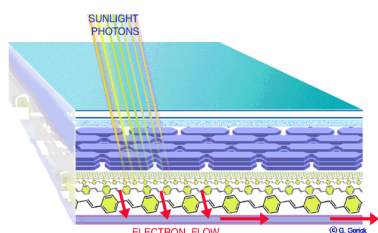


Organic Solar Cell Architectures



PhD Thesis

by

Dipl.Ing. Klaus Petritsch

presented to the

Technisch-Naturwissenschaftliche Fakultät
der Technischen Universität Graz (Austria)

under the supervision of

Cavendish Professor, Prof. Richard Friend,
(University of Cambridge, United Kingdom)

and

Univ.Prof.Dr.techn.Dipl.Ing. Günther Leising
(Technische Universität Graz, Austria)

Cambridge and Graz, July 2000

For my dear mother

“If we did all the things we are
capable of doing, we would
astound ourselves.”

Thomas A. Edison

Acknowledgement

I want to thank both Univ.Prof.Dr.Günther Leising and Univ.Prof.Dr. Richard Friend who together made it possible for me to spend these precious three years in the opto-electronics group at the Cavendish Laboratory in Cambridge (UK) with all its benefits (traveling to conferences, excellent lectures and research facilities etc..) where I could learn so much not only about science but also life in general.

Thanks to the special relationship between the Cavendish Laboratory and its spin-off company Cambridge Display Technology (CDT) I had the opportunity to use the excellent AFM microscope and thereby gain a little insight into the industrial aspect of leading edge technology and research in this exciting new field - for which I am very grateful.

I am particularly indebted to Dr.A.Lux for her patience when explaining organic chemistry to me and pointing out which of my “dream molecules” could be synthesised (and how!).

For many interesting and exciting discussions of conjugated polymer science I want to thank J.J. Dittmer, Dr.M.G. Harrison, Dr.E.Moons, A.Koch as well as Dr.A.N.Ramaprakash who spent many hours to read and comment on different parts of the manuscript. Furthermore Dr.H.Ago, A.C.Arias, T.Brown, F.Cacialli, N.Chawdherry, Dr.G.Denton, Dr.M.Granström, Dr.N.Greenham, P.Ho, Dr.A.Köhler, Dr.R. Lazzaroni, Dr.E.A.Marseglia, Dr.J. de Mello, Dr. G.G.Rozenberg, Dr.H.Sirringhaus, Dr.P.Spearman, Dr.N.Tessler, S.Thomas, V.Wan and B.Weir.

I would like to thank my mother Gertrude Petritsch and my uncle Arnfried Meyer for their generous financial support as well as the TMR-Network SELOA.

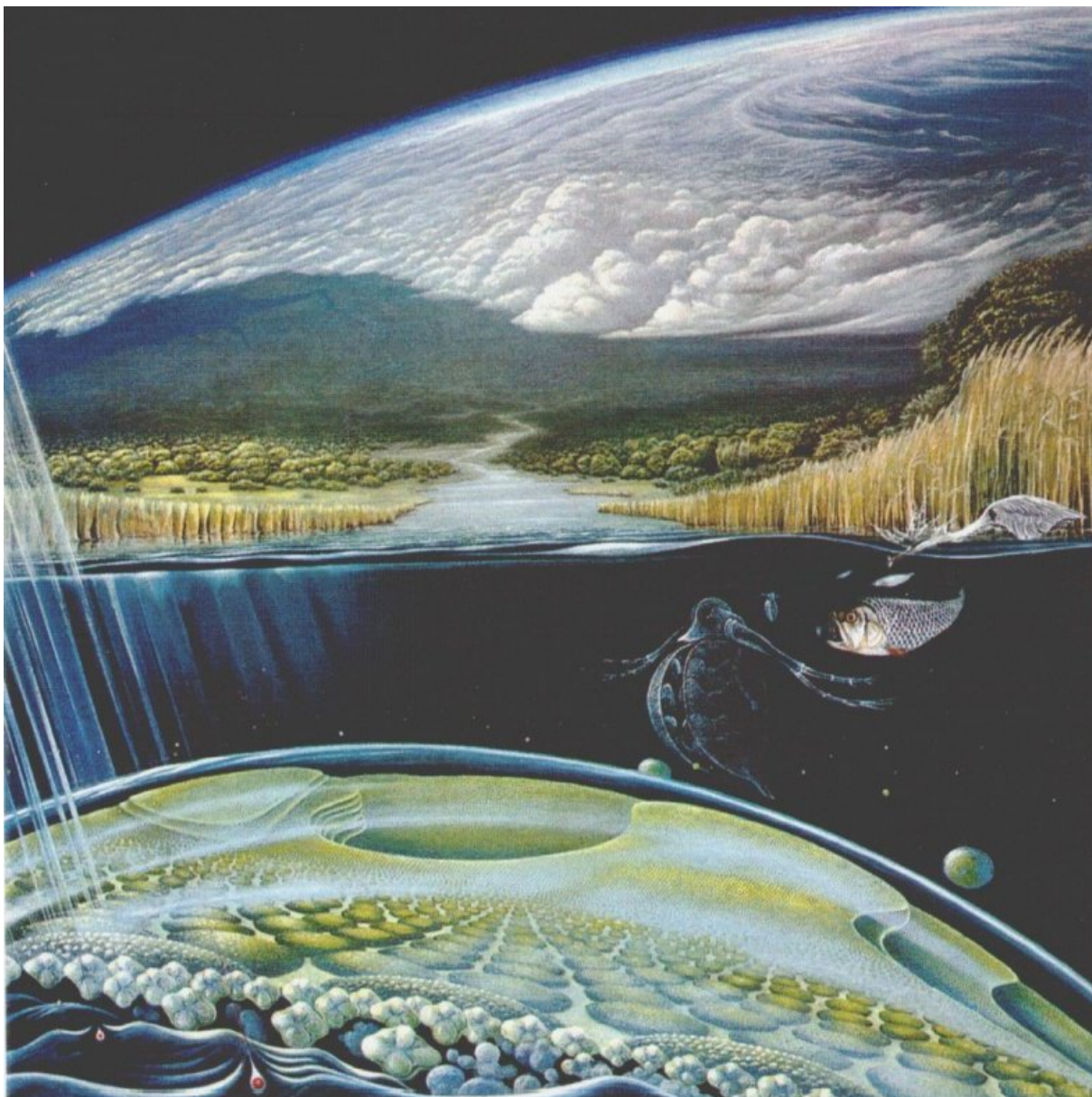
Last but not least, I want to thank all fellow salseros and tangueros who made even my little free time highly enjoyable during these intense three years in Cambridge, Graz, London, Paris, Vienna, Faro, Bologna...

I want to note that, unlike all other results described in this thesis - the experimental part of the Section on the laminated polymer device in Chapter 6 was carried out by Dr. M. Granström. However, the realisation and success of this project was only possible as a result of an excellent collaboration among the coauthors in Ref.[94] - without each of them this work would not have been possible.

With the exception of the laminated polymer device, more than 95% of the actual experimental and theoretical work as well as 100% of the writing was performed by the author.

However, the term “we” is used throughout the text to underline the fact that every single result of the author’s work as presented in this thesis was only possible because of the provision of equipment, materials and scientific input from others.

This is also reflected in the long list of people mentioned in this acknowledgment and consistent with the fact that modern research relies on collaboration and teamwork.



SUNLIGHT HARVESTING

Sunlight provides the energy for almost all life on Earth. It is harvested by plants, including the microscopic algae living in water. Photons of sunlight (represented as red dots) enter the food-producing regions within the algal cell which act like solar panels. Here the molecules of the green pigment, chlorophyll, are arranged in clusters and absorb the energy of the photons. That energy is used to turn carbon dioxide and water into food, releasing excess oxygen. Algae are eaten by daphnia (water fleas) and these are caught by roach, small fish which are preyed on by herons. The heron ultimately depends on a vast number of algal cells to supply it with food. The scale of sizes in the painting gradually changes from

the magnified part of a single algal cell, covering the lower third of the painting, to the Earth's atmosphere at the top of the painting. The oxygen in our atmosphere was itself created by ancestral forms of algae, beginning millions of years ago, when they were among the most advanced life forms on Earth. They changed the ancient atmosphere of the Earth, making it possible for oxygen-breathing animals to evolve. Even today, about 90% of all oxygen production and carbon dioxide use is carried out by algae living in the seas and freshwaters.

From an oil painting by Glynn Gorick, 113 Hemingford Road, Cambridge CB1 3BY, UK. ©G. Gorick 1994

Contents

1	Motivation - Outline	1
1.1	Motivation	1
1.1.1	The Combustion of Fossil Fuels	1
1.1.2	Renewable Energy Sources	1
	Inorganic Solar Cells	2
	Organic Solar Cells	2
1.2	Outline	2
1.3	Abbreviations and Synonyms	3
2	Solar Cells - General	5
2.1	Introduction	5
2.2	General Properties of Organic Semiconductors	8
2.2.1	Polarons and Polaron Excitons	8
2.2.2	P- and n- type Organic Semiconductors	10
	Fermi-level	10
	Doping	10
2.2.3	Structural Properties of Organic Semiconductors	11
2.2.4	Photogeneration of Free Charges	12
	Photogeneration due to Oxygen Traps	12
	The Donor/Acceptor Interface	12
2.2.5	D/A Materials	14
2.2.6	Electrode/Semiconductor Interfaces	15
	Current Through Barriers	16
2.3	Electrode Materials	16
2.4	Photovoltaic Characterisation	18
2.4.1	Power Conversion Efficiency	18
2.4.2	The Equivalent Circuit Diagram (ECD)	19
2.4.3	Open Circuit Voltage	22
	The Ideal Solar Cell	22
	Effect of R_{sh}	22
	Effect of Shorts	22
	The Effect of Photoluminescence	23
	The Upper Limit of V_{oc}	23
	Summary	25
2.4.4	Photocurrent	25
	The Short Circuit Current I_{sc}	25
	The Optical Filter Effect	26
2.4.5	Interpretation of IV Characteristics	27
	Inorganic Solar Cells	27
	Organic Solar Cells	28
2.4.6	Space Charges & Traps	30

3	Single Layer Devices	31
3.1	Introduction	31
3.1.1	Optical Properties of Organic Photovoltaic Materials	31
3.1.2	Performance of Single Layer Devices	33
3.1.3	Doping of Organic Photovoltaic Materials	33
3.1.4	Desired Properties of Organic Photovoltaic Materials	34
3.1.5	Electrodes	36
3.2	LPPPT	36
3.3	MEH	44
3.4	PTV	52
3.5	PIF	55
3.6	THPF	57
3.7	Per	60
3.8	Ter	62
3.9	Single Layer Devices - Summary	64
4	Double Layer Devices	67
4.1	Introduction	67
4.2	The Dye/Pigment Double Layer Device (HPc/Per3)	70
4.3	The Dye/Dye Double Layer Device (CuPc/Per)	73
5	Blend Layer Devices	75
5.1	Introduction	75
5.2	HPc+Per	78
5.3	HPc+PIF	82
5.4	PTV+Per	84
5.5	PTV+Ter	86
5.6	PTV+THPF	89
5.7	PTV+PIF	91
6	Laminated Layer Devices	95
6.1	Introduction	95
6.2	The Laminated Polymer Device	96
	PL Quenching	97
6.3	The Laminated Dye Device	101
	PL Quenching	102
7	Discotic Liquid Crystals as Solar Cell Materials	105
7.1	Introduction	105
7.2	Experimental	107
7.3	Liquid Crystalline Properties	107
7.4	Photovoltaic Properties of HPc	109
7.5	Summary	112
8	Determination of Solar Cell Efficiencies	115
8.1	Introduction	115
8.2	Solar Radiation	115
8.3	Simulation of Solar Radiation	118
	8.3.1 Calculation of the Required AM1.5d Filter	118
	8.3.2 The Simulator Setup	119
8.4	“Numerical” Simulation	120
8.5	Summary	122

9	Summary and Bibliography	123
9.1	Summary	123
9.1.1	Suggestions for Future Investigations	124
9.2	Bibliography	124
10	Appendices	137
10.1	Details of the Sample Preparation	137
10.1.1	ITO Substrates	137
10.1.2	Preparation of the Dye and Polymer Solutions	137
10.1.3	Film Deposition	137
10.1.4	Sublimation of the Top Electrode	138
10.2	Details of the EQE and IV Measurements	138
10.2.1	Note on the Dark Current at 0V	140
10.3	Absorption Measurements	140
10.4	Thickness Measurements	140
10.5	Thermal Polarisation Microscopy	141
10.6	List of Publications	141
10.7	Conferences	142
10.8	Curriculum Vitae of the Author	142

List of Figures

1.1	Atmospheric CO ₂ and human population growth.	1
2.1	Device structure of a typical organic solar cell.	5
2.2	Energy conversion steps and loss mechanism in a solar cell.	6
2.3	The different D/A architectures used in organic solar cells.	7
2.4	IV characteristics related to band energy diagrams.	8
2.5	Polarons and singlet exciton	9
2.7	Examples of structures for the different types of organic semiconductors	11
2.6	Categories of organic semiconductors	12
2.8	Organic semiconductor/semiconductor interfaces	13
2.9	Band bending of D/A devices with electrode interfaces	15
2.10	Solar cell efficiency limits as a function of the semiconductor bandgap.	18
2.11	IV characteristics and fillfactor.	19
2.12	ECD of a solar cell.	19
2.13	Extended ECD of a solar cell.	21
2.14	Optical filter and active layer in device structure.	26
2.15	Two scenarios for the formation of a thin active layer	26
2.16	Effect of R_{sh} on the IV characteristics $10^4 \leq R_{sh} \leq 10^7 \Omega$ - inorganic cell.	27
2.17	Effect of R_{sh} on the IV characteristics $10^1 \leq R_{sh} \leq 10^4 \Omega$ - inorganic cell.	27
2.18	Effect of R_s on the IV characteristics. Inorganic cell.	28
2.19	Effect of R_{sh} on the IV characteristics $10^7 \leq R_{sh} \leq 10^{10} \Omega$ - organic cell.	28
2.20	Effect of R_{sh} on the IV characteristics $10^3 \leq R_{sh} \leq 10^6 \Omega$ - organic cell.	29
2.21	Effect of R_s on the IV characteristics. Organic cell.	29
2.22	Effect of light intensity on the IV curve in an organic cell.	30
2.23	IV characteristics for space charge limited current with deep and shallow traps	30
3.1	Device architecture of a single layer solar cell.	31
3.2	Absorption versus layer thickness (transparent rear contact)	32
3.3	Absorption versus layer thickness (reflective rear contact)	32
3.4	Chemical structure of LPPPT.	36
3.5	EQE and absorption for a thick and a thin LPPPT device.	37
3.6	Thickness dependence of EQE (at 536nm) for LPPPT devices	38
3.7	EQE of LPPP versus thickness at 536nm	39
3.8	Transmission of the Al electrode.	39
3.9	EQE of LPPPT films for different thickness when illuminated through AL.	40
3.10	IV characteristics of the 205nm LPPPT device.	40
3.11	IV characteristics of the 185nm LPPPT device.	41
3.12	IV characteristics of the 122nm LPPPT device.	41
3.13	IV characteristics of the 117nm LPPPT device.	41
3.14	IV characteristics of the 93nm LPPPT device.	42
3.15	IV characteristics of the 67nm LPPPT device.	42
3.16	IV characteristics of the 59nm LPPPT device.	42
3.17	IV characteristics of the 32nm LPPPT device.	42

3.18	V_{oc} and dark current versus film thickness in LPPPT devices.	43
3.19	R_s and R_{sh} (dark) versus film thickness in LPPPT devices.	43
3.20	R_s and R_{sh} (dark and light) versus film thickness in LPPPT devices.	44
3.21	Ratio R_s/R_{sh} as a function of film thickness in LPPPT	44
3.22	IV characteristics of various film thicknesses in LPPPT.	45
3.23	Fitted IV curves for LPPPT.	45
3.24	Chemical structure of MEH-PPV.	46
3.25	EQE and absorption for a thick and a thin MEH-PPV device.	46
3.26	EQE spectra for MEH-PPV thicknesses between 10 and 250nm	47
3.27	EQE of MEH-PPV versus film thicknesses.	47
3.28	IV characteristics of a 250nm thick MEH PPV cell.	47
3.29	IV characteristics of a 210nm thick MEH PPV cell.	47
3.30	IV characteristics of a 54nm thick MEH-PPV cell.	48
3.31	IV characteristics of a 38nm thick MEH-PPV cell.	48
3.32	IV characteristics of a 35nm thick MEH-PPV cell.	48
3.33	IV characteristics of a 10nm thick MEH-PPV cell.	48
3.34	IV characteristics for varying film thicknesses in MEH-PPV.	49
3.35	V_{oc} and I_d in MEH-PPV versus film thickness.	49
3.36	R_{sh} and R_s versus film thickness in MEH-PPV.	50
3.37	R_{sh} and R_s versus film thickness in MEH-PPV.	50
3.38	R_{sh} and R_s versus film thickness in MEH-PPV.	50
3.39	Fitted IV curves for MEH-PPV.	51
3.40	Chemical structure of PTV.	52
3.41	EQE and absorption spectrum of a 90nm thick PTV device.	53
3.42	EQE of a 90nm thick PTV device (semi logarithmic plot)	53
3.43	IV characteristics of the PTV device.	54
3.44	IV characteristics of the PTV cell (double logarithmic).	54
3.45	Chemical structure of PIF.	55
3.46	EQE and absorption spectrum of a PIF device.	56
3.47	EQE and absorption of PIF device (semi logarithmic plot)	56
3.48	IV characteristics of the PIF device.	57
3.49	IV characteristics of the PIF device (double logarithmic plot).	57
3.50	Chemical structure of THPF.	58
3.51	EQE and absorption spectrum of the THPF device.	58
3.52	EQE and absorption spectrum of the THPF device(semi logarithmic plot).	59
3.53	IV characteristics of the THPF cell.	59
3.54	Chemical structure of Per.	60
3.55	EQE and absorption for the Per device.	61
3.56	EQE and absorption of the perylene device (semi logarithmic plot).	61
3.57	IV characteristics of the Per device.	62
3.58	Chemical structure of Ter.	63
3.59	EQE and absorption of the Ter-device (semi logarithmic plot).	63
3.60	IV characteristics of the Ter device.	64
4.1	Device architecture of a double layer solar cell.	67
4.2	EQE and OD of the heated HPc/Per device	68
4.3	HPc/Per3 double layer - architecture and chemical structures	70
4.4	EQE and OD of the pristine and heat treated ITO/HPc/Per3/Al device	72
4.5	IV-characteristics of the pristine and heated HPc/Per double layer device.	72
4.6	Chemical structure of CuPc and Per	73
4.7	Absorption and EQE of the CuPc/Per double layer device	73
4.8	IV Characteristics of the CuPc/Per double layer device	74
5.1	Solar cell architecture comprising a blend of two organic semiconductors	75

5.2	Chemical structure of HPc and Per	79
5.3	PL efficiency versus blend ratio (HPc+Per)	79
5.4	AFM phase contrast images of a HPc+Per blend	80
5.5	Absorption and EQE of the HPc+Per blend device	80
5.6	EQE of the HPc+Per blend device and the single components	81
5.7	IV characteristics of the HPc+Per blend device	81
5.8	Chemical structure of HPc and PIF	82
5.9	Absorption and EQE of the HPc+PIF blend device	83
5.10	Absorption and EQE of the HPc+PIF blend device	83
5.11	IV characteristics of the HPC+PIF blend device	84
5.12	Chemical structure of Per and PTV	85
5.13	EQE and absorption of the PTV+Per blend device	85
5.14	EQE of the PTV/PER blend device (semi logarithmic plot)	85
5.15	IV characteristics of the PTV+Per blend device	86
5.16	Chemical structure of Ter and PTV	87
5.17	EQE and absorption of the PTV+Ter blend device	87
5.18	Absorption versus energy of the PTV+Ter device (vibronic modes)	87
5.19	EQE of the PTV+Ter blend device (semi logarithmic plot)	88
5.20	IV characteristics of the PTV+Ter blend device	89
5.21	Chemical structure of PTV and THPF	89
5.22	Absorption and EQE of the PTV+THPF blend device	90
5.23	EQE of the PTV+THPF blend device (semi logarithmic plot)	90
5.24	IV characteristics of the PTV+THPF blend device	91
5.25	Chemical structure of PTV and PIF	92
5.26	Absorption and EQE of the PTV+PIF blend device	92
5.27	EQE of the PTV+PIF blend device (semi logarithmic plot)	92
5.28	IV characteristics of the PTV+PIF blend device	93
5.29	IV characteristic (dark) of the PTV+PIF blend device (double logarithmic plot).	93
6.1	The lamination technique	95
6.2	PL-quenching of MCP+POPT	97
6.3	Absorption spectra of MCP and POPT	98
6.4	EQE and absorption of the laminated polymer device	98
6.5	AFM image of cross-section of the laminated polymer device.	99
6.6	AFM image of a MCP+5%POPT film.	99
6.7	AFM image of a POPT+5%MCP film.	99
6.8	IV characteristics of the laminated ITO/POPT/MCP+5%/Al device	100
6.9	IV characteristics of the laminated Au/PEDOT/POPT/MCP+5%POPT/Ca device	100
6.10	V_{oc} and I_{sc} versus light intensity of the laminated PEDOT/Ca polymer device	101
6.11	PL-quenching HPc+Per	102
6.12	EQE and absorption spectrum of the laminated dye device	103
6.13	EQE and absorption spectrum of the laminated dye device	103
7.1	Schematic illustration of the solid, liquid crystalline and liquid phase of discotic molecules.	105
7.2	Illustration of the different discotic phases.	106
7.3	Chemical structure of some liquid crystalline phthalocyanines.	106
7.4	DSC trace of HPc.	107
7.5	Image of digitate star texture and birefringent defects.	108
7.6	Sketch of a bend mode as origin for birefringent defects in the mesophase of discotic molecules	108
7.7	Image of a focal conic texture under the polarisation microscope.	109
7.8	TGA of a series of liquid crystalline phthalocyanines.	109
7.9	TGA of CuPcSC12 under nitrogen and air.	110
7.10	Absorption and photoluminescence of HPc.	110
7.11	EQE of the thin HPc device, illumination through ITO.	110

7.12	EQE of the thick HPc cell, illuminated through AL.	111
7.13	EQE of thin HPc device, illumination through Al.	111
7.14	EQE of the thick HPc device in vacuum and air illuminated through ITO.	112
7.15	IV characteristics of the thin HPc device.	113
7.16	IV characteristics of the thick HPc device.	113
8.1	Definition of Air Mass.	115
8.2	Global and direct solar spectrum	116
8.3	Energy distribution in AM1.5d spectrum.	116
8.4	Emission of a QTH-lamp and filter transmission spectra.	118
8.5	Measured and modeled AM1.5d spectra	118
8.6	Transmission of the required, modeled and measured AM1.5d filter.	119
8.7	Measured, modeled and standard AM1.5d spectrum	119
8.11	Solar simulator setup.	120
8.8	Deviation of actual filter absorption from the catalogue.	120
8.9	AM1.5d spectrum and filter calculated from measured filter curves	120
8.10	Calculated spectrum for new filter combination and AM1.5d	121
8.12	Intensity dependence of V_{oc} and I_{sc}	121
10.1	Electrode pattern of the substrate with 8 pixels.	138
10.2	Electrode pattern of the substrate with 8 pixels.	138
10.3	Typical light intensities versus wavelength in EQE/IV measurements.	139
10.4	EQE spectrum and spectral response of the silicon reference diode.	139

List of Tables

1.1	List of synonyms	4
1.2	List of abbreviations	4
2.1	Workfunction of the elements.	17
2.2	Workfunction of molecular electrode materials	18
3.1	Survey of the absorption properties of various organic semiconductors	32
3.2	Survey of important performance parameters of various organic single layer solar cells . .	34
3.3	Survey of solar cell parameters obtained from the IV curves	40
3.4	Survey of various solar cell parameters obtained from the IV characteristics	49
3.5	Survey of photovoltaic parameters of the investigated organic semiconductors	65
4.1	Survey of performance parameters of various organic double layer solar cells	69
5.1	Survey of performance parameters of various solar cells using organic semiconductor blends	77
6.1	Survey of performance parameters of laminated solar cells.	96
7.1	Phase transition temperatures of a series of liquid crystalline phthalocyanine derivatives .	107
7.2	Survey of electron and hole mobilities of important organic and inorganic semiconductors	112
9.1	Overall assessment of the different solar cell architectures incl. pigments	123
9.2	Overall assessment of the different solar cell architectures for soluble materials only	123
9.3	Summary of important performance parameters of various organic solar cells including all types of architectures.	125

Chapter 1

Motivation - Outline

1.1 Motivation

1.1.1 The Combustion of Fossil Fuels

The limited supply of today's main energy sources (oil, coal, uranium) will force us - sooner or later - to replace most of the currently used power plants with *renewable* energy sources. According to recent predictions [123, 36]¹, the inevitable permanent decline in the global oil production rate is expected to start within the next 10-20 years.

Worldwide, oil prices will then rise considerably favouring the introduction of various *renewable* energy sources such as the direct conversion of solar energy (solar cells), but also others like for example, hydroelectric- and wind-power systems.

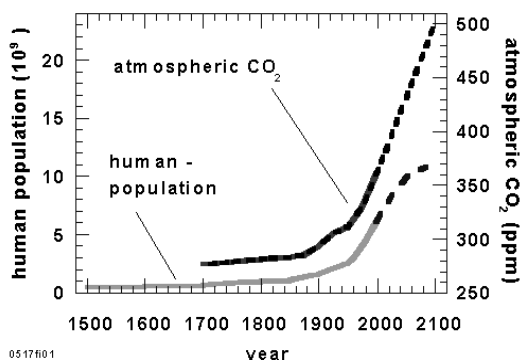


Figure 1.1: The atmospheric concentration of greenhouse gases like CO₂ have grown significantly since pre-industrial times. This can be largely attributed to human activities, mostly fossil-fuel use [136]. Dashed lines are possible (optimistic) future scenarios [136, 10].

¹As a service to the reader, references are listed in *alphabetical* order in Chapter 9. Hence, they do not appear in numerical order in the text.

However, the combustion of fossil fuels in the past has *already* harmful effects on the delicate balance of nature on our planet. Today, about $20 \cdot 10^{12}$ kg of carbon dioxide are put into the atmosphere every year, mainly by burning fossil fuel [17, 136, 252].

Today's plants are unable to absorb this huge amount of extra CO₂. As a result the CO₂ concentration in the atmosphere continues to mount (Fig.1.1) adding considerably to the greenhouse effect which will increase the global mean surface temperature - depending on future emission scenarios and the actual climate sensitivity - by another 0.6-7.0°C by the year 2100 [136].

Global mean surface temperature has increased by 0.3-0.6°C since the late 19th century and the global sea level² has risen by 10-25cm, most likely due to human activities [136].

The consequences of this temperature change have already increased the frequency and severity of natural disasters [252] and are likely to have more devastating effects for humans and other life forms in all parts of Earth within the next decades.

1.1.2 Renewable Energy Sources

Fortunately, we have *renewable* energy sources which neither run out nor have any significant harmful effects on our environment. Naturally, power plants that use wind, the potential, wave or tidal energy of water, the heat from the Earth's crust or direct solar radiation rely on the local supply of their primary energy source. Thus, the amount of power they can supply over a longer period³ often depends on geographical and weather conditions.

It is important to recognise that the installation of these power systems should *always* be preferred as long as they supply more energy throughout their

²Projected sea level rise from the present to the year 2100 is 15-95cm [136].

³Using the existing energy storage technology.

lifetime than they have consumed during their fabrication, installation and maintenance. Although this criterion is fulfilled for all of them their *prices* are not yet low enough.

Unless we can soon develop low cost technologies for renewable energy sources we have to hope that the world's governments start to consider the "costs" of environmental hazards of the majority of existing power sources in the planning of future power plants.

Inorganic Solar Cells

At present, solar cells comprising an inorganic semiconductor such as mono- and multi-crystalline silicon have found markets for small scale devices such as solar panels on roofs, pocket calculators and water pumps. These conventional solar cells can harvest up to as much as 24% [237] of the incoming solar energy which is already close to the theoretically predicted upper limit of 30% [230]⁴. This illustrates that technologies which allow low fabrication costs - rather than somewhat higher conversion efficiencies - are now desired. One approach here would be to reduce the amount of silicon by using thinner films on (cheap) glass substrates.

Today, the production of these solar cells still requires many energy intensive processes at high temperatures (400-1400°C) and high vacuum conditions with numerous lithographic steps leading to relatively high manufacturing costs [162].

Organic Solar Cells

Considerably less effort and production energy is necessary if organic semiconductors are used because of simpler processing at much lower temperatures (20-200 °C) than the above mentioned inorganic cells.

For example, electro-chemical solar cells using titanium dioxide in conjunction with an organic *dye* and a liquid electrolyte [182] already exceeded 6% power conversion efficiencies [237] and are about to enter the commercial market thanks to their relatively low production costs.

Another interesting alternative to inorganic cells is given by the semiconducting *polymers*, which combine the opto-electronic properties of conventional semiconductors with the excellent mechanical and processing properties of polymeric i.e. "plastic" materials. These can be processed from solution at

room-temperature onto e.g. flexible substrates using simple and therefore cheaper deposition methods like spin or blade coating.

Since the discovery of electro-luminescence in conjugated polymers [34], this class of materials has been used to build efficient light emitting diodes [248, 274, 100], field effect transistors [232], optically-pumped LASERs [249, 250] and photovoltaic diodes [112, 278, 213, 94].

The advantage of polymeric photovoltaic cells when compared to electro-chemical cells is predominantly the absence of a *liquid* electrolyte, which generates problems with sealing against air, but also the prospect of even cheaper production using large area devices and the use of flexible substrates. Possible applications may range from small disposable solar cells to power smart plastic (credit, debit, phone or other) cards which can display for example, the remaining amount, to photo-detectors in large area scanners or medical imaging and solar power applications on uneven surfaces.

1.2 Outline

Chapter 2 is aimed to introduce researchers who are planning to work on organic solar cells into this very specialised but also interdisciplinary field. The more general properties of organic semiconductors can be found in many excellent text books and other references and are only summarized briefly in the first part.

The second part gives a more comprehensive insight into the important characteristic solar cell parameters and links between them. In fact, this Chapter contains a unique compilation and summary of "organic solar cell relevant knowledge" that is consistent with the experience, understanding and view of the author.

However, since a full theoretical understanding of organic solar cells is still not possible we have tried to improve understanding of device physics by drawing analogies to inorganic cells using the equivalent circuit diagram and the "traditional" interpretation of current voltage characteristics.

The subsequent Chapters deal with the four known device architectures: the single layer (Chapter 3), double layer (Chapter 4), blend (Chapter 5) and the laminated device (Chapter 6).

Each of them begins with a survey of characteristic parameters of already reported devices - including the results of this thesis - pointing out specific advantages and encountered problems.

⁴Note that using the more expensive GaAs even higher power conversion efficiencies (AM1.5) have been confirmed [237]: 25% (monocrystalline GaAs) and 30% (GaInP/GaAs)

Chapter 7 concerns single layer devices comprising a liquid crystalline semiconductor. The outstanding properties of discotic liquid crystals justify the discussion of this device in a Chapter separated from the single layer device Chapter. It also comprises a survey of the interesting transport (charge carrier mobility) properties of liquid crystalline semiconductors as well as the mesogenic characterization of a series of discotic molecules from which one has been used to fabricate a single layer solar cell.

How solar cell efficiencies can be determined in a reasonable yet practical way either by setting up a solar simulator or numerical simulation is discussed and described in Chapter 8.

Chapter 9 concludes with a summary of the characteristic parameters comprising all four solar cell architecture, an overall assessment, some suggestions for future investigations and a comprehensive bibliography.

Details of sample preparation and measurements as well as a list of publications by the author and a brief CV can be found in the Appendices in Chapter 10.

The object of this thesis was the investigation of various types of organic semiconductors (preferably with low bandgaps) in different solar cell architectures. However, the following findings may be of particular interest for both experts and newcomers in the field:

- We have introduced a new device architecture that combines advantages of double layer and blend devices and opens exciting new possibilities in device design such as selective doping. Two laminated devices are discussed in Chapter 6 and published in Refs. [94, 95, 201].
- We have shown for the first time that dye/dye interfaces can be used for photogeneration of charges in solar cells - see Section 4.3, Section 5.2 and Section 6.3 as well as publications Refs [200, 201].
- In Chapter 7 we have shown that dyes with liquid crystalline properties can be used as active semiconducting components in solar cells. Our results together with the recent literature indicate that heating into the liquid crystalline phase is not necessary.
- All devices discussed in the Chapters on double layer, blends and laminated structures show spectral responses covering at least the

wavelength range of visible light. Two devices even had a clear photo-response down to $\lambda > 1000\text{nm}$ - see Section 5.7 and Section 5.3.

- The single layer device comprising PTV shows a very strong monoton dependency of the EQE on the wavelength so that the device can be used as simple colour - or even - wavelength detector covering the entire visible range - see Section 3.4.
- We have studied effects of film thickness and have found that those devices that have the thinnest films (10-30nm, which is near the estimated exciton diffusion length) give the highest currents - see Section 3.2 and Section 3.3. A method to estimate the optimal thickness has been introduced - see Section 3.2. However, we have also found that the shunt resistor grows 30 to 100 times faster than the series resistor with increasing film thickness favouring thicker films for larger fill factors.
- In Chapter 8 we describe how the standard solar spectrum can be simulated with a relatively simple setup that can be built in most laboratories for a fraction of the cost of commercial simulators. We also discuss a method solely based on intensity dependent photocurrent/voltage measurements that can be used to estimate the AM1.5 efficiency of solar cells.

1.3 Abbreviations and Synonyms

Table 1.1 lists terms which are frequently used as synonyms in literature and throughout the text. Note that the terms "dye" and "pigment" are frequently used as synonyms in literature - while we differentiate clearly between these two in this thesis - see also Section 2.2.3.

Note that, for example, the term IPCE which is sometimes used in publications on organic solar cells, can have two very different meanings:

1. Internal power conversion efficiency. This is the power conversion efficiency when losses due to reflection and transmission are considered. Thus its value can be considerably larger than the external power conversion efficiency.
2. Incident photon to current conversion efficiency. This is often the equivalent to EQE but could also be the IQE.

Table 1.1: List of expressions which are used as synonyms throughout the text or relevant literature.

AM1.5 efficiency	solar (power) conversion efficiency
blend device	blend layer device
conjugated polymer	semiconducting polymer
external quantum-efficiency	photon to current-conversion efficiency
exciton splitting	exciton dissociation
heterojunction	donor/acceptor interface
HOMO/LUMO gap	bandgap
HPc (pig.or dye)	HPcSC12 (dye)
irradiance	light intensity
n-type - laminated device	electron transport - laminated layer device
material	or acceptor material
photocurrent	light current
p-type - material	hole transport or - electron donor material
shunt	parallel resistor
Shottky diode	single layer device
spectral response	photo-response

Moreover, both interpretations of IPCE could refer to monochromatic light (more common) but also to white light exposure or some other light spectrum.

In order to avoid these irritating ambiguities, the big scientific community that has been researching on *inorganic* solar cells for many decades usually quotes the EQE and if required the IQE together with AM1.5 efficiencies to allow meaningful comparisons of solar cell performances all over the world.

Many terms used in organic chemistry or to describe theoretical objects or concepts can grow very long and become unreadable. Hence we have had to use abbreviations most of which are common in the field. These are listed in Table 1.2.

Table 1.2: List of common abbreviations used throughout the text.

A	electron acceptor
CB	conduction band
CN-PPV	cyano substituted PPV
CV	cyclic voltametry
D	electron donor
DSC	differential scanning calorimetry
EA	electron affinity
ECD	equivalent circuit diagram
EQE	external quantum efficiency
FF	fillfactor
FTO	fluorinated tin oxide
HOMO	highest occupied molecular orbital
HPc	metal free phthalocyanine
IP	ionisation potential
ITO	indium tin oxide
LED	light emitting device
LPPP	poly(<i>para</i> -phenylene) type ladder polymer
LPPPT	poly(phenylene-tienylene) type ladder polymer
LUMO	lowest unoccupied molecular orbital
MEH	2-methoxy, 5-(2-ethyl-hexyloxy)
MCP	CN substituted MEH-PPV
MWNT	multiwall nanotubes
OD	optical density
PANI	poly(aniline)
Pc	phthalocyanine
PEDOT	poly(ethylene dioxythiophene)
Per	perylene diimide derivative
PIF	poly(indenofluorene)
PITN	poly(iso-thionaphthene)
PL	photoluminescence
PR-TRMC	pulse radiolysis time resolved microwave conductivity
PPP	poly(<i>para</i> -phenylene)
PPV	poly(<i>para</i> -phenylene vinylene)
PT	poly(thiophene)
PTV	poly(tienylene vinylene)
PVK	poly(vinyl carbazole)
P3HT	poly (3-hexylthiophene)
SCE	saturated calomel electrode
SMU	source measure unit
SR	spectral response
TCNQ	tetra-cyano-quino-di-methane
TGA	thermal gravimetry analysis
TNF	trinitrofluorenone
TO	tin oxide
TOF	time of flight
VB	valence band

Chapter 2

Solar Cells - General

2.1 Introduction

The conversion of solar light into electric power requires the generation of both negative and positive charges as well as a driving force that can push these charges through an external electric circuit. When connected to the external electric circuit any electrical device, such as a computer screen or the motor of a water pump, may then utilise the converted solar energy.

In fact, a solar cell (Fig.2.1) may be seen as a solar-light driven *electron pump*: The maximum height the electrons can be "pumped" is equal to the highest voltage the solar cell can develop. The maximum current is determined by the pump rate.

Suppose the "pump" can promote 100 electrons/s from the valence band (VB) into the conduction band (CB), the highest possible continuous current of electrons flowing through the external circuit is then 100 electrons/s. If the current flow through the external circuit is reduced by e.g. a load resistor to - for example - 80 electrons/s, the remaining 20 electrons/s will drop back into the VB before they can leave the device.

In real semiconductors, these leakage currents are simply realised by the *recombination* of the photoexcited charge carriers or using our analogy: the "pumped" electrons drop back into their VB. These leakage currents are typically caused by defects or other deviations from the ideal semiconductor structure which give rise to the appearance of allowed energy levels *within* the bandgap.

Only if there are virtually no such defects, *radiative* recombination, which occurs on a much larger time scale, will remain as the only decay channel since it does not require the existence of mid-gap levels but can occur directly from band to band.

As a consequence, high PL - efficiency can be regarded as evidence for the absence of the faster and therefore more efficient non-radiative recombination channels. The charge carriers will then have

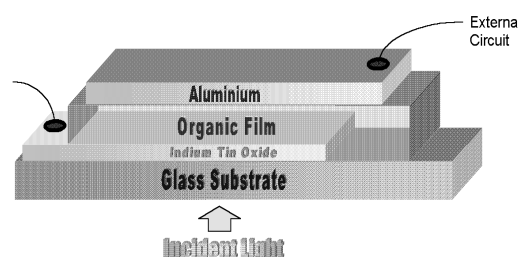


Figure 2.1: Device structure of a typical organic solar cell. The organic film may comprise one [89] or more [245] semiconducting layers, a blend [115] or a combination of these [95]. Figure courtesy of Ref. [63].

much more time to reach the device electrodes before they recombine under the emission of light.

The assumption of the absence of nonradiative recombination allows predictions for the upper limit for both the power conversion efficiency of a semiconductor with a given bandgap and the open circuit voltage. These issues are discussed in more detail in Section 2.4.3.

Fig.2.2 shows the conversion steps of photons into separated charges as it takes place in an organic solar cell. It also shows the associated loss mechanism and the related electrical quantity used in the equivalent circuit diagram (ECD). The latter is described in more detail in Section 2.4.2.

In organic semiconductors, absorption of photons leads to the creation of bound electron hole pairs (excitons) rather than free charges. These excitons carrying energy but no net charge may *diffuse* to dissociation sites where their charges can be separated. The separated charges then need to travel to the respective device electrodes, holes to the anode and electrons to the cathode to provide voltage and be available for injection into an external circuit.

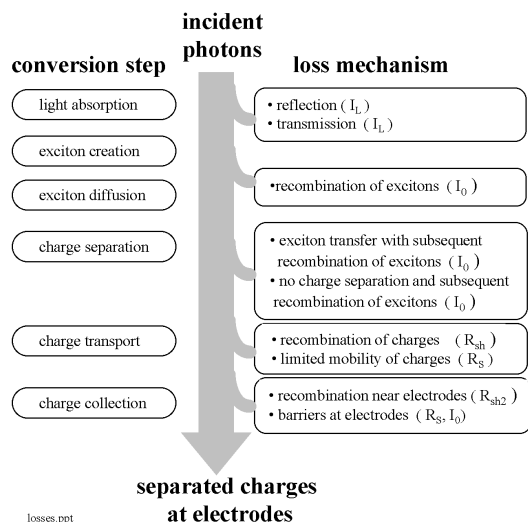


Figure 2.2: Survey of the specific conversion steps and loss mechanisms in an organic solar cell. The symbols in brackets represent the quantities that allow for the specific loss mechanism in the ECD - see Section 2.4.2. For effects of doping see Section 2.2.2.

In the following we comment on the individual conversion steps with regard to the special situation in organic solar cells:

1. Absorption of photons. In most organic device only a small portion of the incident light is absorbed for the following reasons:

- The semiconductor bandgap is too high. A bandgap of 1.1eV (1100nm) is required to absorb 77% of the solar radiation on earth (see Table 8.3 whereas the majority of semiconducting polymers have bandgaps higher than 2.0eV (600nm) limiting the possible absorption to about 30%.
- The organic layer is too thin. The typically low charge carrier and exciton mobilities require layer thickness in the order of 100nm. Fortunately the absorption coefficient of organic materials is generally much higher than in e.g. Si so that only about 100nm are necessary to absorb between 60 and 90% if a reflective back contact is used.
- Reflection. Reflection losses are probably significant but little investigated in these

materials. Systematic measurements of photovoltaic materials are desired to provide knowledge of their impact on absorption losses. Anti-reflection coatings as used in inorganic devices may then prove useful once other losses such as recombination become less dominant.

2. Exciton diffusion. Ideally, all photoexcited excitons should reach a dissociation site. Since such a site may be at the other end of the semiconductor, their diffusion length should be at least equal the required layer thickness (for sufficient absorption) - otherwise they recombine and photons were wasted. Exciton diffusion ranges in polymers and pigments are typically around 10nm [111, 113, 52, 88]. However, some pigments like perylenes are believed to have exciton diffusion lengths of several 100nm [154].
3. Charge separation. Charge separation is known to occur at organic semiconductor/metal interfaces, impurities (e.g. oxygen) or between materials with sufficiently different electron affinities (EA) and ionisation potentials (IA). In the latter one material can than act as electron acceptor (A) while the other keeps the positive charge and is referred to as electron donor (D) - since it did actually *donate* the electron to A. If the difference in IA and EA is not sufficient, the exciton may just hop onto the material with the lower bandgap without splitting up its charges. Eventually it will recombine without contributing charges to the photocurrent. See also Fig.2.8.
4. Charge transport. The transport of charges is affected by recombination during the journey to the electrodes - particularly if the same material serves as transport medium for both electrons and holes. Also, interaction with atoms or other charges may slow down the travel speed and thereby limit the current - see also space charge limited current in Section 2.4.2).
5. Charge collection. In order to enter an electrode material with a relatively low workfunction (e.g. Al, Ca) the charges often have to overcome the potential barrier of a thin oxide layer. In addition, the metal may have formed a blocking contact with the semiconductor so that they can not immediately reach the metal. Semiconductor/metal interfaces are discussed in more detail in Section 2.2.6.

We note that both exciton and charge transport in organic materials usually require *hopping* from molecule to molecule. Thus, close packing of the molecules is assumed to decrease the width of the intermolecular barriers and a flat molecular structure should generally lead to better transport properties than bulky 3 dimensional molecules¹. We note that dense packing also favours a higher absorption coefficient.

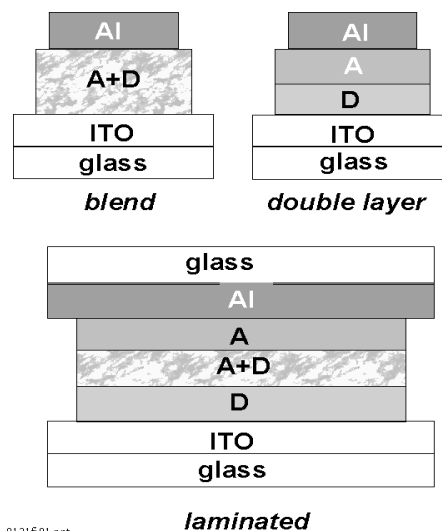
In order to meet these specific requirement for efficient photon to charge conversion different device architectures have been developed in the past. Fig.2.3 shows device designs used for cells comprising two components, an electron donor (D) and an electron acceptor material (A). Charge separation occurs at the interface between those two. Ideally the D- material should only be in contact with the electrode material with the higher workfunction (typically ITO) and the A-material with the lower workfunction electrode (typically Al)².

In the following we give a brief summary including the strengths and weak points of the four different architectures known today:

1. Single Layer Cell. Single layer structures consist of only one semiconductor material and are often referred to as *Schottky* type devices or *Schottky diodes* since charge separation occurs at the rectifying (Schottky) junction with *one* electrode. The other electrode interface is supposed to be of ohmic nature. The structure is simple but absorption covering the entire visible range is rare using a single type of molecule. The photoactive region is often very thin and since both positive and negative photoexcited charges travel through the same material recombination losses are generally high.
2. Blend cell. The strong point of this type is the large interface area if the molecular mixing occurs on a scale that allows good contact between alike molecules (charge percolation) and most excitons to reach the D/A interface. This can usually only be partly achieved so the defects of the network structure - particularly the connectivity with the correct electrode - represents a technological challenge.

¹PL is often quenched considerably if close packing occurs indicating the presence of faster recombination (loss) channels. The reason why many aggregated materials can still be used to give excellent devices is not yet clear. The gain of improved charge transport may compensate the extra recombination channel here.

²See Section 2.2.6 for more information on electrode materials.



0121601.ppt

Figure 2.3: Three different types of D/A architectures for organic solar cells. The blend structure can be obtained by spincoating using a D/A mixture whereas the double layer requires two separate deposition processes. The laminated device can be seen as a hybrid between these two.

3. Double layer cell. This structure benefits from the separated charge transport layers that ensure connectivity with the correct electrode and give the separated charge carriers only little chance to recombine with its counterpart. The drawback is the small interface that allows only excitons of a thin layer to reach it and get dissociated.
4. Laminated device. This relatively recent type represents the successful attempt to unify the advantages of the two structures above. Charge separation occurs in the blend layer in the middle that is obtained after laminating the two separate layers together and charge transport can only occur via the correct transport layer. This structure also features the useful options to treat each layer separately (e.g. doping, physical/chemical conversion) before forming the blend layer and instant encapsulation between the two substrates. The drawback is that certain mechanical properties of the organic semiconductors are required (low glass transition temperature) to form the intermixed layer.

In Section 2.2 we discuss the special general properties associated with organic semiconducting ma-

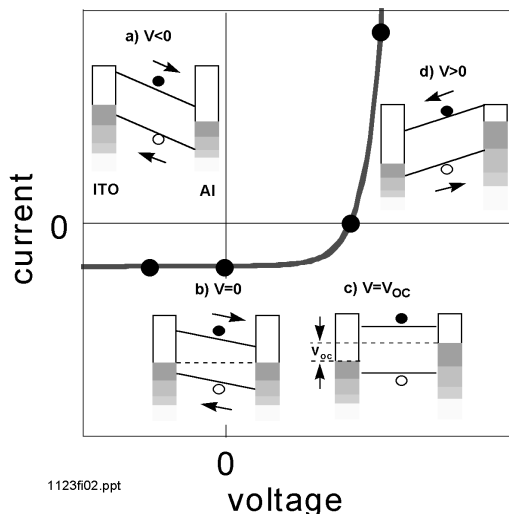


Figure 2.4: Simple model that relates the IV characteristics qualitatively to energy level diagrams. For clarity it is assumed that bands are tilted rather than bent and exciton dissociation occurs throughout the entire device. Tilted bands represent homogeneous electric fields that drive the charge carriers to the respective electrodes.

materials whereas in Section 2.4 we focus on the *photovoltaic* properties. Since solar energy conversion using solar cells is *in principle* the same for both organic and inorganic semiconductors "general tools" like the definition of solar cell parameters (FF, V_{oc} , EQE), the concept of an equivalent circuit diagram (ECD) or the deduction of resistor parameters from the IV characteristics are the same.

2.2 General Properties of Organic Semiconductors

Due to e.g. the strong electron-phonon interaction in organic materials the photo-physics in this class of materials is often different compared to the inorganic semiconductors and not yet fully understood.

One of the main differences is that photo-excitation in these materials does not automatically lead to the generation of *free* charge carriers, but to bound electron-hole pairs (excitons) with a binding energy of about 0.4eV [12, 56, 168].

These excitons need to be split up (or dissociate) before the charges can be transported through the film and collected at the electrodes. For example, exciton *dissociation* can occur at a rectify-

ing interface (Schottky contact) in single layer devices or at the interface between an electron-donor and an electron-acceptor semiconductor material. The larger this interface area the more excitons can reach it and dissociate.

In addition, the small diffusion range of the excitons (typically about 10nm [111, 113, 88, 52]) compared to the film thickness necessary to absorb the major portion of light (typically >100nm) has made it difficult to reach practically interesting conversion efficiencies in organic solar cells.

2.2.1 Polarons and Polaron Excitons

The origin of the term *polaron* for charged quasi-particles can be found in classical polar crystals where the associated charge e.g. the electron repulses adjacent electrons while attracting the nuclei resulting in a *polarisation* of the lattice in its closer vicinity.

Moreover, this accompanying cloud of polarisation causes an increasing effective mass decreasing the mobility of these quasi-particles. Due to the dimerisation³ of the bonds, *conjugated* systems exhibit neither pure covalent nor pure polar bonds.

In fact, they represent a separate class with regard to their bond nature exhibiting huge electron-lattice coupling⁴ compared to the inorganic solids. The strong electron-lattice coupling is responsible for the existence of the quasi-particles such as polarons and polaron excitons in conjugated systems.

These quasi particles can be identified by the additional energy levels [70] associated with them which appear within the semiconductor bandgap⁵ - see Fig.2.5 - using sensitive detection methods like photo-induced absorption spectroscopy [163, 197, 198].

Polarons in conjugated systems affect not merely the polarisation in their vicinity - they even change the nature of bonds from σ to π and vice versa via excitation and while traveling. This usually leads to a more *rigid* structure in the excited state the so called *quinoid* configuration.

Note that photogeneration of *charged* excitations usually requires separation of charges *between*

³The alteration of single and double bonds does not allow determination of which bond is double and which is single bond in degenerate semiconducting systems such as most semiconductors. Thus, the π electron of the double bond can be seen as *delocalised*.

⁴Excitation of the π electron used for the double bond has a strong effect on the "lattice" structure.

⁵upon photoexcitation or chemical doping (upon blending or intercalation with guest material (dopant)).

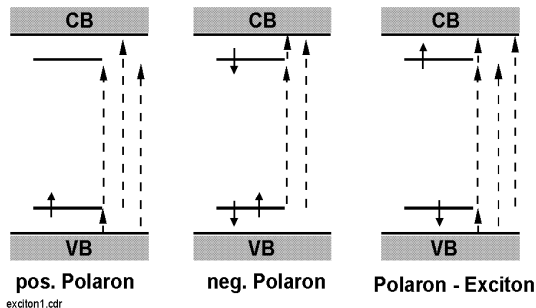


Figure 2.5: Energy levels of the positive and negative polarons as well as the polaron (singlet) exciton. Arrows with solid lines represent electrons with their spin orientation, arrows with dashed lines show possible intra gap transitions that can be used to detect and identify the excited species.

the chains, the most effective generation is photo-excitation with a pump beam that is polarised *perpendicular* to the polymer backbone [76].

In the following we give a brief overview about differences between excitons in the much better understood inorganic systems and the organic ones:

- Excitons in inorganic solar cells. The binding energy E_b of *inorganic* excitons is estimated to be around 16meV which means that these exciton become important predominantly at *lower* temperatures (where kT becomes small compared to E_b)[98]. Unlike its constituents particles, an inorganic exciton is a *Boson* rather than a Fermion, with occupation statistics determined by the Bose-Einstein equation.

These excitons can reduce their energy further if they bind with impurities or defects. Since they are Bosons, *all* of them can occupy the lowest lying state (at once) giving sharp peaks in the light emitted at low temperatures due to radiative recombination of the constituent electron and hole. At high densities and low temperatures, the free exciton gas can condense to give an electron-hole liquid phase with interesting properties [270].

- Excitons in organic solar cells. The binding energy E_b of excitons in *organic* semiconductors - in particular for conjugated *polymers* like PPV and its derivatives - has been subject to intense debates over the past decade. E_b values ranging from very small [158] over intermediate values (around 0.4eV) [56, 168, 12] to very high (up to 0.95eV) [49] have been proposed.

Within the framework of this thesis we assume that binding energy is not larger than about 0.4eV. As a consequence, the energy levels of the exciton are separated from the CB and VB by less than about 0.2eV which have been neglected in all band energy diagrams in this thesis since the bandgaps of the materials used are between 1 and 2eV. However, a clear offset between the HOMO and LUMO levels of the D/A material is still required for the exciton to dissociate at room temperature.

In the following we give a brief description of different types of excitons⁶:

1. Frenkel exciton: The electron hole pair is confined to not more than one molecular unit [75, 195].
2. Mott-Wannier exciton: The distance between electron and hole is much greater than the spacing between unit cell (here molecular units) [175, 265]. Their energy levels can be described as hydrogen-like bound states, calculated with a reduced effective mass.
3. Charge transfer exciton: The exciton extends over only a few adjacent molecular units [138]
4. Inter-chain excitons: This term is used for polymeric semiconductors to indicate that the constituent charges are located on *different* polymer *chains*. It can be regarded as a charge transfer exciton.
5. Intrachain excitons: This term also refers to *polymeric* semiconductors to indicate that the constituent charges are located on the *same* polymer *chain*. It is believed that intrachain excitons represent the main species that is formed after photoexcitation in conjugated polymers [78, 79, 54].

We note that there is another *related* excited species called “excimer” that can play an important role in organic semiconductors. An excimer can be understood as a dimer that is only stable in the excited state [205, 138]. Hence, it is only weakly absorbing and shows little vibronic structure in its emission spectrum. It can be formed by interaction of an excited molecule with a molecule in its ground state. Both singlet and triplet excimers have been observed in organic molecules such as naphthalenes or perylenes [205, 104]. An exciplex is an excimer consisting of two *different* molecules.

⁶Inter- and intrachain excitons may also be seen as sub groups of the three main types.

2.2.2 P- and n- type Organic Semiconductors

Fermi-level

The energetic position of the Fermi-level in semiconductors is important for two reasons:

1. Together with the workfunction of the metal the Fermi level determines whether a blocking or ohmic contact is formed at the semiconductor/metal interface.
2. The relative position of the Fermi levels is a measure for the type of conductivity - whether the semiconductor conducts preferably holes in the VB (p-type) or electrons in the CB (n-type)

The energetic position of the Fermi level in a semiconductor represents the balance between the concentration of holes and electrons that occupy allowed energy levels under equilibrium condition (dark, no applied voltage). If the Fermi-level is closer to the CB the material is called n-type conductor since more electrons are available for conduction than holes - otherwise it is called p-type conducting.

Thus, the position of the Fermi level can be written as a function of both the effective density of states in the conduction band N_C and valence band N_V as well as the concentration of donors N_D and acceptors N_A :

For n-type semiconductors this gives [162]:

$$E_F = E_C - kT \cdot \ln(N_C/N_D) \quad (2.1)$$

whereas for p-type semiconductors the relation is:

$$E_F = E_V - kT \cdot \ln(N_V/N_A) \quad (2.2)$$

E_V and E_C stand for the top edge of the VB and the bottom edge of the conduction band respectively⁷.

When voltage is applied and/or the semiconductor is illuminated, the concept of a Fermi level can no longer be applied. Upon e.g. illumination the increased concentration of electrons in the CB would shift E_f up while the higher concentration of holes in the VB would require to shift E_f down - at the same time. As a consequence, two separate Fermi levels - the so called *quasi* Fermi-levels⁸ - are then introduced to describe the situation under this non equilibrium condition [98, 162]:

$$E_{FN} = E_C + kT \cdot \ln(n/N_C) \quad (2.3)$$

and

$$E_{FP} = E_V + kT \cdot \ln(N_V/p) \quad (2.4)$$

with n and p denoting the concentration of electrons in the CB and holes in the VB. E_{FN} and E_{FP} are the quasi Fermi-levels that are associated with the balance of electrons and holes - both exist at the same time in one semiconductor.

Doping

In inorganic semiconductors doping occurs via the introduction of dopant atoms that provide additional free charge carriers at room temperature so that the extra charges increase the conductivity for this type of charge carrier. As discussed above, the Fermi level would be moved towards the CB if extra electrons are introduced or towards the VB if the concentration of mobile holes has been increased.

In organic semiconductors “doping” is usually achieved by the introduction of foreign *molecules* rather than atoms⁹. Another possibility to achieve doping effects in conjugated systems is electrochemical oxidation or reduction which can be achieved and investigated by e.g. cyclic voltametry [125, 126, 127, 233].

Moreover, changes of the concentration of mobile charges are often achieved by trapping of e.g. electrons in the CB so that the concentration of mobile holes in the VB (relative to the mobile electrons) increases. That way the Fermi level would move towards the VB and make the material a ‘doped’ p-type conductor i.e. a better hole than electron transport material. Since there is no net increase of mobile charge carriers the conductivity cannot increase (unless the mobility of charge carriers is affected).

However, in practice we often find increased conductivity (particularly in light) upon exposure to e.g. oxygen [268, 43]. This effect may be explained by the generation of charge carriers due to exciton dissociation - see discussion below.

Examples for dopants¹⁰ of p-type materials are: Cl_2 , NO_2 , I_2 , Br_2 , organic molecules like o-chloranil, and 2,4,7-trinitrofluorenone, H_2O , O_2 . Other p-type dopants are TCNQ or also high electron affinity *semiconductors* like C60 or CN-PPV or perylene

⁷ E_V may be seen as the HOMO and E_C as the LUMO level in a quasi molecular model.

⁸These are also known as Imrefs (Fermi read backwards.)

⁹Atoms are not used because they are too small. They would diffuse out of the bulk and eventually neutralize with other atomic dopants.

¹⁰In decreasing order of effectiveness.

diimides. Dopants for n-type materials¹¹ are e.g. alkali metals, phenothiazines and also *semiconductors* with low ionisation potentials.

A different form of doping resulting in a truly increased concentration of mobile charge carriers on the semiconducting molecule and therefore considerably increased conductivity (in both the dark and under illumination) can be achieved by complexation with foreign molecules. Such doping molecules are preferably large (polymers) so that they cannot diffuse and penetrate into another material (e.g. in a p/n junction device) where they can possibly neutralize with another (different) dopant to form a salt. Examples are doping of PANI with camphor-sulfonic acid or PEDOT with polystyrene sulphonic acid [38, 6].

We note that compared to doped inorganic semiconductors, organic semiconductors can have very few mobile charges available - particularly in the dark - so that extra mobile charges due to illumination or doping can make a big difference. In fact, they can sometimes be described better using models for photo-conducting *insulators* [138].

More information on doping of molecular semiconductors can be found in Refs. [49, 43, 164, 225, 268, 38].

2.2.3 Structural Properties of Organic Semiconductors

We have seen that the optical and electronic properties of organic semiconductors can be tailored by attaching certain functionalities to the conjugated system. These properties are crucial for the operation of devices such as solar cells or LEDs - however, the “mechanical” i.e. *processing* properties are also very important.

For example the fabrication of devices via thermal sublimation requires high vacuum conditions and high temperatures whereas processing from solution can be done at room temperature at ambient pressure. In addition the fabrication of certain device architectures such as blends or laminated devices requires much more work or are not even feasible if thermal sublimation techniques have to be used. Moreover liquid crystalline systems were not accessible for investigation if only sublimation was available.

Fig.2.6 shows how organic semiconductors can be divided into different categories due to their processing and mechanical properties. We also

distinguish between molecules that have only a few (oligomers) or no (monomer) repeat unit and molecules (polymers) which have more than about 10 repeat units. Oligomers and monomers that absorb visible light are often called chromophores and are referred to as dyes if they are clearly soluble or pigments if they are not¹².

Liquid crystalline materials have only recently been investigated for the use in LEDs and organic solar cells [151, 199, 200]. For a certain temperature range these material exhibit a phase where the molecules move like in a liquid but are still able to sustain or attain a certain structural order among the molecules as in crystalline materials.

Such molecules have to have a strong asymmetry to show structural order and are therefore either rod-like (calamitic) or disc-like (discotic) molecules. We will discuss these interesting molecules in Chapter 7 in more detail.

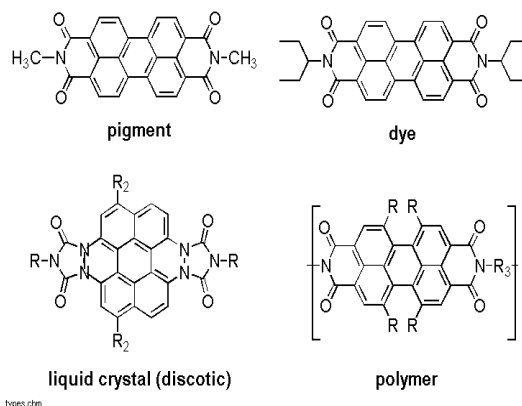
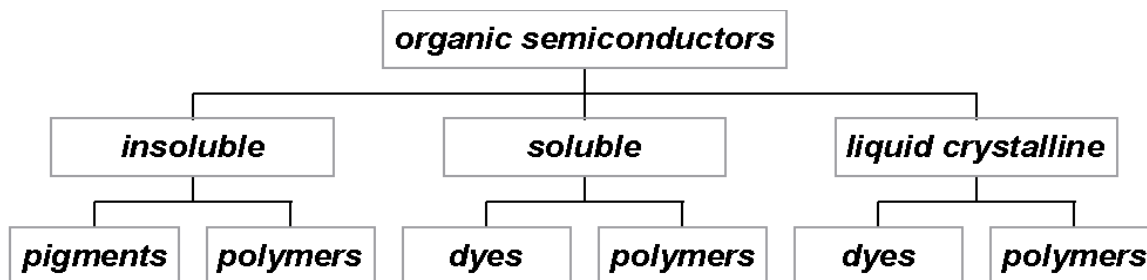


Figure 2.7: The “mechanical” properties of a flat structure like perylene diimides depend to a large extent on the position, number and properties of the side chains rather than the constituent atoms of the main structure. Common solubilising side chains (R, R_1, R_2) are often linear or branched alkyl or alkoxy groups. The synthesis of the perylene dye is reported in [60] while more information about the other shown molecules can be found in Ref. [217]

Fig.2.7 shows that the “mechanical” properties depend mainly on the position and number of side chains. Side chains are usually attached to molecules to introduce or improve solubility. They

¹¹Note that H_2 , NH_3 can be used to compensate radicals or impurities and thereby somewhat enhance the photocurrent.

¹²Note that the terms pigment and dye are sometimes regarded as synonyms among researchers who are not concerned about solubility properties. Recently, a method has been found to process many pigments like dyes using strong acids [283].



orgsem.ppt

Figure 2.6: Organic semiconductors may be divided into three different categories according to their mechanical i.e. processing properties: insoluble, soluble and liquid crystalline. They may be divided further into monomers (dyes, pigments) and polymers.

are more successful in solubilising the molecule the better they can prevent aggregation between molecules.

Flat molecules in particular have a strong tendency to stick together due to π - π interaction and form clusters of solids in many solvents. Bulky side chains can separate these molecules and make it easier for solvent molecules to surround the individual molecules i.e. dissolve them¹³. Typically, smaller molecules are better soluble and/or have lower sublimation temperatures but larger molecules give better films upon spincoating.

2.2.4 Photogeneration of Free Charges

Photogeneration due to Oxygen Traps

It is widely believed that oxygen can act as trap for electrons in the CB of organic materials and thereby lead to a higher number of free holes in the VB. In this sense oxygen can act as a dopant that favours p-type conductivity as discussed above. However, oxygen traps can also act as exciton dissociation sites and therefore generate free charge carriers in the presence of excitons. The proposed mechanism is the following: After a certain period, an electron in the oxygen trap may further decrease its energy by decaying to the VB where it recombines with either a free hole or the hole of an exciton. Thus 3 scenarios may be distinguished:

1. The electron stems from a not yet dissociated exciton and it recombines with a hole that

¹³In liquid crystalline materials solvent molecules are not even necessary since the cores of the molecules are "dissolved" in their own side chains.

comes from a different exciton. Both excitons are dissociated - but only two charges (the hole of the first exciton and the electron of the other) are produced since the other two recombined.

2. Only one recombination partner is associated with an exciton. This means its dissociation produces one free charge but still eliminates two.
3. None of the recombination partners belongs to an exciton. Two charges are lost, none is generated.

Note that both electrons and holes can be produced with the same probability according to the above list. In any case, the electron in the oxygen trap still reduces predominantly the mobility of negative charges thus sustaining its p-dopant character. We note that basically any defect that leads to an allowed free energy level between the middle of the bandgap and the CB may have the same effect as the here discussed oxygen trap - although other effects may become more important. For example, photo-oxidised PPV is believed to contain a good deal of carbonyl-groups which can facilitate exciton splitting but may also decrease both electron & hole as well as exciton transport properties [114, 215].

The Donor/Acceptor Interface

We have seen that photogeneration of charge due to traps is not very efficient since there is always the recombination of two charge carriers involved. Here we describe a more efficient way to generate free charge carriers - the formation of an electron donor

(D)/electron acceptor (A) interface. Although on a first glance, the concept may be reminiscent of the p/n junction in inorganic materials, the physical process are often very different.

Fig.2.8a) shows that the required transfer of charges can be realised at the interface between two materials if one material has a higher electron affinity (EA) whereas the other has a lower ionisation potential (IP). The one with the larger EA can accept an electron from the CB of the other and is therefore called electron acceptor. The material with the lower IP can accept the hole from the VB of the contacting semiconductor may therefore be termed hole acceptor or electron donor since it also donates the electron to the contacting acceptor.

We note that the offset of IP and EA needs to be large enough so that the resulting field (the potential gradient at the junction) can overcome the exciton binding energy which is typically around 0.4eV. Otherwise charge transfer may occur but the excitons do not split into their constituent charges and recombine eventually at the D/A interface¹⁴.

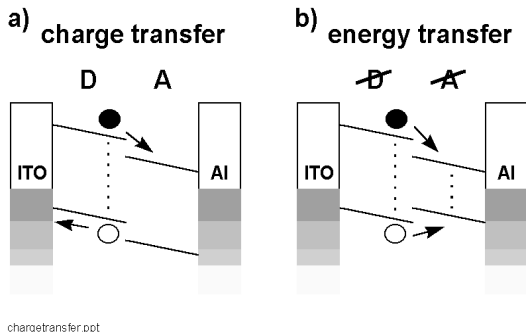


Figure 2.8: The interface between two different organic semiconductors can either: a) facilitate charge transfer (D/A interface), b) energy transfer (no exciton splitting). What kind of interface forms depends on the position of the HOMO and LUMO levels and the direction in which band bending occurs. The latter is determined by the relative position of the Fermi levels.

Fig.2.8 b) shows that an exciton that carries its excitation energy can be transferred from the material with the higher bandgap to the other if both the hole and the electron can decrease their energy thereby. This process of excitation energy transfer

which is accompanied with some energy loss is also known as Foerster transfer [72] and can be used to shift the emission band of the exciton towards lower energies in e.g. LEDs [246].

Foerster transfer also allows the design of a possibly helpful directionality in an organic solar cell since it is an one way mechanism, carrying excitons from the the shorter wavelength absorber to the longer wavelength absorber. This can be helpful to concentrate delivered excitons in a spatially small high field region [267] to enhance dissociation. We note that placing the higher bandgap absorber in front of the lower bandgap material to avoid thermalisation losses is proposed in Ref. [268].

Whether Foerster transfer or charge transfer occurs with a certain combination of organic semiconductor materials is often difficult to assess - particularly if one or both materials do not fluoresce. However, if they do, it is helpful to plot PL versus blend ratio. If the PL of both pure components decreases upon blending Foerster transfer can be ruled out - otherwise the PL of one component would enhance the other. Although, the exciton may still recombine at the D/A interface rather than split into its constituent charges there is a good chance for the latter.

Confirmation of exciton dissociation can be obtained by comparing the EQE of a blend solar cell with equivalent devices comprising only the pure components. If the EQE of the blend cell is clearly higher over the entire spectrum exciton splitting at the D/A interface is most likely. Extra confirmation may be obtained if the experimental and/or theoretical LUMO and HOMO data of the components also suggest a sufficient offset of the band edges to split the exciton. We note that the prediction of the offset of the band edges actually requires the knowledge of the accurate position of the Fermi levels - since those have to equalize upon contact.

The determination of Fermi levels in organic semiconductors can be done¹⁵ but there are very few data in literature [172]. For practical purposes Fermi-level are often assumed to lie around the middle of the semiconductor bandgap. HOMO and LUMO levels are often taken from cyclic-voltametry (CV) measurements where the current through the semiconductor gives a peak at the voltage where oxidation and reduction occurs [125, 126, 127]. The oxidation or reduction potential are then regarded as HOMO and LUMO levels.

We note that this method appears very useful if

¹⁴This is the situation that is desired for the design of light emitting diodes (LEDs) to favour radiative recombination at the interface between an electron and a hole transporting material[100].

¹⁵Using e.g. the Kelvin probe method described in Ref. [172].

all components can be measured at the same setup under comparable conditions. Otherwise care has to be taken if absolute numbers are compared, since the scan rate, and the assessment of the peak (it is not clear if the peak or the onset should be taken) can vary and affect the result considerably. CV values for films and solution may also differ.

Given that photo excitation results in the formation of excitons with a binding energy considerably higher than kT (26meV), photogeneration of charge is always assisted by an external factor such as the presence of traps, a D/A interface or a metal which can also act as an electron or hole acceptor or simply provide an electric field that can split the exciton. Thus photogeneration of charge in these organic semiconductors can be regarded as *extrinsic* as opposed to inorganic semiconductors where separation occurs mainly together with photo excitation.

2.2.5 D/A Materials

For the design of D/A solar cells it is important to know whether a specific material combination is likely to lead to charge transfer + exciton splitting. One way to find out is to build blend devices and look for PL quenching of both components and enhanced EQE with respect to the single components - as discussed above. Much effort, time and money can be saved if the chemical structure of the chosen molecules is considered. In the following we provide some background knowledge that allows guessing not only the D/A properties but also some other relevant properties for organic photovoltaic materials:

1. Donor/Acceptor properties. Since a donor can act as an acceptor for an even stronger donor - these two terms can not really be used separately. There are certain functionalities that are likely to make a material an electron acceptor with respect to most other materials. Examples for functionalities that favour electron acceptor properties are: CN, CF_3 , F , $=O$ (keto-groups) or diimides (all perylene derivatives in this thesis are perylene diimides). These groups are known as electron withdrawing groups if they are attached to an unsaturated (=conjugated) system.

Note that their ability to enhance the electron affinity (EA) of the entire molecule is not purely connected to the electron withdrawing properties of these functionalities. It is essentially a result of both the *inductive* and the

mesomeric effect.

While the inductive effect is determined by the electronegativity of the substituents, the mesomeric effect takes into account the influence of free electron pairs. The latter considers that many conjugated structures can equally be drawn with a different double/single bond i.e. π electron arrangement. The average of these possible π electron locations can be regarded as the overall mesomeric effect of a specific molecular structure. Examples for electron acceptors are CN-PPV, CF_3 substituted PPV and perylene diimides [167, 154]. Most organic semiconductors behave more like electron donors, for example PPV, PT, PPP and phthalocyanines.

2. Bandgap. As a rule of thumb, the bandgap is lower the larger the conjugated π -system is. Examples for large π -systems are phthalocyanines [117, 118, 119, 154], naphthalocyanines [171, 140, 37] and perylenes [154, 155, 267].

Sulfur in a conjugated systems also tends to reduce E_g . The bandgap can also be small if a molecule consists of a donor and an electron acceptor that are connected via a conjugated structure to create a “push/pull system” as in e.g. poly-methines. Such structures can accomplish charge transfer sometimes already in the ground state (e.g. charge transfer salt) or only little extra (light) energy is required to complete it. Examples for charge transfer salts are PVK-TNF [154] and for poly-methines: merocyanines [204, 173, 43].

3. Solubility. Solubility is good if the planar parts of the conjugated π -systems of the molecules cannot get too close to each other. Otherwise they would stick together, driven by their $\pi-\pi$ interaction, to form aggregates i.e. larger clusters i.e. particles which do not contain solvent. Flexible and bulky side chains or atoms that stick out of the molecular plane can prevent molecules from getting too close - see also discussion in Section 2.2.3.

The general rule is: Molecules dissolve in solvents with *similar* structure. *Polar* solvents like water, alcohol or iso propanol dissolve *polar* molecules while less polar solvents (e.g. toluene, xylene) dissolve non-polar molecules. As a rule of thumb, it can be said that a solvent containing other atoms than carbon and hydrogen has a good chance to be more polar - particularly if the structure is asymmetric.

4. Photoluminescence (PL). Practice shows that PL is quenched if the molecules can aggregate. Consequently, molecules in solution fluoresce much stronger.

Materials with higher bandgaps tend to show stronger PL¹⁶.

Moreover, the presence of impurities or structural defects usually leads to energy levels within the bandgap. The energetic decay of an excited electron can occur faster and therefore more efficiently if smaller energy jumps are required.

Also conjugated systems containing certain atoms like sulfur tend to give lower PL than conjugated structures containing only carbon and hydrogen.

2.2.6 Electrode/Semiconductor Interfaces

The theory of contacts between doped semiconductors and metals was developed in 1938 by Mott and Schottky [176, 225]. Since then charge injection from metallic contacts into semiconductors has been studied extensively and is explained in detail in the semiconductor literature [220, 241, 138, 205] to which we refer the interested reader.

However, it is not clear to what extent the developed models can be applied to organic semiconductors we only describe the basic concepts as they are often used to understand and predict the behaviour of organic semiconductor/ electrode interfaces.

In Fig.2.9 we have drawn the band energy diagram as it is expected for the situation before contact and after contact. It can be seen that - after contact - band bending occurs at *all* interfaces and that the Fermi levels and workfunctions equalize. The workfunction of the electrodes are drawn as equal here to show the situation in the short circuit mode.

The depicted band bending can be qualitatively predicted by assuming that the edges of the LUMOs and HOMOs are “pinned” to their absolute energy values as they were before contact. The bulk of the semiconductor sustains the same distance to the equalising Fermi-level.

Interestingly, both the electron affinity and ionisation potential of the semiconductors does not need to change - not even where band bending occurs - since the corresponding vacuum level follows both the band curvature and vertical shifts.

The *direction* the band bending occurs depends on whether the W_f of the electrode is *above* or *below* the Fermi-level of the semiconductor.

In case the workfunctions of both electrodes are deeper inside the bandgap than the Fermi-levels of the materials they are contacting, band bending occurs as depicted in Fig.2.9 b). Note that band bending at the D/A interface would be the other way round (blocking) if both Fermi-levels are assumed to be close to the middle. This may be the case and desired for LEDs [100].

Photoexcited electrons from the CB of the electron acceptor (A) encounter a barrier before they can reach the Al electrode. The same is true for holes from the VB near the ITO contact. These types of contacts are referred to as *blocking* contacts. Since these contacts can become non-blocking upon changing the potential of the electrode they are also called *rectifying* or Schottky contacts.

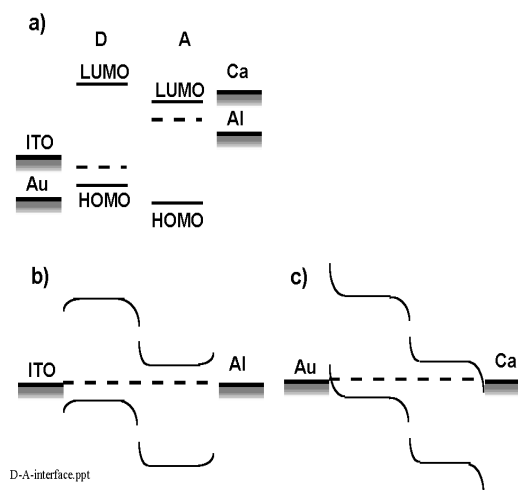


Figure 2.9: Energy band diagrams of D/A devices with the electrode interfaces. a) the situation before contact. After contact the Fermi levels (dashed lines) and W_f equalize and band bending occurs: b) the formation of a blocking contact for holes (ITO/D) and electrons (A/Al). c) the formation of a non-blocking (ohmic) contact for holes (Au/D) and electrons (A/Ca).

Note that Al forms a blocking contact only with the CB of the n-type semiconductor¹⁷ but an ohmic contact with the VB. The reason why this

¹⁶Systematic intentional interruption of the conjugation has been shown to increase the PL in PPV considerably []

¹⁷p type conductivity is assumed for D and n-type for A - see also discussion in Section 2.2.2

particular interface situation is called rectifying is because the n-type conductor is supposed to transport electrons in its CB - and for electrons it is blocking i.e. rectifying. The situation is analog for the semiconductor/ITO interface.

Since charge separation at the D/A interface leads to an excess of electrons in the CB of A (n-type) and holes in the VB of D (p-type), both charge carriers find barriers if they want to get out of the semiconductor. Thus currents through this device are decreased by the contact barriers.

Fig.2.9 illustrates that the situation is improved if Au and Ca are used as contact materials. The W_f of both electrodes is further away from the middle of the bandgap than the semiconductors Fermi-levels. Thus, after contact, band bending occurs the other way round so that electrons in the excited state can reach the Ca electrode and holes the Au electrode without encountering a barrier.

Practice confirms that organic devices using Au and Ca instead of ITO and Al show indeed considerably higher open circuit voltages and often also higher photocurrents and EQE values [114, 94]. However, because of the lower W_f of Ca compared to Al, Ca is more prone to oxidation than Al. Gold electrodes are expensive and have to be very thin to become transparent and are more difficult to pattern via etching. For the above reasons Al and ITO electrodes are actually more suitable for research devices since they can be reproduced easier.

Current Through Barriers

There are two principal mechanisms for the charge carriers to overcome barriers: Thermionic emission and quantum mechanical tunneling (field emission).

For thermionic emission over a triangular barrier of height Φ from a metal into a high-mobility semiconductor, the current density (J) is given by

$$J = A^* T^2 e^{-\frac{\Phi}{kT}} \quad (2.5)$$

where A^* is the effective Richardson constant and T the absolute temperature

If an electric field is applied across the barrier the barrier height decreases by

$$\Delta\Phi = \sqrt{\frac{q^3 E}{4\pi\epsilon_0}} \quad (2.6)$$

where E is the applied electric field, q the elementary charge and ϵ_0 the dielectric constant of vacuum.

In a semiconductor with a low mobility, it is necessary to take into account the diffusion of carriers within the barrier region back towards the contact. The analysis is complicated and depends on the type of barrier assumed. A full treatment is given by Kao and Hwang [138].

At sufficiently low temperatures, or for large barriers at high fields, emission due to quantum mechanical tunneling through the barrier (field emission), can become important. For a Schottky barrier the current is given by

$$J \propto \frac{\Phi_b + qV}{\Phi} e^{K \frac{\Phi^{3/2}}{(\Phi + qV)^{1/2}}} \quad (2.7)$$

where V is the applied voltage and K a material constant.

The essential characteristic of field emission is that the current is insensitive to temperature, but strongly dependent on the applied field (voltage). Since the tunneling rate depends also strongly on the width of the barrier¹⁸, thermal excitation can increase the tunneling current. For a Schottky barrier the current can then be written as

$$J = J_0 e^{qV/nkT} \quad (2.8)$$

where J_0 is essentially a constant for low doping levels and $n \approx 1$ at high temperatures [101].

2.3 Electrode Materials

In organic devices the workfunction of the electrode materials is very important since it determines together with the LUMO/HOMO and Fermi-level of the semiconductor whether the electrode forms an ohmic or a blocking contact for the respective charge carrier (holes in VB, electrons in CB). Moreover a large difference in workfunction of the electrode materials can increase the V_{oc} considerably.

In Table 2.1 we have listed the periodic table of the elements with its values of W_f - as far as it was known in Ref. [170]. The values in Table 2.1 are valid only for poly-crystalline materials. However, many numbers for single crystals which depend on its crystallographic orientation have also been reported in Ref. [170].

Common electrode materials for the electron collecting contact (low W_f required) of organic solar cells are Al, Ca, In, Ag whereas for the hole collecting contact *high* workfunction materials like Au are preferred. For both solar cells and LEDs one

¹⁸This is not considered in Eq. (2.7)

Table 2.1: Workfunction of the elements. The numbers refer to the workfunction in eV of the elements in poly-crystalline form..

IA	IIA	IIIB	IVB	VB	VIB	VIIIB	VIII			IB	IIB	IIIA	IVA	VA	VIA
Li	Be											B	C	N	O
2.9	4.98											4.45	5.0	-	-
Na	Mg											Al	Si	P	S
2.75	3.66											4.28	4.85	-	-
K	Ca	Sc	Ti	V	Cr	Mn	Fe	Co	Ni	Cu	Zn	Ga	Ge	As	Se
2.30	2.87	3.5	4.33	4.3	4.5	4.1	4.5	5.0	5.15	4.65	4.33	4.2	5.0	3.75	5.9
Rb	Sr	Y	Zr	Nb	Mo	Tc	Ru	Rh	Pd	Ag	Cd	In	Sn	Sb	Te
2.16	2.59	3.1	4.05	4.3	4.6	-	4.71	4.98	5.12	4.26	4.22	4.12	4.42	4.55	4.95
Cs	Ba	La	Hf	Ta	W	Re	Os	Ir	Pt	Au	Hg	Ti	Pb	Bi	Po
2.14	2.7	3.5	3.9	4.25	4.55	4.96	4.83	5.27	5.65	5.1	4.49	3.84	4.25	4.22	-
Fr	Ra	Ac	Th	Pa	U										
-	-	-	3.4	-	3.63										
			Ce	Pr	Nd	Pm	Sm	Eu	Gd	Tb	Dy	Ho	Er	Tm	Yb
			2.9	-	3.2	-	2.7	2.5	3.1	3.0	-	-	-	-	-

contact has to be at least partly transparent. Semi transparency can be obtained if the sublimed metal e.g. Au is not much thicker than about 15-20nm compared to about 50-100nm which are typical values for non transparent contact. We note that the sheet resistance of such a thin layer can be considerably increased compared to a 50 to 100nm thick layer and possibly add to the series resistor of the cell significantly. Also the optical properties change considerably in the thickness range from 10-20nm so that devices with slightly different thickness may not be immediately comparable. For these reasons so called conducting glasses are often used.

Particularly Indium Tin Oxide (ITO) which is a degenerated semiconductor comprising a mixture of In_2O_3 (90%) and SnO_2 (10%) with a bandgap of 3.7eV and a Fermi-level between 4.5 and 4.9eV is widely used. The large bandgap allows no absorption of wavelengths longer than about 350nm. The material can be highly conducting if there is excess of In due to a lack of oxygen - so that In acts as n-type dopant leading to very low sheet resistances for already only 100nm thick layers of ITO. ITO covered quartz substrates are commercially available since they are widely used as conducting glasses in the liquid crystal screen industry.

The sheet resistance of these ITO substrates is lower, the thicker the ITO layer is. Typical thickness of ITO in our devices is 100nm. Values smaller than 5 Ω / square are available. The transmission properties of the thicker ITO substrates do not change much since the material does not absorb in the visible but interference effects cause significant spectral dependence of the transmission. Very thick ITO layers (several 100nm - microns)

are problematic because of the increased absolute surface roughness¹⁹ which can cause shorts in the thin organic films.

We note that ITO itself can be used as anti-reflection layer [51] as active semiconductor [122]. The surface can be modified via plasma etching[271, 82] or the semiconducting molecules can even be chemically attached to it[178].

Other conducting glasses are Tin oxide and Indium oxide. Alternatively, conjugated polymers with absorption in the whole visible range can be used if they are doped so that the allowed energy levels move deep into the bandgap and create an absorption minimum in the visible region. Example for such polymers are PEDOT [193, 263, 55] and PITN [272, 222, 191]. An additional advantage of PEDOT is that it can be processed from (water) solution and therefore easily be spincoated.

Moreover, other water- insoluble materials may be spun on top of it²⁰. Some important soluble or transparent conductors are listed with their workfunction and references in Table 2.2.

¹⁹Considering the typical thickness of organic devices (30-150nm) the substrate surface should ideally be smooth on a nm scale.

²⁰Thicker layers of PEDOT can be obtained by repeated spincoating since it seems poorly soluble in water once the film is formed.

Table 2.2: Molecular electrode materials for organic solar cells. The abbreviations are listed in Chapter 1.

material	W_f (eV)	comment
PANI	5.2-5.3eV [33]	sol. polymer[38]
PEDOT		sol. polymer transp.[55, 39]
ITO	4.4-4.9[188, 144] ²¹	transp.
FTO	4.84eV [172]	transp.
TO	[273]	transp.

2.4 Photovoltaic Characterisation

2.4.1 Power Conversion Efficiency

In practice the photoexcited electron can decrease its potential energy by losing energy to phonons until it reaches the lowest lying level in the CB - the LUMO. Since the phonon energy dissipates into heat this process is known as thermalisation. As a consequence of thermalisation the semiconductor bandgap is often regarded as a measure for the achievable voltage. The higher the bandgap the higher the voltage can be.

On the other hand, a low bandgap material can absorb more photons and thus increase the number of photogenerated charge carriers i.e. the photocurrent. The lower the bandgap, the higher the photocurrent. Hence, there must be an optimal bandgap for a given illumination spectrum. Shockley and Queisser were the first who calculated the maximum power conversion efficiency for a semiconductor with a given bandgap assuming only radiative recombination and the solar radiation of earth. They obtained a value of 30% for a semiconductor with a bandgap of 1.12eV like Si. How the maximum conversion efficiency varies with the bandgap can be seen in Fig.2.10.

The semi empirical limits take into account realistic loss mechanism e.g. by assuming realistic values for the fillfactor. AM0 is the solar spectrum above earth's atmosphere while AM1.5 is the standard spectrum at sea level - see Chapter 8. The graphs show that for both the terrestrial and the space solar spectrum a semiconductor bandgap between 1.3 and 1.5eV allows reaching power conversion efficiencies around 30%.

Since a high load resistor reduces the current flux the charges need more time to get out of the semiconductor. This means that recombination can take

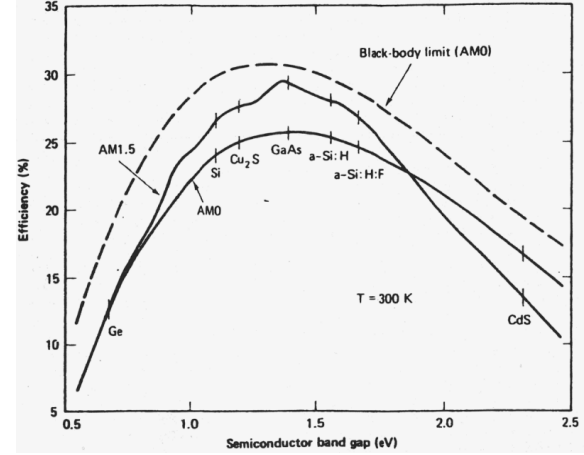


Figure 2.10: Power conversion efficiency limits as a function of the semiconductor bandgap. The solid lines are semi empirical limits assuming AM0 (=space) and AM1.5 (=terrestrial) solar radiation; the dashed line is based purely on thermodynamic considerations for blackbody solar cells under AM0 radiation. The graph shows that for both AM0 and AM1.5 condition a semiconductor bandgap between 1.3 and 1.5eV gives the highest power. Figure courtesy of Ref.[97].

place increasingly and the extracted external current decreases. This behaviour can be seen in the fourth Quadrant of the IV characteristic in Fig.2.11.

Thus considering the voltage dependence of the IV curve - the maximum power is the maximum product of I and V that can be found amongst the data points in the fourth quadrant. This maximum area is larger the more the IV curve resembles a rectangle with the area $V_{oc} \times I_{sc}$. The ratio between these two areas represents a measure of the quality of the shape of the IV characteristics:

$$FF \equiv \frac{(IV)_{\max}}{I_{sc} V_{oc}} \quad (2.9)$$

thus:

$$P_{\max} = (IV)_{\max} = V_{oc} \cdot I_{sc} \cdot FF \quad (2.10)$$

The higher FF the more the IV characteristics resembles a constant current source with a maximum voltage and the higher is the electric power that can be extracted. The voltage/current (V_p, I_p) combination that gives the largest power rectangle is called the maximum power point. Thus, any appliance connected to a solar cell can utilize

the maximum output power only if its supply voltage is around V_p or in other words: The load resistor $R_l = V_p/I_p$. Otherwise power would be wasted in heating the series resistor ($V < V_p$) or via increased current losses through the ideal diode and shunt resistor ($V > V_p$).

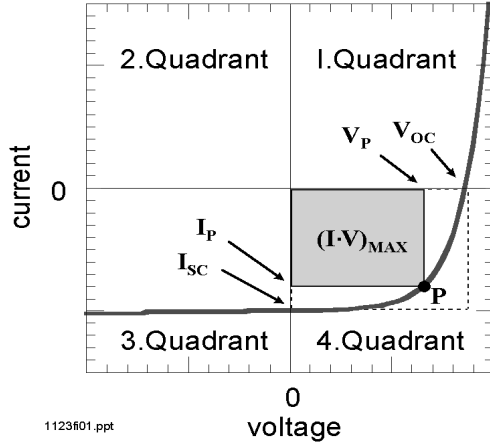


Figure 2.11: Current versus applied voltage of a solar cell. The extracted current is negative. The fourth quadrant represents the voltage and current that is generated by the cell. An externally applied voltage is necessary to obtain data points in the first and third quadrant.

In order to describe the power conversion efficiency η of a solar cell the maximum output power P_{max} has to be related to the power of the incident light P_{light} . Using Eq. (2.10) to express P_{max} considering the wavelength dependence of the parameters involved we can write:

$$\eta(\lambda) \equiv \frac{I_{sc}(\lambda) \cdot V_{oc}(\lambda) \cdot FF(\lambda)}{P_{light}} \quad (2.11)$$

Because of the wavelength and intensity dependence²² power conversion efficiencies are only meaningful for a given spectral distribution and intensity. This can be the solar spectrum or the spectrum of the artificial illumination for indoor applications (for e.g. pocket calculators).

In order to compare efficiencies of solar cells, solar radiation standards have been defined in the past. The most common standard at present is the AM1.5 spectrum which can be approached by commercial solar simulators. We note that, if international

²²the current usually scales linearly with the light intensity but V_{oc} also increases slightly. The latter is neglected in Eq. (2.11).

recognition of a solar power conversion efficiency number of a cell is desired, the cell should be measured by one of the internationally recognised institutions that offer solar cell efficiency measurements such as the National Renewable Energy Laboratories (NREL) in Golden (USA) or the Fraunhofer Institut for Solar Cell research in Freiburg (Germany).

In case its not feasible to send a cell to such an institute, it would still be very helpful to estimate the solar power efficiency of a solar cell rather than quoting monochromatic power efficiencies (or other) to allow at least rough comparisons among different research groups. We note that in Chapter 8 we describe how an inexpensive solar simulator can be built or - alternatively - η can be estimated from intensity dependence measurements of the spectral response.

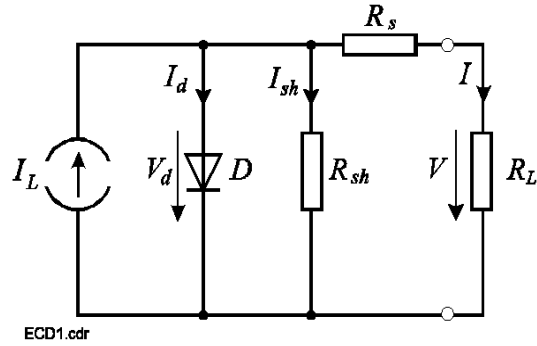


Figure 2.12: ECD of a solar cell. The circuit consists of the following ideal components: A current source I_L that considers the light-generated current, a diode that accounts for the nonlinear voltage dependence and a shunt as well as a series resistor. Also shown is a load resistor R and its voltage drop and current. The current arrows point into the direction the holes flow - according to the standard in electronics. The current I is negative if $V > V_{oc}$ and it flows “into” the device - otherwise it is positive.

2.4.2 The Equivalent Circuit Diagram (ECD)

ECDs are frequently used to describe the electric behaviour of more complex semiconductor devices with a network of ideal²³ electrical components such as diodes, current or voltage sources and resistors.

²³A real current source for example always has losses due to a shunt and series resistor.

Fig.2.12 shows the ECD that is typically used for inorganic solar cells. Although the specific physical processes in organic semiconductors may be different and therefore lead to other parameters, the principal loss mechanisms are the same and we may therefore apply the same circuit. We suggest to associate the following (more general) processes with the single components in the ECD:

- The current source generates current I_L upon illumination. I_L = number of dissociated excitons /s = number of free electron/hole pairs immediately after generation - before any recombination can take place.
- The shunt resistor R_{sh} is due to recombination of charge carriers near the dissociation site (e.g. D/A interface). Provided the series resistor R_s is at least one order of magnitude lower than R_{sh} , it may also include recombination further away from the dissociation site e.g. near the electrode. Otherwise an extra shunt resistor R_{sh2} has to be considered - see Fig.2.13. R_{sh} can be derived by taking the inverse slope around 0V:

$$R_{sh} \approx \left(\frac{I}{V}\right)^{-1} \quad (2.12)$$

This is because at very small voltages the diode D is not conducting and the current driven by the external voltage (positive or negative) is only determined by $R_{sh} + R_s$ with R_{sh} (typically) being much larger.

- The series resistor R_s considers conductivity i.e. mobility of the specific charge carrier in the respective transport medium. For example mobility of holes in a p-type conductor or electron donor material. The mobility can be affected by space charges and traps or other barriers (hopping). R_s is also increased with a longer traveling distance of the charges in e.g. thicker transport layers. R_s can be estimated from the (inverse) slope at a positive voltage $> V_{oc}$ where the IV curves becomes linear:

$$R_s \approx \left(\frac{I}{V}\right)^{-1} \quad (2.13)$$

This is because at high positive external voltages V the diode D becomes much more conducting than R_{sh} so that R_s can dominate the shape of the IV curve.

- ideal diode D = voltage dependent resistor that takes into account the asymmetry of conductivity due to the built in field in D/A cell (difference between the acceptor LUMO and the donor HOMO) or the nature of the semiconductor electrode interface (blocking contact) in single layer cells. This diode is responsible for the nonlinear shape of the IV curves. The diode characteristic is not necessarily Shockley type. Note that the IV characteristic of the ideal diode D is only equal to the IV characteristic of the entire cell (circuit) if $R_s = 0\Omega$ and $R_{sh} = \infty\Omega$.
- solar cell voltage V . The cell can generate a voltage between 0 and V_{oc} depending on the size of the load resistor. In order to obtain IV curve data in other voltage ranges ($V < 0$ and $V_{oc} < V$) in the IV curve an external voltage source is required. We note that also the voltage drop across a load resistor - the range between 0 and V_{oc} - can be simulated by the same voltage source so that the entire range can be scanned by applying an external voltage.

Note that the current for $V > V_{oc}$ and the extra current for $V < 0V$ is delivered from the external voltage source. The external voltage source can then act as a current amplifier to boost the photo sensitivity²⁴ but the actual photon to current conversion efficiency (EQE) of the solar cell or photodiode can not really be increased.

These are the components of a ECD with which we can associate the most important effects in solar cells of all types. However, a more comprehensive ECD for organic devices - see Fig.2.13 may comprise the following extra components:

- another diode D_2 . The formation of an extra blocking contact (e.g. for holes at the ITO electrode) can affect the IV curve in the third quadrant or even lead to FF values < 0.25 . We note that the normal blocking contact for electrons at ITO and holes at Al allows charge injection into the electrodes if a sufficiently high negative voltage is applied. This diode is always present and not considered in any of the ECDs drawn here.
- the capacitor C. The capacitor that takes into account charging/discharging and other time

²⁴Provided the current increases with applied voltage.

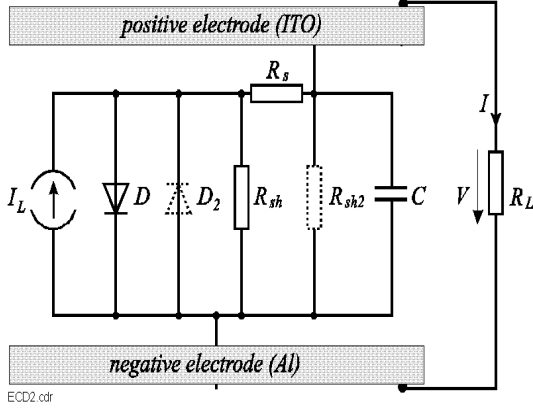


Figure 2.13: Extended ECD of a solar cell. The formation of a counter diode D_2 may sometimes need to be considered as well as another shunt R_{sh} that connects the two electrodes directly. The capacitor accounts for accumulation i.e. storage effects of charges and may be of particular interest for AC measurements i.e. photocurrent measurements with chopped light.

dependent effects that can be significant since the contact area A can be large and the distance between the electrodes d is very small: $C = \epsilon \frac{A}{d}$

- an extra shunt resistor R_{sh2} . It considers shorts due to pinholes or significant conductivity of the bulk material. It may also account for recombination losses near the electrodes. The effect of R_{sh2} is considered in R_{sh} if R_s is considerably smaller than any of the two shunts.

We note that current and resistor values depend on the illuminated area and need to be related to it if comparisons between cells with different illumination areas are desired²⁵. Note that the dark current depends on the actual device area - regardless of the size of the light spot.

Using the simple ECD in Fig.2.12 and Kirchoff's laws for current knots and voltage loops, we can formulate the following relation:

$$\overbrace{(I_L - I_d - I)}^{I_{sh}} R_{sh} = V + IR_s \quad (2.14)$$

which can be transformed into

²⁵Within this thesis the illuminated area was typically around 4mm^2 (only slightly smaller than the active area) which allows immediate comparison of the absolute values.

$$I\left(\frac{R_s}{R_{sh}} + 1\right) = I_L - I_d - \frac{V}{R_{sh}} \quad (2.15)$$

if we now assume that the Shockley diode equation describes the voltage dependence of the current I_d through the ideal diode D

$$I_d = I_0 \cdot \left(e^{\frac{V - IR_s}{nkT/q}} - 1\right) \quad (2.16)$$

and replace I_d in Eq. (2.15) we obtain

$$I = \left(I_L - \frac{V}{R_{sh}}\right) \frac{R_{sh}}{R_{sh} + R_s} - I_0 \frac{R_{sh}}{R_{sh} + R_s} \left(e^{\frac{V - IR_s}{nkT/q}} - 1\right) \quad (2.17)$$

If we now use

$$\frac{R_{sh} + R_s}{R_{sh}} = 1 + \frac{R_s}{R_{sh}} \quad (2.18)$$

we can write Eq. (2.17) as:

$$I = \frac{I_L - \frac{V}{R_{sh}}}{1 + \frac{R_s}{R_{sh}}} - \frac{I_0}{1 + \frac{R_s}{R_{sh}}} \cdot \left(e^{\frac{V - IR_s}{nkT/q}} - 1\right) \quad (2.19)$$

This equation will be used later when we discuss what can be learned from the specific shapes of IV characteristics. Even though the current I in Eq. (2.19) appears also in the exponent which requires numerical methods to find solutions, we can already see the following:

Inorganic solar cells have R_s values²⁶ between 0.3Ω and a few Ohms and R_{sh} larger than 1000Ω so that the ratio R_s/R_{sh} is very small and the term $1 + R_s/R_{sh}$ is virtually 1 and can therefore be neglected in Eq. (2.19). However, even in silicon solar cells the voltage drop across R_s represents an important loss factor and has to be considered as well as the loss current through the shunt. Note that both R_s and R_{sh} still appear in Eq. (2.19) even though $1 + R_s/R_{sh}$ can be neglected. However, the situation can be very different for organic cells.

Organic cells very often suffer from high series resistors and - in addition - relatively small R_{sh} values. As a consequence not only the losses due to both resistors are higher than in silicon cells but also the term $1 + R_s/R_{sh}$ can become significantly different from 1 and has to be considered in Eq. (2.19).

As a result, the *shape* of the IV curves and the absolute currents are more affected by these resistor values in organic than in inorganic cells.

²⁶Related to 1cm^2

2.4.3 Open Circuit Voltage

In the preceding Section we have deduced a formula that allows calculating the output current of a solar cell. In this Section we derive an expression for the open circuit voltage V_{oc} and consider the effects of the single components of the ECD. We will also discuss how PL efficiency can positively affect the solar cell performance and show how the upper limit for V_{oc} can be estimated.

The Ideal Solar Cell

First we consider the case of an ideal solar cell that comprises only the ideal ²⁷ diode D in the dark so that $R_s = 0$ and $R_{sh} = \infty$ in Eq. (2.19) turns into:

$$I_d = I_0(e^{qV/nkT} - 1) \quad (2.20)$$

The current through such a cells or photodiode is determined only by the current through the ideal D - here represented by the Shockley equation. For positive voltages I increases exponentially.

Upon illumination the light generates a photo current I_L that is simply superimposed (added) upon the normal rectifying IV characteristics of the diode D:

$$I = I_0(e^{qV/nkT} - 1) - I_L \quad (2.21)$$

The addition of I_L results in a region of the fourth quadrant where electrical current and voltage can be extracted from the solar cell. The highest voltage in this quadrant develops at the electrodes when I_L just manages to cancel the dark current. Thus, given a constant I_L the V_{oc} is higher the smaller the dark current is - note that I_0 determines the height of the characteristics. Canceling of I_d by means of I_L can be considered in Eq. (2.21) by setting $I = 0$. V_{oc} can than be derived quantitatively using:

$$V_{oc} = \frac{nkT}{q} \ln\left(\frac{I_L}{I_0} + 1\right) \quad (2.22)$$

Note that the effect of the I_L/I_0 ratio is relatively small. Reduction of I_0 by a factor 10x increases V_{oc} only by $25mV \cdot \ln(10)$ (58mV). Typical V_{oc} of silicon cells under solar conditions are around 550mV.

Effect of R_{sh}

A formula for V_{oc} that considers the influence of R_{sh} can be deduced from Eq. (2.19) after setting

²⁷We keep the ideality factor in this equation to consider different shapes. However, the diode D is still ideal in the sense that there are no Ohmic losses.

the output current to zero ($I \equiv 0$) to give²⁸:

$$V_{oc} = \frac{nkT}{q} \ln\left(\frac{I_L - V_{oc}/R_{sh}}{I_0} + 1\right) \quad (2.23)$$

This equation relates the maximum output voltage not only to the light generated current I_L but also to the reverse saturation current and the shunt resistor. Now, also the formula for V_{oc} becomes transcendent and requires numerical modeling to find solution. The value for V_{oc} still depends on the ratio I_L/I_0 but now I_L is decreased by the presence of a finite R_{sh} whereas R_s is unimportant since there is no current flowing through it that can create a voltage drop (loss).

Both the ideal diode D and R_{sh} are now the components that determine V_{oc} : Suppose R_{sh} is not very high and the device is in the dark. If we apply a positive voltage across the cell electrodes we create a voltage drop across R_{sh} that is equal to the voltage V_d across the ideal diode D. The current that can pass through the diode D at V_d is determined by its IV characteristic²⁹. The sum of the currents through D and R_{sh} yields the current through the electrodes of the solar cell for a given applied voltage.

Upon illumination, the current source generates the current I_L some of which passes through the diode where a voltage drop is generated that is big enough to allow the rest of I_L to go through R_{sh} - if the electrodes are open. The same voltage can be measured with a voltmeter with high internal resistor across the device electrodes and is then termed open circuit voltage V_{oc} .

Note that n which determines the shape of the IV curve stands outside the logarithm in Eq. (2.23) and has therefore a stronger influence than a variation of R_{sh} or I_0 . The latter controls the "height" of the IV curve of D. However, since R_{sh} can vary considerably it can seriously decrease V_{oc} if V_{oc}/R_{sh} is not much smaller than I_L . We note that I_0 can be related to PL efficiency as discussed later in this thesis.

Effect of Shorts

Organic solar cells have often values for series resistance which are more than 3 orders of magnitude

²⁸There is no influence of R_s since R_s can only affect the voltage when there is a current flowing through it.

²⁹Note that the IV characteristics of the diode D is not the IV curve one obtains when measuring the entire device (with R_{sh} and R_s)! For inorganic solar cells it is assumed to be the Schottky diode characteristics - while for organic cells it depends on many material and device parameters.

larger. This means that currents measured in short circuit mode still have to get through a large resistor which can seriously limit the output current particularly if also R_{sh} is low. Moreover, since a short across the electrodes represented by R_{sh2} in Fig.2.13 represents a voltage divider in conjunction with R_s according to Eq. (2.24) R_s can actually reduce V_{oc} if R_s reaches values in the order of R_{sh2} . Thus "shorts" do not need to have very low resistances to smaller V_{oc} considerably - they just need to approach the value of R_s which can be as big as $10^7\Omega$ in some small area organic devices!

$$V_{ocs} = V_{oc} \cdot \frac{R_{sh2}}{R_s + R_{sh2}} \quad (2.24)$$

This also makes voltage measurements across the device electrodes more critical. Voltmeters need to have internal resistors larger than $10^7\Omega$ to exclude effects on the circuit that lead to lower readings.

Analogously, recombination that takes place near the electrodes - represented by R_{sh} may be more effective in decreasing V_{oc} than recombination in the middle of the device if R_s is so high.

The Effect of Photoluminescence

Any type of recombination³⁰ represents a less mechanism for the photoexcited charge carriers in a solar cell. However, non-radiative recombination affects the photoexcited charge carriers statistically much faster than the unavoidable radiative decay that does not require any semiconductor defects. Hence, if there is only radiative recombination the charge carriers have much better chances to reach the electrodes and circumvent the radiative decay by entering an external circuit.

If there is no external circuit (open circuit mode) the charges accumulate at the electrodes to build up V_{oc} before they decay showing their maximum PL efficiency. Indeed, it has been shown that the PL of e.g. chlorophyll is about 3% in a living plant, and 30% if the chlorophyll molecules are separated from the rest of the electron transport chain, which corresponds to operation under load and open circuit mode, respectively [208, 234].

In other words, a highly fluorescent material can have relatively low charge carrier mobilities and still generate a high V_{oc} and good photocurrents. According to Ref. [234] radiative recombination Φ_{PL} can be considered as a correction factor for the reverse saturation current I_0 in the diode characteristics

$$I_d = \frac{\overbrace{I_{01}}^{I_0}}{\Phi_{PL}} \cdot (e^{\frac{V}{nkT/q}} - 1) \quad (2.25)$$

Note that the Shottky equation remains unchanged if the photoluminescence efficiency $\Phi_{PL} = 1$ i.e. 100%. Within this thesis we call I_{01} the PL independent reverse saturation current. Thus the expression Eq. (2.23) to derive V_{oc} can be written as

$$V_{oc} = \frac{nkT}{q} \ln\left(\frac{I_L - V_{oc}/R_{sh}}{I_{01}/\Phi_{PL}} + 1\right) \quad (2.26)$$

The reverse saturation current $I_0 = I_{01}/\Phi_{PL}$ can be obtained experimentally by modeling of the IV curve and gives indeed about 10^3 larger values for e.g. silicon cells ($\Phi_{PL} \approx 10^{-4}$) than for cells using organic semiconductors ($\Phi_{PL} \approx 10^{-2}$). Indeed the more fluorescent porous silicon has been reported to show lower I_0 values being consistent within Eq. (2.25). The higher PL (10^{-1}) in GaAs predicts V_{oc} values of 1V under 1 sun which is also in good agreement with the observations [234].

We note that non-radiative recombination losses affect both I_0 and the shunt resistor R_{sh} . For very fluorescent materials the I_0 is small and R_{sh} should be high.

In fact, polymers and dyes with higher PL yield appear to give high V_{oc} values like PPV (1.2V), MEH-PPV (1.3V) in contrast to poorly fluorescent materials like PIF ($V_{oc} < 0.02V$) and HPc ($V_{oc} < 0.2V$). So called non-fluorescent materials may, however, still give reasonable voltages as long as their optical and charge transport properties are very good and the PL is not too low. For example, the low PL of e.g. Si (10^{-3} to 10^{-4}) is still high enough to result in a I_L/I_0 allowing V_{oc} to reach 0.6V [234]. Similar considerations hold for the very good photovoltaic performance of certain organic material with relatively low PL efficiencies.

The Upper Limit of V_{oc}

In the previous Section we have discussed how R_s , R_{sh} and in particular I_0 can affect the value for V_{oc} . In this Section we discuss whether there is an upper limit for V_{oc} and what might determine it.

We have seen that according to Eq. (2.26) the voltage is higher the lower I_0 and the higher I_L is.

In virtually all inorganic cells and many organic ones I_L scales linearly with the light intensity over many orders of magnitude. Possible upper limits with regard to excitation intensity may only be

³⁰Before passing through the external circuit.

reached if the charge carrier density approaches critical values which would typically only occur at unrealistic high excitation intensities.

What determines in practice the absolute value of I_0 in *inorganic* devices has been reported: majority charge carrier and dopant concentration, charge carrier diffusion lengths and recombination velocities [97].

Here we focus on a more general approach to find the V_{oc} upper limit so that it may be applicable to the organic solar cell structures described in this thesis.

Ideally the potential difference between the ground state and the excited state of an electron after photo-excitation can be regarded as a driving force i.e. maximum voltage. Thus the maximum photo-voltage that a semiconductor can develop should increase linearly with the excitation energy. In other words, a 2eV photon should be able to supply a voltage of 2V.

In practice, in both organic and inorganic semiconductors photoexcited electrons can decrease their potential energy very quickly using the high density of allowed states in the CB until they reach the lowest unoccupied molecular orbital (LUMO). Since the lost potential energy is usually converted into phonons i.e. heat this process is called thermalisation. As a consequence the difference between the HOMO and LUMO levels (the bandgap) can be seen as a theoretical upper limit for V_{oc} . Practice confirms that indeed inorganic solar cells made of higher bandgap materials develop higher V_{oc} and the maximum achieved V_{oc} has never exceeded the width of the bandgap.

For organic solar cells, we also find higher V_{oc} for higher bandgap materials. As discussed earlier a high V_{oc} may be favored by a lower reverse saturation current I_0 due to the frequently low non-radiative recombination in these more fluorescent materials. However, it has been observed for many organic solar cells that a higher workfunction difference of the electrodes ΔW_f can also increase V_{oc} . This is often explained by assuming that ΔW_f introduces a “built in field” across the thin semiconducting layer that helps to extract the photoexcited charge carriers.

Qualitatively, as it can be seen from Fig.2.4, a larger ΔW_f results in either a stronger tilting of the semiconductor band for voltages $< V_{oc}$ or a stronger bend bending near the electrode semiconductor interface if there are enough charges to cancel the field³¹ within a fraction of the bulk thickness. Thus,

³¹A gradient of a potential in space can be treated as a

low W_f for the negative and high W_f for the positive hole collecting electrode often helps to increase V_{oc} . The drawback is that the use of low W_f materials such as Ca often requires the sublimation of a protection layer on top because of the increased tendency to form an oxide layer when exposed to air that represents an extra obstacle for charge carrier extraction.

On the other hand *shorts* may be avoided more efficiently which also helps to develop higher voltages at the electrodes. We note that in single layer devices $\Delta W_f > E_g$ is not expected to increase V_{oc} above E_g since charge injection from the LUMO and HOMO into the electrodes is limited.

In D/A cells³², however, $\Delta W_f > E_g$ may result in V_{oc} larger than the “combined bandgap” E_{gDA} since the internal field at the D/A interface can assist the extraction of the charges through the “high” lying electrode workfunction. V_{oc} larger than E_g has been observed in a laminated device as discussed in Chapter 6.

As a result of these considerations the upper limit for V_{oc} in *single* layer devices is expected to be the bandgap whereas in D/A cells ΔW_f of the electrodes or the bandgap - whichever is higher - determines the maximum photogenerated voltage.

In case of $\Delta W_f > E_{gDA}$ the built in field due to the offset of LUMOs ($\Delta LUMO$) and HOMOs ($\Delta HOMO$) between the two components has to be large enough to provide the extra driving force. Hence, the maximum V_{oc} can be written as:

$$V_{oc} \leq |LUMO_A - HOMO_D| + \Delta LUMO + \Delta HOMO \quad (2.27)$$

if only positive numbers are used.

Note that $\Delta LUMO + \Delta HOMO$ has to be greater than the exciton binding energy to split the excitons in D/A devices.

The above formula can be written as

$$V_{oc} \leq E_{gD} + E_{gA} - |LUMO_A - HOMO_D| \quad (2.28)$$

Thus, it can be expected that the bandgaps of the semiconducting components determine the (theoretical) upper limit of D/A cells provided the ΔW_f is large enough.

We note that the consideration of the unavoidable radiative recombination losses already reduces the upper limit for V_{oc} in Si from the bandgap value (1.1V) to about 0.8V [234].

field.

³²In case of D/A devices the voltage relevant bandgap is the difference between the LUMO of A and the HOMO of D.

Summary

According to the described model a high V_{oc} at a given light intensity is expected if:

1. I_0 is low. The reverse saturation current is often low if the PL efficiency is high, the bandgap is high and the conductivity is low.
2. The shape of the IV curve is not too steep. The dark current can then only be canceled by the photocurrent at higher (V_{oc}) voltages.
3. R_{sh} is clearly larger than the DC resistor value of the ideal diode D.

Note that not all requirements to obtain a high V_{oc} coincide with the requirements to obtain a high short circuit current. For example, a large I_{sc} is favored if the bandgap is small and the conductivity is high. However, both V_{oc} and I_{sc} are high if R_s is small and R_{sh} is high.

2.4.4 Photocurrent

The Short Circuit Current I_{sc}

The current I_{sc} under short circuit condition ($R_L = 0$ - see Fig.2.13) can be derived from Eq. (2.19) by setting $V \equiv 0$. If we also consider the influence of the PL as discussed above we can write:

$$I_{sc} = \frac{\overbrace{I_L - I_{sh}}^{I_L - I_{sh}}}{1 + \frac{R_s}{R_{sh}}} - \frac{\overbrace{I_0 / \Phi_{PL}}^{I_d} (e^{\frac{1R_s}{n k T / q}} - 1)}{1 + \frac{R_s}{R_{sh}}} \quad (2.29)$$

From the ECD in Fig.2.12 can be seen that the short circuit current is simply the light current I_L (photogenerated charge carriers/s i.e. number of split excitons/s) reduced by the current through the shunt I_{sh} and the diode D, I_d :

$$I_{sc} = I_L - I_{sh} - I_d \quad (2.30)$$

This is the highest current that can be extracted from a solar cell³³. The light current increases linearly with the illumination intensity. In order to extract a quantity that describes how efficiently photons are converted into charges in the external circuit, I_{sc} has to be related to light intensity. This leads to the definition of the spectral response:

³³Even if an external voltage is applied, only the photo-sensitivity can be amplified - any current higher than I_{sc} current originates in the external voltage source.

$$SR(\lambda) = \frac{J_{sc}(\lambda)}{\Phi(\lambda)} \quad (2.31)$$

with Φ being the light intensity per illuminated area³⁴ (W/m^2) and J_{sc} representing the current density (A/m^2) in short circuit mode.

The spectral response (SR) thus gives the current in the external circuit per watt incident light (A/W). This quantity is frequently used to characterise the light sensitivity of *photodiodes* since the product $SR \cdot J_{sc}$ gives immediately the light intensity³⁵.

For the characterisation of *solar cells* a quantity that considers the actual fraction of the incident photons that can be converted into electrons in an external circuit is of higher interest:

$$EQE \equiv \frac{\text{number of electrons in external circuit}}{\text{number of incident photons}} \quad (2.32)$$

EQE stands for external quantum efficiency and represents, together with the power conversion efficiency η , the most interesting parameter of a solar cell. The EQE can be derived from the spectral response considering that the energy of a photon $E_p = hc/\lambda$ with h being Planck's constant, c the speed of light and q the elementary charge using the following formula³⁶:

$$EQE(\lambda) = SR(\lambda) \cdot \frac{hc}{q\lambda} \quad (2.33)$$

Note that the EQE gives higher values for shorter wavelengths when compared with the SR spectrum. This is because the spectral response relates to the energy of photons whereas the EQE refers only to the *number* of particles. Since the output current is determined by the number of electrons that can be "pumped" into the CB regardless of their energy, the EQE represents a true measure for the photon to current conversion efficiency in contrast to SR.

The EQE can be converted into the internal quantum efficiency IQE if only the fraction of the actually absorbed photons are considered:

$$IQE(\lambda) = \frac{EQE(\lambda)}{1 - R(\lambda) - T(\lambda)} \quad (2.34)$$

with $R(\lambda)$ denoting the fraction of reflected light and $T(\lambda)$ the fraction of the transmitted light.

³⁴The hardly used but accurate term is: irradiance.

³⁵Light intensity measurements are an important application for photodiodes.

³⁶Note that $hc/q = 1240 WnmA^{-1}$.

The IQE is very helpful and frequently used in inorganic devices to investigate the physical processes in the semiconductor material. In contrast to inorganic solar cells where the complete bulk absorbs light and contributes to the photocurrent, organic devices have typically large regions that act only as optical filter.

In addition, interference effects would have to be considered because of the very thin films compared to inorganic cells. This makes the interpretation of IQE spectra in organic cells only more speculative rather than simpler and therefore generally less useful at the present time. The EQE is therefore the preferred quantity in the devices discussed in this thesis.

The Optical Filter Effect

The region in the semiconductor that allows photoexcited excitons to dissociate and the separated charges to reach their respective electrodes is often called the "active region" - see Fig.2.14. Thus, only light absorbed in the active region can contribute to the photocurrent. The layer that absorbs light before it reaches the active region³⁷ is the actual optical filter.

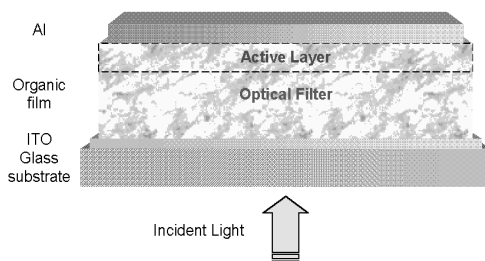


Figure 2.14: In organic devices very often only a thin layer (active layer) near back electrode is electronically active (contributes to the photocurrent). Depending on the thickness and absorption coefficient a significant fraction of photons can be absorbed in the semiconductor bulk (optical filter) *before* this region is reached. Figure from [63].

Fig.2.15 shows two scenarios for the formation of an active region smaller than the bulk which can lead to an optical filter effect:

³⁷Electrode/polymer interfaces often act as dissociation site but also polymer/polymer interfaces or impurities (dopants, oxygen molecules) can act as such - see also Section 2.2.2.

1. Exciton dissociation throughout the entire bulk but small mobility of one charge carrier. Often the mobility of the hole is considerably higher than the mobility of the electron. Thus, free electrons have to be generated close to the negative electrode for charge collection.

Even if the excitons have large diffusion lengths, a considerable fraction of the photogenerated excitons would dissociate too far away from the negative electrode. Thus the width of the active layer is determined by the distance electrons can travel L_e in the specific material i.e. the electron mobility - see Fig.2.15 a).

2. Exciton dissociation occurs only near one electrode interface. If exciton splitting occurs due to a strong local field (band bending), excitons that are generated outside the band bending area have to diffuse into this region to supply charges. Although small hole and electron mobilities can still become limiting factors it is usually the exciton diffusion length that determines the width of the active layer in this case - see Fig.2.15 b).

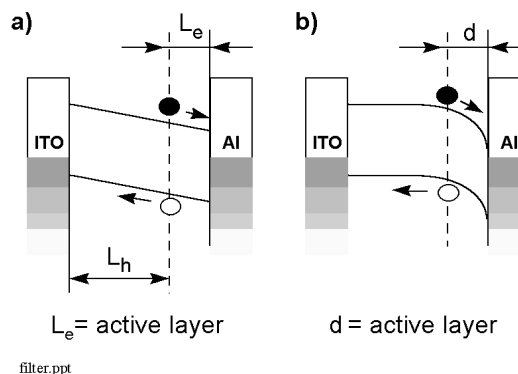


Figure 2.15: Two scenarios that can lead to the formation of an optical filter: a) exciton dissociation occurs throughout the entire bulk but one charge carrier (here the electron) can only travel a very short distance before it recombines. b) exciton dissociation occurs only near the (here negative, Al) electrode due to a local high field. Thus a small exciton diffusion length determines the width of the active layer - provided the charge carrier traveling distance is sufficiently high.

Only if the active region extends across the entire bulk i.e. the bulk is thin enough, most of the disso-

ciated excitons can generate a photocurrent so that the EQE essentially follows the absorption features.

Due to short exciton diffusion lengths most organic cells have a bulk thickness that is considerably larger than the active layer (to avoid shorts). Thus these EQE spectra show a strong filter effect resulting in EQE maxima at wavelengths where the optical density is low and EQE minima where the OD is too high to allow many photons to reach the active region.

Such a spectrum is termed antibatic spectrum in contrast to the symbatic spectrum that shows no offset between absorption and EQE features [120]. Note that a symbatic spectrum can be obtained if the device is illuminated through the other contact - if it is sufficiently transparent.

In Section 3.2 we describe a method to estimate how thick a semiconducting layer can be before it shows the conversion losses due to the optical filter effect.

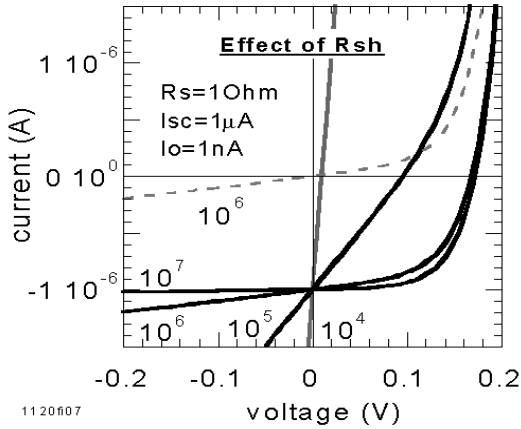


Figure 2.16: Effect of R_{sh} (ranging from 10^4 to $10^7 \Omega$) on the shape of the IV characteristic. A large R_{sh} can reduce both the fillfactor and V_{oc} but *not* I_{sc} . The dashed curve is the dark characteristic at $10^6 \Omega$

2.4.5 Interpretation of IV Characteristics

Inorganic Solar Cells

The higher charge carrier mobility in inorganic semiconductors leads to sufficiently long diffusion lengths which allow most charge carriers to reach

the electrodes before they undergo intense recombination - even though the devices are about 1000 times thicker. In addition R_{sh} is typically more than 3 orders of magnitude larger than R_s . This not only leads to a negligible term $1 + \frac{R_s}{R_{sh}}$ in Eq. (2.19) and Eq. (2.29) but also makes it much easier to distinguish the effects of the two resistors in the IV characteristics.

In addition the reverse saturation current I_0 is typically larger than in organic devices - probably due to the higher PL efficiency in the latter - as discussed in Section 2.4.3. The values for R_{sh} and R_s have been estimated from the IV curve data as described in Section 2.4.2.

Fig.2.16 shows how the IV characteristic changes if the shunt resistor varies between 10^4 and $10^7 \Omega$ assuming the shown³⁸ values for R_s, I_L, I_0 . If $R_{sh} > 10^6 \Omega$ the shape (FF, V_{oc}) of the IV curves remains virtually unchanged and the current shows no significant field dependence for negative bias.

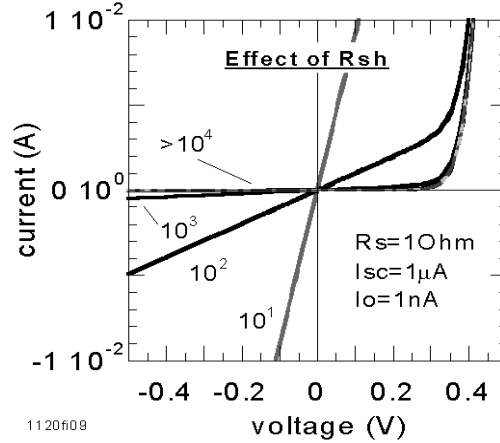


Figure 2.17: Effect of R_{sh} (ranging from 10^1 to $10^4 \Omega$) on the shape of the IV characteristics. V_{oc} is virtually zero and R_{sh} extends its “linearisation effect” into the first quadrant. The photocurrent ($I_{sc} - I_0$) is too small to be visible on this scale.

However, clearly smaller R_{sh} values have enormous bad effects on the IV curve. The slope (field dependence) in the third quadrant increases considerably, V_{oc} approaches zero and the fillfactor reaches its theoretical minimum of 0.25 (Ohmic - linear)³⁹

³⁸The currents given in this Section are related to an area of 1 mm^2 - which is sufficiently close to our experimental conditions ($A \approx 4 \text{ mm}^2$) to get a “feel” for the absolute numbers.

³⁹Lower values than the one for ohmic behaviour may be

very quickly. However, the short circuit current is not affected since the current through the shunt can be neglected if $R_s \ll R_{sh}$.

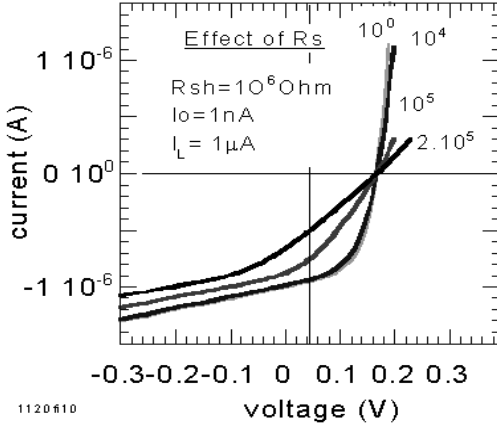


Figure 2.18: Effect of R_s on the shape of the IV characteristics assuming the same values for an inorganic solar cell as above with $R_{sh} = 10^6 \Omega$. R_s reduces FF and the slope in the first quadrant when it reaches the same order of magnitude as R_{sh} . R_s can reduce the short circuit current but not V_{oc} . The slope in the third quadrant is still dominated by R_{sh} .

Note that the reverse slope around 0V or in the third quadrant is equal to the value of R_{sh} . This can easily be seen from the ECD - Fig.2.12. Under reverse bias the diode D is blocking and $R = R_{sh} + R_s$ only determine the voltage dependence of the current ($I = R^{-1}U$). Since R_s is much smaller than R_{sh} it is only R_{sh} that determines the slope R^{-1} .

Fig.2.17 shows how even smaller R_{sh} values affect the IV curve. The slope in the third quadrant increases even further and the “linearisation effect” of R_{sh} extends to about 0.3 V in the first quadrant. Note that V_{oc} is virtually zero. Note that the values for $R_{sh} > 10^4 \Omega$ that have been shown in Fig.2.16 do look exactly the same on this scale.

Fig.2.18 shows what happens if the series resistor increases assuming the same parameters as above and $R_{sh} = 10^6 \Omega$: While the slope in the third quadrant remains unchanged the slope in the first quadrant starts to decrease considerably when R_s reaches the same order of magnitude as R_{sh} . The effect of the large R_s even extends into the 3 quadrant

obtained if another diode (with reverse orientation) is formed (=counterdiode).

thereby decreasing the fillfactor to its minimum.

Moreover, if the two resistors have similar values the IV curve is dominated by their ohmic characteristics (the inverse slope in the 1 quadrant is equal to R_s) and the ideality factor or voltage dependence of D may then have little influence. Note that - in contrast to the effect of R_{sh} - the short circuit current can decrease but the open circuit voltage can not be affected at all - since there is no current through R_s at V_{oc} .

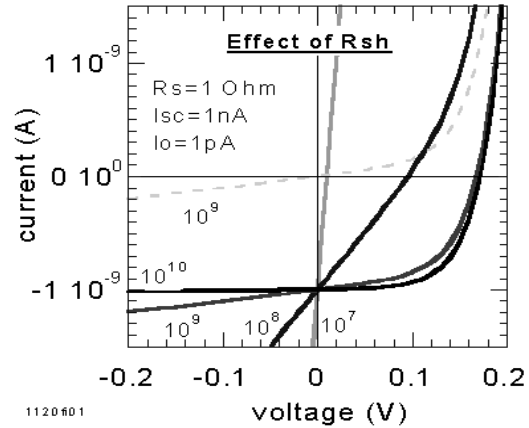


Figure 2.19: Effect of R_{sh} (ranging from 10^7 to $10^{10} \Omega$) on the shape of the IV characteristics assuming typical dark and light currents for an *organic* solar cell. The effect of R_{sh} is qualitatively the same as for the inorganic device in Fig.2.16 but 1000 times larger resistor values are required to give the same shape.

Organic Solar Cells

Lower mobilities and smaller charge carrier concentration lead to considerably smaller currents in most organic solar cells. In fact, both the dark⁴⁰ and light currents are about 1000 times smaller ($I_0 \approx 1 \text{ pA}$ and $I_{sc} \approx 1 \text{ nA}$) so that the light current in these devices is about as big as the dark current in silicon devices while the dark current is still about 1000 times smaller so that according to Eq. (2.22) a similar V_{oc} is expected.

We note that the dark current may be related to the fraction of radiative recombination so that high PL-efficiency - as observed in many organic semiconductors - is expected to give a low dark current.

⁴⁰The dark current I_d scales with I_0

This is discussed in more detail in the Section about V_{oc} (Section 2.4.3).

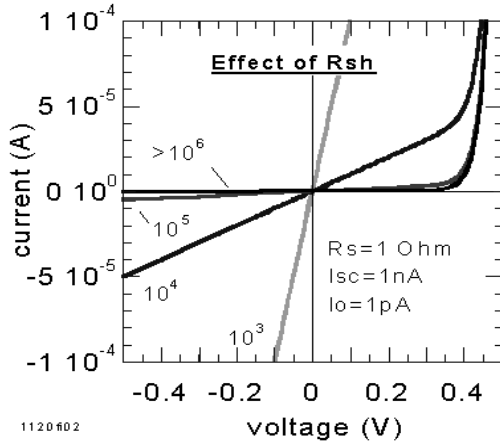


Figure 2.20: Effect of R_{sh} (ranging from 10^3 to $10^6 \Omega$) on the shape of the IV characteristics assuming typical dark and light currents for an *organic* solar cell. The effect of R_{sh} is qualitatively the same as for the inorganic device in Fig.2.17 but 1000 times larger resistor values are required to give the same shape.

Fig.2.19 shows the effect of a decreasing R_{sh} on the IV curve using current values typical for organic solar cells. In order to show the influence of *only* R_{sh} we assumed an unrealistic low value (1Ω) for R_s .

Even lower values for R_{sh} are considered in Fig.2.20. Note that the IV curve for values larger than $10^6 \Omega$ - like e.g. all curves shown in Fig.2.19 - look exactly the same on this scale.

Both figures show qualitatively the same effect of a decreasing R_{sh} : a steeper slope in the third quadrant and eventually reduction of V_{oc} . However, although the I_{sc}/I_d ratio is exactly the same the R_{sh} value has to be 1000 times higher to cause the same effect. For example, an R_{sh} as low as $10^5 \Omega$ in the *inorganic* cell (Fig.2.16) is necessary to decrease V_{oc} by 50% whereas a value of $10^8 \Omega$ can show the same effect in the *organic* device (Fig.2.19).

Fig.2.21 shows the effect of R_s with currents typical for organic cells and assuming $R_{sh} = 10^9 \Omega$. Again, we observe the same effects as in for the inorganic device upon increasing: decrease of the slope in the first quadrant and reduction of I_{sc} . However, the output current is 1000 times smaller and the resistor value 1000 times higher - compare with

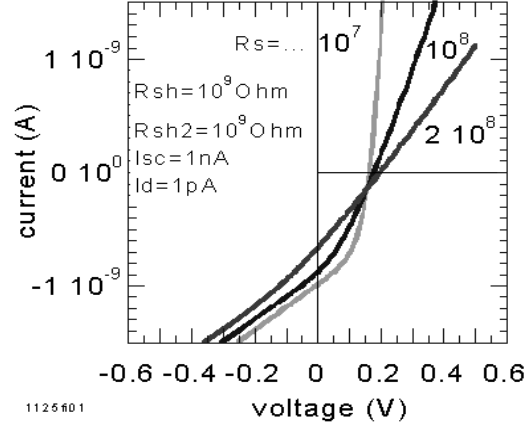


Figure 2.21: Effect of R_s on the shape of the IV characteristics assuming the same values for an *organic* solar cell as above with $R_{sh} = 10^9 \Omega$. R_s decreases FF and the slope in the first quadrant if it reaches the same order of magnitude as R_{sh} . R_s can decrease the short circuit current but not V_{oc} . The slope in the third quadrant is still dominated by R_{sh} .

Fig.2.18.

Fig.2.22 shows that - apart from high R_s and/or R_{sh} values - a low light current can cause both a low FF and a low V_{oc} . Thus, IV curves should only be compared if light intensities are similar and FF and V_{oc} values (mW/cm^2) should be quoted together with light intensity numbers.

In fact, IV curves of inorganic solar cells are usually measured under standard (AM1.5) conditions to allow direct comparisons. The problem with many organic solar cells is that they may not be stable enough under such high light intensities and that depending on the material, device type and measurement condition, IV curves - particularly of very inefficient devices - can vary significantly from pixel to pixel or even over time⁴¹.

As a guideline it may be said that the light current should be at least 3 orders of magnitude higher than the dark current before the fillfactor can be regarded as light intensity independent and used for direct comparisons. Otherwise, the potential fill factor and V_{oc} for realistic conditions may be underestimated considerably.

⁴¹We note that unlike many IV curves the EQE spectra are usually very well reproducible.

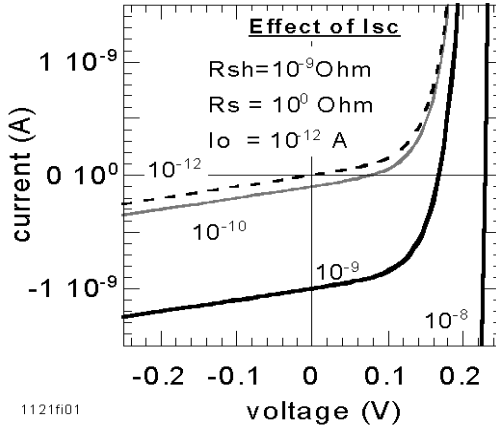


Figure 2.22: Effect of I_{sc} on the IV characteristics of an organic solar cell. The dashed curve is the dark characteristic. It can be seen that low I_{sc} values can result in a considerably smaller fillfactor and also lower V_{oc} values compared to higher I_{sc} numbers.

2.4.6 Space Charges & Traps

The comparatively low charge carrier mobilities in most organic semiconductors⁴² in conjunction with the need to drive high currents through the device can lead to accumulation of charges in the semiconductor bulk. These excess charges build up a space charge that creates a field which reduces the throughput i.e. increases the transit time of charges between the device electrodes. This phenomenon is termed space charge limited current (SCLC).

Provided there are no traps, the total current (I) through a semiconductor considering space charge formation as a function of voltage (V) can be expressed as [138]:

$$I = \underbrace{qp_0\mu_p \frac{V}{d}}_{\text{ohmic}} + \underbrace{\frac{9}{8}\epsilon\mu_p \frac{V^2}{d^3}}_{\text{SCLC}} \quad (2.35)$$

p_0 is the density of the thermally generated free carriers, μ is the mobility, d is the semiconductor thickness, ϵ the dielectric constant of the semiconductor.

As long as the density of the the thermally generated free carriers p_0 is dominant the current follows Ohm's law. Otherwise the current increases with the square of the voltage according to the second term in Eq. (2.35). This second term is known as

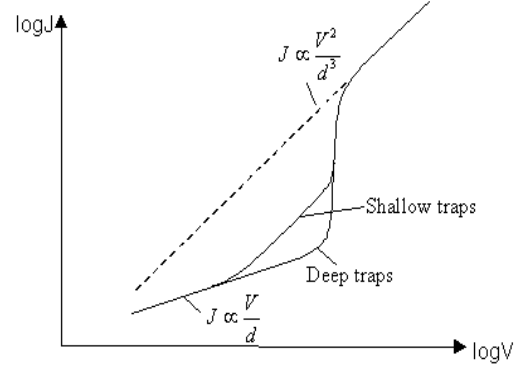


Figure 2.23: Schematic log-log plot showing the shape of the current-voltage characteristics for space charge limited current with deep and shallow traps.

the Mott and Gurney equation for trap free space charge limited currents. The transition from the ohmic to the space charge conduction here is very smooth.

If the material contains shallow traps the residence time inside the traps is shorter than the charge carrier transit time. The space charge is then composed of the mobile free carriers and those carriers that are thermally freed from the shallow traps. The trap free Mott and Gurney equation will still be applicable, if the mobility μ is multiplied by a factor F defined as the proportion of free charge carriers, giving an effective mobility:

$$\mu_{\text{eff}} = F\mu \quad (2.36)$$

Once the applied electrical field is strong enough to release the charge carriers from the traps, the current will return to obey the trap free Mott and Gurney equation - see Fig.2.23.

If the material contains deep traps the residence time inside the traps is longer than the charge carrier transit time. The SCLC depends then on both the density of traps and their distribution inside the bandgap. The transition from the ohmic conduction to the trap free condition occurs sharper than for shallow traps - see Fig.2.23.

⁴²Typical values are below $10^{-4} \text{ cm}^2 \text{ V}^{-1} \text{ s}^{-1}$

Chapter 3

Single Layer Devices

3.1 Introduction

In its simplest form, an organic solar cell consists of a single polymer layer sandwiched between two different electrode materials as depicted in Fig.3.1. Solar photons can enter the cell through the transparent contact (ITO) and create excitons upon absorption in the organic film. Not all photons will be absorbed in the thin film - some will be reflected by the back contact and have another chance to be absorbed in the film before they can leave the device again through the ITO layer.

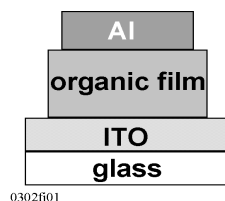


Figure 3.1: Device architecture of a single layer solar cell as it is used throughout this thesis. The organic film (dye, pigment, polymer) is sandwiched between the transparent ITO covered quartz substrate and a sublimed Al layer. The ITO and Al electrodes are sometimes replaced by other materials in the cited literature. The thickness of the organic layer is typically between 40 and 200nm.

3.1.1 Optical Properties of Organic Photovoltaic Materials

Table 3.1 gives insight into the absorption properties of some important organic semiconductors. The (half peak) absorption coefficient $\alpha_{1/2}$ are listed together with the wavelength range that exceeds this value to give a “feel” for the spectral dependence of the absorption.

We have also calculated the percentage of absorbed photons α_{10} using $\alpha_{1/2}$ for a 10nm thin¹ film. Note that the percentage of absorbed photons in a 10nm film in the cited range would require integration of the absorption over the given range. The quoted number for α_{10} is therefore somewhat underestimated² if it wants to be interpreted as absorption in the given range.

PPV being the only precursor polymer in the list has clearly the highest absorption coefficient followed by its well known soluble derivative MEH-PPV that has to accommodate also the bulky and optically non active side-chains in the film. Interestingly the absorption coefficient of MEH-PPV is still twice as large as the other soluble polymers indicating it can arrange its aromatic system in a very compact fashion.

The metal-free phthalocyanine has virtually the same $\alpha_{1/2}$ regardless if eight bulky thio-alkyl chains are attached (HPc(dye)) or nothing at all (HPc(pig)) as in the insoluble version. The perylene diimide pigments (Per(pig)), however, is somewhat stronger absorbing when compared with the soluble derivative (Per(dye)). This is actually expected because the absence of bulky side chains in the pigment should favour denser packing. In any case, it appears as if the differences between absorption properties of dyes and pigments do *not* differ tremendously.

On the other hand, the introduction of a metal like Cu in the phthalocyanine core can lead to an *increase* of the absorption. Pigments also tend to have slightly broader absorption bands.

In Chapter 2 we have discussed this in context with the exciton diffusion range and the importance to reach dissociation sites. In single layer devices

¹10nm were chosen since this is the typical thickness of the active layer i.e. exciton diffusion length - see Section 2.1.

²For example: 50% of $\alpha_{1/2}$ would have to be added if the absorption spectrum is approximated as being triangular.

Table 3.1: Survey of the absorption properties of various organic semiconductors. $\alpha_{1/2}$ is half the value of the absorption peak in the visible. The range parameter refers to the part of the absorption band that exceeds this value. α_{10} is the percentage of absorbed photons using $\alpha_{1/2}$ in a 10nm film without and with (brackets) a fully reflective rear contact.

material	$\alpha_{1/2}$ nm^{-1}	range nm	α_{10} %
PPV	0.017	320-480	16(29)
MEH-PPV	0.013	440-560	12(23)
CuPc(pig) [43]	0.012	570-740	11(21)
Per(pig) [133]	0.010	450-590	10(18)
Per(dye)	0.007	450-560	7(13)
CN-PPV	0.006	410-550	6(11)
MCP	0.006	370-510	6(11)
HPc(dye)	0.004	610-750	4(8)
HPc(pig) [68]	0.004	590-???	4(8)

such a dissociation site is typically the low workfunction electrode (Al)/semiconductor interface³. Only if the organic material can be regarded as good electron acceptor material, the high workfunction electrode (ITO)/semiconductor interface can become active.

The absorbed fraction A as a function of layer thickness d in Fig.3.2 and Fig.3.3 have been derived using Lambert Beer's law to express the fraction of transmitted light T yielding:

$$A = 1 - \overbrace{e^{-\alpha dr}}^T \quad (3.1)$$

with α being the absorption coefficient (here $\alpha_{1/2}$) and $r=1$ for the transparent rear contact or $r=2$ for the fully reflective one.

It is helpful to know that the reciprocal of α gives the layer thickness that is necessary to absorb 63% ($1-1/e$) light. The layer can be half as thin if a reflective rear contact is used - compare with Fig.3.2 and Fig.3.3.

However, interference and multiple reflections have been neglected above. We note that interference effects may be more important to consider in double layer, blend or laminated device structures. In these structures the active layer can either be

³Interestingly oxygen molecules that can also act as dissociation site do not seem to increase the active layer significantly - see Chapter 2 and end of this Section.

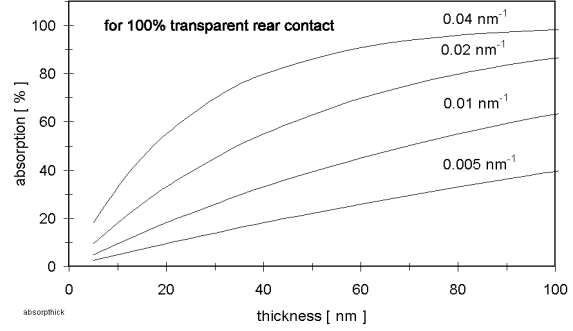


Figure 3.2: Percentage of absorbed photons in a film for various absorption coefficients $0.005 < \alpha < 0.04 \text{ nm}^{-1}$ as a function of film thickness.

placed in an optimal distance from the electrode using a second layer as optical spacer material [213] or the active layer can be made thick enough to allow a significant fraction of the visible light-wave to enter the device.

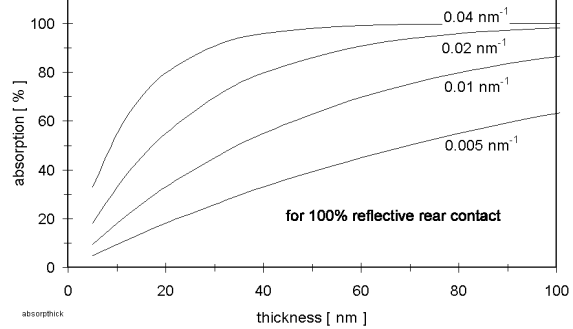


Figure 3.3: Percentage of absorbed photons in a film for various absorption coefficients $0.005 < \alpha < 0.04 \text{ nm}^{-1}$ as a function of film thickness assuming a reflective rear contact.

Since the active layer is usually located next to the reflective electrode interface and not much more than 10nm thick with a refractive index of about 2, interference with the reflected waves is not expected to cause dramatic changes of the exciton density in a 50nm single layer structure. More information on interference effects that may be used to optimise reflection⁴ and absorption properties in solar cells - particularly in multi-layer structures (considering

⁴Anti-reflection coatings like the SiO_2 , Ta_2O_5 or MgF_2 layer in silicon solar cells [162] may also be employed for organic cells.

also the about 100nm ITO film)- can be found in Ref. [281, 282].

The inability to absorb more photons in the 10nm layer represents a *main loss mechanism* in single and double layer organic solar cells. According to Fig.3.2 and Fig.3.3 even with the best absorbing materials ($\alpha_{1/2} \approx 0.02\text{nm}^{-1}$ - see Table 3.1) and reflective rear contacts, 70-80% of the photons in the absorption range are lost for the photovoltaic conversion process if the active layer is only 10nm.

We note that 80% of the solar radiation on earth is distributed over wavelengths ranging from 400 to 1200nm - see Table 8.3. Indeed, most currently available organic semiconductors loose more than 60% of the (mainly) low energy solar photons because their bandgap is too large - independently of the thickness of their active layer i.e. exciton diffusion range. Thus, the development of new low bandgap materials is highly desirable.

Fortunately, organic semiconductors have very high absorption coefficients compared to their inorganic counterparts so that the extremely thin active layer of 10nm can still absorb more than 20-30% of the light in the absorption range.

For example, the peak absorption coefficient of pure silicon at room temperature is 0.0004nm^{-1} at 600nm⁵. Thus, a 10nm Si layer would only absorb 0.8% of light at 600nm - even with a reflective rear contact.

3.1.2 Performance of Single Layer Devices

A survey of the photovoltaic performance of various single layer materials is given in Table 3.2. Blends with a non conjugated polymer binder molecules are treated as single layer here. PEDOT in conjunction with PPV here is heavily doped and therefore treated as a conductive transparent electrode film rather than a second semiconductive layer.

It can be seen that EQE values of 62 and 73% have been achieved with voltages of 1.1 and 0.45V many years ago. However, these cells have still some way to go to become practically interesting since e.g. illumination through the poorly transparent indium electrode was required or sub-linear intensity dependence of the photocurrent decreases the actually achieved solar power conversion efficiency down to 2.5% [164]. The recently published doped pentacene cell in Ref. [224] shows a solar power conversion efficiency of 2.4%.

⁵In fact, α_{Si} varies over 3 orders of magnitude ranging from 0.00001nm^{-1} at 1000nm to 0.01nm^{-1} at 400nm [98].

As can be seen from Table 3.2 cells using *pigments* have reached the highest EQE, V_{oc} and fill factors. However, although they have been investigated intensely in the past three decades and they have replaced many inorganic photo-receptors in xerography - they could not quite conquer the field of commercial solar cells.

Even though some can now be processed - with some effort from (acidic) solution [283] - or dispersed in binder materials [164] and thereby circumvent thermal sublimation, film formation is still considerably simpler, cheaper and less harmful using dyes, polymers or liquid crystals which are soluble in *common* and less harmful solvents. More information on coating techniques - especially for pigments can be found on page 295 in Ref.[29] and in Ref. [268] as well as references therein.

3.1.3 Doping of Organic Photovoltaic Materials

It is well known that molecular substances can have a "doping" effect on organic semiconductors [268, 231]. It has been found - and we can confirm this from our own experience - that often exposure to ambient air of only a few seconds is required⁶ to obtain a photoresponse in hole transport materials i.e. good electron donors⁷. This relates to materials like PPV, MEH-PPV, PTV, phthalocyanines, merocyanines and porphyrins.

Note that in phthalocyanines, for example, it is found that the influence of the central metal ions on the photovoltaic performance strictly follows their *oxygen* binding ability - since oxygen acts here as dopant. It was found that the photovoltaic efficiency of metal containing phthalocyanines follows the following order [231]:

$$PcMg > PcBe > PcFe > PcCu > PcCo \quad (3.2)$$

In other words: the easier they bind oxygen the higher the photocurrent.

Dopants with even greater electronegativity than oxygen, such as halogens, NO_2 , *o*-chloranil or 2,4,7-trinitrofluorenone result in an even greater enhancement of the photoresponse[43] in such hole transporters.

⁶Typically there are marked concentration effects: Exposure over many hours might be required before the photocurrent reaches its *maximum* which is then followed by slow decrease.

⁷Good electron donors have a high lying LUMO = small electron affinity.

Table 3.2: Survey of important performance parameters of various organic single layer solar cells. The abbreviation for materials are listed in Chapter 1. Best parameters parameters are printed **bold** while *italic* print marks devices discussed later in this Chapter.

EQE %	V_{oc} V	FF %	range nm	device –	comments –	year
73	0.45	33	400-800(?)	In/HPc+polymer/NESA	pigment in polymer [43]	1981
62	1.1	33	400-800(?)	Al/HPc+polymer/SnO ₂	pigment in polymer [43]	1979
??	??	??	400-800(?)	doped pentacene	pigment [224]	2000
33	1.2	25	400-800(?)	Al/merocyanine/Ag	pigment [43]	1978
14	0.7	39	400-800(?)	Al/CuPc/Au	pigment [43]	1981
3	0.6	34	400-800(?)	Al/merocyanine/Au	pigment [43]	1978
1	1.2	20	400-500	PPV	polymer [168]	1994
0.7	0.32	25	400-700(?)	Cr/chlorophyll-a/Hg	dye [43]	1975
0.5	1.0	23	400-500	Al/PPV+PEDOT/ITO	polymer [8]	1998
0.15	0.85	25	400-800(?)	Al/MgPc/Au	pigment [43]	1974
0.1	0.7	25	400-750	Al/THPF/ITO	<i>polymer</i>	2000
0.1	0.1	25	400-560	Al/LPPPT/ITO	<i>polymer</i>	2000
0.09	0.5	27	400-570	Al/CN-MEH-PPV/ITO	polymer [114]	1997
0.08	0.19	25	400-600	Al/Per/ITO	<i>dye</i>	2000
0.07	0.7	25	400-570	Al/MEH-PPV/ITO	<i>polymer</i> [196]	2000
0.05	0.37	25	400-750	Al/PTV/ITO	<i>polymer</i>	2000
0.03	< 0.02	25	400-650	Al/P3HT/ITO	polymer [63]	2001(?)
0.015	0.1	25	400-650 ⁺	In/HPc/Au	pigment [68]	1978
0.007	0.15	25	400-820	Al/HPc/ITO	<i>liquid crystal</i>	2000
0.005	< 0.02	25	400-1000	Al/PIF/ITO	<i>polymer</i>	2000

On the other hand, organic *electron* transporters can be doped effectively with H₂, NH₃ or phenothiazine.

In general, the photocurrent is much more affected by the presence of dopants than the dark current. Although exciton dissociation should therefore occur throughout the whole film, optical filter effects that indicate a thick electronically passive layer are often found. We consider therefore that excitons can dissociate at e.g. oxygen molecules and increase the concentration of one type of free charge carrier - while the other one is trapped in the dopant within the inactive layer. This would locally improve the charge transport properties but does not add to the photocurrent.

A high photocurrent requires both the generation of a free electron in the CB and a free hole in the VB. In that way they can both meet *after* passing through the external circuit. Consequently, molecular doping can be seen as essentially different from D/A blend (or laminated) structures since the latter allow *both* charge carriers to be free to travel to the electrodes through their percolation paths. Only then, the entire layer - and not only a layer as thin as the exciton diffusion length (≈ 10 nm) - can become active. For more information on oxygen doping see Chapter 2.

Since the presence of oxygen appears to enhance

the EQE in single layer devices we have exposed all our single layer device samples to air for at least 3 days. Hence, different concentrations of water & oxygen - due to different air exposure times of our samples - should not have a significant effect on our results. We note that the adsorption of water molecules also affects the photovoltaic performance [50].

3.1.4 Desired Properties of Organic Photovoltaic Materials

A very interesting review of photovoltaic, fluorescence and redox properties of 60 semiconducting molecules - most of which are (soluble) merocyanine derivatives - is given in Ref. [204]. These devices were structured like Al⁸/dye/Ag and reached quantum efficiencies of up to 16%. In the following we list the desired properties for photovoltaic molecules as they have been identified in Ref. [204]. The list is followed and complemented by comments found in other studies.

1. The chromophoric⁹ core of the dye must be essentially planar and free from steric crowding

⁸ A AlO₂O₃ layer on top of Al was considered.

⁹Chromophoric core = the pi conjugated part of the molecule is responsible for the optical properties in the visible and near IR range.

effects which tend to twist the dye, predisposing it to photo-isomerisation or internal conversion, instead of sensitisation by electron injection. Small groups projecting out of the plane of the chromophore¹⁰ play a critical role in “indexing” the packing of adjacent molecules to obtain the desired aggregate structure.

2. The dye must be a stable material and a strong absorber.
3. The performance of photovoltaic dyes can be correlated with their chemical parameters. In the configuration of Al/Al₂O₃/dye/Ag, the adhesion of the dye to the Al surface is critical and can be analyzed by studying the chromatography of the dyes on the Al substrates.

The electron rich end of the dye molecule should be chemisorbed at the Al surface. For example, dyes with COOH groups have a much stronger bond to the Al surface and result almost always in much higher photovoltaic quantum yields.

4. The reduction potentials of the dyes should be more negative than -1.3V vs. SCE for efficient electron injection through the Al₂O₃ barrier.
5. Dyes should not be subject to protonation or deprotonation by ambient materials in the pH-range from 3 to 10.
6. Dyes having central conjugated chains and steric crowding are to be avoided since such materials can readily degrade excitons to heat by torsional internal conversion. High PL of the isolated molecules in e.g. fluid solutions signal the effect of less torsional stress and is therefore preferable.
7. The quadrupolar charge distribution of e.g. squaric acid dyes may pack into a “brick-stone” i.e. J-aggregate structure which seems to favour mobility of *low energy* excitons. Merocyanines on the other hand pack in deck of cards or stacks showing only up to 15% photovoltaic quantum efficiency in their main absorption band but up to 100%¹¹ on the short wavelength edge of the absorption band.

8. Low bandgap materials seem to have difficulties to maintain a large negative reduction potential i.e. a low lying LUMO level. This would mean that low bandgap electron acceptors are harder to find i.e. synthesise.

We are not aware that any of these early findings have been proven wrong but many have been confirmed, complemented and further elaborated as can be seen from the following list of comments:

ad 1): The finding that a flat, rigid¹², aromatic molecule favors close packing and good photovoltaic properties - in particular high exciton mobility - has been recognized in other publications [268, 267, 154, 245].

The importance of this point may become obvious by referring to the fact that C.Tang actually included a claim in his patent regarding the use of *flat large* aromatic molecules as photo-active materials in solar cells. In Ref. [154] it is stated that the inter-planar distance should be short ($\approx 3.5\text{\AA}$) between photo-conductive molecules to achieve good performance. We note that close packing also increases the absorption coefficient. However, we also want to emphasise that exciton mobility loses its importance in e.g. blend structures - so that even spheric molecules like C60 can act as excellent electron acceptor and *transport* materials.

ad 3): We note that COOH groups play indeed an important role in bonding sensitizer molecules like the ruthenium dye in electrochemical photovoltaic cells to the TiO₂ surface [182].

ad 6): While PL in *solution* provides information about the isolated molecule and its ability to dissipate excitation energy through e.g. intra-molecular vibrations, PL studies of organic *films* can provide further insight into a material’s photovoltaic properties.

High PL in the solid state has been found to be *desirable* since it means that the life time of excitons is relatively long and allows excitons to diffuse over longer distances. If there is little or no PL, this would indicate that other - faster - decay channels for excitons are present. These fast decay channels reduce the time an exciton has to reach a dissociation site.

The effect of PL efficiency in the solid state on the reverse saturation current and the theoretically

¹⁰Chromophore = coloured molecule

¹¹Photovoltaic quantum efficiency numbers in Ref. [204] consider transmission and reflection losses and are more likely identical with the internal quantum efficiency (IQE) - which gives higher numbers - rather than the usually used EQE. This is discussed in Chapter 2.

¹²Rigid molecules are preferred to flexible structures since they have lower probability for those internal conversions that dissipate the energy carrying species before transport can occur.

achievable open circuit voltage is discussed in more detail in Chapter 2 and Ref. [234].

ad 8): If low bandgap materials tend to have higher lying LUMO levels, then they are more suitable as electron donor (D) materials rather than electron acceptors (A) - when used in combination with another semiconducting component to form a D/A system.

In fact the combination phthalocyanine & perylene representing a system with a low bandgap electron donor and a high bandgap electron acceptor works very well. The other possibility using a low band gap electron acceptor with high bandgap electron donor gives indeed only very low photocurrents (e.g. HPc+PIF in Chapter 5 or MEH-PPV+PIF [202]).

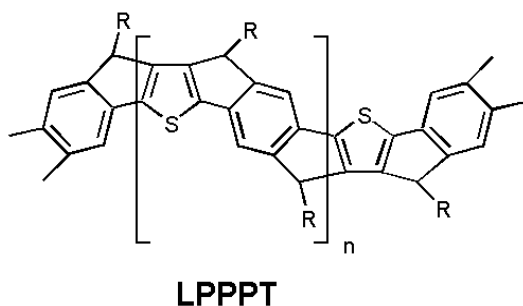


Figure 3.4: Chemical structure of the polymer used in this Chapter. It is ladder poly(para-phenylene thienylene) or short: LPPPT. The bridge between the phenylene-rings enforce a planar structure despite the proximity of the thiophene and phenylene units. $R = -1,4-C_6H_4-n-C_{10}H_{21}$ and $n = 20-25$.

Hence, the conclusion is that a low bandgap material in a D/A solar cell is likely to act as electron donor and thus require a partner with high electron affinity to enable charge transfer i.e. exciton splitting at their interface.

3.1.5 Electrodes

The workfunction and adsorption properties of electrodes have a clear effect on the performance of organic solar cells. The latter has to do with band bending due to equilibration of the workfunctions with the Fermi-levels of the semiconductors upon contact - as discussed in Chapter 2.

In the following Sections of this Chapter we have always used the same combination of electrodes (ITO and Al) to decrease the number of changing parameters. Moreover, both electrodes have been

proven to give more reliable and reproducible results than most other materials under laboratory conditions.

However, higher open circuit voltages and sometimes higher photocurrents can be obtained using electrodes like e.g. Au and Ca instead of ITO and Al.

3.2 LPPPT

It has been found that a poly(para-phenylene)-type ladder polymer exhibits many interesting properties such as high PL not only in solution (90%) but also in the film (50%) enabling the fabrication of efficient organic multi-colour LEDs [246] and even optically pumped blue solid state lasers [279].

The unique performance of this polymer is likely related to a very low concentration of electronically active traps such as structural defects or impurities [96] and the high charge carrier mobility (up to $10^{-3} cm^2/Vs$ for holes at room-temperature) [128]. However, the bandgap of this polymer with 2.7eV is too high to absorb a large fraction of the solar spectrum.

A well established method to shift the absorption onset towards lower energies is the replacement of benzene by electron rich hetero-arylene moieties such as 2,5 thienylene units.

For example the bandgap of PPV could be lowered by about 0.5eV by replacing every benzene unit with a 2,5 thienylene unit to give poly-thienylene vinylene (PTV) [275, 137]. The reason for this effect is the lower aromatic resonance energy of the thiophene building block when compared to that of benzene. This results in a reduced $\pi - \pi^*$ transition energy between the benzoid ground state and the quinoid excited state.

Indeed by replacing every other phenylene unit with a thiophene ring the structure of LPPPT - see Fig.3.4 - the low bandgap version of LPPP could be obtained. The bandgap in solution was lowered by 0.45eV compared to LPPP - which means a red-shift by about 85nm.

Both polymers exhibit a dominating 0-0 transition and an extraordinary small Stoke's shift of 35meV (LPPP) and 17meV (LPPPT) [74]. The latter (small stokes shift) is a consequence of the geometrically fixed, planar structure which allows only minimal changes of the polymer geometry during the transition from the ground to the excited state i.e. photoexcitation [160].

We note that planarity of aromatic systems is also suspected to favour charge and energy (exci-

ton) transport as discussed in Chapter 2 and below.

The well resolved vibronic structure allows better attribution of EQE features to absorption features - which we were exploiting by studying thickness effects in this special material.

Experimental

The chemical structure of the polymer used in this Section is shown in Fig.3.4. LPPPT has been provided by and synthesised at the MPI-Mainz. Details of the synthesis can be found in Ref [74].

LPPPT films were prepared by spin coating from chloroform solution onto ITO covered quartz substrates (12x12mm) after filtering ($0.45\mu\text{m}$). In order to obtain a wide range of different film thicknesses, solutions with concentrations of 10, 15, 20 and 30 mg/ml have been prepared and spincoated at 1600 and 3200rpm.

More details on the preparation of substrates and the EQE/IV measurements can be found in Chapter 10.

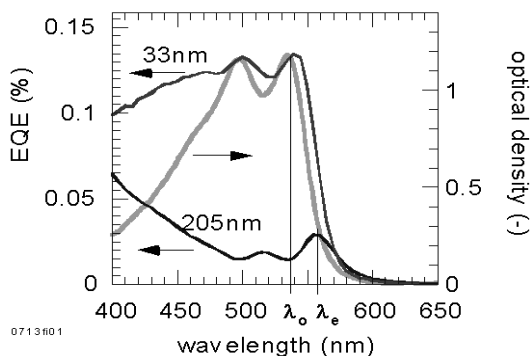


Figure 3.5: Features of the EQE spectrum of a thin (33nm) LPPPT device do almost coincide with the absorption features. The very thick (205nm) device shows not only smaller absolute numbers but also a distinct offset to the absorption i.e. strong antibatic behaviour.

Results and Discussion

Absorption and EQE Spectra

Fig.3.5 shows the EQE spectrum of a thick and a very thin LPPPT device when illuminated through the ITO contact as well as the linear absorption curve. The absorption spectrum shows two dominant peaks at 535nm (2.32eV) and 495nm (2.51eV)

and a shoulder at 460nm (2.70eV). The energetic spacing of 190eV is constant and can be attributed to the dominant vibronic (C-C) mode that has been observed in the absorption of films of other higher ordered polymers such as stretch oriented PPV [108] or the methyl substituted ladder type polymer comprising only benzene rings [197, 198].

The suppression of the rotational degree of freedom between adjacent benzene rings in the latter results in a particularly small Stoke's shift, high photo- and electro-luminescence quantum yields but also in a clearly resolved vibronic structure in both PL and absorption [238, 239, 197].

The EQE spectra of both the thick and the thin device show roughly the same features (the vibronic peaks 0-0 and 0-1); however, there are some differences:

- The EQE of the thinner device is almost “in phase” with the absorption while the thick one shows a clear red shift by 20nm.
- The EQE of the thicker device increases while the EQE of the thin device decreases in the shorter wavelength region.
- The second EQE peak (at 500nm) is virtually as high as the first which is not the case for the thick device.
- The EQE of the thinner device reaches values that are about 5 times larger than those for the thick one.

The peaks in the photoresponse of the thick cell occur not exactly at wavelengths with absorption maxima. In fact the second photoresponse maximum coincides with the absorption *minimum* between the two dominant vibronic peaks. This has been observed in organic solar cells before and is sometimes termed as *antibatic* behaviour [120] - see also Chapter 2.

The peak shift¹³ can be quantitatively explained with the so called *optical filter effect*[120]- see Chapter 2.

Only if the bulk is thin enough, most of the dissociated excitons can generate a photocurrent so that the EQE essentially follows the absorption features. This seems to be approached for the 30nm thin device since there is only a small peak offset left. In the thick device only light which is absorbed less - for example in the onset or the minimum between the vibronic peaks in the absorption spectrum - can

¹³but not the *shape* of the EQE peak

create excitons in the active region so that absorption maxima actually turn out as EQE minima and *vice versa*.

Assuming the filter effect¹⁴ is the main factor that determines the offset between absorption and EQE peaks we can estimate the maximum thickness of the organic film d_{opt} , that can be used in single layer devices without losses due to the optical filter effect. First we need to know the wavelength λ_e of the EQE peak in the onset of the antibatic absorption spectrum. The optical density (OD) at this position together with the OD at the absorption peak (Fig.3.5) and the film thickness d_0 of the measured EQE spectrum can then be taken to get and estimate for the optimal thickness d_{opt} , using:

$$d_{opt.} = \frac{OD(\lambda_e)}{OD(\lambda_0)} \cdot d_0 \quad (3.3)$$

This equation is solely based on Lambert Beer's Law:

$$\frac{I(\lambda)}{I_0(\lambda)} = e^{-\alpha(\lambda)d} = 10^{-OD(\lambda)} \quad (3.4)$$

(with I_o being the incident and I the transmitted intensity) and the resulting simple relation:

$$d \propto OD \quad (3.5)$$

The error of the optimal thickness Δd_{opt} , due to the error of the input variables is:

$$\left(\frac{\Delta d_{opt}}{d_{opt}}\right)^2 = \left(\frac{\Delta OD(\lambda_e)}{OD(\lambda_e)}\right)^2 + \left(\frac{\Delta OD(\lambda_0)}{OD(\lambda_0)}\right)^2 + \left(\frac{\Delta d_0}{d_0}\right)^2 \quad (3.6)$$

Using the data for the 205nm thick device and estimated errors ($OD(\lambda_e) = 0.0696 \pm 45\%$, $OD(\lambda_0) = 0.22 \pm 2\%$ and $d_0 = 205nm \pm 5\%$) we obtain:

$$d_{opt} = 65 \pm 30nm \quad (3.7)$$

The large error of 30nm or 45% for $OD(\lambda_e)$ is due to the steep slope in the absorption onset and the relatively broad peak in the EQE spectrum of the thick device.

We obtain a considerably smaller error and value for d_{opt} using the data for the thinnest investigated device (10nm): $OD(\lambda_e) = 0.201 \pm 12\%$, $OD(\lambda_0) = 0.22 \pm 2\%$ and $d_0 = 33nm \pm 15\%$. Here we obtain:

$$d_{opt} = 30 \pm 6nm(20\%) \quad (3.8)$$

This is a more reasonable result considering that we know already that d_{opt} has to be (slightly) smaller than 33nm. Given that we are trying to avoid the optical filter effect we can justify to use the lowest number within the error bars and calculate the mean in case of several results. This would yield in our case:

$$\overline{d_{opt}} = (36 + 24)/2 = 30nm \quad (3.9)$$

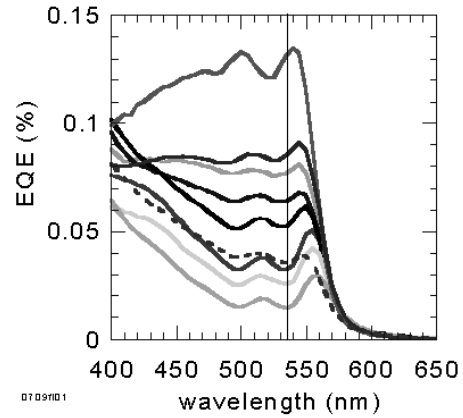


Figure 3.6: The EQE of LPPPT at 536nm when illuminated through ITO decreases according to the layer thickness of 33,59,67,93,127,117 (dashed line),163,168 and 205nm.

Generally, d_{opt} , may be regarded as an *upper limit* of the exciton diffusion range for this material. The actual value might be smaller if e.g. there is an effect of other dissociation sites such as impurities or dopants¹⁵ in addition to the electrode-polymer interface.

We also need to consider the high electric field across the thin layer due to the difference in workfunctions of the electrodes ($0.5V/30nm \approx 2 \cdot 10^5 Vcm^{-2}$). Hence, we cannot be sure that the exciton diffusion length is as long as 30nm but at least we know that the absorbed light is most efficiently used in a device with about 30nm thickness.

On the other hand, a relatively large diffusion length in LPPPT is not surprising knowing that planar structures are expected to favour exciton transport. In any case, the large value for d_{opt} , compared to about 10nm for MEH-PPV devices makes this material an interesting candidate for use in D/A cells.

¹⁴See Section 2.4.4

¹⁵oxygen can act as such in electron donors

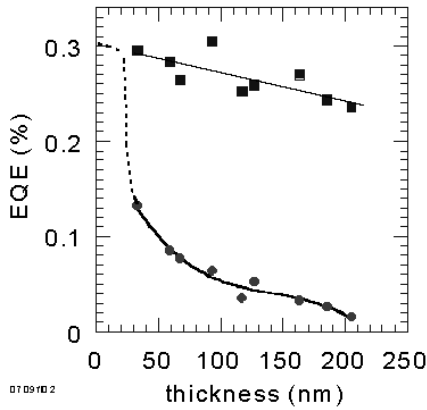


Figure 3.7: EQE versus film thickness when illuminated ($\lambda=536\text{nm}$) through ITO (circles) and Al contact (squares). The solid line in the circles is a fit with a polynomial of 3rd order whereas the solid line in the squares is a linear fit. The dashed line illustrates a possible trend.

How the shape of the EQE spectra varies with layer thickness is shown in more detail in Fig.3.6. The antibatic behaviour of the 205nm thick device gradually changes into a more and more sybatic response by going to thinner cells. This also holds true for the short wavelength range (400-500nm). Only the 117nm thick device seems to behave differently.

Optical interference effects between the incident and the reflected beam from the Al rear contact may be super-imposed here. In fact, numerical simulation using the described model and taking into account interference effects showed that there is indeed a dip around this wavelength in the thickness dependence curve of the EQE for such a device [266].

We plotted the experimental data of the EQE at 536nm versus thickness in Fig.3.7. The figure clearly shows the trend to higher EQE for thinner devices as well as the dip at 117nm.

The figure also shows the curve for EQE at 536nm obtained upon illumination through the semitransparent Al contact taking into account the transmission losses through the Al layer (Fig.3.8). We obtain then even higher values than with illumination through ITO. This is expected since there should be no losses due to optical filtering¹⁶.

¹⁶The slight increase of the EQE for thinner devices is probably due to improved electric properties such as a

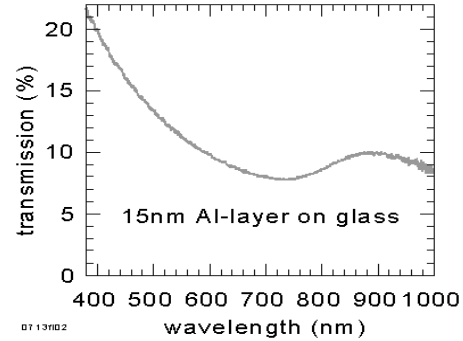


Figure 3.8: Optical transmission spectrum of the 15nm thick Al layer i.e. electrode of the LPPPT devices discussed in this Chapter.

Hence, this curve displays the maximum EQE that is achievable for a single layer device of this material using ITO/Al electrodes regardless of film thickness or which side of the cell is illuminated.

Thus, we can expect that the strong increase of EQE with thinner devices when illuminated through ITO will slow down considerably when reaching the trend line from the Al illumination curve. The thickness at this point can be assumed to coincide with optimal layer thickness d_{opt} . As expected in the described picture, the shape, peak positions and absolute value of the EQE do not vary considerably when illuminated through Al¹⁷ - see Fig.3.9.

IV Characteristics

The IV characteristics in the dark and under monochromatic illumination (550nm) of the *thickest* device (205nm) is shown in Fig.3.10. Even though the open circuit voltage is relatively small (106mV) this device shows a good rectification i.e. diode behaviour: The current that can pass through the device at 0.4V is about 15 times (=rectification ratio) higher than at -0.4V.

Dark and light characteristics have virtually the same shape i.e. lie on top of each other at this scale. The parameter I_d should not be confused with the reverse saturation current I_o which can only be obtained via numerical modeling of the IV curves. I_d here is the actual current measured at

smaller series resistant.

¹⁷The small variation seen in this figure may well be due to random errors in the measurement.

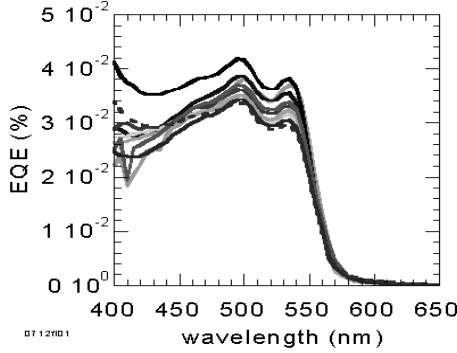


Figure 3.9: EQE of the LPPPT films when illuminated through the semitransparent Al contact (not corrected for the Al transmission) for different thickness (same data as in Fig.3.7-full circles). Shape and ratio of the features do not vary significantly with film thickness. The highest EQE was obtained with a 93nm thick film.

0V¹⁸.

With decreasing film thickness - see Fig.3.11 to Fig.3.16, the rectification ratio also decreases until the IV characteristics of the *thinnest* device - see Fig.3.17 resembles more the characteristic of an ohmic resistor (constant slope) with virtually no rectification and only a small (≈ 30 mV) open circuit voltage. The steep slope reveals a significantly higher conductivity (under illumination and in the dark) in comparison to the thick device.

A survey of parameters obtained from the IV

¹⁸For the suspected origin of I_d see Chapter 10

Table 3.3: Survey of solar cell parameters obtained from the IV curves and the EQE (at 536nm) for LPPPT films of varying thickness.

d nm	EQE $10^{-3}\%$	V_{oc} mV	I_d pA	R_{sh} $M\Omega$	R_s $M\Omega$
32	132	28	33	16(17)	4.8(5.0)
59	85	105	31	83(200)	7.5(11)
67	77	126	31	150(530)	6.3(9.5)
93	64	141	26	170(700)	7.5(10)
117	36	176	18	250(1400)	—
122	52	120	38	200(500)	6.3(8.8)
185	26	99	27	250(600)	7.5(11)
205	15	106	10	—	—

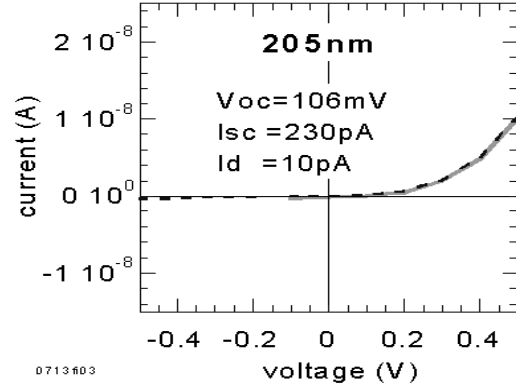


Figure 3.10: IV characteristics of the 205nm thick LPPPT device.

curves with different film thickness is given in Table 3.3. Although there might be a trend towards lower dark currents with increasing thickness and increasing V_{oc} it is not completely conclusive. However, a correlation between dark current and V_{oc} seems to emerge though if the data are plotted on a suitably chosen scale - see Fig.3.18. The conductivity in the dark seems to be high enough to reduce the open circuit voltage.

Larger open circuit voltages appear to require a shunt higher than about $80M\Omega$ here. However, the table also shows that V_{oc} does not necessarily increase for even higher shunts.

A very interesting result is that R_s does increase relatively slowly ($11k\Omega/nm$) with film thickness whereas the shunt increases more than 100 times faster ($1.5M\Omega/nm$) - see Fig.3.19. While the increase of R_s can be qualitatively explained by the fact that charge carriers have simply more semiconducting material to travel through to reach the electrodes, the distinct growth of the *shunt* is harder to understand.

In Chapter 10 we have stated that *recombination losses* somewhere between the dissociation site and the electrodes can be associated with a small R_s .

However, it is not obvious why the absolute number of recombinations should go up if the charges travel through less material. It would be easier to accept that the number of recombinations per second *increased* since the charges need more time to get out of the thicker semiconductor.

Fig.3.20 shows that the shunt also increases for thicker films when measured in the *dark* - although there seems to be some consolidation for $d > 60nm$.

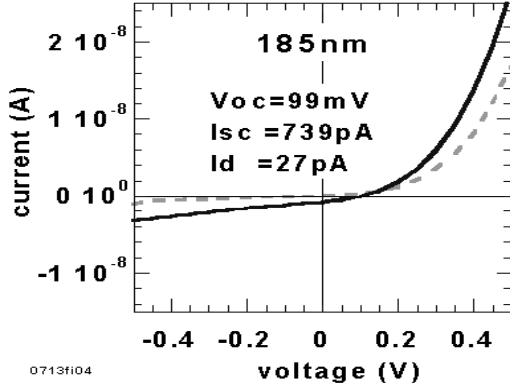


Figure 3.11: IV characteristics of the 185nm thick LPPPT device.

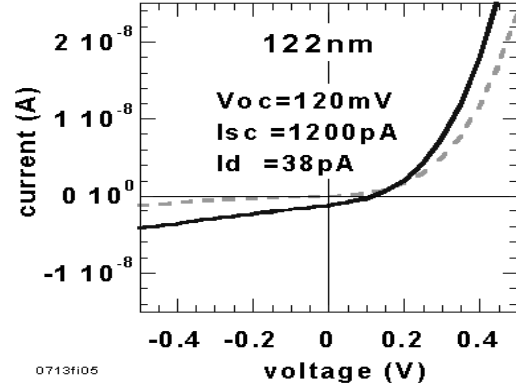


Figure 3.12: IV characteristics of the 122nm thick LPPPT device.

The thickness dependence of R_s appears unchanged in the dark with absolute numbers about 30% larger than under illumination.

R_s is expected to decrease significantly with increasing light intensity simply because more charge carriers become available for the conduction process. A considerable decrease of R_s is required to allow both high voltages as well as high photocurrents and thus high power conversion efficiencies [206, 214].

In Chapter 2 we have seen that the ratio R_s/R_{sh} not only affects the fillfactor strongly but also the output current in a solar cell. According to Eq. (2.19) the current through a solar cell is reduced by the factor β :

$$\beta = 1 + R_s/R_{sh} \quad (3.10)$$

In Fig.3.21 we have plotted β versus film thickness. The figure shows that the factor β is close to 1 for film thicknesses larger than about 60nm. For thinner films the reduction factor can increase from 1.04 (60-200nm) to at least 1.3 (30nm) in light. Although this does not affect the photocurrent dramatically it indicates that there is an additional effect for devices thinner than 60nm in LPPPT.

In the preceding Section we have already seen that with decreasing thickness the EQE is indeed rising.

In order to see the effect of film thickness on the shape of the IV curves, we have plotted the light IV curves in a single graph - see Fig.3.22. The graph illustrates clearly the distinct changes of slopes and open circuit voltages.

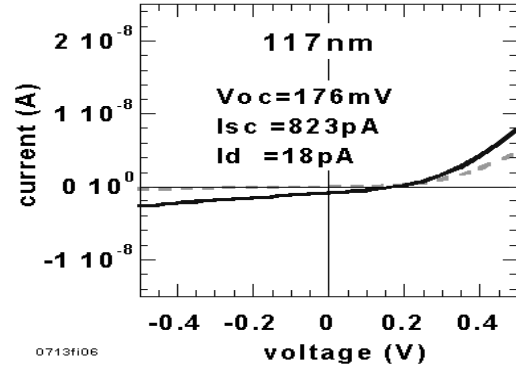


Figure 3.13: IV characteristics of the 117nm thick LPPPT device.

The increasing R_{sh} can be recognized immediately from the decreasing slope in the 3 quadrant (negative voltage range here) although there are exceptions in the expected order.

As we have seen in Fig.3.18 before the V_{oc} reaches a maximum value for the 117nm thin layer and not for the thickest device as it may be expected from the flat slope in Fig.3.22.

In fact, V_{oc} of the 32nm device is as small as 28mV whereas the highest voltage in LPPPT is 176mV (117nm). Such a large difference cannot be explained with the effect of the R_s/R_{sh} - which essentially works as a voltage divider. According to Eq. (2.24) the value for $R_s/R_{sh} = 0.3$ for this device can only account for a reduction of V_{oc} by about 30%. Hence, apart from a low shunt, there

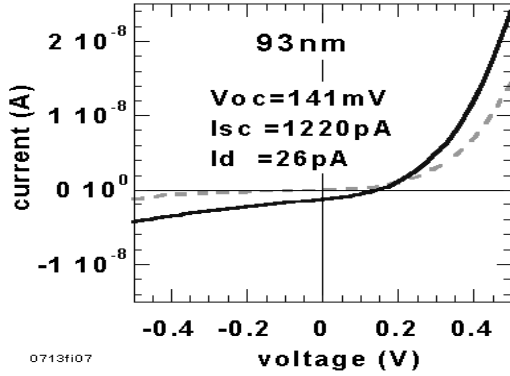


Figure 3.14: IV characteristics of the 93nm thick LPPPT device.

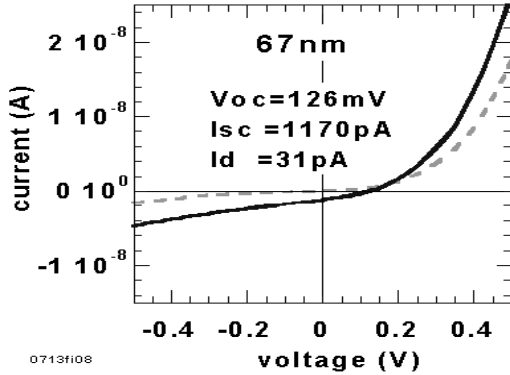


Figure 3.15: IV characteristics of the 67nm thick LPPPT device.

must be another not yet known reason to cause the low open circuit voltage in this device.

Fig.3.23 shows again the dark and light characteristics of the ITO/LPPPT/Al device (59nm thick). It also shows the fit with Eq. (2.19) that could be applied for the region -0.1V to 0.4V using the following fit parameters:

1. ideality factor $n=1.10$
2. reverse saturation current $I_0 = 10\text{pA}$
3. resistors in the dark: $R_{sh} = 18 \cdot 10^7\Omega$, $R_s = 2.3 \cdot 10^7\Omega$
4. resistors under illumination ($0.1\text{mW}/\text{cm}^2$): $R_{sh} = 8.8 \cdot 10^7\Omega$, $R_s = 1.8 \cdot 10^7\Omega$ and $I_L = 1610\text{pA}$

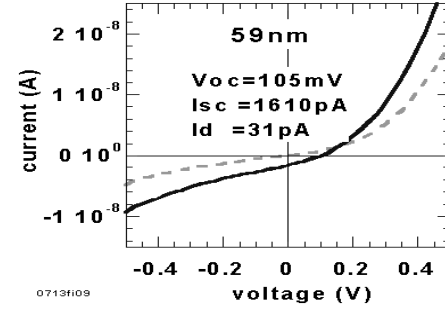


Figure 3.16: IV characteristics of the 59nm thick LPPPT device.

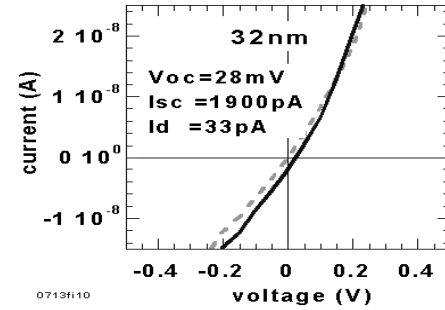


Figure 3.17: IV characteristics of the 32nm thick LPPPT device.

Note that the resistor values shown in this list are somewhat different from the values shown in Table 3.3. In the latter the numbers were derived directly by taking the slopes of the characteristics at 0V (R_{sh}) and the highest voltages around 0.5V (R_s) whereas in the former the formalism considered effects of n , I_0 , I_L . The results for the shunt are fairly similar and the values for R_s are about 4 times higher in the fit.

We consider the numbers for R_s values which are derived from the slope around 0.5V to be more accurate than the value obtained from fitting the *entire* curve since R_s really starts to dominate only at higher voltages¹⁹.

In any case, the comparison of these two methods indicates that the error for R_s is much higher than the one for R_{sh} . This is because of both the steeper slope at higher voltages which results in stronger

¹⁹Unless the IV curve becomes clearly linear for higher voltages the (inverse) slope can only represent an upper limit of R_s - see Chapter 2.

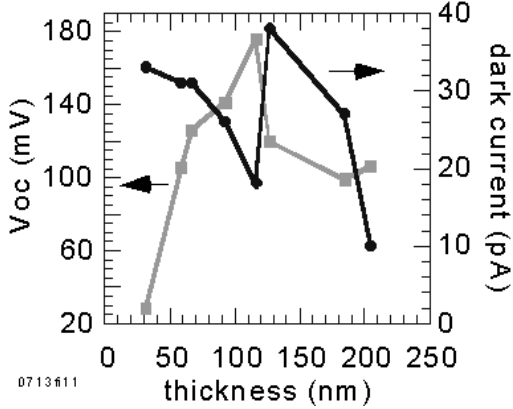


Figure 3.18: Open circuit voltage and dark current seem to be “out of phase” when plotted versus film thickness on the shown scales.

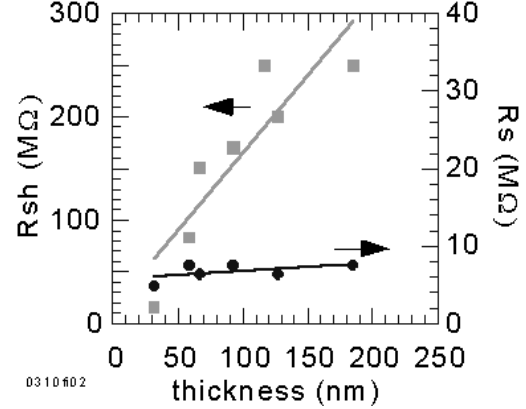


Figure 3.19: Series and shunt resistor as obtained from the slopes in the IV curves under illumination for varying film thickness.

dependence and voltage fluctuations of the source measure unit in the low mV range.

According to the discussion on the photoluminescence effects we can now take the reverse saturation current together with the PL efficiency of LPPPT of about 1.2% [35, 63] to obtain a value for the PL independent component of the reverse saturation current according to Eq. (2.25):

$$I_{01} = I_0 \cdot \Phi_{PL} = 12\text{pA} \cdot 0.012 = 0.12\text{pA} \quad (3.11)$$

The value for I_{01} is close to the 0.091pA obtained for the later discussed MEH-PPV. Thus, it can not be ruled out here that I_0 depends only or at least predominantly on the PL efficiency. This would then indicate that the maximum performance of both materials LPPPT and MEH-PPV showing the used PL efficiency has been closely approached in these devices.

The higher EQE numbers of thinner devices would possibly disappear if the optical losses like the filter effect were considered or - in other words - the internal quantum efficiency (IQE) was calculated.

A more detailed study comprising a higher number of samples and systematic IV analysis is necessary to confirm this possibility and explain the observed variation of V_{oc} with thickness.

Summary

In this Section we have found for LPPPT that:

- Thickness is an important parameter. The optimal thickness can be estimated from the absorption spectrum and an antibatic EQE spectrum.
- The EQE increases from 0.029% for the thickest (205nm) devices to 0.135% for the thinnest (32nm) device.
- The highest EQE is almost twice as high as the best i.e. thinnest (10nm) MEH-PPV device.
- The highest EQEs were achieved for the thinnest cells where the optical filter effect has virtually disappeared. Since the entire 30nm layer contributes to the photocurrent - the exciton diffusion length could be as high as 30nm in this material - if the polymer/Al interface has to be reached.
- Since LPPPT is a very large flat molecule but without any other obvious outstanding structural properties the high EQE in this material and the lack of an optical filter effect supports the suspicion that planar rigid structures favour exciton diffusion.
- Although the EQE increases with thinner devices without reaching a maximum in the observed range (30-200nm) the V_{oc} appears to reach a maximum value at 117nm.
- Both shunt and series resistor increase with increasing film thickness but R_{sh} grows more

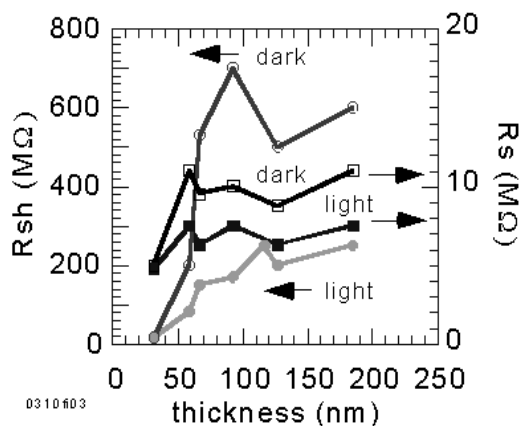


Figure 3.20: Series and shunt resistor as obtained from the slopes in the IV curves in the dark and under illumination for varying film thickness.

than 100 times faster ($1.5\text{M}\Omega/\text{nm}$) than R_s under illumination ($\lambda = 536\text{nm}$, $0.1\text{W}/\text{cm}^2$) for an area of 4mm^2 .

- The PL efficiency is rather low (1.2%).
- The PL efficiency multiplied with the reverse saturation current (12pA) gives approximately the same number for LPPPT (0.12pA) as for MEH-PPV (0.091pA). This is consistent with a strong correlation between the IV curve i.e the photovoltaic performance and the PL as discussed in Chapter 2 and Ref. [234].
- Films of LPPPT which are thinner than about 60nm show a strong increase of EQE, more similar R_s and R_{sh} values, a fast decreasing V_{oc} , a fast decreasing R_{sh} in the dark. Hence, the physics in these thin devices seems to be dominated by other effects which are not yet understood.

3.3 MEH

After the discovery of EL in conjugated polymers [34] the next step towards inexpensive device manufacturing was the design of a molecule with similar semi-conducting properties but even easier processibility.

At that time PPV films could only be obtained via spincoating a precursor solution and a subsequent heat conversion step at about 200C for 5 to

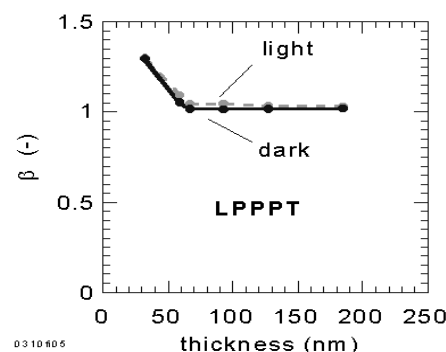


Figure 3.21: Current reduction factor β as a function of film thickness in LPPPT - calculated using the numbers under illumination.

10hrs²⁰.

Already in 1991 researchers in Santa Barbara (CA, USA) were successful at obtaining a PPV derivative with branched saturated side chains [124]. These bulky side chains allow solvent molecules to penetrate into the space between the polymer chains thus allowing device fabrication using simple spin-casting techniques ([32] and References therein). These side chains are also not conjugated so they do not alter the semiconducting or electronic properties significantly.

This was the birth of MEH-PPV, probably the worlds first *soluble* semiconducting polymer. Single layer MEH-PPV cells have already been subject to photocurrent spectroscopy [120], impedance and photo-voltage spectroscopy [121] as well as deep level transient spectroscopy [92].

The availability of a soluble semiconductor not only opened the way towards cheaper processing via numerous coating methods - even inkjet printing²¹ has already been reported [19] - but also made it possible to investigate blends with other semiconductors such as C60 while maintaining the advantages of solution processing.

Photo-induced electron transfer from MEH-PPV onto the fullerene C60 has been discovered and exploited in solar cells reaching EQE as high as 29% for monochromatic light [278]. Shortly afterwards, blends of MEH-PPV with its more electro-negative derivative CN-PPV that also benefit from photo-

²⁰Recently, another deposition method which can be applied for PPV such as laser-ablation has been found and investigated [240].

²¹This technique could be used to fabricate not only computer or video screens but also photosensitive CCD arrays.

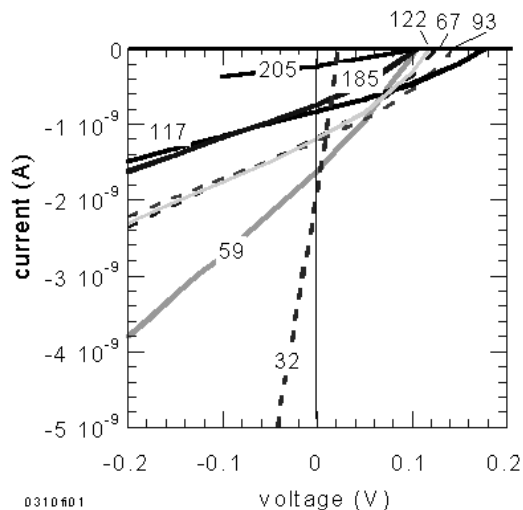


Figure 3.22: 3rd and 4th quadrant IV characteristics of LPPPT devices under light. The numbers represent the film thickness.

induced charge transfer with 6% monochromatic EQE have been reported[112].

Here we investigate to what extent the thickness (between 10 and 250nm) of the MEH-PPV layer effects the photovoltaic properties.

Experimental

We fabricated ITO/MEH-PPV/Al photodiodes with different thickness of the MEH-PPV layer ranging between 10 and 250nm. MEH-PPV was synthesised by H. Rost, at the Melville Laboratory for Polymer Synthesis in Cambridge. information on the synthesis can be found in Ref. [181, 124] and references therein.

The MEH-PPV films were spincoated in air after filtering (5 μ m) from chloroform solution (1 - 6 mg/ml) onto ITO coated glass substrates (Balzers). Unless stated otherwise all devices were measured when illuminated through the ITO contact. We measured the thickness of the thicker films (50 to 250nm) with a profilometer (Dektak) after 2 days drying in air in darkness which is necessary to obtain films hard enough to avoid the profilometer needle to scratch the polymer considerably. Together with the absorption data we calculated the absorption coefficient which we used in order to confirm the thickness of the thinner films.

More details on sample preparation and the used setup can be found in Chapter 10.

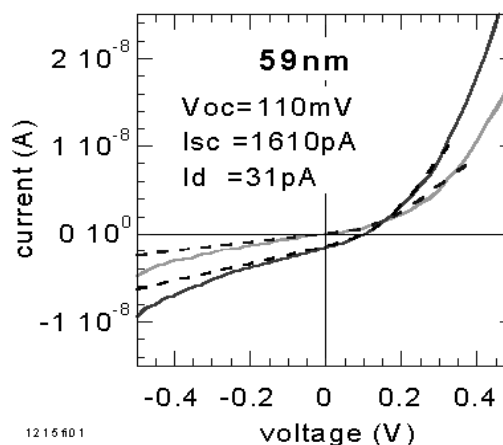


Figure 3.23: IV characteristics (solid lines) in the dark and under illumination of a ITO/LPPPT/Al device (59nm thick) and calculated curves (dashed lines) using Eq. (2.19).

Results and Discussion

Absorption and EQE Spectra

Fig.3.25 shows the linear absorption of MEH-PPV together with the EQE spectra for two different thicknesses. The absorption spectrum reveals essentially one broad feature with the peak at 505nm (2.46eV). The onset of absorption is not very sharp, starting at 600nm which corresponds to a bandgap of 2.07eV.

According to Table 8.3 a sufficiently thick MEH-PPV film can absorb about 28% of the solar radiation. Note that the bandgap has been significantly reduced with respect to the insoluble PPV.

For the EQE spectra of these two devices we found that:

- The thickest (250nm) device shows an EQE peak in the onset of the absorption spectrum while the EQE peak coincides with the absorption peak for the thinnest (10nm) cell.
- The EQE of the thin cell *increases* again for shorter wavelengths after reaching its maximum at the absorption peak whereas the optical density continues to fall. Such behaviour is unexpected for an otherwise sybatic EQE spectrum and indeed in contrast to the results in e.g. LPPPT where the 30nm device keeps following the absorption.

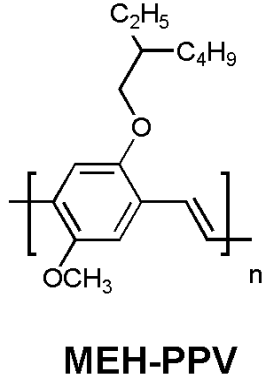


Figure 3.24: Chemical structure of the polymer used in this Chapter. It is a poly(2-methoxy-5-(2-ethyl-hexyloxy)-1,4-phenylene vinylene - referred to as MEH-PPV.

- The EQE peak of the 10nm device is almost 5 times as high as for the 250nm cell.

The EQE values for thicknesses ranging from 10 to 250nm with some intermediate values are plotted in Fig.3.26. All films show an increasing EQE in the short wavelength range - although the slope is flatter for medium thickness (35, 54nm) but higher again for the 10nm film.

Apart from the raising EQE of the 10nm film, all spectra show very similar features and trends as observed in the LPPPT film - see previous Section. The EQE increases clearly with thinner films.

However, if we apply Eq. (3.3) to estimate the thickness of the active layer from the antibatic EQE of the 35nm cell, we obtain:

$$d_{opt} = 26 \pm 7nm \quad (3.12)$$

which is 17nm higher than the value found for PPV [113, 111]. The large error stems from the uncertainty of the peak position of the 35nm film in conjunction with the steep slope of OD which results in a relative error of $\lambda_e = 22\%$. Note that the 54nm film actually has its peak closer to the absorption peak than the 35nm film. We consider this mainly to be due to the low resolution of the EQE scan (10nm) but also random errors related to the photocurrent measuring process.

A plot of the EQE versus film thickness taken at $\lambda = 505nm$ shows how the efficiency increases by nearly a factor 50 from 0.0014% for a thickness of 250nm to 0.064% for 10nm - see Fig.3.27.

The fact that the efficiency is highest in a layer as thin as 10nm is particularly interesting in the

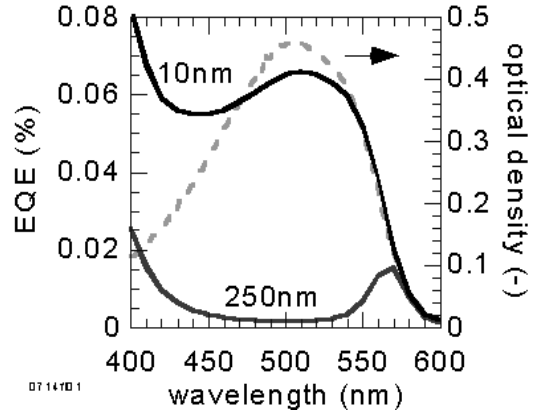


Figure 3.25: EQE spectrum of a thick (250nm) and very thin (10nm) MEH-PPV cell. Also shown is the absorption of a 38nm MEH-PPV film.

view of other discoveries: For example, it has been shown that non radiative energy transfer - in other words - the transfer of an exciton from an excited molecule to the metal electrode can generate surface plasmons. The energy transfer onto these plasmons represents an effective decay channel particularly if the excitons are close ($\approx 20nm$) to the metal film [40]. More recently, effective photo- and electroluminescence quenching has been found in organic films near ($< 20nm$) metal electrodes [14, 15, 103].

Both these earlier findings would let us expect lower EQEs in such thin films since the lost excitons are believed to be transferred onto the metal where their energy dissipates into heat rather than being split into their constituent charges. Hence, the high EQE in our thin devices may be affected by the generation of surface plasmons but the gain of a smaller filter effect and higher field due to the small distance between the two electrodes seems to over-compensate those quenching effects.

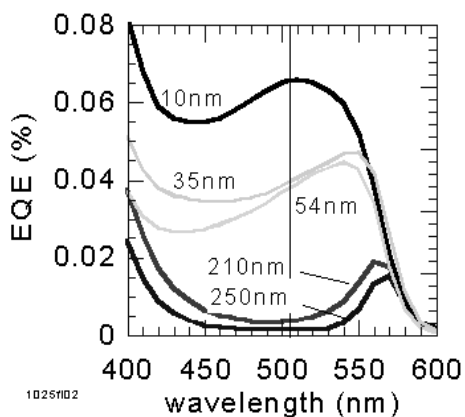


Figure 3.26: EQE spectra for MEH-PPV devices with thicknesses ranging from 10 to 250nm.

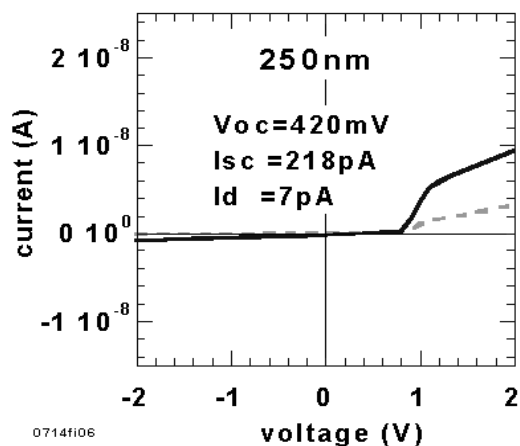


Figure 3.28: IV light (solid line) and dark (dashed line) characteristics of a 250nm thick MEH-PPV device.

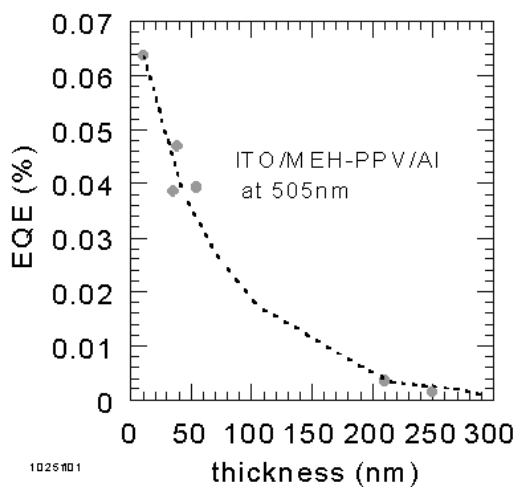


Figure 3.27: EQE versus film thicknesses for the MEH-PPV devices ranging from 10 to 250nm. The dashed line is a guide to the eye.

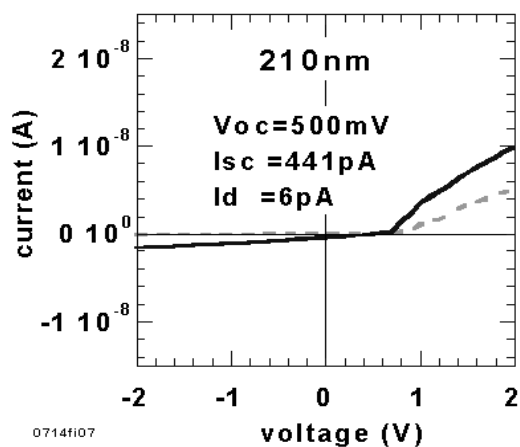


Figure 3.29: IV light (solid line) and dark (dashed line) characteristics of a 210nm thick MEH-PPV device.

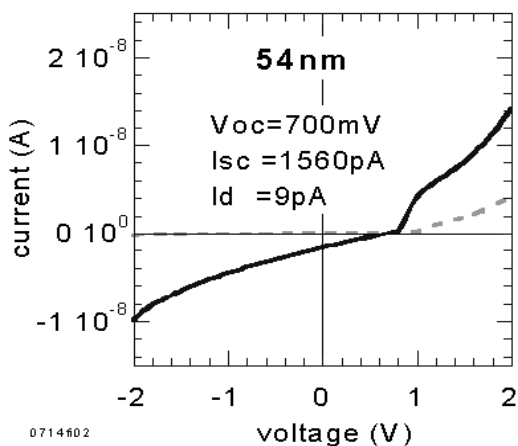


Figure 3.30: IV light (solid line) and dark (dashed line) characteristics of a 54nm thick MEH-PPV device.

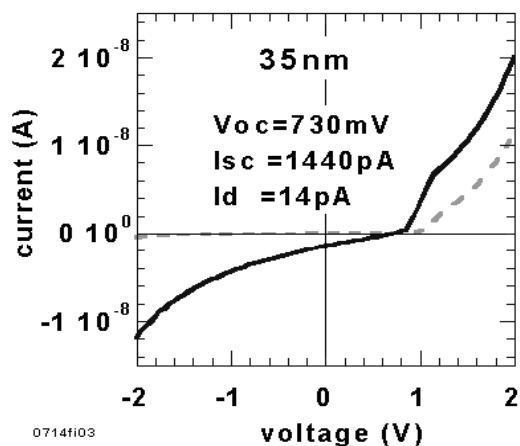


Figure 3.32: IV light (solid line) and dark (dashed line) characteristics of a 35nm thick MEH-PPV device.

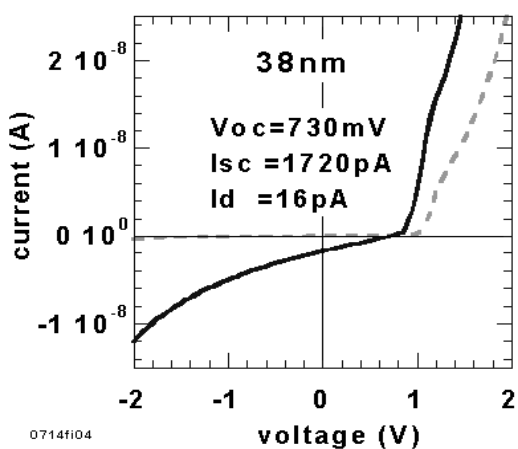


Figure 3.31: IV light (solid line) and dark (dashed line) characteristics of a 38nm thick MEH-PPV device.

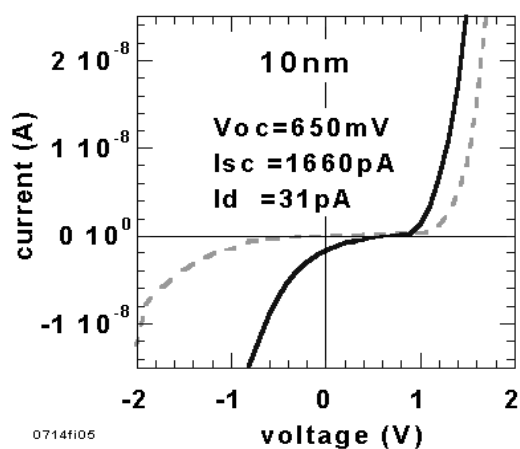


Figure 3.33: IV light (solid line) and dark (dashed line) characteristics of a 10nm thick MEH-PPV device.

Table 3.4: Survey of various solar cell parameters obtained from the IV curves and the EQE (at 536nm) for MEH-PPV films of varying thickness.

d nm	EQE %	V_{oc} mV	I_d pA	R_{sh} $M\Omega$	R_s $M\Omega$
10	0.064	650	31	200(2400)	7.5(8.0)
35	0.039	730	14	500(11000)	40(74)
38	0.047	730	16	400(12000)	14(23)
54	0.039	700	9	380(18000)	40(270)
210	0.004	500	6	1400(21000)	100(170)
250	0.001	420	7	2400(24000)	54(220)

IV Characteristics

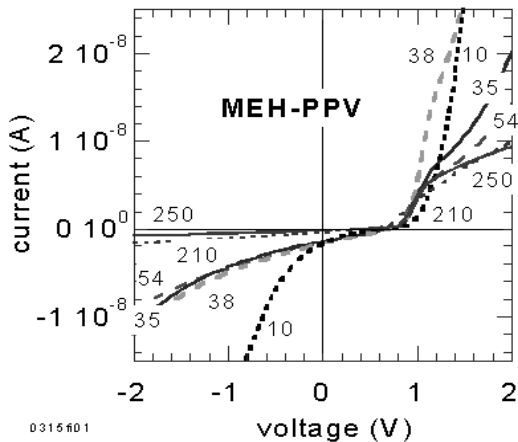


Figure 3.34: IV characteristics under illumination for different film thicknesses in MEH-PPV. The numbers represent the thickness in nm.

Fig.3.29 to Fig.3.33 show the IV characteristics for various film thicknesses in darkness and under illumination (through ITO) with $\lambda = 550\text{nm}$ at about 0.2mWcm^{-2} . The dark current I_d is the actually measured current at 0V in darkness and should not be confused with the reverse saturation current which can only be obtained by fitting the IV curve. For more information on the dark current which is an experimental artifact see Chapter 10.

In contrast to the findings in LPPPT films the IV characteristics in the dark for MEH-PPV do not change their shape much for different thicknesses in the negative voltage range (3rd quadrant). Apart

from the thinnest device the IV curves for positive voltages (1 quadrant) under illumination reveal two different slopes. The slope at lower voltages is always steeper than the other. The latter also decreases with thickness while the other remains more or less constant. The changes of the shape of the IV curves under illumination can be assessed more easily in Fig.3.34.

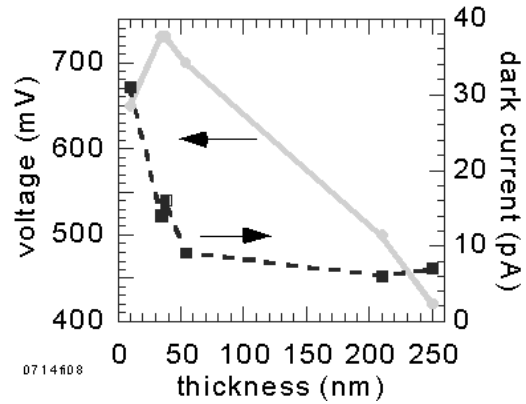


Figure 3.35: V_{oc} and I_d in MEH-PPV versus film thickness. The lines are guides to the eye.

Table 3.4 gives a survey of important cell parameters obtained from these IV curves plus the EQE values at $\lambda = 505\text{nm}$. The R_{sh} and R_s values were taken from the inverse slopes around 0V and the steeper slope in the 1st quadrant. A rough comparison with the table for LPPPT reveals that both the shunts (R_{sh}) and R_s in MEH-PPV are generally about an order of magnitude higher and V_{oc} by about a factor 6. The dark currents I_d are only slightly smaller than for LPPPT. However, the EQE is reduced by a factor of 2-3 with respect to the ladder type polymer.

These results can be understood if we consider the equivalent circuit diagram ECD - as discussed in Chapter 2 qualitatively: Higher R_s results in lower photocurrents and a large shunt favours higher V_{oc} . The slightly smaller dark currents I_d are also consistent with the higher V_{oc} in MEH-PPV.

In Fig.3.35 we have plotted V_{oc} and dark current versus film thickness. As in LPPPT there seems to be an opposite trend between V_{oc} and I_d : For similar film thickness the V_{oc} is smaller if I_d is higher and *vice versa*.

The series and shunt resistors are plotted versus film thickness in Fig.3.36. As in the LPPPT films we find that the shunt increases much faster

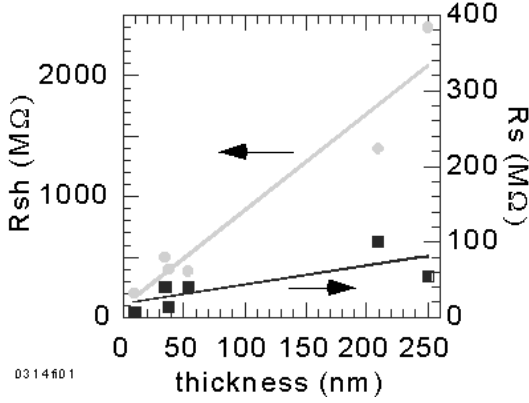


Figure 3.36: Series and shunt resistor versus film thickness in MEH-PPV cells. The lines are linear fits.

(8MΩ/nm) than the series resistor (250kΩ/nm). Considering the average size of $R_s \approx 40\text{M}\Omega$ in MEH-PPV the increase for a device with e.g. polymer film thickness of 100nm is 25MΩ which is about 60% is relatively small.

Very interesting and somewhat surprising is that R_{sh} increases very quickly (350MΩ/nm) and virtually linearly up to a thickness of at least 54nm. The shunts in light and darkness are plotted in Fig.3.38.

However, for larger thicknesses we find consolidation at around 23000MΩ. We note that the differences in dark currents around 0V for the thicker films become less than 1pA which is close to the resolution limit of the source measure unit. Thus the shunts for these two thick films do contain a large relative error and can therefore only give an indication²².

In Chapter 2 we have seen that the ratio R_s/R_{sh} does not only affect the fill factor but also the output current of a solar cell. According to Eq. (2.19) the current through a solar cell is reduced by the factor β

$$\beta = 1 + R_s/R_{sh} \quad (3.13)$$

In Fig.3.37 we have plotted β versus film thickness. The figure shows that - unlike the situation in LPPPT where we found a strong increase for $d < 60\text{nm}$ - β in MEH-PPV is not much different from 1 for thicknesses ranging from 10 to 250nm. Hence, the R_s/R_{sh} ratio is small enough so that

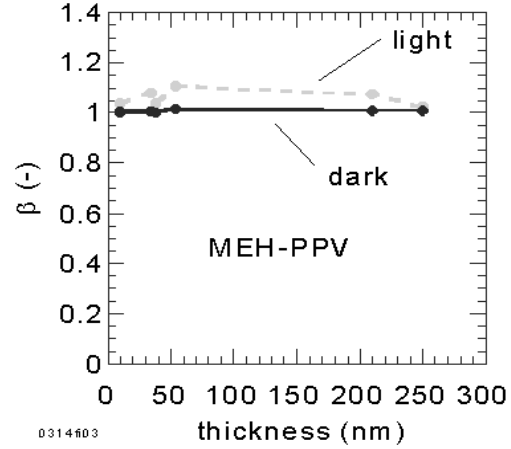


Figure 3.37: Reduction factor β versus film thickness in MEH-PPV under illumination ($\lambda = 550\text{nm}$) and in the dark.

reasonable fill factors should be possible for higher light intensities.

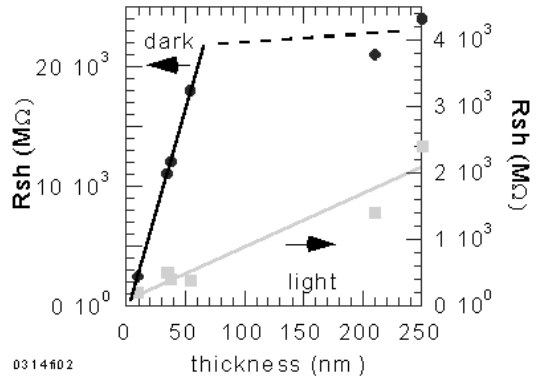


Figure 3.38: Shunt resistor of MEH-PPV devices in the dark and under illumination versus film thickness. The solid lines are linear fits while the dotted line represents a possible saturation.

Fig.3.39 shows again the dark and light characteristics of the ITO/LPPPT/Al device (59nm thick). It also shows the fit with Eq. (2.19) that could be applied for the region -0.4V to 1.2V using the following fit parameters:

1. ideality factor: $n=4.54$

²²Similar considerations could apply for LPPPT and thickness values larger than 120nm.

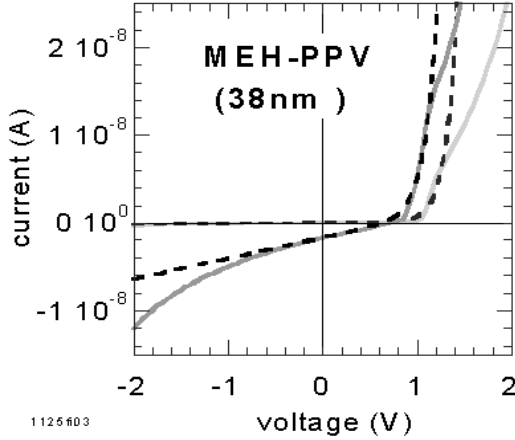


Figure 3.39: Experimental IV curves (solid lines) in the dark and under illumination of a ITO/MEH-PPV/Al device (38nm thick) and fits (dashed lines) using Eq. (2.19).

2. reverse saturation current: $I_0 = 0.7\text{pA}$ (light), $I_0 = 0.1\text{pA}$ (dark)
3. resistors in the dark: $R_{sh} = 1130\text{M}\Omega$, $R_s = 1.3\text{M}\Omega$
4. resistors under illumination: ($0.2\text{mW}/\text{cm}^2$): $R_{sh} = 400\text{M}\Omega$, $R_s = 2.0\text{M}\Omega$ and $I_L = 1720\text{pA}$

Note that the resistor values shown in this list are somewhat different from the values shown in Table 3.4. In the latter the numbers were derived directly by taking the slopes of the characteristics at 0V (R_{sh}) and the highest voltages around 0.9V (R_s) whereas in the former the formalism considered effects of n , I_0 , I_L . The results for the shunt are very similar but the values for R_s are about 10 times larger in the fit.

We consider the numbers for R_s values which are derived from the slope around 0.9V to be more accurate since R_s really starts to dominate only at higher voltages²³.

Note that in contrast to the fit for the LPPPT device we had to choose two *different* values for I_0 in MEH-PPV to obtain a reasonable fit.

According to the discussion on the photoluminescence effects in Chapter 2 we can now take the reverse saturation current I_0 together with the PL ef-

iciency of MEH-PPV of about 13% [63]) we obtain a value for the PL independent component of the reverse saturation current according to Eq. (2.25) - of:

$$I_{01} = I_0 \cdot \Phi_{PL} = 0.7\text{pA} \cdot 0.13 = 0.091\text{pA} \quad (3.14)$$

The value for I_{01} is close to the 0.12pA obtained for LPPPT. Thus, it can not be ruled out here that I_0 depends only or at least predominantly on the PL efficiency. This would then indicate that the maximum performance of both materials LPPPT and MEH-PPV showing the used PL efficiency has been closely approached in these devices.

A more detailed study comprising a higher number of samples and systematic IV analysis is necessary to confirm this possibility and explain the observed variation of V_{oc} with thickness.

Summary

In this Section we have found for MEH-PPV that:

- Thickness is an important parameter. The optimal thickness can be estimated roughly from the absorption spectrum and an antibatic EQE spectrum.
 - The EQE increases from 0.0014% for the thickest (250nm) devices to 0.064% for the thinnest (10nm) device.
 - The highest EQE efficiencies were achieved for the thinnest cells where the optical filter effect has virtually disappeared. Since the entire 10nm layer contributes to the photocurrent - the exciton diffusion length can be at least as high as 10nm in this material - if the polymer/Al interface has to be reached.
- The maximum active layer was estimated to be around $26 \pm 7\text{nm}$ which is an estimate for the upper limit for the exciton diffusion length in MEH-PPV.
- For similar thicknesses devices with lower dark current I_d shows higher open circuit voltages.
 - Both resistors increase with increasing film thickness, but R_{sh} grows more than 30times faster ($8.0\text{M}\Omega/\text{nm}$) than R_s ($250\text{k}\Omega/\text{nm}$) under illumination ($\lambda = 550\text{nm}$, $0.2\text{W}/\text{cm}^2$) for an area of 4mm^2 .
 - The PL efficiency multiplied with the reverse saturation current (0.7pA) gives approximately

²³Unless the IV curve becomes clearly linear for higher voltages the (inverse) slope can only represent a upper limit of R_s - see Chapter 2.

the same number for MEH-PPV (0.091pA) as for LPPPT (0.12pA). This is consistent with a strong correlation between the IV curve i.e the photovoltaic performance and the PL as discussed in Chapter 2 and Ref. [234].

The following observations are in contrast to the findings for LPPPT:

- V_{oc} in MEH-PPV is generally about 6 times higher and V_{oc} also tends to increase with thinner films.
- The *dark current* in MEH-PPV is virtually voltage independent for negative voltages and the thickness range 30 to 250nm. Only the 10nm device shows clear dependence for (negative) bias larger than 0.6V.
- R_s is on average about 15 times smaller than R_{sh} so that the output current reduction factor β is not very different from 1 for all thicknesses.
- The EQE of the thinnest MEH-PPV device follows the main absorption band but increases again in the blue, while the absorption still decreases.

3.4 PTV

With an EQE of about 1% and V_{oc} of 1.2V, PPV has shown some of the highest solar cell parameters for polymers in single layer devices. Unfortunately, the high bandgap ($\approx 2.4\text{eV}$) does not allow sufficient absorption of photons in the visible range. This is not only an obstacle for the application as photo-detector material but also for the use in solar cells.

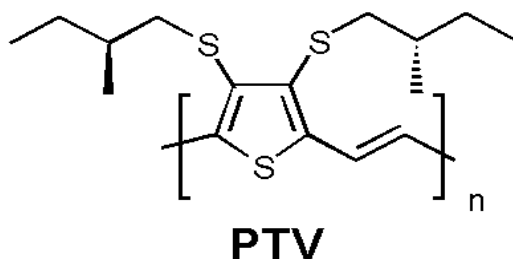


Figure 3.40: Chemical structure of Poly[3,4-bis-(S)-(2-methylbutylthio) thienylenevinylene], PTV. Here $n \approx 120$ (Mn)

With a bandgap of 2.4eV, only about 15% of the solar light on earth could be absorbed in a

very thick film of PTV - see Table 8.3. The introduction of alkoxy substituents could lower the bandgap by about 0.4eV and lead to good solubility in many solvents. One of these derivatives (MEH-PPV) has been investigated in the previous Section and showed broader wavelength sensitivity but otherwise poorer photovoltaic properties than PPV.

In this Section we investigate a molecule where the benzene ring of MEH-PPV is replaced by a thiophene ring and the alkoxy by the stronger electron donating thioalkyl chain. Note that replacement of carbon atoms with sulfur in a conjugated systems generally decreases the bandgap. Thus we obtain a polythiophene (PT) derivative with ethylene linkages PTV - see Fig.3.40.

If we compare PTV with poly-thiophene derivatives, we find that the introduction of ethylene linkages between the thiophene rings should lead to a more rigid structure with less rotational disorder and lower aromatic character²⁴ and therefore higher electron delocalisation. Hence the bandgap should be even lower than in many PTs.

Moreover, the side-chains are chiral and can therefore induce interesting optical properties such as the ability to turn the plane of electromagnetic waves (optical activity) by means of aggregation of the main chains into chiral superstructures. This has already been observed for other semiconducting polymers [156].

Experimental

PTV has been synthesised via the McMurry reductive polymerisation by Francesca Goldoni, University of Technology (Eindhoven, The Netherlands). Details of the synthesis, solvatochromic effects and circular dichroism (a bisignated signal has been observed for this polymer) can be found in Ref.[90, 91]. The molecular weight of the polymer is high but also shows strong polydispersity ($M_n = 38600$, $M_w = 146680$). The number of repeat units can therefore be calculated as 120 (M_n) and 470 (M_w).

The polymer was spincoated from chloroform solution (15mg/ml) onto pre-etched ITO coated quartz substrates with 2000rpm in a laminar flow box.

Absorption and photocurrent measurements were performed in air. More details on the preparation of substrates, devices and the EQE/IV measurements can be found in Chapter 10.

²⁴Directly linked aromatic rings tend to twist

Results and Discussion

Absorption and EQE Spectra

Fig.3.41 shows the EQE spectrum of an ITO/PTV (70nm)/Al device when illuminated through the ITO contact as well as the linear absorption curve. The absorption spectrum shows features of the vibronic structure - similar to the ones observed in solution[90]. The low bandgap suggests well ordered regions with extended conjugation along the polymeric backbone. The onset of absorption is at around 720nm which corresponds to a bandgap of 1.73eV. According to Fig.8.3 a sufficient thick layer of a material with such a bandgap can absorb about 42% of the solar light (ranging from 300 to 720nm).

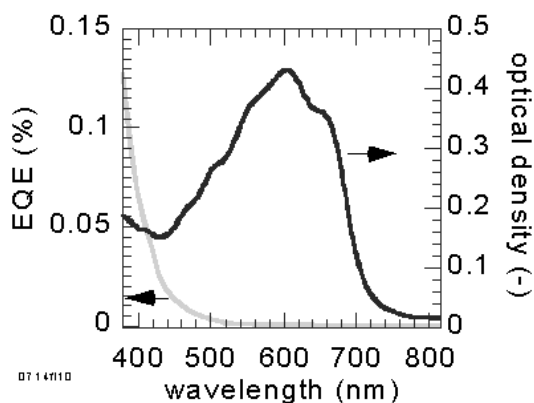


Figure 3.41: The EQE of a 90nm thick PTV device is very low in the main absorption region but reaches values similar to MEH-PPV in the blue range.

The EQE spectrum as shown in Fig.3.41 does not reveal any response in the region of the main absorption band (not even at the absorption onset) but reaches its maximum EQE at around 0.07% around 400nm. This number is very similar to peak EQEs of good single layer materials such as MEH-PPV (see Ref.[196]) or other soluble polythiophenes [202] but clearly lower than the 1% found in PPV [168]. Such a behaviour, neither a symbatic response nor a clear sign of an optical filter effect is rather unusual.

A possible explanation may have to consider the special optical properties (optical activity) due to a chiral superstructure²⁵ or simply be the result of a

²⁵A bisignated circular dichroism spectrum was found for aggregates in solution [90]

combination of two extrinsic charge generation processes such as a photoactive Al/polymer interface and the presence of exciton dissociation sites such as oxygen distributed within the bulk.

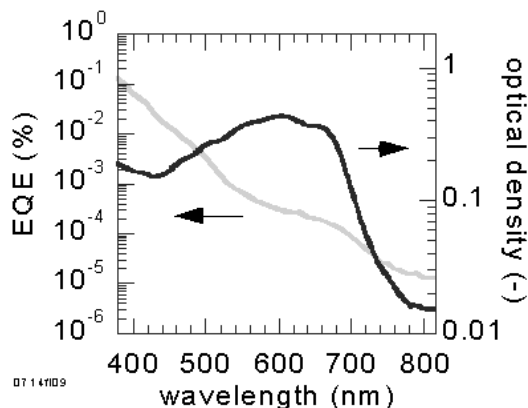


Figure 3.42: The semi logarithmic plot of the EQE spectrum of the same device as in Fig.3.41 reveals that the photoresponse starts in fact with the onset of light absorption and increases nearly by a factor of 10 every 100nm. We found that $EQE \propto \lambda^{-9}$ fits very well for $\lambda > 480\text{nm}$

The EQE plotted on a logarithmic scale - Fig.3.42- reveals a nearly single exponential increase of the EQE starting from the absorption onset at 720nm. The photoresponse covers the full visible range with virtually unequivocally correlated EQE values distributed over 4 orders of magnitude. The photocurrent increases by about an order of magnitude when illuminated with e.g. 500nm instead of 600nm. As a consequence, this device can be used as a colour or wavelength detector for a wavelength range as wide as 400 to 800nm (the full visible range). For comparison: Tada et al. had to use the photoresponse of a thick *and* a thin layer of a poly thiophene derivative (Poly(3-hexylthiophene) to obtain a colour sensor with similar sensitivity but much narrower spectral range (550 and 630nm) [243].

IV Characteristics

The IV characteristics in the dark and under monochromatic illumination (420nm) is shown in Fig.3.43. Even under the low illumination intensity (0.05mW/cm²) the device develops an open circuit voltage of 370mV with a fill factor of $\approx 30\%$.

Another interesting result is that despite the rea-

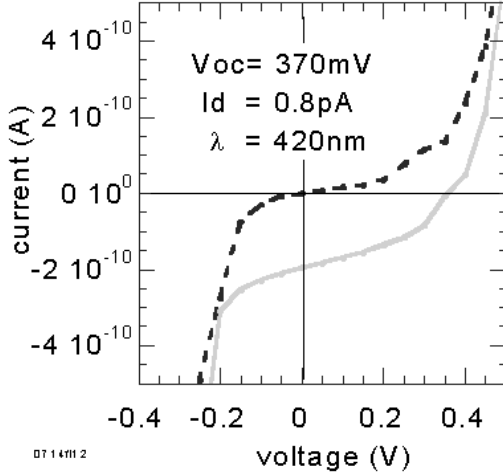


Figure 3.43: IV characteristics of the PTV device in the dark (dashed line) and when illuminated with $\lambda = 420\text{nm}$ (solid line).

sonable V_{oc} and relatively good fill factor, this device shows no strong rectification ratio since there is no clear off state current. It looks more as if a counter-diode has been formed with a even lower breakthrough voltage than in forward bias. This has probably to do with the low bandgap that is more likely to lead to low interface barriers for both forward and reverse bias. From the slopes in Fig.3.43 we have extracted the following resistor values:

- light: $R_s = 200\text{M}\Omega$ and $R_{sh} = 3000\text{M}\Omega$
- dark: $R_s = 200\text{M}\Omega$ and $R_{sh} = 6400\text{M}\Omega$

The series resistor is about 10 times higher than in MEH-PPV or LPPPT - possibly because of the lower light intensity here. A study of R_s as a function of light intensity would be desirable as part of a future project. The smaller difference between the shunt in dark and light compared to LPPPT and MEH-PPV may also be due to the lower illumination intensity here.

We note that the R_s values taken from the first (around 0.45V) or the third quadrant (counter-diode, around -0.25V) are virtually identical.

Fig.3.44 shows a double logarithmic plot of the same IV characteristics as in Fig.3.43. There are two different slopes fitting the dark characteristics in the positive bias voltage range: For voltages up to

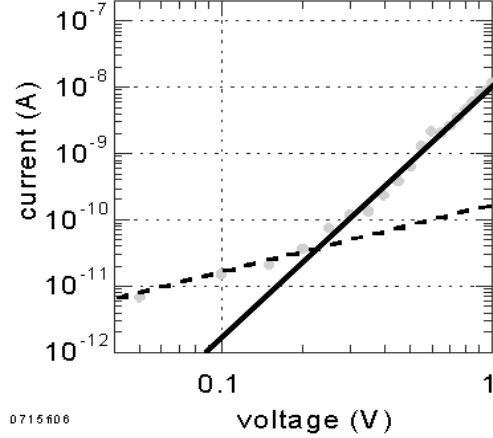


Figure 3.44: A double logarithmic plot of the dark characteristics. Ohm's law seems to fit for lower voltages while the $I \propto V^4$ relation may be due to charges released from deep and/or shallow traps.

0.2V, current and voltage obey Ohm's law of direct proportionality.

For voltages larger than 0.2V up to 1V we find an $I \propto V^4$ relationship. According to the Mott-Gurney equation [138, 231] for trap free space charge limited current the current through the diode obeys:

$$I \propto \frac{V}{d} \quad (3.15)$$

for low voltages and

$$I \propto \frac{V^2}{d^3} \quad (3.16)$$

for high voltages

However, the presence of deep and/or shallow traps can lead to an even stronger dependence in a limited range of V before returning to obey the trap free equations above. The range from 0.2 to 1 V in Fig.3.44 may display the trap dominated region.

Summary

In this Section we have found that:

- A semiconducting polymer with a bandgap as small as 1.76eV can be used to built a ITO/polymer/Al cell.

- The EQE is very low at long wavelengths but very sensitive to the illumination wavelength and obeys $\text{EQE} \propto \lambda^{1/9}$ between 480 to 720nm. This enables direct determination of the wavelength of incident light from the photocurrent using the spectral response curve. Thus, this device can be used as colour sensor covering the full visible range.
- The cell shows a relatively good fill factor for a single layer polymer cell of about 30% with an open circuit voltage of 370mV
- The device shows low breakthrough voltages for both negative and positive voltages. Thus it can be used to amplify positive and negative voltages.
- The EQE reaches 0.07% at 400nm.
- The EQE spectrum is neither antibatic nor symbatic - possibly due to the optical activity in conjunction with a chiral superstructure
- Resistor values derived from the IV curves at 0.05mW/cm² are: $R_s = 200\text{M}\Omega$ and $R_{sh} = 3000\text{M}\Omega$ and in the dark: $R_s = 200\text{M}\Omega$ and $R_{sh} = 6400\text{M}\Omega$

3.5 PIF

Up to now, all polymers that have been discussed in this Chapter can be used as electron donors because of their small ionisation energy i.e. high lying HOMO level. Fig.3.45 shows the chemical structure of a polymer (PIF) that has the potential to be both a low bandgap absorber as well as an electron acceptor with respect to many other polymers.

The short distance between the fairly large repeat units causes a twisting angle of 33° [210]. The distinct twist between the monomer units and the short but bulky side chains allow for plenty of space between the molecules so that it dissolves readily in many common solvents.

Despite the distortion of the conjugated backbone this molecule can still have a very low bandgap thanks to the large π system of the single repeat units. The quinoid character was expected to lead to relatively high electron affinity which would classify this material as an electron acceptor with regard to the majority of other conjugated polymers.

In this Section we will discuss the absorption and photovoltaic properties of ITO/PIF/Al devices.

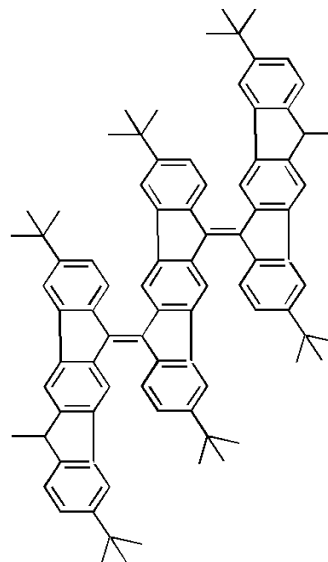


Figure 3.45: Chemical structure of poly indeno fluorene, referred to as PIF. The quinoid character, the large π - system and the bulky side chains make this material a candidate for a low bandgap electron acceptor. $n = 20-25$.

Experimental

PIF has been synthesised by H. Reisch and U. Wiesler at the MPI in Mainz, Germany. Details about the synthesis can be found in Ref. [210]. The polymer was spincoated from chloroform solution (8mg/ml) onto pre-etched ITO coated quartz substrates at 2000rpm in a laminar flow box. Absorption and photocurrent measurements were performed in air. More details on the preparation of substrates, devices and the EQE/IV measurements can be found in Chapter 10. The thickness of the organic layer was about 30nm.

Results and Discussion

Absorption and EQE Spectra

Fig.3.46 shows the absorption spectrum of PIF together with the EQE of an ITO/PIF/Al device (20nm thick). The absorption peak is at 800nm whereas the onset of absorption is around 1100nm which corresponds to a semiconductor bandgap of 1.13eV. A sufficiently thick device of a semiconductor with this material can absorb 77% of the direct solar radiation on earth - see Fig.8.3.

Note that the bandgap is virtually identical to the one of crystalline silicon. Thus, this might be the

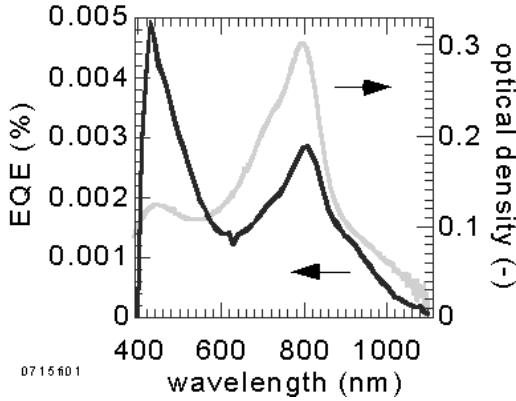


Figure 3.46: EQE and absorption spectrum of a PIF device when illuminated through ITO and measured in air. The whole bulk is active since we observe a symbatic behaviour. The photoresponse covers the same range as commercial silicon photodetectors (400-1100nm)

first photodiode based on a soluble semiconductor that covers the same spectral range as commercial silicon photodiodes. Organic semiconductors with very low bandgaps often lack photo-stability.

However, with this material we did not observe any signs of photo-degradation before or during the measurements where the polymer was exposed to light intensities of up to $0.2\text{mW}/\text{cm}^2$ for several minutes in air. Although these intensities are still relatively low, the device was working and could serve, for example, as photo-detector at such intensities.

The EQE spectrum closely follows the absorption indicating that the entire bulk contributes to the photocurrent. The absolute EQE numbers (0.003% at 800nm), however, are about an order of magnitude lower than in e.g. MEH-PPV.

A semi logarithmic plot - see Fig.3.47 - confirms that the photoresponse coincides very well not only with the peaks but also with the onset of absorption. The EQE is again higher for the shorter wavelengths. We want to note here that the error of the EQE spectrum between 400 and 500nm can be as high as $\pm 50\%$. This is because the signal to noise ratio is very low due to the low emission intensity of the QTH-lamp and the low EQE of PIF in this region.

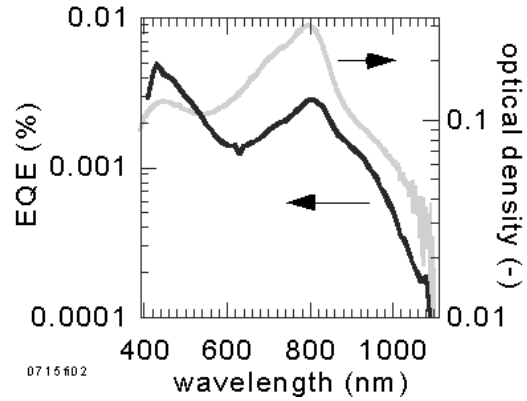


Figure 3.47: The semi logarithmic plot of the same data as in Fig.3.46 shows that absorption and EQE are very much “in phase” even at the onset at 1100nm

IV Characteristics

The dark and light characteristics of the same PIF device are shown in Fig.3.48. Despite a significant I_{sc} , there is neither a significant V_{oc} nor a reasonable rectification ratio. Both the dark and the light characteristics appear almost symmetrical and on top of each other at the scale shown.

Note that the current through this device is about 10 times higher than in MEH-PPV so that the slope around 0V is actually very steep i.e. the material is very conductive already without applying a voltage. Thus, the relatively few photogenerated charge carriers cannot change the shape of the dark characteristic significantly.

From the slopes in Fig.3.49 we have extracted the following resistor values:

- light: $R_s = 1.7\text{M}\Omega$, $R_s = 5.7\text{M}\Omega$ (negative voltage range) and $R_{sh} = 66\text{M}\Omega$
- dark: $R_s = 1.7\text{M}\Omega$, $R_s = 5.7\text{M}\Omega$ (negative voltage range) and $R_{sh} = 83\text{M}\Omega$

Note that according to the discussion in Chapter 2 all R_s values obtained from the slope in the IV curve can only represent *upper limits*. The values are considerably smaller than in e.g. MEH-PPV which may indicate either partial shorts due to pin-holes or high conductivity due to dopants or rather low barriers in the pathway of the charges. The lack of a reasonable V_{oc} is most likely related to the low shunt resistor.

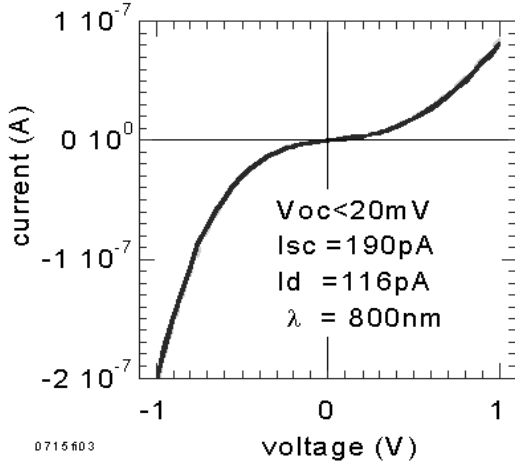


Figure 3.48: IV characteristics of the PIF device (32nm thick). Dark and light curve coincide on this scale. The device was illuminated at $\lambda=800\text{nm}$

The extraordinary low bandgap among today's polymers (1.13eV) may well lead to low electrode/polymer - interface barriers for both injection and extraction of charges and therefore lead to the formation of a counter-diode as in the low bandgap polymer PTV. Such a steep slope with a low V_{oc} seems to occur more often in electron transport materials particularly if they have a low bandgap [150, 64].

In Fig.3.49 we plotted the dark curve of Fig.3.48 on a double logarithmic scale. The IV curve follows the Mott-Gurney equation (Child's Law) for trap free materials ($I \propto V^2$) between 0.1 and 1V.

Summary

In this Section we have found that:

- The conjugated polymer PIF with a bandgap as low as 1.13eV can be used to manufacture a photovoltaic cell with a photoresponse covering the same range as a commercial crystalline silicon based solar cells.
- The EQE of this material reaches 0.003% at its absorption peak (800nm)
- There is only little rectification and a negligible V_{oc} (smaller 20meV) - most likely due to the low shunt resistor.
- Resistor values derived from the IV curves at $0.2\text{mW}/\text{cm}^2$ and $\lambda = 800\text{nm}$ are: $R_s =$

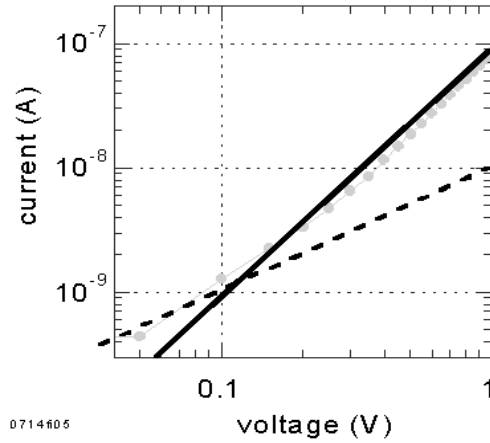


Figure 3.49: The IV curve (filled circles) fits the Mott and Gurney equation (Child's law) for trap free materials ($I \propto V^2$, solid line) and shows no ohmic behaviour as expected for such low voltages ($I \propto V$, dashed line). There are also no clear signs for deep or shallow traps. The steep slope i.e. strong voltage dependence of the current around 0V seems to occur more often in electron transport materials.

$1.7\text{M}\Omega, R_s = 5.7\text{M}\Omega$ (negative voltage range) and $R_{sh} = 66\text{M}\Omega$ and in the dark: $R_s = 1.7\text{M}\Omega, R_s = 5.7\text{M}\Omega$ (negative voltage range) and $R_{sh} = 83\text{M}\Omega$

- Child's law for trap free materials fits the IV characteristics between 0.1 and 1V

3.6 THPF

In this Section we are going to investigate a polymer with a molecular structure which has a number of interesting peculiarities - see Fig.3.50: A dialkoxy substituted phenylene ring is coupled via a triple bond to a thiophene with a pyrazine fused to it. Moreover, two fluoro substituted phenylene rings extend the the conjugated system further.

The triple bond does not break the conjugation in these poly-yne²⁶; in fact, *extended* conjugation has been found in both organic and organo-metallic poly-yne [142]. The large and electron rich π system should be reasonably flat and therefore result in a particular low bandgap - see below.

²⁶The term -yne denotes the triple bond.

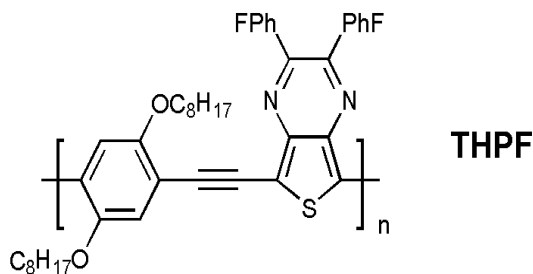


Figure 3.50: Chemical structure of the polymer THPF used in this Chapter. $n \approx 22$

In addition, the introduction of the fluoro substituted phenylene could increase the electron affinity significantly and make it - together with the low bandgap - an interesting candidate as electron acceptor in D/A solar cells. However, the spatial separation from the thieno-pyrazine via the phenylene could weaken their effect to some extent.

From the comparison with a derivative that lacks the fluor atoms, we know that their effect on e.g. the bandgap is negligible - which is consistent with the findings for MEH-PPV and its cyano substituted analogue²⁷.

In any case, low bandgap acceptor materials are particularly promising for the use in D/A solar cells but still very hard to find among polymeric semiconductors. More information on organic and organo-metallic poly-ynes can be found in Refs. [141, 146, 147, 184].

Experimental

THPF has been provided and synthesised by M. Khan, University Chemical Laboratory (Cambridge, UK). Details of the synthesis can be found in Ref. [143]. The polymer was spincoated from chloroform solution (16mg/ml) onto pre-etched ITO coated quartz substrates with 2000rpm in a laminar flow box.

Absorption and photocurrent measurements were performed in air. More details on substrate, device preparation and the EQE/IV measurements can be found in Chapter 10.

²⁷Cyano (CN) groups are like fluor atoms strong electron withdrawing and therefore often used to increase the electron affinity of an organic compound.

Results and Discussion

Absorption and EQE Spectra

Fig.3.52 shows the linear absorption spectrum together with the EQE spectrum of a 110nm thick ITO/THPF/Al cell. The onset of absorption is at 720nm (1.72eV). A sufficiently thick layer with this bandgap can absorb about 48% of the direct solar radiation on earth - see Fig.8.3. The absorption spectrum shows a dominant peak at 620nm and a shoulder at 680nm.

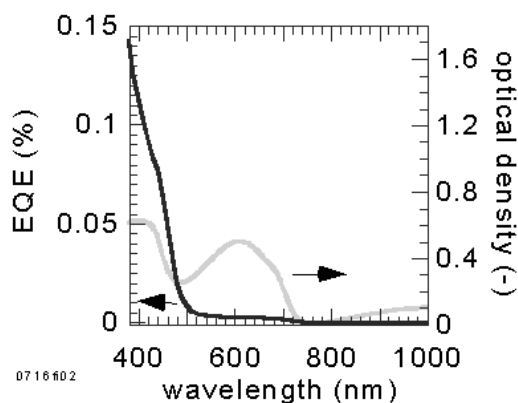


Figure 3.51: The EQE of an ITO/THPF/Al device reaches 0.15% around 400nm. However, in the main absorption range (500-700nm) the efficiency is only 0.003% which is an order of magnitude lower than in analogous MEH-PPV cells.

The EQE exceeds values of 0.1% at 400nm which is more than twice as much as typical MEH-PPV devices. The shape as well as the absolute numbers with the considerably high peak EQE around 400nm resemble the EQE spectrum found in the PTV device. Note that in both materials the EQE in the main absorption band is considerably lower than near 400nm.

Unlike the results in PTV devices, the semi logarithmic plot - see Fig.3.51 - shows no exponential dependence on the wavelength for THPF. The plateau around 600nm makes an application as colour sensor clearly more difficult. In addition, the shoulder in the EQE curve at 700nm might indicate the presence of the optical filter effect.

IV Characteristics

The IV characteristics of the same device is shown in Fig.3.53. The IV curves show ohmic

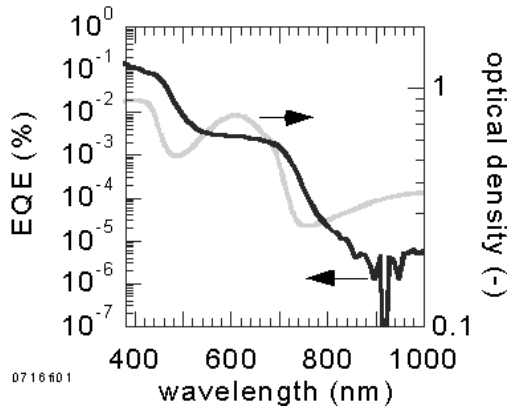


Figure 3.52: A semi logarithmic plot of the EQE spectrum in Fig.3.52 reveals that the EQE follows the absorption - although some signs of an internal filter effect are visible.

behaviour between -1 and +1V but develop a reasonable open circuit voltage of 600mV (at $\lambda = 552\text{nm}$, $0.2\text{mW}/\text{cm}^2$) and 700mV (at $\lambda = 440\text{nm}$, $0.06\text{mW}/\text{cm}^2$). We can also see that the EQE can be doubled by increasing the reverse bias voltage by 1V.

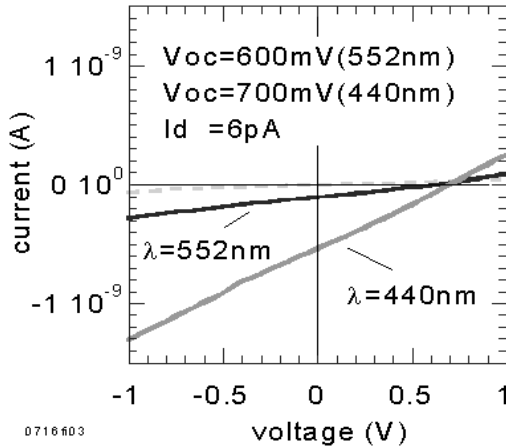


Figure 3.53: IV dark (dashed line) and light characteristics (solid lines - shown here for two excitation wavelengths) of the THPF device. The behaviour is ohmic.

From the slopes in Fig.3.53 we have extracted the following resistor values:

- light: $R_s < 6300\text{M}\Omega$ ($\lambda = 552\text{nm}$), $R_s < 1400\text{M}\Omega$ ($\lambda = 440\text{nm}$) and $R_{sh} = 6300\text{M}\Omega$ ($\lambda = 552\text{nm}$), $R_{sh} = 1400\text{M}\Omega$ ($\lambda = 440\text{nm}$)
- dark: $R_s < 17000\text{M}\Omega$ and $R_{sh} = 17000\text{M}\Omega$

Note that according to the discussion in Chapter 2 all R_s values obtained from the slope in the IV curve can only represent *upper limits*. This is particularly important here since the voltage range is probably not large enough to exceed the onset of the diode breakthrough voltage - so that both the shunt and the series resistors are equal here. However, R_s could be considerably smaller.

The values are somewhat higher than in e.g. MEH-PPV which indicates the absence of significant shorts through pinholes and thus account for the good open circuit voltage.

Note that the shunt (and the upper limit for R_s) at the wavelength with the lower light intensity is almost 5 times smaller as is the short circuit current. Considering that the OD for the two wavelengths is roughly the same (0.51 at 440nm and 0.37 at 552nm) the higher conductivity at lower light intensity is rather surprising.

However, the unusually big difference between the EQE in the main absorption and around 400nm suggests that there may be other wavelength dependent effects dominating. This would require further investigation preferably involving light intensity dependent EQE/IV for different wavelengths in future studies.

Summary

In this Section we have found for ITO/THPF/Al devices:

- The EQE is relatively low (0.003%) in the main absorption band (500-700nm) but reaches more than 0.1% around 400nm.
- The photo-responsive range covers a broad wavelength range (400 to 800nm).
- A relatively high open circuit voltage of up to 700mV.
- The EQE can be doubled by applying a reverse bias voltage of 1V.
- Resistor values derived from the IV curves at $0.2\text{mW}/\text{cm}^2$ and $\lambda = 552\text{nm}$ are: $R_s < 6300\text{M}\Omega$ and $R_{sh} = 6300\text{M}\Omega$ and in the dark: $R_s < 17000\text{M}\Omega$ and $R_{sh} = 17000\text{M}\Omega$

3.7 Per

The most frequently used perylene pigments are diimides and bis imidazoles of perylene-3,4,9,10-tetracarboxylic acid. They show good light and water fastnesses and are best known for their use as colourants for automobile paints and plastics.

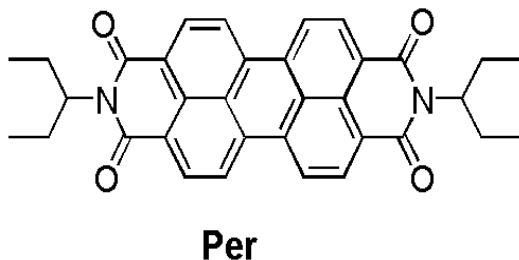


Figure 3.54: Chemical structure of the soluble perylene diimide (Per) used in this Section.

Also photo-conducting properties of perylenes have been recognized as early as 1972 when Regensburger and Jakubowski studied the xerographic behaviour of a number of perylenes in bi-layer devices[218]. Their motivation to investigate these molecules were likely driven by the fact that many perylene diimides are strongly absorbing in nearly the entire visible range and that they were available. We note that perylene bis-imidazole absorb at longer wavelengths relative to those of perylene diimide due to the extended π -conjugation[154].

Later it was discovered that charge separation in perylenes primarily takes place at an interface with a hole accepting molecule unless the exciton decays non-radiatively to the ground state [154], [244].

Furthermore, it has been found that the photo-sensitivity of perylenes is higher, the more planar the molecule is [154].

The following formulation can be found in claim 17 of Chin Tang's Patent on a multi-layer organic photovoltaic device which underlines the importance of size²⁸ and planarity of photovoltaic molecules *in general* - not only perylene derivatives [245]: "...materials comprising a compound containing a generally planar polycyclic nucleus having a surface area of at least about 40 square Å and a width of at least about 5 Å." In this basic patent he also mentions that *electron-acceptor compounds* should have at least 7 aromatic rings and 8 for elec-

tron donors to avoid shorts due to pinholes in the about 40 to 50nm thin films.

Following these guidelines, he managed to fabricate one of the best organic solar cells until today using a double layer comprising two large and flat aromatic molecules such as a perylene bis-imidazole together with a copper phthalocyanine [244].

Interestingly at least one device in the patent was even better than in Ref. [244]: A NESATRON²⁹/diimide-perylene/Ag device with V_{oc} =440mV, I_{sc} = 3.0V, FF = 0.6 and a power conversion efficiency as high as 1.0% under AM2 conditions. The particular diimide perylene used in this cell had a phenyl ring coupled to both nitrogen atoms.

However, in order to fabricate thin film solar cells with pigments, energy intensive and expensive thermal sublimation has to be employed since their solubility in common solvents is very low.

Only very recently (1998), chemists at Xerox have found a method to process many heterocyclic pigment classes from *solution* to facilitate cheaper manufacturing [283]. In this Lewis-acid pigment solubilisation (LAPS) process, the pigments are mixed with a solution of a Lewis-acid in nitromethane. The solubilisation involves coordination of the acid with the pigment molecules' hetero atoms to form a soluble electron donor-acceptor complex which is later removed by washing. Unfortunately this method does not work for all pigments and the acid might attack the pigment and/or the electrode material causing other complications.

In this Section we investigate a photovoltaic cell using a perylene derivative (a dye) that allows for simple processing via spincoating from solution. Other soluble perylenes have been reported, most of which also exhibit photoluminescence efficiencies around 100% in solution [69].

We note that in the meanwhile also soluble perylene containing *polymers* are available [217]. One has already been employed successfully in LED structures to produce white light by means of excitation energy and charge transfer from a blue emitting ladder type polymer in a blend [246].

Experimental

The perylene dye has been purchased from Synthec (Germany). Details of the synthesis can be found in Ref.[60]. The polymer was spin-coated from chloroform solution (8mg/ml)³⁰ onto pre-etched ITO

²⁹NESATRON is a trademark for a material with similar properties as ITO - mainly used in the 1970s

³⁰According to Ref [60] up to 70mg(!) can be dissolved in 1ml.

²⁸The actual perylene structure (4 aromatic rings fused together around a central ring) measures about 7x6Å

coated quartz substrates with 2000rpm in a laminar flow box.

We obtained very tractile films of reasonable thickness (about 100nm) - with no spin marks but the surface appeared rough in contrast to the shiny surface of e.g. MEH-PPV films. Absorption and photocurrent measurements were performed in air. More information on sample and device preparation can be found in Chapter 10.

Results and Discussion

Absorption and EQE Spectra

Fig.3.55 shows the EQE spectrum of a 40nm thick ITO/Per/Al cell when illuminated through the ITO as well as the linear absorption curve. We find virtually no antibatic behaviour so that the two main features can be found in both spectra: A dominant peak at 495nm and another peak at 540nm. In addition, the EQE reveals another local maximum at 370nm.

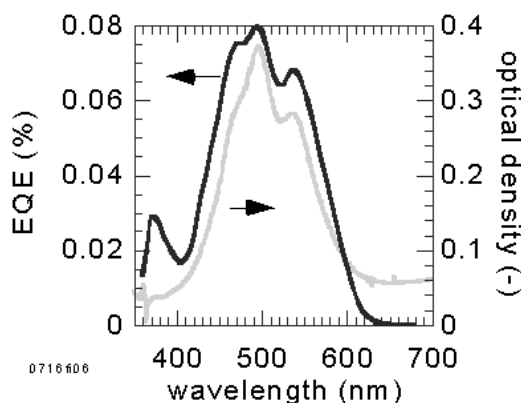


Figure 3.55: The EQE of this Per device follows the absorption spectrum closely reaching numbers comparable to MEH-PPV but covering a larger spectral range.

The lack of an optical filter effect upon illumination through ITO in this 40nm thick device is consistent with the assumption that perylene can be regarded as n-type semiconductor: N-type semiconductors form an rectifying i.e. active interface with ITO rather than Al which is expected to result in a symbatic EQE spectrum when illuminated through ITO - regardless of the actual exciton diffusion length.

Further confirmation of the n-type nature of this particular organic dye could be obtained from field

effect measurements following the argumentation in Ref. [134]. In the same reference a very similar perylene diimide has been classified as n-type semiconductor by means of the symbatic response³¹ and field-effect-transistor IV curves.

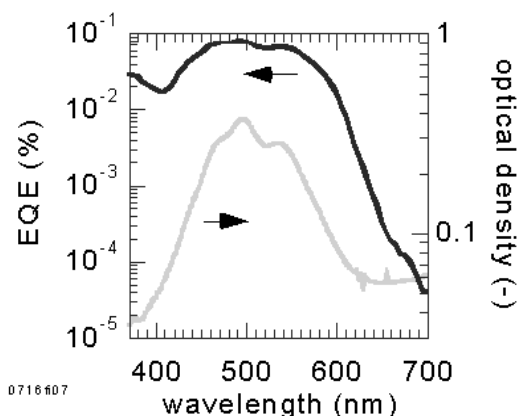


Figure 3.56: The semi logarithmic plot of the data in Fig.3.55 reveals an onset of the photoresponse even before the onset of absorption (as determined by our absorption setup). Photo-thermal deflection (PDS) measurements may be useful to investigate this further.

The EQE reaches about 0.08% which is about twice as high as MEH-PPV cells with the same thickness. This is still between one and two orders of magnitude smaller than the values for perylene diimide *pigments* published in Ref. [245]. Thus, the same side chains that facilitate solubility prevent the molecules from close packing as in pigment films. Hence, strong inter molecular interaction seems to favour efficient charge transport and/or exciton generation.

The logarithmic plot in Fig.3.56 reveals that the onset of the EQE spectrum does not exactly coincide with the onset in the absorption at 620nm. Significant photoresponse can already be found at about 700nm. Photoresponse before the absorption onset has also been found in THPF - earlier in this Chapter. Both materials have electron withdrawing groups that are expected to lower the LUMO to make them stronger electron acceptors - see also Chapter 2.

³¹when illuminated through SnO₂

IV Characteristics

The light and dark characteristics of this device is shown in Fig.3.57. We found very large currents indicating high conductivity and a rectification ratio of about 20 at $\pm 1V$. Note that similar to the previously described PTV and PIF devices there is a relatively small negative breakthrough voltage indicating the presence of a counter-diode.

From the slopes in Fig.3.57 we have extracted the following resistor values:

- light: $R_s = 0.9M\Omega$ and $R_{sh} = 50M\Omega$
- dark: $R_s = 0.9M\Omega$ and $R_{sh} = 60M\Omega$

Both the series and the shunt resistors are more than an order of magnitude smaller than in e.g. MEH-PPV or LPPPT. This would probably account for the relatively small V_{oc} and the high positive dark current. The value for the series resistor has been taken from the slope in the negative voltage range - since the slope there is smaller than the one in forward bias representing the “lower” upper limit for R_s .

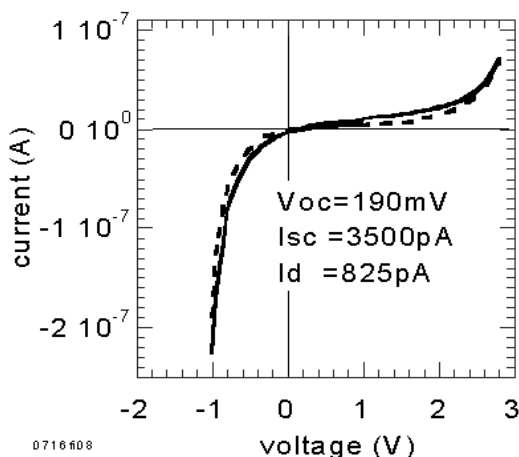


Figure 3.57: IV dark (dashed line) and light ($\lambda = 550nm$, solid line) characteristics of the Per device. A clear rectification for voltages above 1V is observed.

We note that the formation of crystals has been observed in Per/P3HT blends but also to a smaller extent in single layers [62, 63]. Crystal formation is a known problem with dye films and can lead to pinholes and partial shorts - which might be - at

least partly - responsible for the high conductivity here.

In addition, the dark and the light characteristics have similar shapes even in the negative bias region. This means that the EQE cannot be increased by increasing the negative bias voltage as in MEH-PPV or THPF. Note that photocurrent multiplication as large as 10 000 times has been observed in other perylene diimides sandwiched between Au electrodes [133].

Summary

In this Section we have found that:

- A soluble perylene (Per) derivative can be used to fabricate an ITO/Per/Al solar cell from solution avoiding the usual high temperature sublimation steps hitherto used for perylene derivatives.
- The EQE reaches up to 0.08% which is twice as much as comparable MEH-PPV devices but 10 to 100 times less than the best pigment devices. Hence, compact packing of molecules (as with pigments or using the LAPS method) seems to be required to obtain the best efficiencies.
- The Per/ITO interface is the “active” interface which is consistent with the n-type semiconducting properties of other known perylene derivatives.
- The V_{oc} (190mV) of the dye device is somewhat smaller than in pigment devices (280-530mV) - although different illumination conditions and electrode material have to be considered.
- The EQE onset appears to be significantly before the absorption onset which requires further clarification in future studies.
- A counter-diode has been formed similar to PTV and PIF devices.
- Resistor values obtained from the slopes in the IV curves are:
 - light: $R_s = 0.9M\Omega$ and $R_{sh} = 50M\Omega$
 - dark: $R_s = 0.9M\Omega$ and $R_{sh} = 60M\Omega$

3.8 Ter

As we have mentioned earlier, there is some evidence that large polycyclic aromatic hydrocarbons

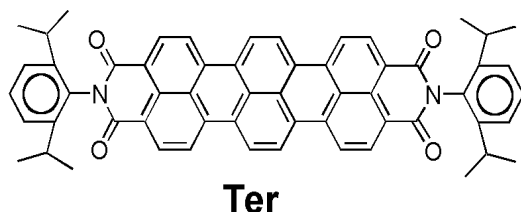


Figure 3.58: Chemical structure of the soluble terrylene derivative, Ter, investigated in this Section.

are likely to give good photovoltaic conversion efficiencies - see e.g. Ref. [245].

The reason for that may be found in the possibility of a more compact arrangement of the molecules in the thin films that leads to the following list of advantages:

- The relatively undisturbed π system of planar molecules favours exciton and charge transport as well as a low bandgap.
- The higher molecular density makes the occurrence of pinholes i.e. shorts more unlikely.
- The higher concentration of π - electrons per unit volume increases the absorption coefficient.

Well-known examples for large polycyclic aromatic hydro-carbons are phthalocyanines and perylenes. The “pure” perylene structure can be regarded as two peri-condensed naphthalene compounds. Theoretically three or more naphthalene compounds can be condensed together to form a series of oligo-rylenes leading to a rylene-polymer. Such a polymer i.e. large rylene should have a vanishing bandgap indicating the possibility of intrinsic electrical conductivity (metallic behaviour) according to theoretical predictions - see Ref. [145] and references therein. In fact a decreasing bandgap has been found for a series of increasing rylene units: terrylene ($\approx 620\text{nm}$ or 2.02eV), quaterrylene ($\approx 800\text{nm}$ or 1.58eV) and pentarylene ($\approx 950\text{nm}$ or 1.32eV) [145].

The cited bandgaps have been obtained for thin films after thermal sublimation. These oligo-rylenes were also amenable to spectroscopic measurements in solution (1,4 dioxane) thanks to substitution with four *tert*-butyl side chains [145].

We note that such a terrylene derivative has played an important role in nano-science where single molecule spectroscopy was possible even at room

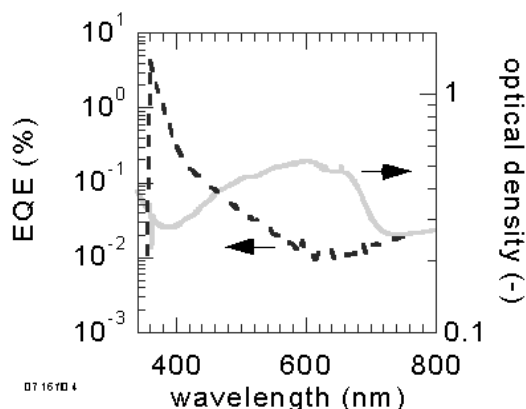


Figure 3.59: The EQE of a Ter-device shows a very broad spectral response (UV to near IR) reaching high numbers in the short wavelengths range (around 1%).

temperature [153, 71]. In the foreseeable future, the application of, for example, heat to a single molecule and thereby the initiation of an optically detectable chemical reaction affecting the PL of a single molecule may lead to optical data storage on a molecular scale.

In this Section we investigate the photovoltaic properties of this well soluble terrylene diimide derivative as active material between ITO and Al.

Experimental

The terrylene has been synthesised by Stefan Becker at the Max Planck Institut (Mainz, Germany). Details of the synthesis can be found in Ref. [16].

The polymer was spin-coated from chloroform solution (6mg/ml) onto pre-etched ITO coated quartz substrates with 1600rpm in a laminar flow box. We note that the solubility ($< 1\text{mg/ml}$ in Chloroform) of the *quaterrylene* of the same series (same side-chains) was not sufficient to produce continuous films via spincoating.

Absorption and photocurrent measurements were performed in air. More details about the sample i.e. device preparation and the IV/EQE measurements can be found in Ref. Chapter 10.

Results and Discussion

Absorption and EQE Spectra

Fig.3.59 shows the EQE spectrum of an ITO/Ter ($\approx 15\text{nm}$ thick) /Al cell when illuminated through

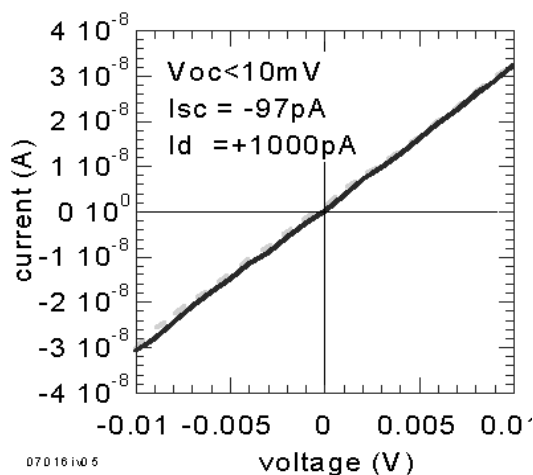


Figure 3.60: The IV dark (dashed line) and light (solid line, $\lambda = 650\text{nm}$, $0.28\text{mW}/\text{cm}^2$) characteristics of this Ter device could only be recorded for a very small voltage range due to the steep slope i.e. high conductivity ($330\text{k}\Omega$).

the ITO as well as the linear absorption curve. The absorption spectrum of the Ter film is very broad (410 to 700nm) and featureless apart from a little dip at 630nm.

The EQE spectrum resembles the spectrum observed in PTV with no clear antibatic peak in the absorption onset but reaching the highest EQE in the UV range with the local absorption minimum. In fact the EQE is surprisingly high for a single layer cell with values above 0.01% throughout the visible spectrum reaching about 4% in the UV.

However, since the IV curve suggests a very conducting and/or strongly pinhole dominated and therefore partly shorted film, we have to take into account that the EQE might be affected here by small fluctuations in the voltage applied by the source measure unit. For example, a voltage change of 1mV can lead to an increase of current of 3nA equivalent to change in EQE of nearly 1% here.

Generally, both the HOMO and the LUMO is expected to become lower with increasing π system i.e. the terrylene should be a better electron acceptor than the perylene.

IV Characteristics

The light and dark characteristics of this device is shown in Fig.3.60. The very steep slope that should represent the shunt resistor (here only $330\text{k}\Omega$) sug-

gests that the device is considerably shorted via pinholes in the only 15nm thin film. This is not surprising considering the observations of crystal formation even to a larger extent than in previously investigated related molecule Per [64]. The partial shorts would also explain the lack of a detectable open circuit voltage 10mV.

However, upon illumination the current at 0V changes from +1000pA to -97pA. The positive dark current is most likely an artifact related to a slight ground potential of the source measure unit. Note that an offset of only 1mV would change the current by about 3nA here. IV curves with very high conductivities and small open circuit voltages tend to be observed more often in electron conductors like PIF and others [150, 64].

Summary

In this Section we have found that:

- A soluble terrylene derivative can be used to produce a photocurrent. The EQE around 500nm is even in the same order of magnitude as in e.g MEH-PPV reaching higher values of up to 1% around 400nm.

However, since we could not obtain a detectable V_{oc} we believe the device performance may be affected by local shorts due to the formation of crystals causing a resistance of only about $900\text{k}\Omega$. As a consequence, the IV and EQE characteristics of this particular device have therefore to be interpreted with caution.

3.9 Single Layer Devices - Summary

In Table 3.5 we have listed the most important solar cell parameters for the different organic semiconductors investigated in this Chapter. Many of these materials will be investigated further in blend and/or double layer devices in the subsequent Chapters.

Where possible, we have chosen a device with a “typical” characteristic. The EQE value of the Ter device has to be treated with caution since the device showed non-ideal IV and EQE characteristics.

The list shows that only devices with shunt resistors above $100\text{M}\Omega$ and dark currents under 30pA do develop a V_{oc} larger than about 200mV. We also have to consider that the values for R_s are only *upper limits* and that the actual values could be considerably smaller.

Table 3.5: Survey of photovoltaic parameters of the investigated organic semiconductors. The number in brackets are obtained from the dark characteristics. d stands for the thickness of the organic layer. EQE values were taken at peak wavelength.

material	d	EQE	V_{oc}	I_d	R_{sh}	R_s	comment
–	nm	$10^{-3}\%$	mV	pA	$M\Omega$	$M\Omega$	–
Ter	15	4000	0	1000	0.9(0.9)	0.9(0.9)	dye
THPF	110	100	600	6	6300(17000)	6300(17000)	polymer
LPPPT	59	85	105	31	83(200)	7.5(11)	polymer
Per	40	80	190	825	50(60)	0.9(0.9)	dye
PTV	90	70	370	0.8	3000(6400)	200(200)	polymer
MEH-PPV	35	45	730	14	500(11000)	40(74)	polymer
PIF	30	3	0	116	66(83)	1.7(1.7)	polymer

Hence, a suspected correlation of the EQE with the series resistor or the ratios between R_s and R_{sh} cannot be ruled out here.

The list also reveals that both polymers and dyes give peak EQE values of approximately the same size ranging from 0.04 to 0.10% - with MEH-PPV being near the lower end in terms of the photo-current but on the high end with respect to the open circuit voltage.

Chapter 4

Double Layer Devices

4.1 Introduction

In the previous Chapter we have found that the main losses in single layer structures are due to short exciton diffusion lengths and recombination of the excited charge carriers. The short exciton diffusion length causes a very thin active region of the device whereas recombination losses before and after charge separation can reduce the shunt resistor considerably.

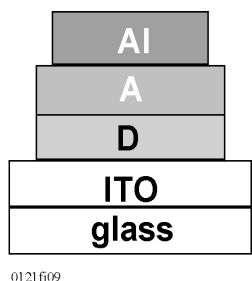


Figure 4.1: Device architecture of a double layer photovoltaic cell. The electron acceptor A and electron donor D are sandwiched between the transparent ITO contact and an Al layer.

With the introduction of an electron acceptor layer between the active material and the negative electrode (Al), both the exciton diffusion range and the poor shunt resistor can be improved - see Fig.4.1.

Provided the offset between the HOMO and LUMO levels of both materials upon contact are sufficient to split excitons, the separated charges can travel to the respective electrode with very small chances of meeting a recombination partner. The active region is now extended to the exciton diffusion length of *both* materials.

Moreover, the use of two different semiconduc-

tors allows tuning of the absorption spectrum for e.g. maximum coverage of the spectrum of the light source. The latter is not only desired for optical photodetectors but also essential if high solar cell efficiencies are required.

In fact, absorption of photons from 300 to 1000nm is required to utilise 70% of the solar radiation on earth. Only about 22% of the solar radiation can be exploited with a single layer material like MEH-PPV.

One of the first organic double layer solar cells is the one reported by Tang in 1985 [244]. He sublimed two pigment films, a copper phthalocyanine and a perylene derivative on top of each other, sandwiched between an ITO and Ag contact, and obtained one of the hitherto most efficient organic photovoltaic devices. The separation of the charge carriers resulted in a higher shunt and low series resistor such that the fillfactor was comparable to commercial Si photodiodes.

Since the absorption of the perylene derivative and the Cu-phthalocyanine complement each other very well, the device showed a good EQE over the full visible range. The open circuit voltage at AM1.5 condition ($75\text{mW}/\text{cm}^2$) was 450mV.

Although a rough similarity to the P/N junction in inorganic solar cells can often be drawn, care has to be taken using such comparison. However, in both cases *equalisation* of the Fermi-levels occurs at the interfaces between semiconductors and/or metals. In both organic and inorganic solar cells the equalisation of Fermi levels leads to a significant potential gradient that can drive the photoexcited charge carriers (minority carriers) through the rest of the bulk towards the electrodes.

However, as discussed in Chapter 2 the nature of *doping* in *organic* semiconductors can be very different from the usual doping in inorganic materials. Although, the Fermi-levels are still important the offset of the valence band (VB) and conduction

band (CB) at the interface after equalisation of the Fermi-levels is a crucial factor for the function of these devices. This is largely because there are excitons in organic devices that need to be split at the first place.

Thus, a device with sufficient VB/CB offset can split excitons and separate charges efficiently if both materials are e.g. p-type conductors. As a consequence, it is more appropriate to speak about a D/A -rather than P/N junction in case of organic solar cells. Note that the term *heterojunction* is also found in the literature but we prefer D/A junction in this thesis since a junction between two different semiconductors does not necessarily lead to the required splitting of the excitons.

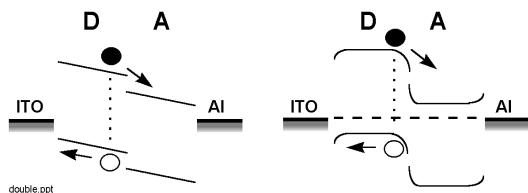


Figure 4.2: Band energy diagrams for a D/A double layer device in short circuit mode. Left: the built-in field due to ΔW_f of the electrodes leads to tilted bands if only few free charge carriers are present. Right: For higher charge carrier concentration the bands can remain flat in the bulk but blocking contacts may be formed

The figure on the left in Fig.4.2 shows the band energy diagram for a double layer device with a low concentration of free charge carriers. The difference of workfunctions of the electrodes ΔW_f can cause the bands to tilt, as shown, which creates a constant field across the bulk. Although band bending at the electrodes can still occur, it may be considered insignificant in such devices¹.

The figure on the right in Fig.4.2 shows the situation for a device with a concentration of free charge carriers that is high enough to compensate the built-in field due to the electrode workfunctions within a fraction of the layer thickness. As a consequence, accumulation and depletion of charges near the electrodes can cause distinct band bending².

According to this picture the driving force i.e.

V_{oc} is mainly determined by the offset at the D/A junction although the increased built-in field (tilted bands) can help to transport charges through the bulk [223].

In Table 4.1 we have listed D/A double layer devices from the literature. The device with * has been measured at only 0.015 mW/cm^2 so that significantly higher values for V_{oc} may be achieved if measured under intensities in the order of 0.5 mW/cm^2 .

The table shows that the highest efficiencies have been achieved with insoluble molecules (pigments). Pigments have been successfully used as photo-receptors and charge transport media in colour copying machines and related devices (Xerography) replacing many inorganic materials³.

However, the prospect of easier processing by e.g. spin or blade coating from non-acidic solution⁴, lamination or even inkjet printing, makes soluble molecules technologically more interesting. The table also shows that technically pigments can *already* be replaced by polymers, dyes and even liquid crystals but at the expense of lower efficiency.

We note that only recently, a modification of the double layer device, the laminated device structure (see Chapter 6), allowed semiconducting polymers to exceed in performance values for the best pigment devices [94].

Both Pcs and Per pigments show very high stability, good absorption and good photo-conductive properties which makes them the probably most investigated photovoltaic materials in the past [268, 43, 29, 154, 231, 267].

On the other hand, the easier processible soluble derivatives have attracted the interest of researchers more recently - driven by the fast progress of polymer based devices and the discovery of outstanding electronic properties of liquid crystalline (LC) materials [228, 226, 227, 184, 253, 254, 255, 259, 260, 262, 1, 2].

Although the successful synthesis of perylene dyes has been reported already 18 years ago [209], phthalocyanine dyes and polymers of both have only been synthesised in the more recent past - see Refs above.

We note that many other molecules that have been proven suitable as photo-active pigments in solar cells, may also be of utmost interest to be chemically modified so that they can be used as dyes, liq-

¹Here we have also neglected the band bending at the D/A junction.

²We have drawn the formation of blocking contacts, ohmic contacts are more likely to form using Au and Ca instead of ITO and Al.

³In 1993 more than 90% of the xerographic photo-receptors were made of organic photo-conductors [154]

⁴Recently a method was found to dissolve certain pigments in acids [283]. Although, this simplifies film deposition, the use of acids introduces other problems.

Table 4.1: Survey of performance parameters of various organic double layer solar cells. The abbreviation for materials are listed in Chapter 1. Polymers and dyes in this table were processed from solution whereas pigment films have been formed by thermal sublimation. The EQE for devices marked with ⁺ was estimated from the information given in the respective papers. Per denotes the soluble perylene derivative while Per1,2 and 3 refer to different perylene pigments. Best parameters are printed **bold** while results discussed in this Chapter are printed *italic*.

EQE %	V_{oc} V	FF %	range nm	materials D/A	comments –	year
30⁺	0.5	65	400-800	CuPc/Per1	pigment/pigment [244]	1985
23	0.5	≈ 30	400-700+	HPc1/Per2	pigment/pigment [131]	1990
23	0.3*	40*	400-600	PEDOT/PEOPT/C60	polymer/pigment [213]	1998
9	0.8	48	400-560	PPV/C60	polymer/pigment [111]	1996
6	1.0	60	400-620	PPV/Per3	polymer/pigment [113]	1996
$\approx 3^+$	1.0	23	400-620	PPyV/P3HT	polymer/polymer [242]	1997
2	1.0	51	400-590	PEDOT/PPV/Per	polymer/dye [9]	1999
0.6	0.12	25	400-800	CuPc2/Per	<i>dye/dye</i> [200]	2000
0.4	0.35	20	400-850	HPc/Per3	<i>liquid crystal(dye)/pigment</i> [199]	1999

uid crystals or polymers in solar cells. Among those should be mentioned: squaraines, quinacridone, azulenium, but also charge transfer complexes like PVK:TNF [154] and certainly the large number of different merocyanines and azo pigments [154, 29]. Many dyes are commercially available from suppliers for the copy industry (Xerography) like Synthec/Synthone in Germany but also laser dye manufacturers like Kodak.

The following we list some ideas that have been published to improve the performance of double layer photovoltaic structures:

1. It has been shown that the device efficiency of a double layer (PEOPT/C60) is strongly connected to the geometry and optical field distribution [213].

Choosing suitable electrodes and thicknesses of the involved layers in such a device allows to optimize the optical field taking into account interference effects at the active interface and thus enhance the exciton concentration within a layer with thickness comparable to the short exciton diffusion length.

2. F. Zhu and J. Singh have published an optical analysis method to optimise the structure of multi-layer thin film solar cells with respect to the thickness of the layers and the electrode materials [281, 282]. Their model takes into account multiple reflections of multi-junction structures composed of absorbing and non absorbing materials.

They have applied their analysis on e.g. glass/ITO/p/i/n/rear-contact where p,i, and n stands for the doped and intrinsic layer of amorphous silicon. Their method may be of interest for application on organic multi-layer structures to maximise the effects of the incident radiation.

3. Another possibility to optimise organic double layer cells is to place the material with the higher bandgap (e.g. a perylene derivative) next to the transparent (ITO) contact and the lower bandgap material (e.g. a phthalocyanine) behind. Although, a higher workfunction material than Al might then be required to avoid the formation of blocking contacts, such structure can show better efficiencies than the reverse order of layers [268, 187].

As possible reasons⁵ for such an improvement may also be considered: longer exciton diffusion lengths in the high bandgap material or simply lower thermalisation losses of the photoexcited carriers in the first layer.

⁵We note that in Ref. [187] Foerster energy transfer facilitating exciton diffusion to the active junction is given as explanation for better performance in these devices.

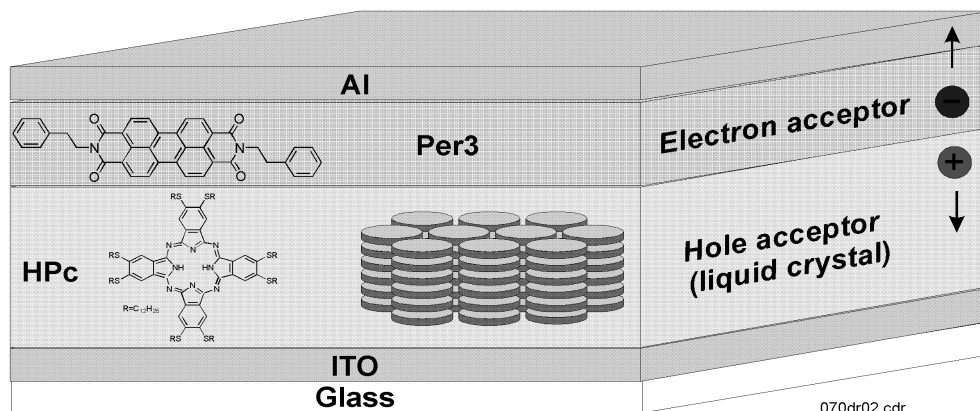


Figure 4.3: The figure shows the chemical structure of the two organic semiconductors (HPc, Per3) and the architecture of the double layer device structure. Charge separation typically occurs at the HPc/Per3 interface so that electrons and holes can travel individually without a high chance to meet a recombination partner. Thus, only the exciton diffusion range determines the width of the active region in such a structure. One device has been heated and slowly cooled in order to obtain the alignment of the discotic molecules of HPc, as shown here, which is expected to affect the charge and exciton transport properties. The characteristics (IV, EQE) of this device were compared with the figures of a non-heated reference cell.

4.2 The Dye/Pigment Double Layer Device (HPc/Per3)

As mentioned above the small exciton diffusion length in most organic semiconductors represents a serious limitation for double layer structures. More recently researchers have discovered not only long diffusion lengths (several 100nm) for excitons, but also particularly high mobilities ($0.1\text{--}0.5\text{cm}^2\text{Vs}^{-1}$) for charges in discotic liquid crystalline materials [1, 57, 21].

It is the strong intermolecular interaction of the flat disc-like molecules which acts as driving force to induce a higher degree of order. The formation of such a highly ordered phase requires a certain degree of mobility of the molecules themselves which can be found in the liquid crystalline phase (mesophase).

Indeed, PR-TRMC studies have revealed that both solid (crystalline) and mesophases of many discotic molecules allow have higher charge carrier mobilities than in most pigments or polymers [57]. The same study revealed also that the *crystalline* phase of the same liquid crystalline materials shows even higher numbers than the mesophase of a given material. Our own studies of HPc in single layer devices are consistent with these improved transport properties at room temperature- see Chapter 3.

In practice liquid crystalline molecules had plenty of opportunities to rearrange themselves during purification steps (e.g. column chromatography, recrystallisation) or simply during the last synthesis steps which typically involves solutions. Moreover, materials with transition temperatures $< \approx 40^\circ$ may have seen sufficiently high temperatures during their storage or transport period prior to their use. The decreased motion (vibrations) of the molecules at lower temperatures i.e. the solid phase allows even closer packing and even less disorder once the molecules have arranged themselves.

Although the PR-TRMC studies seem very conclusive there are also signs for poorer transport properties in the crystalline phase. For example, alkoxy substituted metal free phthalocyanine shows very high PL (50%) at low temperatures (4.2K) which is considerably quenched at the transition to the mesophase (372K) [21]. This quenching effect is interpreted as increased mobility of the excitons in the mesophase so that they can now reach more nonradiative decay sites ⁶.

In other words it is *a priori* not clear whether or not the effort to orient the columns perpendicular to the electrodes pays off in terms of photo-

⁶We note that breaking the conjugation (reducing the exciton diffusion length) of PPV chains by the introduction of acetylene units has also increased the PL[]

voltaic performance. One advantage of liquid crystalline phases is that they are self-repairing and can thereby minimise defects that can act as recombination sites. In any case, already the high solubility that allows simple spin-coating like normal dyes - is technologically very interesting.

After characterisation of a number of mesogenic phthalocyanines - see Chapter 7 we found that only one compound, HPc, forms a liquid phase while all the others started to decompose before the isotropic liquid can be formed. The particularly high *mobility of the molecules* in the liquid phase allows the formation of the perpendicular arrangement at the transition to the discotic phase as observed for HPc in Chapter 7 or for a similar derivative in Ref.[152]. HPc, is also soluble enough to allow spin coating from solution and sufficiently viscous to form excellent films on the ITO substrates despite the relatively low molecular mass compared to polymers.

During the transition from the solid to the liquid phase the surface tension leads to the destruction of the continuous thin film. As a consequence, instead of a thin film, much thicker droplets which are surrounded by areas of no or very little material are created. Hence, subsequent sublimation of the Al top contact inevitably results in a shorted device. In order to avoid these shorts the electron acceptor Per was sublimed prior to the deposition of the Al top contact.

Thus, this device may in fact be regarded as a hybrid between a single layer device (ITO/Per3/Al) and a double layer device (ITO/HPc/Per3/Al) with varying thickness of both organic layers. Hence, it is not possible to probe the effect of alignment via comparison with a pristine device directly⁷.

However, such a device has not been investigated yet and it should at least be possible to see to what extent the two materials can contribute to the photocurrent⁸ in such a hybrid structure.

After spin-coating HPc onto ITO, we heated the phthalocyanine until it forms an isotropic liquid (clearing point =292°C) and cooled it slowly down to room temperature - according to the procedure described in Chapter 3. After that we sublimed a thin layer of Per3 as electron acceptor and transport layer. The double layer device was then completed

by the sublimation of an Al layer as top contact. Then we compare the external quantum efficiency (EQE) of this device with the same device architecture which has not been heat treated.

Experimental

Films of HPc have been fabricated in air by spin coating from solution onto indium tin oxide (ITO) coated glass substrates. HPc was dissolved in chloroform (30mg/ml) and filtered with 0.1mm PTFE-filter. One HPc film on ITO was heated to 292°C (20°C /min) under a constant nitrogen flow and slowly (5°C/min until 270°C, then 20°C/min) cooled down to room temperature using a hot stage (Linkam).

The transition into the liquid phase as well as the formation of a few linear defects - see Chapter 3 (visible with crossed polarisers) has been observed simultaneously under the microscope (Vickers) which has been adapted for temperature-dependent polarisation microscopy. Exposure to the illumination source (tungsten) has been minimised to avoid photo-degradation effects. The Al top contact was obtained through thermal evaporation. The thickness of the HPc film after spincoating was 450nm and the Per3 film was about 20nm.

Current- voltage curves and photocurrents were measured using a Keithley 237 source measure unit. Monochromatic illumination was provided by the output of a tungsten lamp dispersed by a Bentham M300 single-grating monochromator. Quantum efficiencies were determined by normalisation with a calibrated silicon photodiode at the sample position. The sample was kept under vacuum ($< 10^{-5}$ mbar) during the measurements. Reflection losses were neglected for all measurements. Absorption spectra were taken with a UV-Vis spectrometer (HP 8453).

Results and Discussion

Absorption and EQE Spectra

Fig.4.4 shows that - for the pristine device - illumination through ITO results in an EQE spectrum with maxima where the absorption is low and EQE minima at absorption peaks. This suggests that a considerable part of the HPc layer absorbs light but does not contribute to the photocurrent (optical filter effect). The thickness of the active layer can be estimated using Eq. (3.3) and gives about 180 ± 90 nm. This value is in good agreement with

⁷Note that according to Ref.[57] see Table 7.2 the difference of charge carrier mobilities in HPc at the solid to mesophase transition is only very small. Also the exciton diffusion length is likely much longer than the layer thickness - see Chapter 3 and Ref.[21]. Thus a dramatic change in performance is not expected even if a non hybrid double layer could be fabricated.

⁸Such a distinction is possible since Per3 does not absorb around 650-850nm but HPc does.

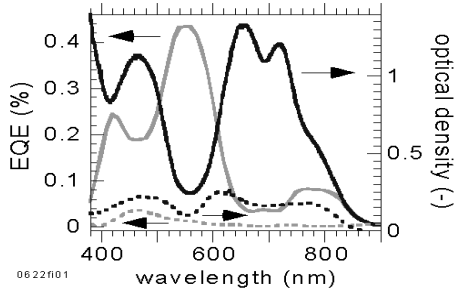


Figure 4.4: EQE and optical density of the pristine (solid lines) and the heat treated (dashed lines) device. Illumination through ITO.

the $200 \pm 80\text{nm}$ obtained from the measurements of the single layer HPc - see Eq. (7.2).

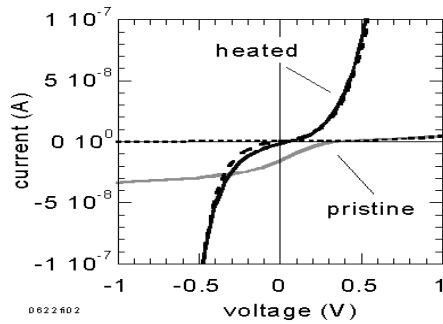


Figure 4.5: IV-characteristics in light at 570nm and $0.19\text{mW}/\text{cm}^2$ of the heated device and the pristine device.

Fig.4.4 shows also that the heat treated device only reaches about 1/10 of the EQE of the pristine device. The heated device using the same materials and structure was heated until it turned into a liquid at 292°C and slowly cooled down to room temperature to obtain the perpendicular orientation of the discotic molecules. Interestingly the absorption spectrum of the heated device is broader in the range where HPc absorbs only (650-850nm).

Upon illumination through the semitransparent Al contact (transmission about 2%) the EQE of the pristine device follows the features of the absorption spectrum (not shown here, see [199]). This is expected in this device since the Per3 layer is rather thin (about 20nm) so that a filter affect due to a passive Per3 layer can not be very strong.

If we consider the transmission losses of the Al

contact the EQE reaches up to about 1%. This number is not very different from the EQE obtained in double layer structures containing at least one polymer layer - see Table 4.1. The photo-response spectrum of this device is very broad. The V_{oc} is 350mV which is slightly smaller than in devices made of insoluble molecules.

The low OD of the heated device is expected since droplets have been formed leading to very thick but also very thin layers. The latter dominate the absorption spectrum leading to the shown low OD numbers. The redistribution of oscillator strength into the low energy region may be due to the high ordered phase of HPc.

IV Characteristics

The IV curves in vacuum for both the pristine and the heated device are shown in Fig.4.5. The pristine device shows only little rectification but an V_{oc} of 350mV.

The heated device shows higher currents for small voltages and also little rectification. The V_{oc} is only about 50mV. In addition the heated device reveals a stronger voltage dependence in both reverse and forward bias. This may be explained by the formation of a “counter”-diode in conjunction with a vanishing HPc layer for parts of the device.

We note that the shape of the IV curves can be changed considerably upon exposure to air approaching the shape of the pristine device [199]. Increased conductivity of the thick HPc droplets may here increase the contribution of HPc. However, the parts of the device which contain only Per3 seem to be responsible for the low V_{oc} . Interestingly the photocurrent of the heated cell reaches a maximum after about 4 hours exposure to air [199].

Summary

In this Section we have shown that:

- A layer of discotic liquid crystals can be used to manufacture a working D/A double layer photovoltaic device.
- Heat treatment to align the discotic columns perpendicular to the electrodes could not improve the efficiency.
- The efficiency (EQE) of the pristine device is between 0.5 and 1% which is about 30 times smaller than comparable devices using only pigments. The V_{oc} was 350mV - similar to typical pigment devices.

4.3 The Dye/Dye Double Layer Device (CuPc/Per)

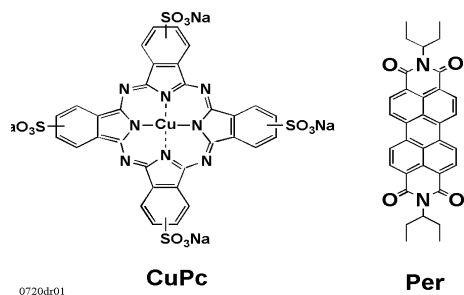


Figure 4.6: Chemical structure of the two dyes used in this section: A perylene tetracarboxylic acid-bis imide with aliphatic side chains (Per) and a copper phthalocyanine with polar side chains (CuPc).

The D/A double layer cell reported by Tang who sublimed *insoluble* CuPc and perylene derivatives onto ITO with a silver top electrode is still one of the most efficient organic solar cells [244].

In this Section we investigate a double layer solar cell using *soluble* derivatives (see Fig.4.6) of Tang's pigments. That way we could circumvent the thermal sublimation process and simply manufacture the device at room temperature via spincoating.

The essential differences to Tang's pigments are the polar side chains attached to the phthalocyanine structure and the short but bulky aliphatic side chains of Per. Since these side chains are not electronically active, we might expect that these molecules would have very similar electronic properties to those in Ref. [244]. These side chains do alter the *mechanical* properties since they prevent aggregation in solution although they do not induce liquid crystalline phases here.

However, they are also likely to change the intermolecular arrangement in the solid (film) which can affect both charge and exciton transport and the optical properties of the films. Indeed, we have found that the absorption coefficient at the absorption maximum of HPc is about 20% smaller than in typical phthalocyanine pigment films.

Experimental

The chemical structures of the two dyes used in this section are shown in Fig.4.6. Per and CuPc are commercially available (Synthec, Aldrich). The

double layer device (Fig.4.1) was fabricated by spin coating onto an ITO/quartz substrate from a solution containing 30mg/ml CuPc in distilled water followed by 10min annealing at 150 °C in air. Per/chloroform solution (30mg/ml) was spin coated on top of the CuPc layer with subsequent sublimation of the Al electrode. The Per film was about 60nm thick and the CuPc film 15nm. The CuPc solution is not very viscous despite the high concentration and did not only give very thin films with moderate quality. The device was prepared in air but measured after 1 hour in vacuum.

Results and Discussion

Absorption and EQE Spectra

Fig.4.7 shows the EQE spectrum together with the optical absorption spectrum of the dye-based double layer cell. Because of the very thin CuPc layer (15nm) the optical density is less than 0.1 at wavelengths where Per does not absorb (650-800nm).

However, even though only about 10% of the incident photons around 700nm are absorbed the EQE spectrum is almost constant between 450nm and 720nm. The EQE roughly follows the absorption spectrum suggesting the absence of significant filter effect.

The EQE around 700nm seems to be enhanced compared to the rest of the spectrum. This indicates that unlike the 15nm thin CuPc layer the Per layer can not facilitate dissociation of all absorbed photons. Hence, the thickness of the active region, which is the exciton diffusion range of *both* the Per and the CuPc layer, is likely shorter than the 60nm thick Per film.

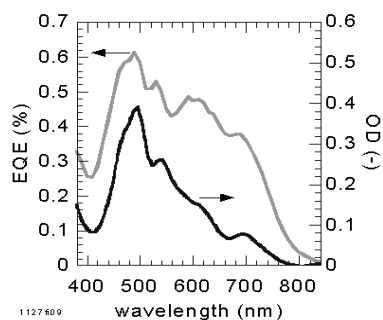


Figure 4.7: Linear optical absorption and EQE of the double layer device.

A more efficient device may be obtained by re-

ducing the thickness of Per and increasing the thickness of CuPc. The highest EQE would then be expected when both layers are as thick as their respective exciton diffusion lengths. Note that the fairly symbaric response spectrum indicates that the exciton diffusion length of CuPc is possibly higher than 15nm. We also note that the CuPc film also contains Na^+ ions which may affect the electronic properties.

IV Characteristics

The (IV) characteristics in the dark and under illumination are shown in Fig.4.8. This device develops a relatively low open circuit voltage of 120mV. V_{oc} for other double layer devices at comparable intensities is typically a few hundred mV. Although there is only little rectification for all shown curves certain features are interesting: The linear IV characteristics for small positive voltages indicates that the series resistant affects the shape and FF in this region. It even extends into the negative voltage range so that the EQE at 0V is directly affected and reduced by resistive losses.

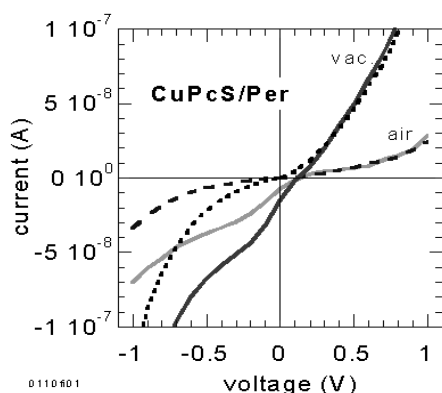


Figure 4.8: IV characteristics in the dark and under illumination at 610nm and an intensity of 0.25mW/cm^2 . The thickness of the CuPc layer was about 15nm and the Per layer was about 60nm thick.

An analysis of the slopes at -0.3V and +0.5V gives values of $R_{sh}=1.4 \cdot 10^7\Omega$ and $R_s=0.7 \cdot 10^7\Omega$. Although the R_s is not unusually high⁹ the shunt is relatively low. In Chapter 2 we have seen that the effect of the series resistor becomes important if the shunt is not at least an order of magnitude

higher. The reason for a low shunt resistor can be recombination at the interface or local shorts.

We note that Per tends to form crystals that may easily penetrate the thin CuPc film and thereby favour a lower¹⁰ R_{sh} . The small shunt compared to R_s may also be responsible for the low V_{oc} . Moreover the hyper-linear increase of current for negative bias suggests the presence of a diode with reverse polarity (=“counter”-diode).

We note that according to the IV curve the EQE, judged from the difference between dark and light characteristics, can be more than doubled if a small negative bias voltage is applied. This can be used if the device is used as a photo-diode with a broad spectral response - or as solar cell with e.g. Ca instead of Al electrodes.

Summary

In this Section we have found that:

1. A whole new class of organic semiconductors - small soluble organic molecules (dyes) - can be used to built double layer photovoltaic cells.
2. The efficiency of dyes in these first studies is about an order of magnitude lower than e.g. polymer devices and about 30 times lower than the pigment double layer structures.
3. Both R_s and R_{sh} appear to play an important role as limiting factors in these devices. The surprisingly high R_s for a double layer structure may be due to larger intra-molecular barriers (hopping distance is increased by the insulating side chains) that limit both the charge and exciton transport in the investigated material. Thus, further studies that focus on reducing R_s by e.g. doping are necessary to estimate the potential of these molecules.
4. The device shows a very broad spectral response for a solution processed cell. This may be exploited if used as a photodiode - where the sensitivity can also enhanced by at least a factor 2 by applying a small bias voltage.
5. The exciton diffusion length of Per is smaller than 60nm whereas the number for CuPc is likely larger than 15nm.

⁹We found values around $0.210^7\Omega$ in MEH-PPV devices

¹⁰Also the Na^+ ions may contribute to the higher conductivity.

Chapter 5

Blend Layer Devices

5.1 Introduction

In the previous Chapter we have seen that the introduction of an electron acceptor (A) i.e. electron transport layer between the negative electrode (Al) and the electron donor material (D) can increase the EQE with respect to single layer architectures¹.

In such double layer structures exciton dissociation takes place at the D/A interface. At the same time the acceptor material transports the electrons to the negative electrode (Al) while the hole acceptor provides a pathway for the holes to the positive electrode (ITO). Both are spatially well *separated* so that mutual recombination of the photoexcited charges during their journey out of the device is reduced.

In addition, the thickness of the active layer can be increased compared to single layer structures since excitons created within their diffusion length from *both* sides of the D/A interface can now contribute to the photocurrent. Furthermore, the spectral range of the photoresponse can be greatly increased if the absorption spectra of the components (D and A) complement each other.

In this Chapter we discuss another D/A-device architecture: *Blends* i.e. mixtures of donor and acceptor materials (Fig.5.1). Since both blend and double layer structures use *two* materials that can form a *charge separating D/A interface* they share many advantages over single layer devices - for example: separate charge transport and a thicker active layer.

However, the main advantage of the *blend* device over *double layers* is that the active layer can be considerably thicker than the sum of the exciton diffusion lengths in the D and A material *as long as the blend comprises an interpenetrating network*

¹Note that not everything could be improved, for example, the open circuit voltage is generally higher in single layer devices than in double layers.

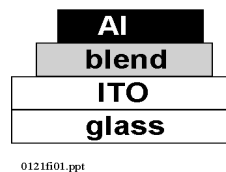


Figure 5.1: Solar cell architecture comprising a blend of two organic semiconductors as used in this Chapter. Thicknesses of the blends vary between 20 and 120nm.

with domains not larger than twice the exciton diffusion length. The latter is typically only about 20nm (2x10nm).

If we consider both the spectral dependence of the absorption as well as the absorption coefficient of the majority of presently available organic semiconductors, the layer thickness has to be at least 150nm of the pure material to approach 100% absorption over a broader wavelength range.

Even with a very low bandgap, a single layer can only use about 7% and a double layer about 14% of the incident light - assuming an exciton diffusion length of 10nm in the constituent material(s).

Consequently, since blends could have active regions as thick as necessary to absorb most light, they have the potential to utilise 15 times more photons than typical single layer structures and 7 times more than double layer devices.

However, blend devices have also drawbacks as can be seen from the following list:

1. If processing from solution is desired, blends require high solubility of both components²

²Note that *double layer* have similar restrictions: they require at least one component to be insoluble in the other components solvent or high thermal stability in order to use

2. For maximum performance, blends require a defect-free interpenetrating network for efficient percolation of charges to the electrodes i.e. phase separation on a scale near or smaller than the double exciton diffusion length in the respective material.
3. Despite the larger active region, most blends tend to develop lower open circuit voltages than single layer structures - for reasons which are not well understood to date.
4. The random network of a blend device benefits strongly from a *driving force* that directs the separated charges from the D/A interface to the respective electrodes. The difference between the workfunctions of the electrodes and/or an externally applied electric field (bias voltage) can represent such a driving force.

As a consequence, blends generally show *stronger field (voltage) dependence* of the photocurrent which often decreases the fill factor and may cause lower V_{oc} . Double layer structures, on the other hand, are less dependent on external fields and do therefore not always benefit from an extra driving force.

In Table 5.1 we give a survey of the four key parameters for solar cell efficiency in various blend structures extracted from our own results and from literature.

Note that already two of these parameters (sensitivity range, open circuit voltage) reach i.e. even surpass the numbers of their silicon counterparts using the blend architecture. However, the EQE of the best organic cell (29%) is yet only a third and the best fillfactor in blends (44%) about 50% of typical commercial silicon solar cells. The blend of MEH-PPV with the hardly soluble C60 could only be accomplished in a very strong solvent (1,2 dichlorobenzene). Since C60 is virtually insoluble in most known solvents we regard it as pigment within this thesis - in contrast to the C60 derivative in Ref. [278] which is readily soluble in more common solvents and therefore rather a dye than a pigment. The table also illustrates that there are problems to realise all of these performance parameters in the *same* device.

In the following list we will comment on many of these structures in order to point out specific novelties and strengths³:

thermal sublimation for film deposition.

³Here we follow the historical order

- The first report on D/A solar cells with conjugated polymer blends has been reported by Halls et. al. [112]. Blends comprising an electron accepting (CN-PPV) and an electron donating (MEH-PPV) polymer have shown EQE values of up to 6% which boosted the EQE with respect to single layer cells by about two orders of magnitude.

The EQE of the single layer structures is 0.001% (CN-PPV) and 0.04% (MEH-PPV) respectively. Phase separation on the scale of 10-100nm was demonstrated and a V_{oc} of 0.6V with fill-factors of 25% were obtained. The low fill-factor is most likely due to the a relatively small shunt that also causes the field dependence of the light current.

However, the shunt must be large enough to allow the device to develop the relatively high open circuit voltage (0.6V). Another problem here is the higher polarity of the *electron* transporting CN-PPV that favours it's accumulation on the positive ITO electrode⁴ during the spincoating process [114].

- The highest EQE values (29%) among blend devices have been achieved with a blend between MEH-PPV and a soluble C60 (Fullerene) derivative as electron acceptor sandwiched between ITO and Al [278]. Photoexcited charge transfer from the polymer donor to the C60 is about 1000 times faster⁵ than radiative and nonradiative recombination[83]. Thus the D/A interface between MEH-PPV and C60 serves as an efficient exciton dissociation site.

Under high monochromatic light intensities (20mW/cm²) this device develops a V_{oc} of 0.68V using ITO and Al electrodes but - interestingly - only little more (0.82V) with Ca instead of Al. Unfortunately, "internal resistive" losses⁶ do not allow the use of thicker devices to circumvent the 40% transmission and reflection losses at the absorption maximum in these devices. The MEH-PPV/C60 blends also show the field dependent photocurrent that leads to low fill-factors (here still only about 30%) typically encountered in blend devices.

Despite the mentioned obstacles for further improvement, the achieved performance with the

⁴Molecular dipoles on the ITO surface attract the polar CN groups.

⁵Radiative and nonradiative decay of singlet excitons occurs typically between 100 and 1000ps [102].

⁶Probably related to charge and exciton transport problems through the C60 network.

Table 5.1: Survey of performance parameters of various solar cells comprising at least one organic component in a blend. The abbreviations for materials are listed in Chapter 1. Best parameters are printed **bold** while results of this work are in *italic*.

EQE %	V_{oc} V	FF %	range nm	materials –	comments –	year
29	0.5	≈ 25	400-550	MEH-PPV+C60	polymer+dye [278]	1995
23	0.4	≈ 33	400-550	MEH-PPV/C60	polymer+pigment [83]	1998
12	0.5	26	400-640	MEH-PPV+CdSe	polymer+nanocrystals [102]	1996
11	0.35	41	400-620	P3HT+Per	polymer+dye [65]	2000
6	0.6	25	400-600	MEH-PPV+CN-PPV	polymer+polymer [112]	1995
1.8	0.9	23	400-500	PPV+MWNT	polymer+nanotubes [3]	1999
1.0	0.1	25	400-800	HPc+Per	<i>liquid crystal+dye</i> [200]	2000
0.7	0.4	44	400-600	MEH-PPV+Per	<i>polymer+dye</i> [62]	1999
0.4	0.2	25	400-850	PTV+Per	<i>polymer+dye</i>	2000
0.4	0.12	25	400-900	PTV+Ter	<i>polymer+dye</i>	2000
0.2	0.6	25	400-800	PTV+THPF	<i>polymer+polymer</i>	2000
0.02	<0.01	25	400-1000	PTV+PIF	<i>polymer+polymer</i>	2000
0.0007	<0.01	25	400-1100	HPc+PIF	<i>polymer+liquid crystal</i>	2000

C60 cells was sufficient to stimulate commercial interest in organic solar cells. We note that a further breakthrough towards economically attractive organic devices has been achieved with the introduction of the laminated device structure - see Chapter 6.

- Blends of MEH-PPV with CdSe nanocrystals⁷, sandwiched between ITO and Al, have also been used to fabricate solar cells. The devices show EQE values up to 12%, V_{oc} of 0.5V and again the strong field dependence leading to a fillfactor no larger than 0.26 [102].

These nanocrystals turn out to be good *electron acceptors* with the extra advantage that their absorption properties can be tailored by varying their size during the synthesis; for example, upon changing their diameter from 6 to 2nm, the energy gap can be increased from 2.0 to 2.6eV. Apart from the small shunt resistant that causes the field dependence, *charge transport* between the nanocrystals seems to be the limiting factor in these cells.

- More recently, blends of MEH-PPV and a perylene dye (Per) as electron acceptor have been investigated. The IV characteristics show that a fill-factor as high as (44%) can be achieved in blends despite the relatively low V_{oc} of 0.4V and an EQE of about 1% [62]. Phase sensitive

AFM images revealed the formation of a large electron conducting network consisting of very long (μm) Per crystals in addition to phase separation on a scale of 50nm upon annealing.

The surprising fact that the formation of such large crystals does still allow the device to perform reasonably well, opens new possibilities - particularly with respect to the use of non polymeric semiconductors such as dyes which are prone to form crystals in the solid state. Indeed blends with $2\mu\text{m}$ long nanotubes have been made - see below.

- A blend between a polymer (PPV) and multi-wall carbon nanotubes (MWNT's) has been investigated with respect to its photovoltaic properties in Ref. [3]. Although the MWNTs were as long as $2\mu\text{m}$ (and only 10nm in diameter) and show relatively high conductivity (8S/cm) the devices developed the highest open circuit voltage in our list of blend devices (0.9V) instead of the expected shorts in the only about 200nm thin films.

This confirms the feasibility of fabrication of working solar cells using materials containing or forming large crystals - consistent with the results and conclusions in Ref. [62] as mentioned above. The EQE however, is only about twice as high as in the pure PPV device. This small but significant improvement is considered to be due to the high workfunction of the nan-

⁷Both can be dissolved i.e. dispersed in chloroform

otubes (5.1eV) and/or the increased interface area due to the formation of an interpenetrating network.

- The first D/A blend between two dyes with one showing liquid crystalline properties at room-temperature has been published [200] and will be discussed in detail in this Chapter.
- Blends with the low bandgap semiconductor PIF allowed for the first time to extend the spectral response of an organic D/A blend beyond the 1000nm range. The EQE however is yet only modest (0.02%) and in one case (EQE= $7 \cdot 10^{-4}\%$) even smaller than the single layer device. Both devices will be discussed later in this Chapter.

For all these blend structures discussed above, strong photoluminescence quenching has been found, ranging from a factor of 5 for MEH-PPV+CN-PPV blends to a factor of 10^4 for MEH-PPV+C60 blends. This indicates that the vast majority (over 80%) of photoexcited excitons can reach a dissociation site (D/A interface) within their diffusion length and dissociate before they can recombine under the emission of light (PL).

Hence, the dominant loss mechanism has to be on the way of the charges to their respective electrodes. The charge transport to the electrodes can be affected by:

- inter-molecular barriers (e.g. long distances for the hopping process)
- intra-molecular barriers (e.g. distortion of conjugation along the polymer backbone by e.g. twisting of aromatic units)
- super-molecular structural defects (e.g. “dead ends” of aggregates in blends)
- formation of blocking contacts at the electrodes
- charge carrier traps that can lead to recombination or built up space charges that limit the current

Large flat aromatic molecules like perylenes, phthalocyanines or ladder-type structures⁸ like LPPPT have a good chance to overcome the problems described in the first 3 points in the list above.

⁸Polymers that are planarised through bridges between i.e. aromatic units are said to resemble a “ladder” along their backbone.

It is also noteworthy that *low bandgap* materials are more likely to form non-blocking (ohmic) contacts with metals simply because the workfunction of the electrode material is less likely to lie within the bandgap. On the other hand, *trap levels* in the bandgap of a low bandgap polymer are likely relatively close to both the HOMO and the LUMO so that they can facilitate fast i.e. efficient *recombination* representing “deep traps”.

In this Chapter we investigate the photovoltaic properties of blends comprising the materials discussed in Chapter 3.

The specific combinations of semiconducting materials has been chosen with the aim to accomplish both charge transfer which would indicate a D/A interface and a extended photoresponse covering at least the visible range (400-800nm).

With the exception of Per (2.1eV, 600nm) all components have low bandgaps ranging from 1.77eV (700nm) to 1.12eV (1100nm) and most of them are flat aromatic molecules. We note that HPc also exhibits liquid crystalline properties as discussed in Chapter 7.

5.2 HPc+Per

In this Section we explore the possibilities to form a D/A blend network in a photovoltaic device using the two small soluble molecules (dyes) Per and HPc - see Fig.5.2.

Both molecules have been investigated in both single and double layer devices earlier in this thesis. Although there are reports of dye doped⁹ polymers [276] and mixtures of D/A pigments [264, 251], we are not aware of any reports of photovoltaic D/A blend structures using solely dyes before this work.

The reason for the lack of published work on this interesting subject in literature is presumably related to difficulties in synthesising of soluble semiconducting molecules with the desired optical and electronic properties. Presently, various soluble derivatives of pigments (dyes) with promising photovoltaic properties can be purchased from suppliers that specialise in chemicals for xerography e.g. Syntec/Synthone in Germany.

Two well soluble small molecules like Per and HPc are likely to mix on a *molecular* level to form a *solid solution* rather than showing phase

⁹Note that mixtures containing less than about 10% by weight - sometimes even more - of the guest material are often regarded as “doped” materials in the field of organic semiconductor devices.

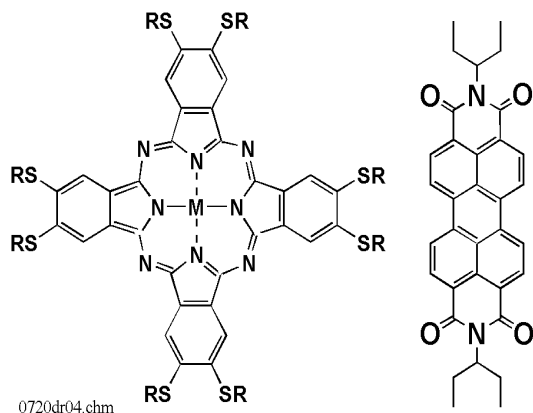


Figure 5.2: Chemical structure of the two dyes investigated in this Section: A perylene tetracarboxylic diimide with aliphatic¹¹ side chains (Per) and a metal free phthalocyanine with aliphatic side chains (HPc).

segregation¹² as usually observed between polymers. Such an intimate mixture may then be regarded as a “new” *material* rather than a *blend* with a large D/A interface.

However, it is not clear a priori to what extent percolation paths are present in such solid solutions. Charge carriers might be able to find their way to the respective electrodes via intermolecular hopping between like molecules even if they are not always in direct contact with each other.

Our hope was that these specific dyes would allow sufficient percolation of charges through molecular clusters (small aggregates) since both show strong aggregation as individual components. We know that Per has a tendency to form crystals during spincoating from solution or upon heat treatment [62] while HPc is liquid crystalline at room temperature and forms even aggregates in solutions that quench the PL - see Chapter 7.

However, we did not know if the dyes still prefer to form aggregates with like molecules¹³ and if the size of the aggregates would be on a suitable scale. Too large aggregates for example would quench excitons before they reach the D/A interface whereas too small aggregates may not provide percolation paths. In the following we try to shed light on these questions.

¹²Phase segregation in dyes often happens at higher concentrations resulting in the formation of crystals.

¹³They might aggregate with the other material and/or form exciplexes.

Experimental

PL efficiency measurements were performed using an integrating sphere coupled to a CCD spectrometer (Oriel) via a liquid light guide. Details of the procedure can be found in Ref. [169].

Images were recorded using an atomic force microscope (NanoScope IIIa Dimension 3100) operated in the tapping mode which is located at and provided by Cambridge Display Technology (CDT).

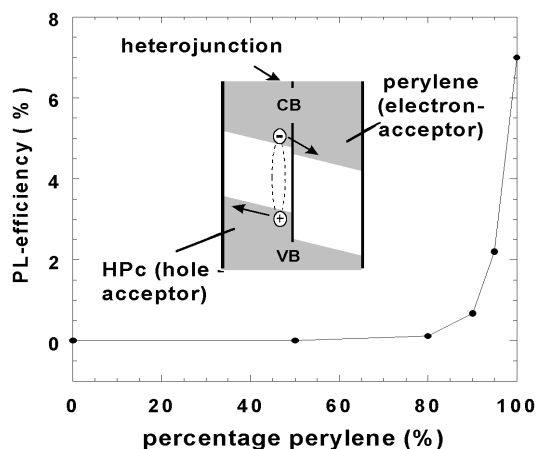


Figure 5.3: The absolute photoluminescence efficiency of the Per+HPc blend film on a quartz substrate plotted as a function of composition. The excitation wavelength was 488nm (1.0mW light intensity). The line shown represents a guide to the eye. HPc does not fluoresce in the film due to aggregation (π -stacking).

The 1:1 (weight) blend device was fabricated by spin coating onto an indium tin oxide (ITO) coated quartz substrate from chloroform solution containing 30mg/ml HPc and 30mg/ml Per followed by sublimation of the Al electrode. IV characteristics and photocurrent measurements were done in vacuum ($< 10^{-5}$ mbar).

The chemical structure of the dyes investigated in this Section are shown in Fig.5.2. Per was used as received from Synthec (Germany) while HPc has been synthesised and purified by G.G. Rozenberg and A. Lux as reported elsewhere [165].

The liquid crystalline properties of HPc are discussed in Chapter 7 and have been published in Ref. [199]. We note that a double layer device with a sublimed perylene derivative is discussed in Chapter 4.

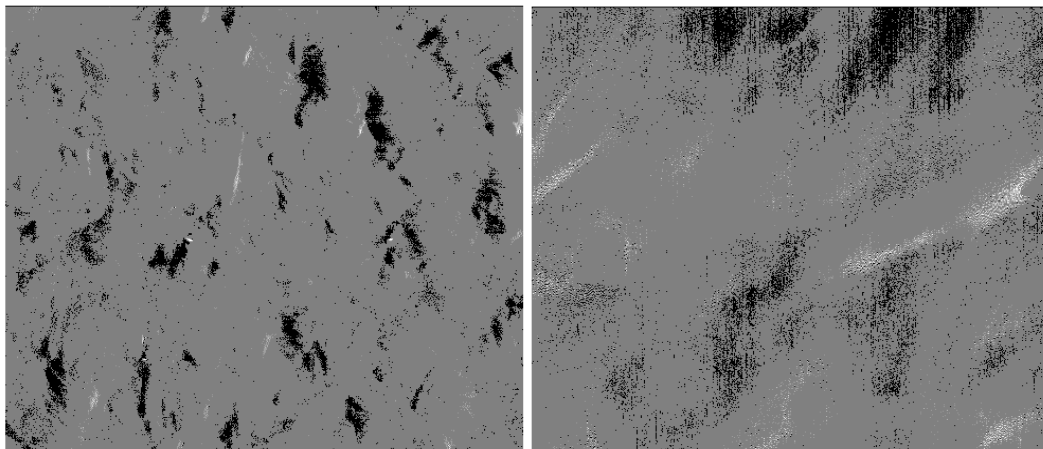


Figure 5.4: AFM images (phase contrast) of a 1:1 (by weight) blend of HPc and Per. *Left*: Scan size is 2x2 microns. *Right*: Scan size is 200x200nm. The lack of contrast suggests that there are no crystals or aggregates between about 20-1000nm. Thus possible aggregates can only be smaller than about 20nm.

Results and Discussion

PL-Quenching

Photoexcited excitons can decay either radiatively showing photoluminescence (PL) or dissipate their energy via direct conversion into heat. Fig.5.3 shows that in a film of 100% Per about 7% of the excitons decay under emission of light. This ratio can be considerably decreased upon the addition of HPc. For example, a 50% Per blend shows virtually no PL indicating that most excitons are affected by the presence of HPc. The photoexcited excitons can undergo several processes:

- recombination at the interface
- energy transfer to the material with the lower bandgap followed by radiative or nonradiative recombination
- charge transfer (exciton splitting) at the interface

We consider the last process (charge transfer) to occur in these devices since we found enhanced photocurrents in the blend compared to devices made of the single components Fig.5.6. Moreover, the interface of similar phthalocyanine and perylene derivatives has been recognized as the active site for exciton dissociation elsewhere [244, 267].

We note that the PL quenching shown in Fig.5.3 for Per+HPc is more than one order of magnitude

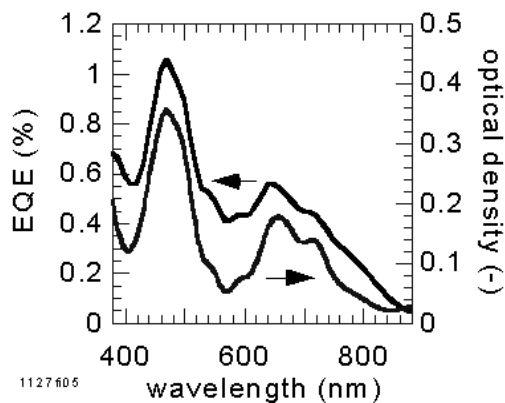


Figure 5.5: Linear absorption and EQE of the blend device.

higher than in the 1:1 (by weight) blend between MEH-PPV and CN-PPV [112]. Since the aggregates in the latter are between 10 and 100nm, the strong PL quenching in our dye blend is consistent with the formation of aggregates on a scale <20nm. In fact, if the dyes do not form aggregates at all, the blend may be regarded as a solid solution (= blend on a molecular scale) rather than a phase segregated mixture.

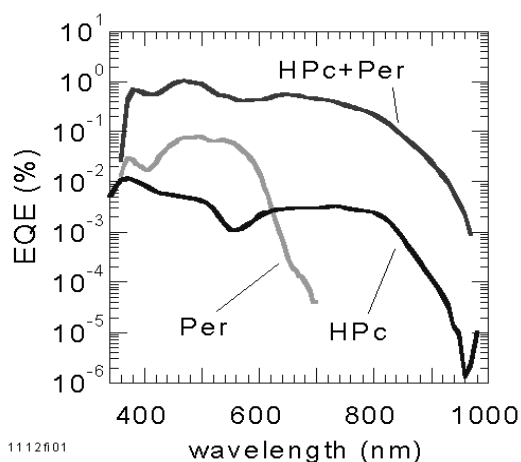


Figure 5.6: EQE of the HPC+Per blend device and the single components. The blend show clearly enhanced EQE over the entire range indicating the presence of a D/A interface and percolation paths to the electrodes.

Absorption and EQE Spectra

The EQE and optical absorption spectrum of the 1:1 (by weight) HPC+Per blend cell are plotted in Fig.5.5 showing that the cell is able to utilise light from the entire visible spectrum. The absorption band between 600nm and 850nm corresponds to HPC whereas Per starts to absorb at around 650nm reaching its peak at 500nm.

From the fact that the EQE spectrum follows the absorption features we can infer that most of the bulk of the cell contributes to the generation of the external current. The EQE spectrum reaches its peak ($\approx 1\%$) at around 500nm which exceeds the EQE of a double layer cell made with very similar materials (Chapter 4) by a factor of 2. The onset of the EQE is around 900nm as in the single layer and double layer devices comprising these components.

IV Characteristics

The (IV) characteristics in the dark and under illumination are plotted in Fig.5.7. The open circuit voltage is 110mV and the fill factor 25 percent under these conditions. Both the dark and the light current depend highly on the applied field. The device shows little rectification in the depicted voltage range.

A voltage and light dependent device like a photodiode can be formed if exciton splitting occurs (here

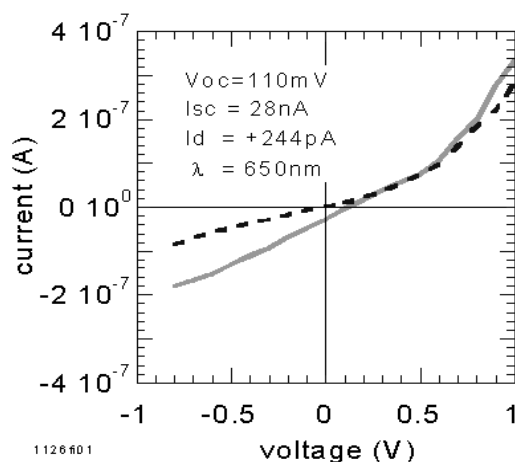


Figure 5.7: IV characteristics of the HPC+Per blend in the dark and under illumination with light at 650nm and an intensity of $0.25\text{mW}/\text{cm}^2$. The thickness of this device was about 70nm.

at the D/A interface) and the built in field drives the separated charges through percolation paths to the different electrode materials.

Indeed, both the light and the dark IV curves in Fig.5.7 show a weak but significant diode behaviour under forward bias. However, the experiment reveals a strong linear voltage dependence under *negative* bias. Thus we conclude that the shunt is too small which may be the case for the following reasons:

1. A short has been formed through a pinhole that results in a shunt resistor approaching the value of the series resistor.
2. There is significant recombination of the separated charges during their journey through the fine interpenetrating network

Since we did not find any pinholes under the AFM and the device is not particularly thin (70nm) we may exclude the presence of shorts due to pinhole formation.

Instead, the formation of a very fine network may account for the observed strong PL quenching, the enhanced photocurrents and the high series resistor¹⁴. Hence, the separated charge carriers have many opportunities to recombine at this large but presumably not very conducting D/A interface.

¹⁴Which is caused by the “fine” percolation paths.

This loss mechanism could be assisted by the presence of trap levels in the bandgap.

Summary

In this Section we have found that:

- Photovoltaic devices with a photoresponse ranging from 400 to 800nm can be built using a blend between two soluble derivatives of a perylene diimide and a phthalocyanine.
- The high solubility of both molecules appears to facilitate the formation of a large D/A interface - possibly even a solid solution - that enables efficient exciton splitting.
- Such a very fine interpenetrating network (<20nm) is probably also responsible for the small shunt resistor since it offers increased possibilities for recombination during the journey of the separated charges.
- The small shunt may be the main reason for the relatively low V_{oc} of 110mV and fill-factor (0.25).

5.3 HPc+PIF

Experimental

Fig.5.8 shows the chemical structure of the organic semiconductors used for the device fabrication in this Section. The liquid crystalline properties of HPc are discussed in Chapter 7 and have been published in Ref. [165]. PIF has been synthesised by H. Reisch and U. Wiesler at the MPI in Mainz, Germany [210]. HPc has been synthesised by G.G. Rozenberg and A. Lux, Melville Laboratory for Polymer Synthesis, Cambridge (UK) as reported elsewhere [165].

We note that a double layer device with a sublimed perylene derivative is discussed in Chapter 4 of this thesis and published in Ref. [199].

The ITO/HPc+PIF(1:1 by weight)/Al devices were fabricated by spin coating onto an ITO coated quartz substrate from chloroform solution containing 30mg/ml HPc and 10mg/ml Per followed by sublimation of the Al electrode. More details about preparation of substrates and the setup can be found in Chapter 10.

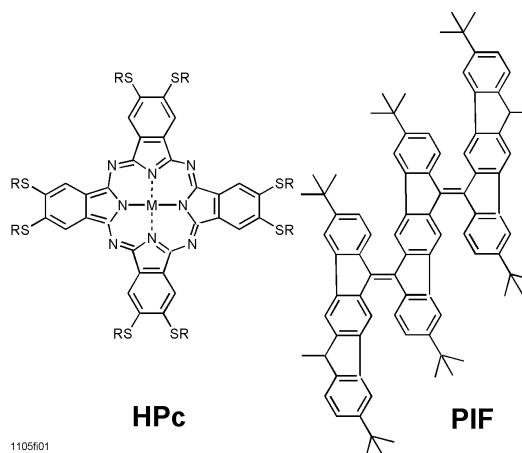


Figure 5.8: Chemical structure of the two organic semiconductors investigated in this Section: A poly-indenofluorene with short aliphatic side chains (PIF) and a metal free ($M=H_2$) phthalocyanine (HPc) with thio-alkyl side chains ($R = C_{12}H_{25}$). While HPc is very flat, the short distance between the repeat units of PIF causes a 33° distortion between adjacent indenofluorene moieties [210].

Results and Discussion

Absorption and EQE Spectra

The EQE and optical absorption spectrum of the HPc+PIF blend cell are plotted in Fig.5.9.

The features around 440, 680 and 720nm are due to the HPc absorption whereas the peak at 800nm can be found in the absorption of PIF - see also Chapter 3. Both components have a small absorption coefficient around 550nm. However, since the absorption onset is indeed around 850nm for HPc and at 1040nm for PIF, the broad peak in the infrared (1040nm) is probably due to enhanced aggregation of PIF in the presence of HPc rather than poor background correction or interference effects in the absorption measurement. Another reason why the latter can be ruled out is that we observe a significant photocurrent in the absorption onset.

We point out that the absorption range of this device is larger than the range of the spectrometer using a *silicon* based CCD array.

The EQE spectrum follows the absorption features very well indicating that the entire bulk - involving both components - contributes to the generation of the external current. However, the EQE does not reach more than $6.5 \cdot 10^{-4}\%$ which is lower than in devices comprising the pure components only: $3 \cdot 10^{-3}\%$ in HPc as well as in PIF - see

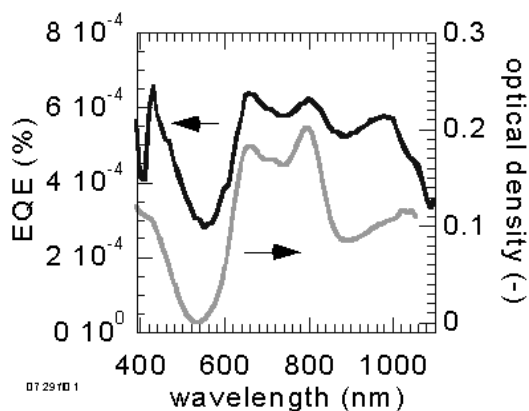


Figure 5.9: Linear absorption and EQE of the HPc+PIF blend device.

Fig.5.10.

The following reasons may be considered to explain such low external quantum efficiencies:

1. Pinholes in the device that can cause shorts when filled with e.g. Al during the sublimation of the electrode.
2. A defect-rich charge transport network in the blend. Such defects could be “dead ends”, isolated areas, accumulation of a homolayer on the wrong electrode. In addition, the blend ratio of 1:1 (weight) may be far from the percolation threshold¹⁵.
3. The offset between the LUMO and HOMO levels between PIF and HPc is not larger than the exciton binding energy¹⁶ which is required to separate the charges i.e. to enable photoexcited charge transfer at the D/A interface.
4. The formation of new recombination channels for the photoexcited species upon mixing the two components.

ad 1): Shorts caused by e.g. pinholes in the organic film can be ruled out since the IV characteristics shows very low currents in the dark - even under bias voltage (Fig.5.11).

ad 2): In MEH-PPV+CN-PPV blends the EQE values are at least two orders of magnitude higher than the devices made of the single components -

¹⁵which is difficult to estimate here

¹⁶ ≈ 0.4 eV according to Ref. [56, 168, 12]

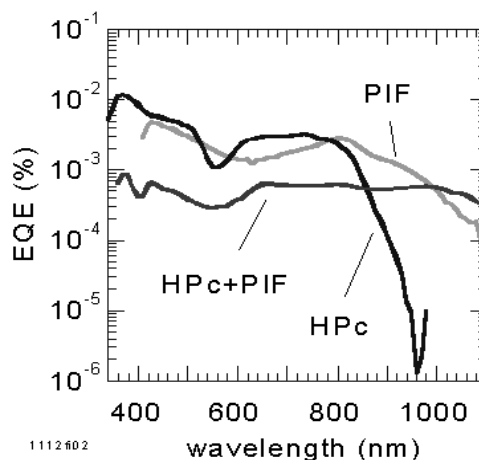


Figure 5.10: EQE of the HPc+PIF blend device and the single components. The blend shows a significantly lower EQE than each component - indicating that there is no charge transfer between HPc and PIF.

despite serious network defects such as the formation of a homolayer of CN-PPV¹⁷ near the wrong electrode (ITO) [114].

In addition, network defects such as “dead ends” cannot account for EQE numbers lower than the single components because extra exciton splitting should always lead to enhanced photocurrents compared to the single layer. This is like introducing oxygen in a single layer device using a hole transport material - see Chapter 2. Molecular oxygen would be the electron acceptor with probably no percolation path at all - and is still better than the oxygen free material. Hence insufficient network formation cannot easily be blamed alone for the poor performance of the HPc+PIF blend.

ad 3): The quinoid structure of PIF and the known donor properties of phthalocyanine derivatives suggest that the difference between the HOMO and LUMO levels of HPc and PIF should be sufficient to allow charge transfer. However, since both materials do not show enough PL we cannot test for PL quenching and have therefore no indication that excitons are split at the interface between these two molecules.

ad 4): In fact, the combination of low bandgaps in both components and the (probably) different electron affinities may bring the LUMO of PIF rel-

¹⁷The more polar CN-PPV is attracted by the polar ITO surface.

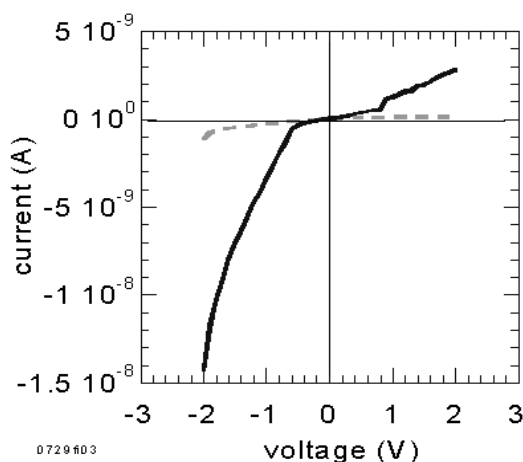


Figure 5.11: IV characteristics in the dark (dashed line) and under illumination with light at 700nm and an intensity of $0.35\text{mW}/\text{cm}^2$. The thickness of this device was about 40nm.

actively wide into the middle of the HPc bandgap. PIF with its low LUMO may then capture an electron to act as a “deep trap” and allow recombination with a hole in the HOMO of HPc (electron back transfer).

The mirror process, photoexcitation of an electron from the HPc directly into the LUMO of PIF may then account for the new absorption band around 1100nm. Note that a pure PIF film does not absorb wavelengths longer than about 1000nm - see Chapter 3 and [221]. Recombination via this “deep trap”, PIF, could then even outnumber the extra photoexcited charge carriers if exciton splitting actually occurs at the PIF/HPc.

IV Characteristics

The (IV) characteristics in the dark and under illumination are plotted in Fig.5.11. The dark current is small and relatively independent of the voltage in both forward and reverse bias in the depicted range¹⁸. Upon illumination the device generates a small but significant photocurrent that can be increased considerably (up to 15 times) by applying an electric field. We can identify a threshold ($\approx 0.5\text{V}$) under negative bias where the photocurrent enhancement seems to begin. The device, however, does not develop a significant open circuit voltage

¹⁸This rules out the presence of a short - as discussed above.

(<10mV).

The device also shows only little rectification in the depicted voltage range.

Summary

In this Section we have found that:

- A working photovoltaic device comprising a 1:1 blend with *low bandgap* dye and a low bandgap polymer has been built.
- The device shows a photoresponse in a wavelength range as wide as 400 to 1100nm which is virtually identical to commercial photo-detector systems based on silicon.
- The blend between such low bandgap materials with different electron affinities may open new decay channels for the photoexcited species that lead to EQEs that are lower than in devices with only the single component. This may be seen as a first hint for the lower limits of the size of the semiconductor bandgap in organic solar cells.
- The EQE can be tremendously increased by applying -2V bias voltage.

5.4 PTV+Per

Experimental

The chemical structure of the organic semiconductors discussed in this Section are shown in Fig.5.12. Per was purchased from Synthec (Germany) while PTV has been synthesised by F. Goldoni, University of Technology (Eindhoven, The Netherlands). Details of the synthesis, solvatochromic effects and circular dichroism can be found in Ref. [90].

We note that single layer devices with both components are discussed in Chapter 3 of this thesis.

The 1:1 (weight) blend device was fabricated by spin coating onto an indium tin oxide (ITO) coated quartz substrate from chloroform solution containing 15mg/ml PTV and 8mg/ml Per followed by sublimation of the Al electrode. More details about preparation of substrates and the EQE/IV setup can be found in Chapter 10. The thickness of the organic layer was measured with a Dektak profilometer and found to be 80nm.

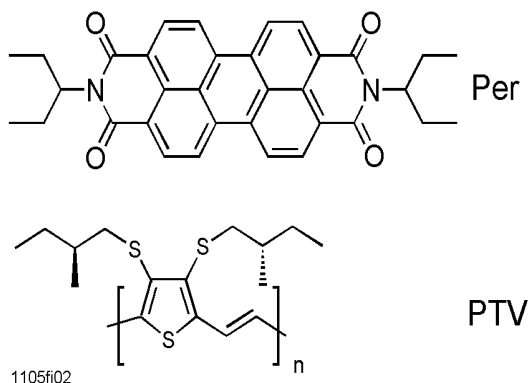


Figure 5.12: Chemical structure of the two organic semiconductors discussed in this Section: A polythienylene vinylene with chiral aliphatic side chains (PTV) and a perylene diimide with aliphatic side chains (Per).

Results and Discussion

Absorption and EQE Spectra

The EQE and optical absorption spectrum of the 1:1 (by weight) PTV+Per blend cell are plotted in Fig.5.13. The two peaks around 500nm correspond to the absorption of a single Per layer whereas the shoulder at 650nm is due to an absorption maximum of PTV. The relatively strong and broad band between 800 and 1000nm is most likely an artifact and probably related to the low signal to noise ratio that affects the background correction.

However, since we find a significant photocurrent down to about 900nm, there must be *some* absorption in that region. We note, that we find a more pronounced - and probably real feature with a fine structure in the absorption onset of the PTV+Ter device discussed in a later Section of this Chapter.

The EQE reaches 0.44% in short circuit mode and 8% under 3V negative bias. The EQE spectrum follows the main absorption bands. Since the EQE values for single layer devices made of the pure components PTV - see Fig.5.14 are clearly lower, we can assume that *charge separation* takes place at the PTV/Per interface. Interestingly, the EQE spectrum of the blend extends further into the infrared than the EQE of the single components. This indicates that there is a long absorption tail in the blend film.

We consider that the presence of the rigid and planar Per molecules may favour a more planar arrangement of the PTV molecules which are ex-

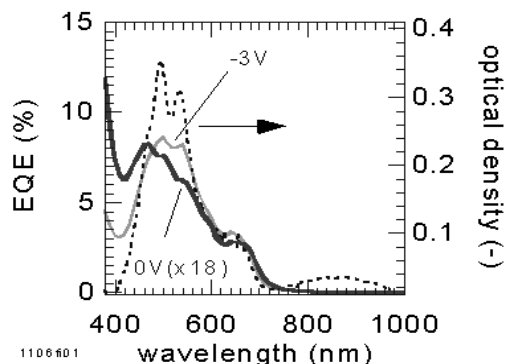


Figure 5.13: EQE of the PTV+Per blend device with 0 and -3V bias and its absorption spectrum.

pected to form a chiral superstructure¹⁹ in the *pure* film. Such a more planar molecular arrangement may then lead to a lower bandgap due to increased conjugation compared to the pure PTV molecule. In addition enhanced aggregation or even crystallisation may take place due to the flatter alignment which has been suggested to be responsible for enhanced exciton splitting leading to enhanced photocurrents in the absorption onset in MEH-PPV [120].

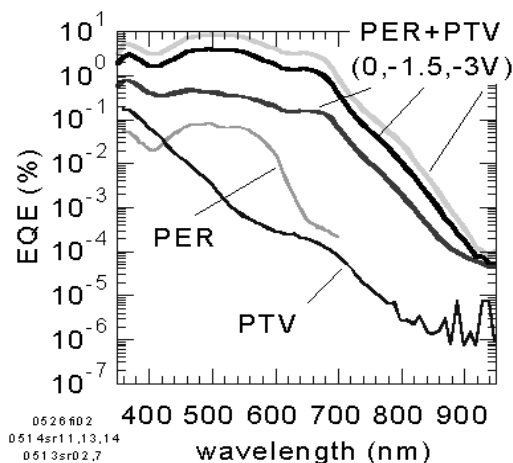


Figure 5.14: EQE of the PTV+Per blend device with 0,-1.5 and -3V bias and the single layer device efficiencies at 0V.

¹⁹because of the chiral side chains [90]

IV Characteristics

The IV characteristics in the dark and under illumination are plotted in Fig.5.15. The open circuit voltage is 150mV and the fill factor 0.25. The dark current is very low and virtually field independent over a wide voltage range as observed in many D/A blend devices. The light current, however, is *highly* field dependent following Ohm's law between +3 and -3V.

What is remarkable here is that the shunt of the dark IV curve decreases by at least²⁰ 3 orders of magnitude from $1.3 \cdot 10^{10}\Omega$ to $1.3 \cdot 10^7\Omega$ upon illumination with light while there is no indication for a significant decrease of R_s .

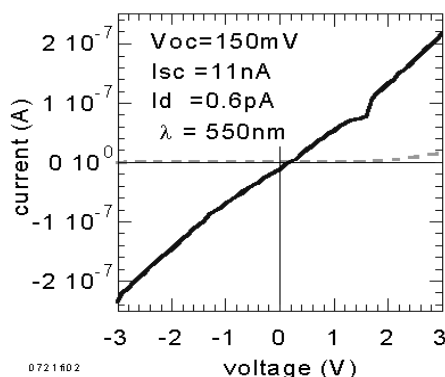


Figure 5.15: IV characteristics of the PTV+Per blend in the dark and under illumination with light at 550nm and an intensity of $0.15\text{mW}/\text{cm}^2$. The thickness of the organic film is 80nm.

From the observation that photoexcitation reduces predominantly the shunt rather than R_s we consider that a new recombination channel near the D/A interface opens under illumination. The low shunt can also explain the moderate open circuit voltage (150mV).

The relatively high EQE (despite the low shunt) suggests efficient exciton splitting at the D/A interface. The linear dependence of the photocurrent shows that the current is not trap limited. The ohmic IV characteristics of the light IV curve does not allow any rectification. We note that the rectification ratios under light are also low for other organic semiconductor blends MEH-PPV/CN-PPV,

²⁰Note that the ohmic characteristics as obtained for the light IV curve represents the sum of both R_s and R_{sh} as discussed in Chapter 2 so that R_{sh} is possibly even smaller than $1.3 \cdot 10^7\Omega$.

MEH/CdSe and MEH/C60 mixtures with low C60 ratios [112, 102, 83].

In any case, the strong field dependence of the photocurrent can be used to increase the photo-sensitivity i.e. EQE by a factor of 20 (reaching about 8%) by applying either -3V (photodiode mode) or +3V (photo-resistor mode).

Summary

In this Section we have found that:

- The external quantum efficiency of a photovoltaic device comprising a 1:1 blend between a small soluble perylene derivative (Per) and a poly-thiophene derivative (PTV) is considerably higher than the EQE of the pure single layer devices.
- Thanks to the low bandgap of PTV the photovoltaic cell shows a very broad photoresponse surpassing the visible wavelength range.
- The EQE can be increased by a factor of 20 (reaching 8%) by applying a negative *or* positive voltage of 3V.
- The distinct difference between the dark and the light IV characteristics makes it possible to operate this device not only as a photo-diode, solar cell but also as light dependent resistor (photo-resistor).
- In short circuit mode the solar cell reaches an EQE up to 0.4% with V_{oc} of 150mV
- The shunt resistor decreases by at least 3 orders of magnitude upon illumination with monochromatic (550nm) light of $0.15\text{mW}/\text{cm}^2$.

5.5 PTV+Ter

Experimental

The chemical structure of the organic semiconductors used in this Section are shown in Fig.5.16. PTV was synthesised by F. Goldoni at The University of Technology (Eindhoven, The Netherlands). Details of the synthesis can be found in Ref. [90]. Ter was synthesised by S. Becker at the MPI (Mainz, Germany). More information about the synthesis of various perylene-, terrylene-, quaterylene-, derivatives including polymers can be found in Ref. [217].

Single layer devices comprising the pure compounds have been investigated in Chapter 2.

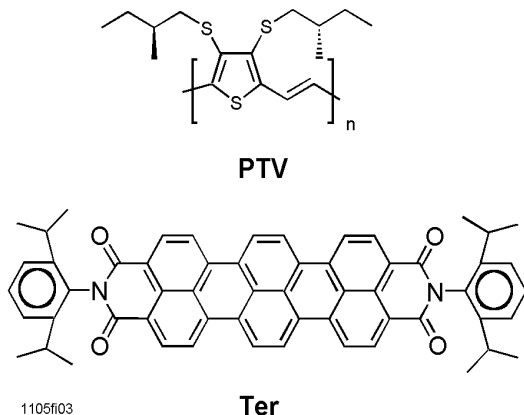


Figure 5.16: Chemical structure of the two organic semiconductors discussed in this Section: A polythienylene vinylene with with chiral aliphatic side chains (PTV) and a terrylene diimide (Ter) with aliphatic side chains.

The 1:1 (by weight) blend device was fabricated by spin coating onto an ITO coated quartz substrate from chloroform solution containing 15mg/ml PTV and 6mg/ml Ter followed by thermal sublimation of the Al electrode. The thickness of the organic film is 32nm. More details about preparation of substrates and the setup can be found on Chapter 10.

Results and Discussion

Absorption and EQE Spectra

The optical absorption spectrum and EQE at 0V and -1.5V of the 1:1 PTV+Ter blend cell are plotted in Fig.5.17. Both PTV and Ter have very similar absorption spectra with features at 600 and 660nm and the onset at 750nm. The spectrum of the blend in Fig.5.17 shows qualitatively the same features but they are much more pronounced than in the single compounds - see Chapter 3.

Also interesting is the occurrence of a broad absorption band between 780 and 1100nm where none of the single components absorbs at all. We note that we have observed a similar absorption band in the PTV+Per blend as discussed in the previous Section in this Chapter. The band here is different from the one in PTV+Per in that the band here is stronger and structured.

In fact, the same data plotted on an energy scale (Fig.5.18) reveal a constant energetic spacing typical for vibronic modes. We found peaks at 1.237,

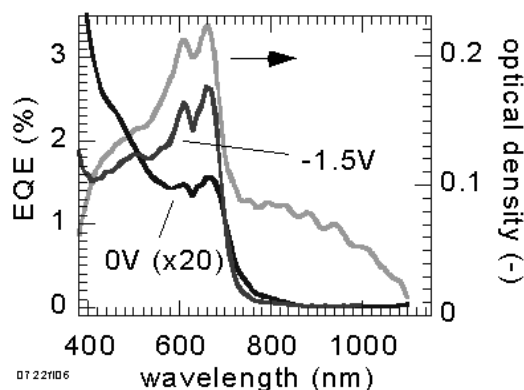


Figure 5.17: EQE of the PTV+Ter (32nm thick) blend device with 0 and -1.5V bias and its absorption spectrum. The EQE at 0V is multiplied by 20 for clarity.

1.320, 1.402, 1.485, 1.567, 1.649, 1.732 which correspond to an energetic spacing of 83meV. The two main peaks are at 1.878 and 2.043eV with a spacing of 165meV - which is 83 times 2. We consider that these two peaks reflect the 0-0 and 0-1 vibronic transition with the 0-0 peak being the dominant feature.

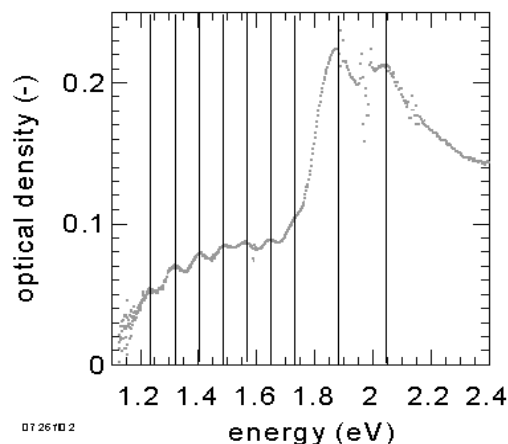


Figure 5.18: Linear absorption of the PTV+Ter blend versus energy. Two vibronic modes can be found: 165meV and 82meV.

A similar vibronic mode of 50meV in addition to the dominant C-C mode of the polymer backbone (180meV) has been found in the absorption

spectrum of the well defined poly-phenylene derivative (m-LPPP). Both the occurrence of such well resolved vibronic structures and a dominant 0-0 transition have only been found either in small molecules or well ordered conjugated polymers like m-LPPP and PPV [198, 197, 163]. The latter had to be especially synthesised [109, 110] or stretch oriented [108] to obtain the required degree of order i.e. maximum conjugation length²¹.

However, regardless of the vibronic structure such a band in the absorption onset may be caused by e.g.:

1. The introduction of sub-bandgap levels via unintentional doping by e.g. the presence of impurities.
2. Interference effects in the thin film.
3. Aggregation effects.

Since the band is very strong and does usually not appear in films of comparable optical properties we consider the first two possibilities (doping, interference) to be very unlikely. However, they could be ruled out by performing photo thermal reflection (PDS) measurements as part of a more detailed study of these types of blends.

We believe it is more likely that the $\pi - \pi$ interaction of the large planar Ter molecules favours a more planar (less disturbed) molecular arrangement of the PTV molecules thus leading to longer effective conjugation lengths and enhanced aggregation and the observed vibronic structure in the polymer. Although this could explain the observation of both the well structured absorption spectrum and the broad absorption band around 900nm further structural investigation - such as the one mentioned above - are desirable to confirm such a possibility.

From the fact that the EQE spectrum follows essentially the absorption features we can infer that most of the bulk of the cell contributes to the generation of the external current. However, in the range between 400 and 500nm the EQE with 0V increases despite the local decrease of absorption in this range.

We note that we found the same effect in the PTV+Per blend discussed in a previous Section. In fact the pure PTV single layer shows a monotonic increase of EQE with shorter wavelengths despite a local absorption minimum at 420nm - see Chapter

²¹Different lengths of conjugated segments on a polymer chain smear out the absorption spectrum - unless they are all longer than the effective conjugation length.

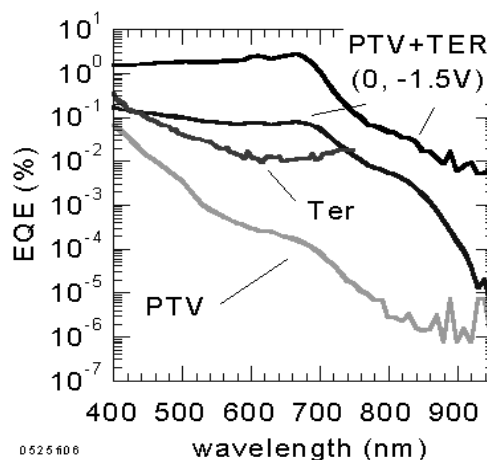


Figure 5.19: EQE of the PTV+Ter blend device with 0 and -1.5 bias voltage and the single layer device efficiency of PTV at 0V. EQE data for the pure Ter film may not be representative due to the formation of shorts - see Chapter 3.

3. In other words, photons carrying higher energies contribute more efficiently to the photocurrent already in the pure PTV (containing oxygen and water) than photons with lower energy. Hence, although we cannot identify the exact nature of this effect, we consider that the PTV component is responsible for this effect.

Another interesting observation is that photons absorbed in the low energy absorption band contribute to the photocurrent the more, the higher their photon energy (Fig.5.19). In fact, 1.55eV (800nm) photons are almost 100 times more efficient in contributing to the photocurrent than photons with only 1.38eV (900nm). Under negative bias voltage the sensitivity to photon energy decreases considerably in both the high energy (400 to 600nm) and the low energy range (800 to 900nm).

IV Characteristics

The IV characteristics in the dark and under illumination are plotted in Fig.5.20. The device develops an open circuit voltage of 120mV upon illumination with light at 600nm.

The dark current is low and stays virtually constant under negative bias whereas the light current depends strongly on the applied field. Similar to the PTV+Per device discussed earlier, the photo-sensitivity can be enhanced by a factor of 20 by

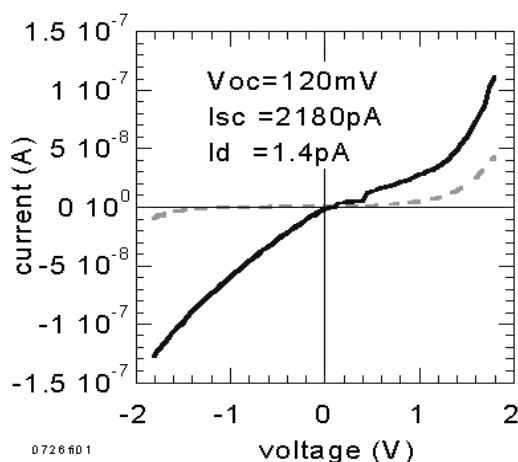


Figure 5.20: IV characteristics of the PTV+Ter blend in the dark and under illumination with light at 600nm. The thickness of this device was about 32nm.

applying a voltage of -1.5V.

Note that strong electric field dependence dependence of the photocurrent under negative bias is often observed in blend devices - especially if the open circuit voltage is relatively low ($< 300\text{mV}$ at typical light intensities around 0.2mW cm^2). This has probably to do with a tendency towards low shunt resistors in blends since separated charges have more opportunities to recombine within the large D/A network.

In contrast to the PTV+Per cell the PTV+Ter device shows *some* rectification in the dark but virtually none under illumination.

Summary

In this Section we have found that:

- The external quantum efficiency of a device comprising a 1:1 blend between a soluble terrylene derivative (Per) and a soluble polythienylene vinylene derivative (PTV) is considerably higher than in the pure PTV device.
- The device shows a photoresponse exceeding the visible wavelength range (400-900nm)
- The photoresponse can be increased by a factor of 20 reaching 2.4% at 670nm by applying a negative voltage of 1.5V.

- The device can operate as a photodiode, solar cell and a photo-resistor.
- The EQE reaches up to 0.4% with an open circuit voltage of 120mV.
- We find little rectification (5 at $\pm 1.8\text{V}$) in the dark but virtually none under illumination.
- The absorption of the blend shows a sharp vibronic mode (165meV) with a dominant 0-0 transition indicating high molecular order i.e. long effective conjugation of the PTV in the presence of Ter.

We also found an extra absorption band at low energies (1.2 to 1.8eV) with a vibronic mode (83meV).

5.6 PTV+THPF

Experimental

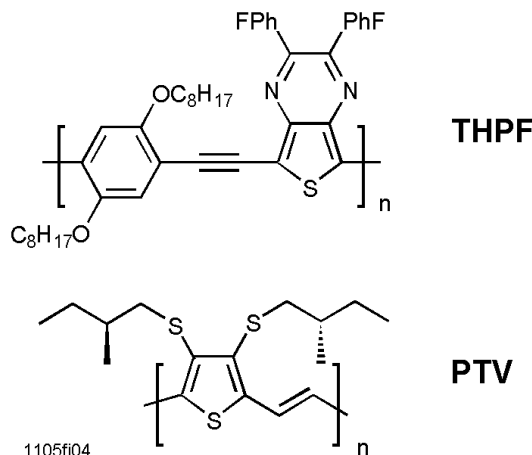


Figure 5.21: Chemical structure of the two organic semiconductors discussed in this Section: A polythienylene vinylene with chiral aliphatic side chains (PTV) and a fluorinated poly-yne, THPF.

The chemical structure of the organic semiconductors discussed in this Section are shown in Fig.5.21. PTV was synthesised by F. Goldoni at the University of Technology (Eindhoven, The Netherlands). Details of the synthesis can be found in Ref. [90]. THPF was synthesised by M. Khan, Imperial College London. The synthesis has not been published yet but some information about D/A interaction in fluoro-substituted phenylene containing organic and organo-metallic poly-yenes can be found in

Ref. [141]. The average molecular weight is 15440 corresponding to $n=22$ repeat units [142].

Single layer devices comprising the pure compounds have been investigated in Chapter 3 of this thesis.

The 1:1 (by weight) blend device was fabricated by spin coating onto an ITO coated quartz substrate from chloroform solution containing 15mg/ml PTV and 16mg/ml THPF followed by sublimation of the Al electrode. The organic film has been measured with a Dektak profilometer and found to be 50nm thick. More details about preparation of substrates and the setup can be found in Chapter 10.

Results and Discussion

Absorption and EQE Spectra

The EQE and optical absorption spectrum of the 1:1 (by weight) PTV+THPF blend cell are plotted in Fig.5.22. Both components have very similar absorption spectra with features at 600 and 660nm - see also Chapter 3. They do not absorb light with wavelengths longer than 800nm. Since there is no photocurrent beyond 800nm we consider the band around 900nm to be an artifact or due to interference effects.

The low bandgap of THPF shows that the triple bond is not breaking the conjugation of the backbone - thus charge transport along the backbone should be efficient. A sufficiently thick layer of such a blend can absorb 54% of the solar radiation on earth - see Table 8.3.

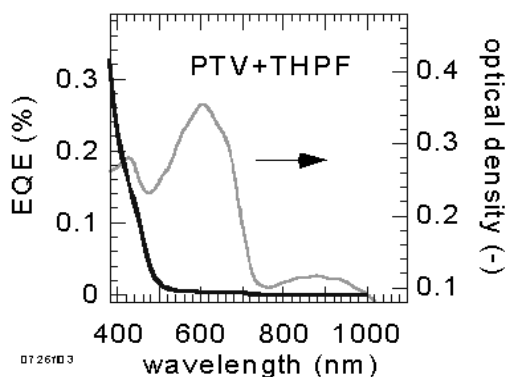


Figure 5.22: Linear absorption and EQE of the PTV+THPF blend device. The thickness of the organic film is 50nm.

PTV blends the EQE increases for shorter wavelengths and reaches values greater than 0.1% around 400nm.

The semi logarithmic plot of the EQE (Fig.5.23) shows clearly that the photoresponse actually starts at around 800nm and increases over more than four orders of magnitude when reaching shorter wavelengths. The blend shows about 10 times higher numbers than in the pure PTV device but only little (2x) more than in the pure THPF cell. The EQE numbers between 800 and 900nm are not significant due to the low signal to noise ratio in this region so that the actual bandwidth of operation of this device is 400 to 800nm.

However, the small improvement of the EQE compared to the pure THPF device may be explained in that charge separation is not particularly effective at the interface between those two molecules. This would mean that THPF is not a very strong electron acceptor as expected because of the electron withdrawing fluor atoms that couple to the conjugated system.

It may be that the rather long distance between the fluor atoms and the conjugated polymer backbone - they are separated not only by the thiophene but also the pyrazine and phenyl units - weakens the electronic effect. Such a weak effect of the fluor atoms is also consistent with the observation of an unchanged bandgap²² regardless whether the fluor atoms in this particular systems are present or not [142].

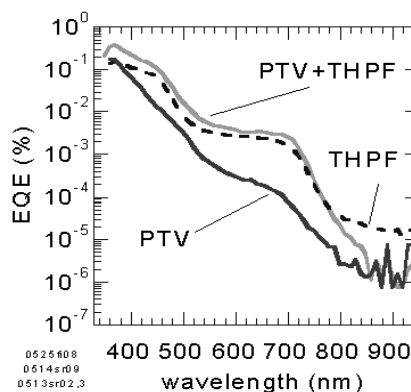


Figure 5.23: EQE of the PTV+THPF blend device and the single layer device efficiencies at 0V.

As observed in the pure PTV device and other

²²The bandgap in both systems was found to be around 1.7eV (730nm) in solution.

IV Characteristics

The IV characteristics in the dark and under illumination are plotted in Fig.5.24. This device develops a relatively high open circuit voltage (550mV) which is close to the difference in workfunctions of the electrodes. Similar open circuit voltages have been observed for e.g. MEH-PPV+CN-PPV blend devices under comparable conditions [112].

Indeed, the open circuit voltage in blend devices appears mainly to be determined by the workfunction of the electrodes and increases only very little with light intensity [102]. The IV characteristics resemble the curves obtained for blends of PTV with Per and Ter of the previous Section but with the exception that the (light) currents are lower and V_{oc} is higher.

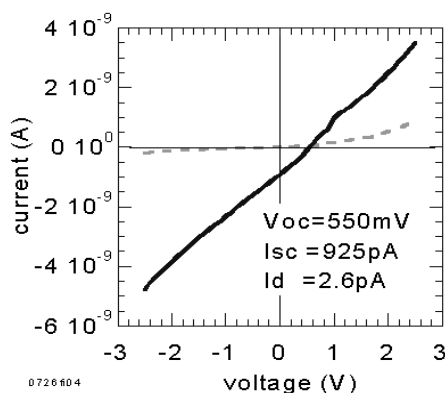


Figure 5.24: IV characteristics of the PTV+THPF blend in the dark and under illumination with light at 550nm and an intensity of 0.2mW/cm². The thickness of this device was about 50nm.

The shunt - calculated from the slope in the 3 quadrant - decreases considerably (from $10^{10}\Omega$ to $6 \cdot 10^8\Omega$). Note that the (inverse) slope of the ohmic IV curve in Fig.5.24 equals $R_s + R_{sh}$. There is no significant rectification in the investigated range (-3V to +3V).

Another result often found in blends is the low *dark* current even under higher negative bias voltage - as opposed to the rather voltage dependent light current.

Summary

In this Section we have found that:

- The external quantum efficiency of a device comprising a 1:1 blend between THPF and a

polythiophene derivative (PTV) is about two times higher than the EQE of the more efficient single material device (THPF).

- The device shows a photoresponse covering the entire visible wavelength range (400-800nm).
- The photoresponse can be increased by a factor of 4 by applying a negative voltage of 2V.
- Thanks to a linear IV curve the device can operate as a photodiode, solar cell and a photoreistor.
- The EQE reaches up to 0.2% with V_{oc} of 550mV which is close to the difference of workfunctions of the electrodes.
- We find some rectification (5) at $\pm 1.8V$ in the dark but virtually none under illumination.
- The dark current is very small and voltage independent in contrast to the photocurrent.

5.7 PTV+PIF

Experimental

The chemical structure of the organic semiconductors used in this Section are shown in Fig.5.25. PTV was synthesised by F. Goldoni at the University of Technology (Eindhoven, The Netherlands). Details of the synthesis can be found in Ref. [90]. PIF has been synthesised by H. Reisch and U. Wiesler at the MPI in Mainz, Germany [210].

Single layer devices comprising the pure compounds have been investigated in Chapter 3 of this thesis.

The 1:1 (weight) PTV+PIF blend device was fabricated by spin coating onto an indium tin oxide (ITO) coated quartz substrate from chloroform solution containing 15mg/ml PTV and 8mg/ml PIF followed by thermal sublimation of the Al electrode.

The thickness of the organic film was determined with a profilometer (Dektak) and found to be 55nm. More details about preparation of substrates and the setup can be found in Chapter 10.

Results and Discussion

Absorption and EQE Spectra

The EQE and optical absorption spectrum of the 1:1 PTV+PIF blend cell are plotted in Fig.5.26. The broad absorption band at 600nm stems from PTV whereas the peak at 800nm with the band

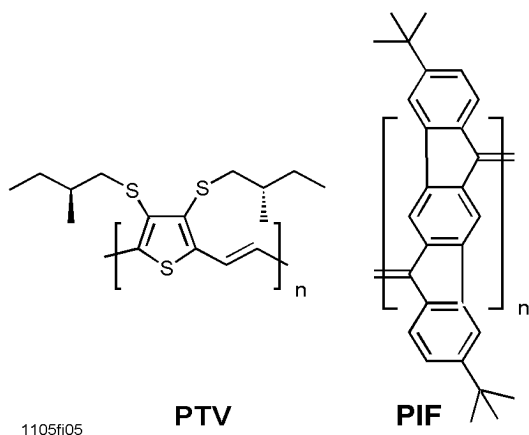


Figure 5.25: Chemical structure of the organic semiconductors discussed in this Section: A polythienylene vinylene with chiral aliphatic side chains (PTV) and a poly indenofluorene (PIF).

between 900 and 1100nm is due to the absorption of PIF - see Chapter 3.

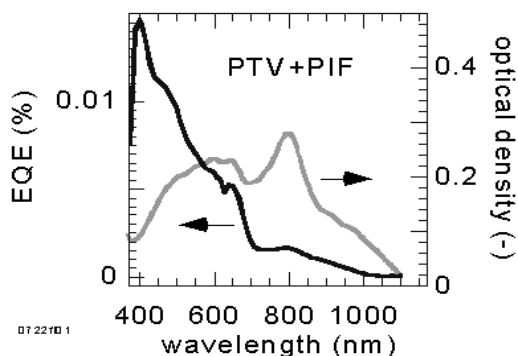


Figure 5.26: Linear absorption and EQE of the PTV+PIF blend device. The thickness of the organic layer is 50nm.

The onset of absorption of PTV is around 790nm. Since the absorption spectra of the low bandgap material PTV and the *very* low bandgap semiconductor PIF complement each other, this device can utilize light with wavelengths ranging from less than 400 to up to 1100nm.

A sufficiently thick layer of such a blend can absorb 77% of the solar radiation on earth which is comparable to commercial silicon based photodetectors and solar cells - see also 8.3. As observed in

both the pure PTV and the pure PIF device as well as other PTV blends the EQE *increases for shorter wavelengths* reaching its maximum around 400nm (0.014%).

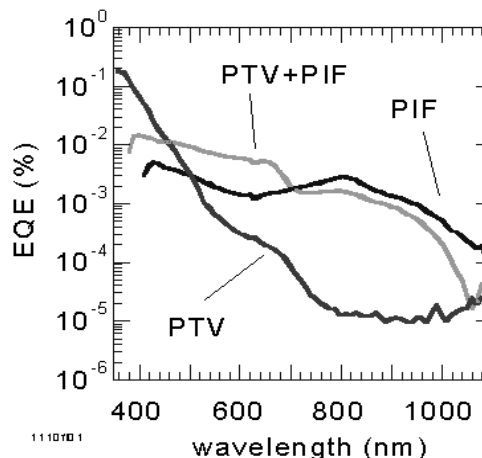


Figure 5.27: EQE of the PTV+PIF blend device and the single layer device efficiencies at 0V.

The semi logarithmic plot of the EQE (Fig.5.27) reveals that the photoresponse of the blend really starts at 1100nm. From the symbatic photoresponse we can exclude charge separation at the ITO/bblend interface. The figure also shows that the EQE of the blend is higher than both pure components only around 600nm.

Thus, we can conclude that photo-induced charge transfer takes place at the D/A interface but there must be another decay channel present that causes the device to lower its performance - possibly wavelength independent.

An alternative²³ and more likely possibility to explain the partial enhancement of the blend compared to the single layer is the presence of partial shorts i.e. a low shunt resistor. This would be consistent with the results of the IV measurements - see following Section.

IV Characteristics

The IV characteristics in the dark and under illumination are plotted in Fig.5.28.

Although the device shows a more than significant photoresponse we believe that the device is

²³ Another possibility is that the organic layer of PIF device was close to its optimal thickness - whereas thickness effects of the double layer here are not investigated or optimised.

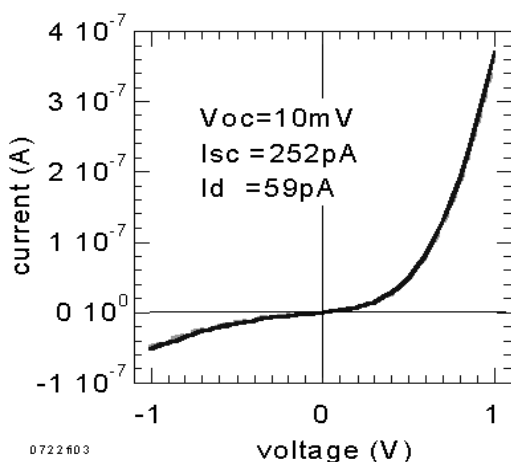


Figure 5.28: IV characteristics of the PTV+PIF blend in the dark and under illumination with light at 550nm and an intensity of about $0.2\text{mW}/\text{cm}^2$.

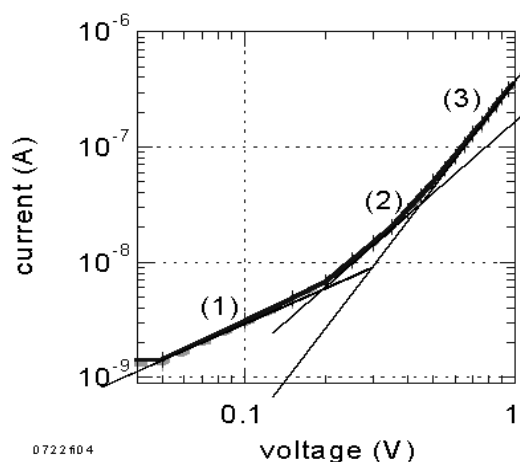


Figure 5.29: Double logarithmic plot of the dark IV curve of the PTV+PIF device (forward bias only). Three different slopes fit the curve suggesting the presence of shallow traps - see text.

partly shorted by e.g. pinholes for the following reasons:

1. The dark current²⁴ is relatively high (more than 20 times higher near 0V than in the other blend devices discussed in this thesis). Also the current is relatively voltage dependent in both the dark and under illumination which results indeed in a low shunt resistor $R_{sh} = 4 \cdot 10^7 \Omega$.

We note that $R_s = 10^6 \Omega$ (derived from the slope in the first quadrant).

2. The open circuit voltage is expected to reach about 0.5V (the workfunction difference between the electrodes), but is much lower here ($\approx 10\text{mV}$)

Fortunately, the shunt resistor is still high enough to avoid complete cancelling of the photogenerated current so that at least a qualitative evaluation of this blend is possible.

A double logarithmic plot of the dark IV curve reveals three distinct slopes (regimes)- see Fig.5.29. The first slope is clearly Ohmic, the second is $\propto V^2$ and the third $\propto V^3$. The quadratic dependence of the current may be due to shallow traps while the third slope may represent the transition to the trap free condition - see also Chapter 2.

²⁴This is the current at 0.00V which is driven by potential fluctuation of the source measure unit which are in the mV range.

We note that the low shunt resistance requires higher fields across the device to release the trapped charges but should not affect this analysis otherwise .

Summary

In this Section we have found that:

- The external quantum efficiency of a solar cell comprising a 1:1 blend between PIF and a polythiophene derivative (PTV) can reach at least 0.015% but can most probably increased considerably if partial shorts can be avoided.
- The photoresponse is - at least partly - enhanced with respect to devices comprising only the pure component suggesting photoexcited charge transfer between the two components
- The device shows a very wide photoresponse exceeding the visible wavelength range (400-1000nm).
- We found evidence for the presence of shallow traps from the analysis of the IV characteristics.

Chapter 6

Laminated Layer Devices

6.1 Introduction

In the previous chapters we have seen that single layer devices can be considerably improved by introducing a second semiconducting component resulting in a D/A type solar cell.

Both types of D/A cells, double layer and blend structures, have certain strengths but also disadvantages. For instance, the fabrication of a blend device requires solubility of both components in the same solvent - while the situation is reversed for the double layer structure. Unfavourable dimensions and/or defects of the interpenetrating network structure are the main problem in blends whereas short exciton diffusion lengths limit the performance of double layers severely.

Moreover, both types would benefit a lot if there was a possibility for separate treatment such as doping or heating of the specific D or A layer in order to modify the electrical and optical properties. Recently we have published a new device architecture i.e. manufacturing method that allows to realise all these possibilities in a surprisingly simple way [94, 200, 95].

The basic idea is to deposit both the D and A layer on separate electrodes (on substrates) before they are laminated together to obtain a D/A double layer device structure. The lamination process can lead to an improved D/A interface when compared to both a standard double layer and even a blend. This is because molecules in each layer have the opportunity to diffuse into the other layer during the lamination process.

The quality of the D/A interface can be controlled by heating, applying pressure or exposing the layers to solution vapor before, during or after the fabrication. The so obtained network structure is less likely to result in both isolated areas and - thanks to the separate charge transport layers - the (unwanted) connectivity with the wrong electrode.

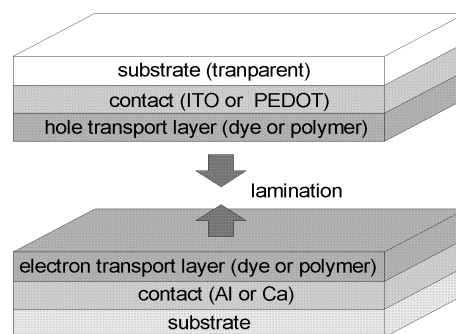


Figure 6.1: Scheme of the manufacturing method and architecture used to obtain the laminated solar cell. After lamination, charge-separation can occur at the interface of the hole and electron transport layers. Here we investigate both a device comprising polymeric semiconductors and another using dyes.

Both of which represent serious problems in normal blend devices.

In the following we list the strong points of the laminated structure:

1. Improved D/A network structure.
2. Relatively simple fabrication - from solution applying the technologically well known lamination technique.
3. Opportunity to treat each layer separately to improve the electronic and optical properties by e.g. doping or heat treatment.
4. Automatic encapsulation of the two semiconducting layers between the substrates.
5. The quality of the D/A interface may be controlled by treating the layers before, during and after the lamination process

Table 6.1: Survey of performance parameters of laminated solar cells.

EQE %	V_{oc} V	FF %	range nm	materials –	comments –	year
30	1.3	33	400-700	POPT/MCP	<i>polymer/polymer</i> [94]	1998
0.2	0.37	23	400-900	HPc/Per	<i>liquid crystal(dye)/dye</i> [200]	2000

Among the listed advantages of laminated devices we want to emphasize that the possibility of separate treatment of the D and the A layer represents a crucial point if commercially interesting efficiencies are to be achieved [277].

In practice, the following limitations using the lamination technique have to be considered:

1. Both components have to be compatible i.e. preferably dissolve in the same solvent and form aggregates not larger than about twice the exciton diffusion length - similar to the requirements for a blend structure, see Chapter 5.
2. Both material need to be sufficiently “soft” to enable lamination. Many polymers can be heated above a certain temperature (glass transition) where they become soft and “rubber-like”. Liquid crystalline phases are particularly “soft”.
3. The *curvature* of the substrates can become important since the films are only about 100nm thin and good contact over the entire area is desired. Particularly *flat* ITO covered glass substrates or *flexible* substrates are commercially available and may be used to overcome such problems.
4. Dust particles or others (crystallites..) between the electrodes could deteriorate the quality of the interface.

In the following sections we investigate first how soluble polymers can be used to obtain a device whose performance exceeds even the best pigment based device in terms of solar efficiency. The second device in this Chapter comprises the two soluble small molecules HPc and Per.

A survey of the performance parameters of both devices - which represent the only reported structures of this type in literature to date - is given in Table 6.1. Note that - despite some advantages of

the used dyes over the polymers as discussed in Section 6.3, the performance of the laminated *dye* device was surprisingly poor. In fact, it was even lower than the blend structure using the same molecules.

6.2 The Laminated Polymer Device

In this section we investigate a laminated device structure using two polymers (Fig.6.2) that have been chosen because of the following properties:

1. PL quenching experiments indicate exciton splitting at the polymer/polymer interface - a crucial requirement for building a D/A solar cell.
2. Both polythiophenes and polyphenylene-vinylenes have been showing good photovoltaic properties within the class of conjugated polymers [112, 213].
3. The bandgap of the spincoated film of POPT can be lowered by about 100nm upon moderate heat treatment. Together with MCP virtually the entire visible range can be covered which increases efficiency.
4. Both materials show suitable mechanical and film forming properties together with the required thermal stability.

Experimental

Current voltage curves and photocurrents were measured using a Keithley 237 source measure unit. Monochromatic illumination was provided by the output of a tungsten lamp dispersed by Bentham M300 single-grating monochromator. Quantum efficiencies were determined by normalisation with a calibrated silicon photodiode in the sample position. Absorption spectra were measured with a Hewlett Packard 8453 UV-Vis spectrometer. Reflection losses were neglected for all measurements.

The chemical structures of the polymer semiconductors used in this work are shown in Fig.6.2. MEH-CN-PPV or MCP is a fluorescent cyano substituted derivative of poly(*p*-phenylene vinylene) with a large electron affinity as a result of the electron withdrawing cyano-groups [174].

The device was fabricated in a nitrogen-filled glove box (oxygen<3ppm). One half of the device comprises the electron acceptor material(MCP) spincoated from filtered (0.45 μ m) chloroform solution (5mg/ml) on Ca which was sublimed on a glass substrate. The other half of the device comprises the hole acceptor material (POPT) spincoated from filtered (0.45 μ m) chloroform solution onto a conducting polymer (PEDOT, commercially available) film. PEDOT was spincoated from water onto a transparent gold layer to decrease the sheet resistance of PEDOT. Note that PEDOT and Au have approximately the same workfunction.

The gold layer was sublimed on a glass substrate. We added 5% (by weight) POPT to the MCP solution which has improved the efficiency considerably. The half with the POPT layer was heated to 200 °C under vacuum before the device was laminated together by applying a gentle pressure while one half was still at elevated temperature.

Heating of the polymer device prior to lamination was required for two reasons: 1) to introduce a transition of POPT into the more crystalline phase [18, 4] which absorbs more in the red region of the spectrum 2) to exceed the glass transition temperatures so that both polymers become “soft”.

The total thickness of the semiconducting layers was about 80nm and the active area 2.5mm². PL-efficiencies were measured using an integrating sphere and an argon ion laser as described previously[169]. The AFM images were obtained using phase sensitive detection, and were taken with a NanoScope IIIa Dimension 3100 (Digital Instruments Inc, Santa Barbara).

Results and Discussion

PL Quenching

Fig.6.2 shows that the single components are fluorescent and the PL of both is quenched upon addition of a small amount of one polymer to the other. This indicates efficient exciton dissociation in both polymers when blended.

Energy transfer between the blend partner as an alternative explanation has been ruled out¹ since

¹Only in the unlikely case that energy transfer is followed

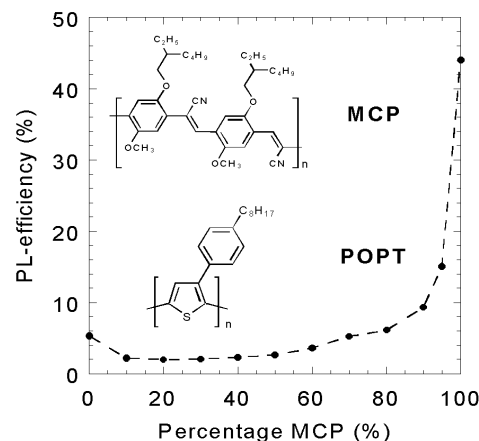


Figure 6.2: Chemical structures of the polymers used in the polymer double-layer blend and PL efficiency as a function of the blend ratio.

the PL of *both* materials is quenched in the blend. Such a “bath tub” shape of the PL versus blend ratio plot may therefore be taken as indication for charge transfer at the polymer/polymer interface - particularly if the electron affinity of one component (here MCP) is higher.

Note that MCP with 45% PL efficiency is *very* fluorescent. In other words, as much as 45% of all excitons generated in MCP recombine radiatively in the pure film. Upon the addition of only 5% POPT the number of radiative recombination is reduced to only 15%. This means a good deal of the photoexcited excitons is now split into its constituent charges with the holes trapped on the POPT molecules and extra *free* electrons in the conduction band of MCP.

Note that PL quenching ratios of 100 to about 10000 have been reported for blends involving relatively small molecules whereas quenching ratios in *polymers* are typically (here:20) about one order order of magnitude lower [112, 278, 62].

In order to sustain the photo-induced *charge generation mechanism* over time the trapped hole in POPT eventually has to recombine with an electron. From the fact that we do observe “continuous PL quenching” - not only in the first few ms - we can infer that these trapped holes do find a recombination partner such as e.g. the electrons in the CB of *adjacent* MCP molecules.

by strong non-radiative recombination, a similar “bath tub” shape may be obtained.

Note that this charge generation mechanism is not as efficient as the one at D/A interfaces of *double layer* structures where *both* charges of an exciton can travel to the electrodes. In fact the generation mechanism here resembles more the situation as we find it with oxygen traps distributed throughout an organic semiconductor - as discussed in Chapter 2.

The main difference to oxygen induced charge generation is that unlike the oxygen atoms, POPT is a semiconductor with a sufficiently low *bandgap* and can therefore also produce excitons. This results in the generation of extra charge carriers in the host system - here electrons in MCP, which contribute to the photocurrent and the reduction of the series resistor.

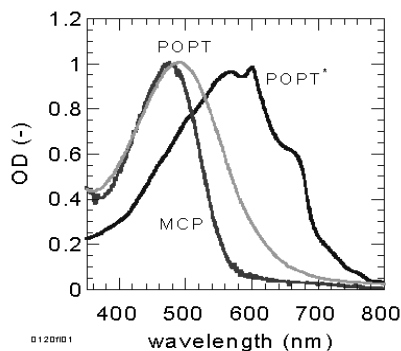


Figure 6.3: Absorption spectra of the pure MCP and POPT layer. Upon heat treatment the POPT film can shift its absorption onset by about 100nm towards the infrared, POPT*.

The described scenario is consistent with the observed incomplete PL quenching for higher concentrations (e.g. 20%) of the guest molecule (Fig.6.2): When the concentration of the guest material approaches a certain threshold, it becomes more difficult to get rid of the trapped charge since there are more and more like molecules in the neighborhood carrying the same trapped charges and no recombination partner.

The addition of 5% of MCP to the POPT layer reduces the fraction of radiatively recombining excitons from 5 to 3%. This is about the same PL reduction factor as for the quenching of the PL of pure MCP.

However, *pure* POPT shows already only 5% photoluminescence. Thus, the relatively few *extra* charges due to exciton splitting in the blend are not expected to make much of a difference. Indeed, we

found that the addition of 5% MCP to POPT could not improve the device performance [94].

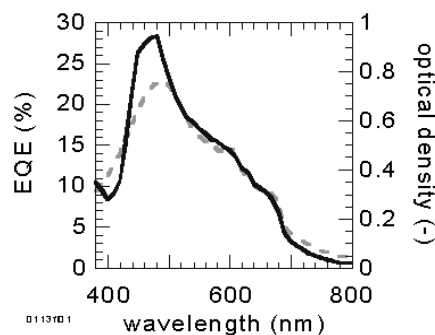


Figure 6.4: External quantum efficiency and absorption spectrum of the laminated polymer cell.

Absorption and EQE Spectra

Fig.6.3 shows the absorption spectra of MCP and POPT films. The absorption of the POPT film can be considerably improved (broadened) upon thermal annealing. This has been observed before in the same molecule by Bergren et al. [18] and is probably related to a temperature induced structural reorganisation of the regio-regular POPT molecules.

Fig.6.4 shows the linear absorption as well as the EQE spectrum of the laminated device (ITO/PEDOT/POPT+5%MCP/MCP/Ca). The absorption spectra of the heated POPT and the MCP film complement each other well so that relatively high OD can be achieved over a wide spectral range. The EQE follows the shape of the absorption spectrum nicely so that the entire semiconducting bulk can be regarded as active layer. The EQE is generally high and reaches 28% near the peak of the absorption (480nm).

Fig.6.5 shows the cross section of a laminated structure: There is inter-penetration between the two layers following the lamination and annealing procedure, on a length scale of 20-30nm. The cut to reveal the cross section was made at low temperature. We note that finer scale inter-penetration is not expected to be revealed in these images. These (and the other) AFM images are shown in phase contrast mode, most of which is due to differences in viscoelastic properties of the two polymers; height differences are no more than 5nm.

Fig.6.6 and Fig.6.7 show an in-plane image of the two semiconducting polymers mixed with 5% of the other component. Apart from the formation of the

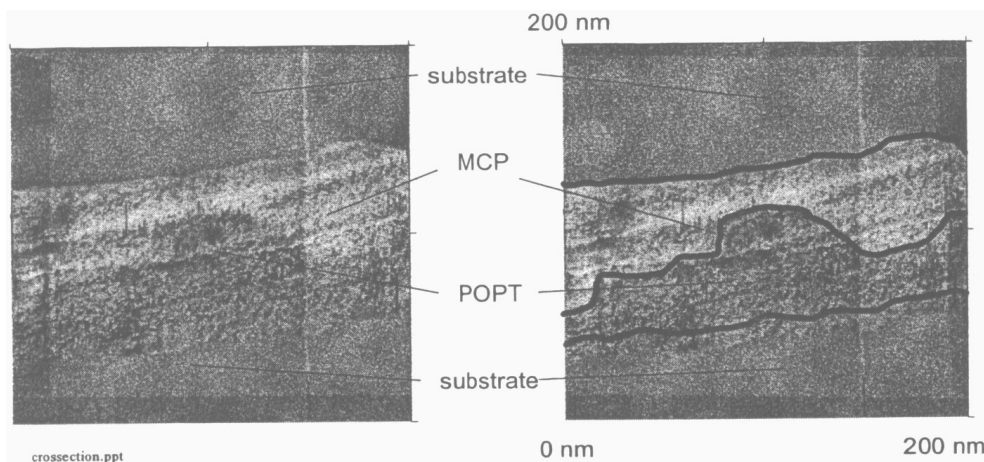


Figure 6.5: AFM phase contrast image of a cross-section of a laminated MCP/POPT+5%MCP polymer interface without metal electrodes sandwiched between polyester substrates. An increased D/A interface (outlined on the right picture) on a 40nm scale can be seen.

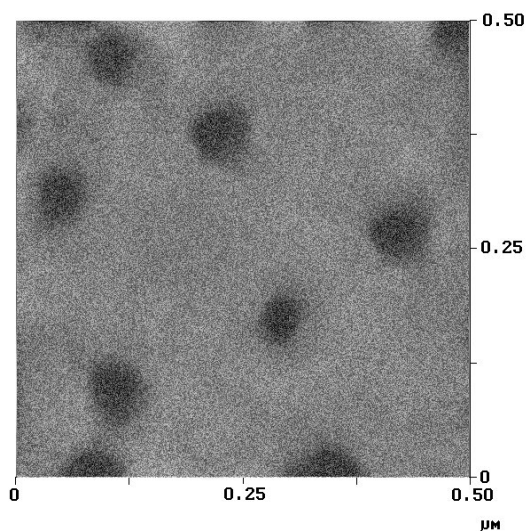


Figure 6.6: AFM phase contrast image of a MCP+5%POPT film. The larger spots are most likely islands of POPT clusters in the MCP matrix.

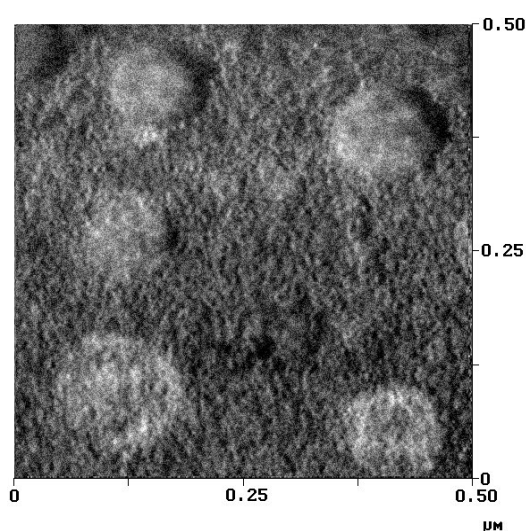


Figure 6.7: AFM phase contrast image of a POPT+5%MCP film. The larger spots are most likely islands of MCP clusters in the POPT matrix.

shown clusters or islands - finer scale mixing is suspected.

We note that a comparable device that does not contain 5% POPT in the MCP film showed only EQE values around 5% which is comparable to “conventional” polymer blend devices [112].

IV Characteristics

The IV characteristics of the laminated polymer cell with ITO and Al contacts in both the dark and under illumination is shown in Fig.6.8. The open circuit voltage of 600mV is comparable to good double layer devices and close to the difference of work-functions of the electrodes.

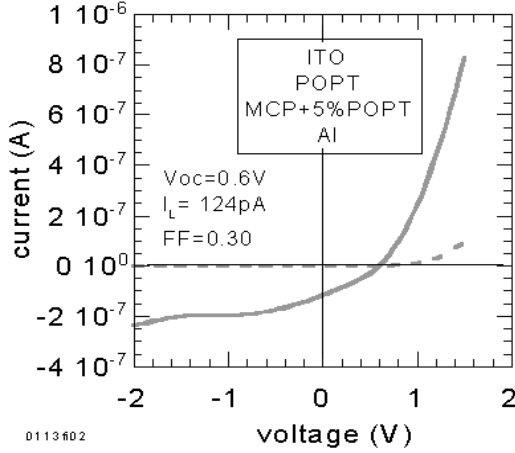


Figure 6.8: IV-Characteristics of the laminated polymer cell with ITO and Al contacts in the dark (dashed line) and under monochromatic illumination with $\lambda=480$ nm, illuminated area = 2.5mm^2 , irradiance = $35\text{mW}/\text{cm}^2$ (solid line).

From the slope in the first and third quadrant we obtain an upper limit for the series resistor of $7 \cdot 10^4 \Omega$ and a shunt resistor of approximately $10^7 \Omega$. These resistor values are in the order of inorganic cells of comparable dimensions - see Chapter 2. Hence, the both the high photocurrent and open circuit voltage with a relatively good FF - is not surprising. However, it is the shunt and not the series resistor that limits both the photocurrent and the fillfactor in this device. Interestingly, the current in the region between -1 and -1.5V shows particularly little voltage dependence for which we have no conclusive explanation yet.

The IV characteristics of the laminated polymer cell with Au/PEDOT and Ca contacts in both the dark and under illumination is shown in Fig.6.9. The open circuit voltage reaches now 1.3V whereas the photocurrent and the fillfactor (0.33) remains the same as in the ITO/Al device. The light characteristic can be fitted well with the Shockley equation (see Chapter 2) using $R_s = 1 \cdot 10^5 \Omega$, $R_{sh} = 2 \cdot 10^7 \Omega$, $I_L = 114\text{nA}$, $I_0 = 6\text{pA}$ and $n=5.8$.

Both resistor values are only little better than in the laminated polymer device with ITO and Al contacts. However, the open circuit voltage is considerably higher and the shape of the IV curve is now clearly dominated by the two resistor values (R_{sh} and R_s). The high value for n (and the low I_0) was necessary to fit the high V_{oc} .

The dark characteristics remains unchanged and

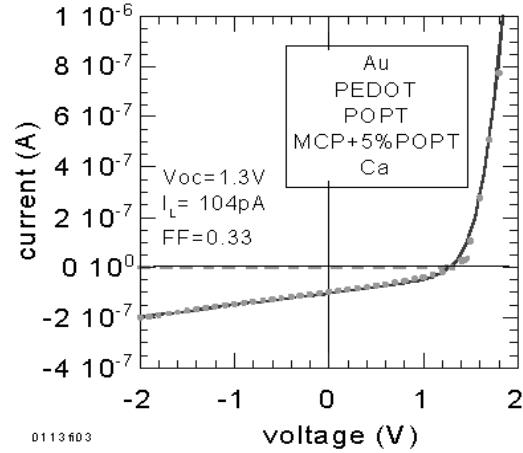


Figure 6.9: IV-Characteristics of the laminated polymer cell with Au/PEDOT and Ca contacts in the dark (dashed line) and under monochromatic illumination with $\lambda=480$ nm, illuminated area = 2.5mm^2 , irradiance = $35\text{mW}/\text{cm}^2$ (solid line). Circles represent data points while the solid line shows the modeled curve using the Shockley equation - see Chapter 2.

the increasing difference between light and dark curve (associated with a not negligible R_{sh}) allows to double the EQE or spectral response if -2V are applied. With such bias voltage at least 58% can be achieved in the photodiode mode.

In Fig.6.10 we plotted the open circuit voltage and the photocurrent versus intensity (irradiance) of the incident light. The figure shows that the photocurrent increases linearly with light intensity over at least 6 orders of magnitude. V_{oc} also increases with light intensity but slower and levels out around 2.2V. In fact, the slope of V_{oc} can be fitted well with

$$V(E) = 2.1V + 0.206V \cdot \ln(E) \quad (6.1)$$

if we ignore the offset value of 2.1V we can see that Eq. (6.1) resembles the expression as derived from the Shockley equation in Chapter 2:

$$U = n \frac{kT}{q} \cdot \ln\left(\frac{I_L}{I_0} + 1\right) \quad (6.2)$$

with $kT/q=26\text{mV}$. Using $nkT/q = 0.206V$ we obtain a diode ideality factor $n=8.0$ which is reasonably close to the $n=5.8$ obtained from the IV curve. The large offset value of 2.1V may be caused by the driving force that can be associated with

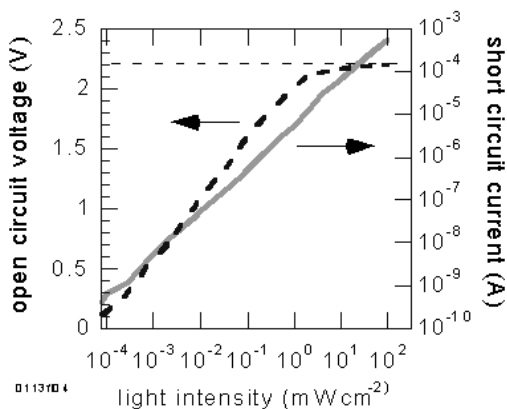


Figure 6.10: Dependence of V_{oc} and I_{sc} on the light intensity (E) at $\lambda=488\text{nm}$ for the laminated PE-DOT/Ca polymer solar cell. $I_{sc} \propto E^{1.02}$ while $V_{oc} \propto \ln(E)$ up to 20 mW/cm^2 and saturates then around 2.2V .

the difference of workfunctions of the electrodes ($W_{f,Au} = 5.1\text{eV}$, $W_{f,Ca} = 2.9\text{eV}$).

Under the assumption that I_{sc} and V_{oc} scale with intensity in the same way for all wavelengths we calculated a power-conversion efficiency for the polymer solar cell under solar conditions on earth (AM1.5d, 76mW/cm^2) of 1.9% - for details see Chapter 8.

This number is remarkable since it is almost twice as high as the hitherto best organic devices with reported solar efficiencies [244] and was achieved even without sublimation of an active layer.

Summary

In this Section we have shown that:

1. The lamination method allows the fabrication of organic solar cells that surpass the power efficiencies of earlier organic device architectures such as sublimed double-layers or blends, featuring many technological advantages.
2. Selective treatment of the two laminated layers, for example, annealing or "doping" of the organic semiconducting components in a D/A structure is now possible and can lead to high EQE and V_{oc} numbers.
3. The laminated polymer device can utilise light over a broad spectral range (400-750nm).

4. The workfunction difference of the electrode materials seems to determine the achievable V_{oc} in this device.
5. The shunt resistor rather than R_s are responsible for remaining EQE and fillfactor losses in this device.
6. The electronic transport properties of the electron acceptor material could be improved considerably upon mixing a small amount (5%) of the donor material into it.

We note that the method of lamination is already well established in (general) polymer & plastics industry and often realised as a roll to roll process using self supporting sheets.

Nevertheless, before it comes to its first industrial applications, such as large-area photosensitive arrays for scanners and medical imaging etc., further efforts to improve charge transport and absorption are necessary and possible stability problems will have to be addressed.

6.3 The Laminated Dye Device

In this section we investigate a laminated device structure using soluble small molecules (dyes) instead of polymers. We have chosen the two soluble derivatives of a metal-free phthalocyanine (HPc) and a perylene diimide (Per) - see Fig.6.11.

A combination of these two materials looked particularly promising to achieve good performance values using the new technique for the following reasons:

1. Both materials are relatively small molecules which dissolve readily in the same solvent. Thus inter-diffusion after lamination may lead to a very fine and therefore efficient interpenetrating network sandwiched between to transport layers.
2. Insoluble derivatives of these molecules have shown good performance in both single layer and double layer solar cells.
3. Both molecules have high light-fastness and thermal stability.
4. The liquid crystalline properties of HPc may favour the lamination process.

5. Efficient PL quenching has been observed suggesting efficient exciton quenching at the dye/dye interface.
6. The photovoltaic properties of HPc as a single layer may be improved by introducing more charge free charge carriers by the addition of a few % Per.

Experimental

Current voltage curves and photocurrents were measured using a Keithley 237 source measure unit. Monochromatic illumination was provided by the output of a tungsten lamp dispersed by Bentham M300 single-grating monochromator. Quantum efficiencies were determined by normalisation with a calibrated silicon photodiode in the sample position. Absorption spectra were measured with a Hewlett Packard 8453 UV-Vis spectrometer. Reflection losses were neglected for all measurements.

The chemical structures of the dyes used in this work are shown in Fig.6.11. Per is commercially available from Synthec/Synthone (Germany) while HPc has been synthesised as reported elsewhere[165]. The electron-accepting dye (Per) was spincoated from chloroform solution (15 mg/ml) onto indium tin oxide (ITO) covered glass substrate. The hole accepting dye (HPc) was spincoated from chloroform solution (35 mg/ml) onto a 50nm thick Al layer which was thermally sublimed on glass. We also added 10 percent (by weight) Per to the HPc solution, which - as discussed below - increased the performance significantly. Both solutions were filtered with 0.1mm PTFE filters.

The lamination was performed under gentle pressure in a laminar flow box after exposing both halves of the device for 15 min to chloroform vapor.

Results and Discussion

PL Quenching

If exciton splitting occurs in a blend with at least one fluorescent material, it is usually faster than its radiative decay and can therefore be observed as photoluminescence (PL) quenching.

Fig.6.11 shows that the relative high PL of pure Per is almost completely quenched if the blend contains more than about 20% HPc. This means that virtually all excitons in the blend film are affected by the presence of HPc molecules suggesting a good

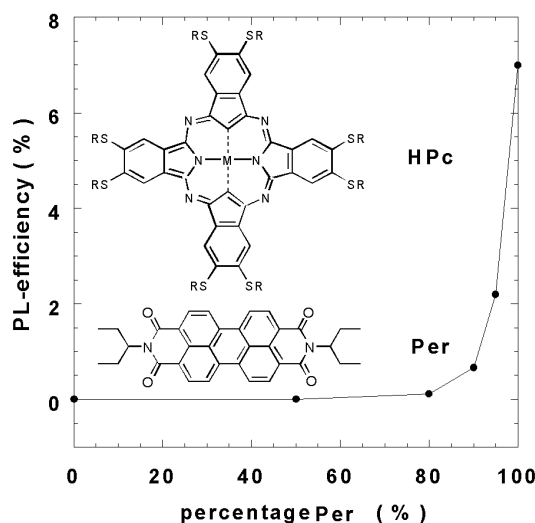


Figure 6.11: Chemical structure of the dyes used ($R=C_{12}H_{25}$, $M=H_2$) and photoluminescence efficiency as a function of the blend ratio. Radiative recombination of Per is strongly reduced for all blend ratios indicating charge-separation at the HPc/Per interface. HPc does not fluoresce in the solid state.

solution and/or a sufficiently long diffusion range for excitons in Per.

The pure HPc layer does not show any detectable PL at room-temperature. However, PL efficiency of about 50% has been reported in a metal-free Pc with alkoxy substituents at low temperature (4K). The low temperature PL decreases with rising temperature until a sharp drop occurs at the solid to mesophase transition where the PL is virtually quenched completely [21]. This sharp drop has been associated with an increase of the exciton diffusion length in the mesophase that enables more excitons to reach quenching sites.

We note that our photovoltaic measurements of cells involving HPc in different architectures suggest exciton diffusion lengths of around 200nm at room-temperature - see Chapter 3 and Chapter 4. In addition, PR-TRMC measurements indicate very high charge carrier mobilities in the crystalline and the mesophase of HPc.

Because of the absence of PL in the solid state, it is not possible to probe for quenching of the PL of HPc upon addition of Per. As a consequence, we cannot completely exclude that transfer of the exciton from the high bandgap material Per to the lower bandgap material HPc is taking place.

However, the investigation of the HPc+Per blends in Chapter 5 indicates that charge transfer

takes place at the interface of HPc/Per mixtures. In the same Chapter we show AFM images that are consistent with the formation of a very fine network with these molecules. Note that, if the network is too fine, the connectivity between molecules may not be very good leading to a high recombination rate i.e. low shunt and high series resistor.

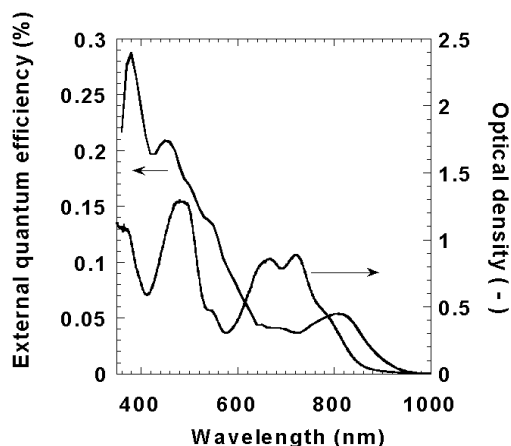


Figure 6.12: External quantum efficiency (EQE) and absorption spectrum of the laminated dye cell.

Absorption and EQE Spectra

The EQE of this device is plotted together with the absorption spectrum in Fig.6.12. The cell is able to harvest light from the UV to the near infrared (900nm). The EQE spectrum is strongly antibatic in the wavelength range where only HPc absorbs (600-900nm) indicating the presence of a filter effect due to a too thick HPc layer. The thickness of HPc is about 400nm to avoid shorts in this soft material.

The EQE approaches 0.3% at the short wavelength end of the visible range. This value is slightly smaller than in a comparable double layer device (0.42%) and only about a third when compared with the standard blend device (1.0%).

IV Characteristics

The IV characteristics of the laminated dye cell is shown in Fig.6.13. The slope in the first quadrant can be associated with a series resistor of $0.5 \cdot 10^8 \Omega$ whereas the inverse slope in the 3 quadrant gives a shunt of $0.1 \cdot 10^8 \Omega$. Although the value for R_s can only represent an upper limit (since the slope could

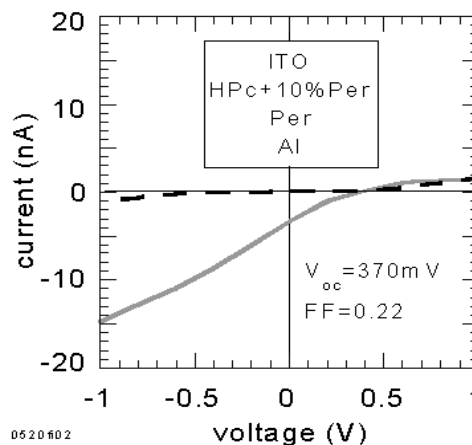


Figure 6.13: IV characteristic in the dark (dashed line) and under illumination (solid line) of the laminated dye device.

increase for higher voltages) the low fillfactor and flat continuation of the curve after leaving the third quadrant suggests that R_s is truly large.

We note that according to the considerations of IV curves in Chapter 2 a series resistor that is larger than the shunt would dominate the entire IV curve. The IV curve would then become completely linear with a inverse slope according to the value $R_s + R_{sh}$.

Since this is not the case here we consider that there is an effect of a counter-diode that increases the slope in the negative voltage range. This would also comply with the small fillfactor < 0.25 . The photocurrent to dark current ratio can be increased by a factor three upon applying a bias voltage of -1V.

Summary

In this Section we have shown that:

- Small soluble molecules (dyes) can be used to manufacture a laminated solar cell.
- The efficiency could not be increased with respect to neither the double layer nor the blend cell.
- The laminated dye cell can harvest photons ranging from 400 to about 900nm over the entire visible range with EQE comparable to good polymeric single layer devices like ITO/MEH-PPV/Al.

- The EQE can be increased by a factor 3 in the photodiode mode by applying -1V bias voltage.

Chapter 7

Discotic Liquid Crystals as Solar Cell Materials

7.1 Introduction

Molecules in the solid phase have virtually no opportunity to move and orient themselves with respect to one another. They have a certain degree of positional and orientational order that cannot be changed in this phase. However, if the same solid melts to a liquid both types of order are lost completely; the molecules can now move and tumble randomly.

The situation is different when a solid melts to a *liquid crystal*¹: The positional order is then lost - since the single molecules are free to move in the same fashion as in a liquid - but at least some of the orientational order remains or even increases. Fig.7.1 illustrates how both orientational and positional order may be improved since the molecules are free to move and to orient themselves. This can be the case for disc shaped (discotic) aromatic molecules since their strong $\pi-\pi$ interaction acts as driving force that favours aggregation in stacks i.e. columns². The disc like shape also favours hexagonal arrangement of the columns.

However, Fig.7.2 shows that the degree of order within such a liquid crystalline phase can vary and mesophases with a different degree of positional order can form. The nematic phase for example can occur with e.g. molecules that have one or more atoms sticking out of the middle of the disc which limits the achievable degree of positional order. Note that even these molecules are still able

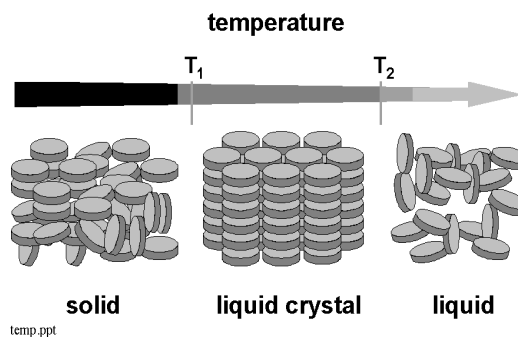


Figure 7.1: Schematic illustration of the solid, liquid crystal, and liquid phases that can be formed by disc-shaped molecules. The degree of order of the solid phase depends on its (thermal) history. The liquid crystalline phase allows self-organisation of the molecules in a limited temperature range (discotic phase).

to sustain a certain degree of *orientational order* since all discs can still arrange such that they face the common substrate plane - which is sufficient to distinguish the phase clearly from a liquid.

In 1994, Adam et. al. reported high charge carrier (hole) mobility in the liquid crystalline phase of a discotic molecule (hexa-hexyl-thio triphenylene, HTTP) based on time of flight (TOF) measurements [2]. The mobility in HTTP increased by a factor of 10 at the transition from the liquid to the hexagonal discotic phase and gains further two orders of magnitude in a higher ordered discotic phase.

With the exception of organic single crystals [139] the reported mobility ($0.1\text{cm}^2\text{V}^{-1}\text{s}^{-1}$) for photo-induced charge carriers of HTTP was higher than

¹The first man who discovered this special phase of matter was F. Reinitzer, an Austrian botanist. He noted the double melting behaviour of cholesterol acetate and cholesteryl benzoate [219]. Reinitzer collaborated with O. Lehmann who was the first to use the term liquid crystal [159].

²S. Chandrasekhar reported the first observation of thermotropic mesomorphism of a disc like molecule (benzene-hexa-n-alkanoate) [44].

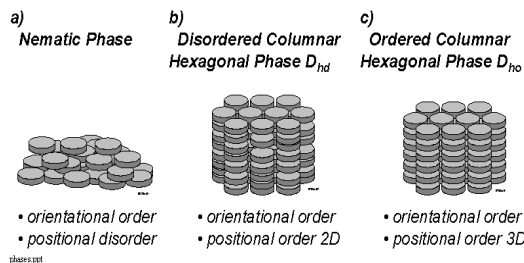


Figure 7.2: Schematic illustration of three different types of liquid crystalline discotic phases. The ordered columnar phase is expected to show the best transport properties.

for any other organic system reported at that time. The distance between adjacent discs in a column was found to be 3.6 Å whereas the distance between the columns was 21.7 Å.

As a consequence, charge (and exciton) transport is expected to occur preferably along the columns whereas the mobility in directions perpendicular to column axes can be more than 500 times smaller [23] since the excited species have to tunnel through a saturated hydro-carbon mantle (the insulating side chains). Such columns may be used to transport efficiently not only charge carriers but also excitons and ions [262].

The discotic phases may even be frozen in, simply upon suitable cooling or become temperature independent if the molecules are polymerised i.e. cross-linked in the mesophase [262]. Moreover, both hole and electron transporting discotic liquid crystals can already be prepared [23].

Columnar discotic molecules (triphenylenes) have already been used in LEDs where they showed strong reduction of the onset voltage upon perpendicular alignment of the columns [53].

Because of these interesting opportunities molecular wires made of discotic liquid crystals are considered a promising alternative to conjugated polymers which can also be seen as molecular wires since transport occurs most efficiently along their conjugated backbone.

The HTTP molecule in which the high mobility was first measured is a relatively small conjugated system and absorbs not much light in the visible range. Larger aromatic molecules like phthalocyanine pigments with their strong absorption and high stability despite the low bandgap have been proven very successful in the past as semi-conducting layers in photovoltaic cells and therefore

have been intensely investigated over many decades [268, 43, 29, 154, 231, 267, 59, 67].

A. Lux and G.G. Rozenberg have synthesised phthalocyanine derivatives which carry 8 thio-alkyl side chains (Fig.7.3) to facilitate solubility and possibly liquid crystallinity [165]. These particular derivatives are subject of our investigation in this Chapter.

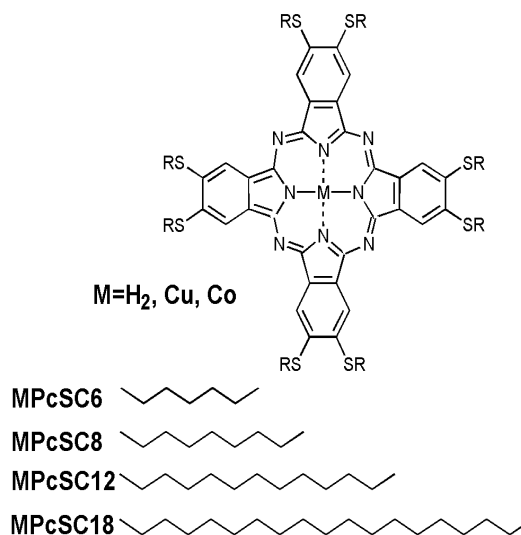


Figure 7.3: Chemical structure of the liquid crystalline phthalocyanines studied in this thesis.

Although their monomers are well known in literature, these soluble and probably liquid crystalline phthalocyanines have either not been synthesised before or not investigated in terms of their liquid crystalline and photovoltaic properties. CV data and aggregation effects have been reported for similar derivatives in Ref. [180]).

In order to exploit the full potential of our molecules in photovoltaic devices it was important to know the "mechanical" properties such as film forming properties, solubility but also the temperature range of the mesophases. Only then can we orient the columns such that their axes points perpendicular to the electrodes.

Thus a hotstage with a polarisation microscope and video camera to record images of the developed textures was set up and access to the equipment for essential thermal characterisation (TGA, DSC) of other research groups has been arranged.

After a description of the experimental details in the next section we present and discuss the results of the liquid crystalline properties. The obtained information is then used to fabricate two double

layer devices, both comprising a liquid crystalline phthalocyanine (HPc) with a perylene pigment as electron acceptor. One device was heat treated to orient the columns perpendicular to the electrodes while the other one was kept at room temperature. These results are discussed in Chapter 4 which treats double layer devices structures.

In this Chapter we investigate the photovoltaic properties of a simple device comprising a single layer of the liquid crystalline semiconductor sandwiched between ITO and AL.

7.2 Experimental

Current voltage curves and photocurrents were all measured *in air* using a Keithley 237 source measure unit. Monochromatic illumination was provided by the output of a tungsten lamp dispersed by Bentham M300 single-grating monochromator.

External quantum efficiencies were determined by normalisation with a calibrated silicon photo diode in the sample position. A more detailed description of how we calculated the EQE can be found in Chapter 10. Absorption spectra were taken using a Hewlett Packard 8453 UV-Vis spectrometer. Reflection losses were neglected for all measurements.

The chemical structure of the dyes used in this section are shown in Fig.7.3. Information on the synthesis of the different phthalocyanine's can be found in Refs. [165, 269, 105, 73]. All materials were purified carefully by column chromatography and the structures established by IR, NMR and mass spectroscopy. HPc was spincoated from chloroform solution (90 mg/ml for the thick (450nm) and 30mg/ml for the thin (80nm)layer) onto either an ITO covered quartz substrate to built a device or a spectroil substrate for an optical measurements (polarisation microscopy). The solution was filtered with a 0.1 μ m disposable PTFE-filter.

The spin-speed for the thick layer was 1600rpm and 2000rpm for the thin film. The Al top contact for the two devices was obtained via thermal sublimation. The oriented HPc film was obtained by heating to 292 °C (20K/min) under constant nitrogen flow and then slowly (5K/min until 270°C, then 20K/min) cooled down to room temperature using the hotstage (Linkam).

DSC and TGA measurements were performed with a Perkin Elmer DSC7 at a heating rate of 10K/min. In order to perform polarisation microscopy, an adapted Vickers microscope has been equipped with a hotstage (Linkam) and a set of polarisers.

Table 7.1: Phase transition temperatures (°C) of a series of liquid crystalline phthalocyanine derivatives. All temperatures have been determined using DSC scans and there was no contradiction with the results from polarisation microscopy. Brackets indicate transitions upon cooling. K=crystalline, D=discotic=liquid crystalline, I= isotropic (liquid).

semicond. molecule	K		D		I
H ₂ PcSC ₁₂	•	20 (4)	•	292	•
CoPcSC ₁₂	•	52(20)	•	–	•
CuPcSC ₈	•	79(-)	•	–	•
CuPcSC ₁₂	•	63(9)	•	–	•
CuPcSC ₁₈	•	52(45)	•	–	•

7.3 Liquid Crystalline Properties

As a result of our investigations of these phthalocyanines in the hotstage under the polarisation microscope together with DSC analysis, we could determine the transition temperatures as summarised in Table 7.1. Since all mesophases were found to be very viscous at lower temperatures not all DSC peaks could be confirmed under the polarisation microscope.

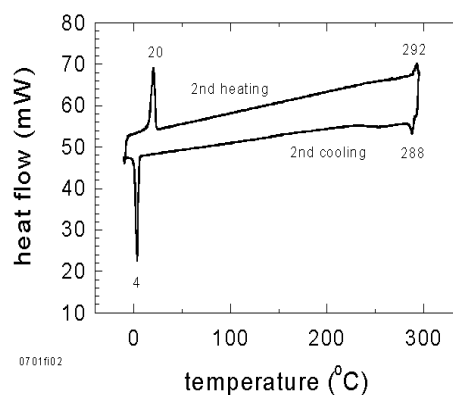


Figure 7.4: DSC trace of HPc. The peaks at 292 and 288°C indicating the transition to the liquid phase are clearly visible here - which is fairly rare for discotic phthalocyanines.

The transition temperatures of both the crystalline (K) to the discotic phase (D) and the discotic (=liquid crystalline) to the isotropic liquid (I)³ of

³Which were in fact only found for HPc.

the octakis(alkylthio)-substituted phthalocyanines investigated here are generally lower than those of their analogues with alkoxy side chains [73] and decrease even further with increasing chain length as reported for similar derivatives in Ref. [253].

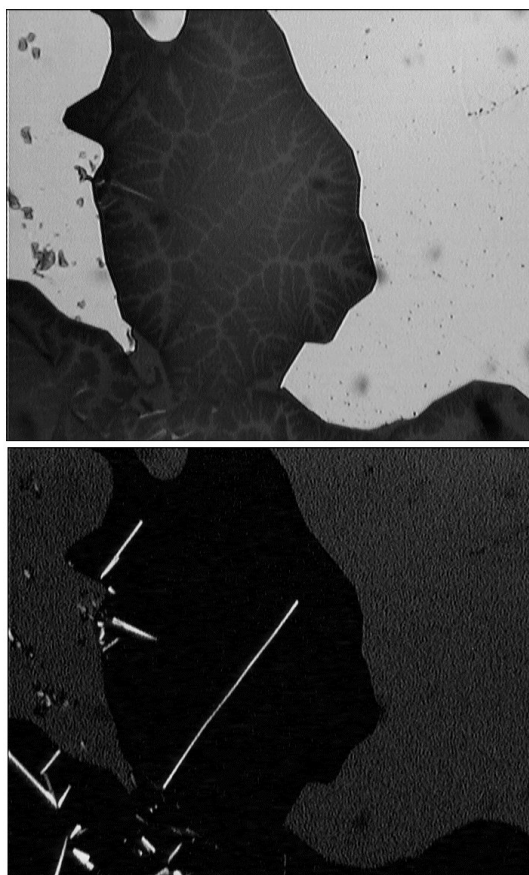


Figure 7.5: The image on the top (A) shows the digitate stars as they appear under parallel polarizers upon cooling from the liquid phase of HPc. Image B shows the same section but with crossed polarizers which reveals the linear birefringent defects that indicate perpendicular orientation of the columns. Both pictures were taken at 280 °C after cooling from the liquid phase.

Note that even lower transition temperatures can be achieved generally by replacing the thio alkyl side-chains with alkyl or alkoxy chains with ethylene oxide units [152].

For HPc the K→D transition temperature is reduced to such an extent that the mesophase can form already at room temperature (20°C). It is also the only material for which the transition to the isotropic liquid phase - the clearing temperature -

could be detected by DSC (see Fig.7.4).

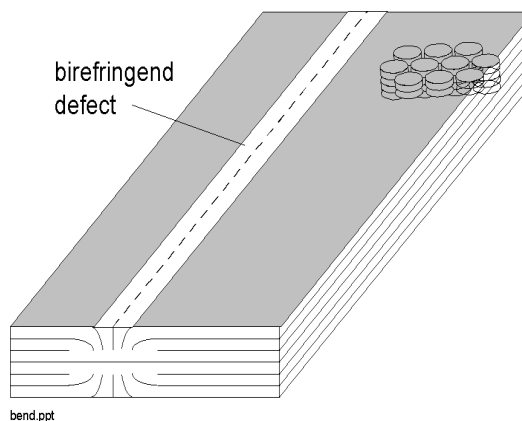


Figure 7.6: Proposed molecular arrangement of discotic molecules to explain the formation of birefringent defects: The main deformation mode is a bend mode [253]. The observation of such defects may be taken as indication for perpendicular alignment of the columns with respect to the substrate plane.

For all other materials the mesophases are stable up to about 290-350°C (see also the TGA results below) where they start to decompose before a liquid phase can be detected.

Upon cooling HPc from the isotropic liquid at a rate of 10K/min, digitate stars appear under parallel polarizers (Fig.7.5 A). Such a texture has been observed for alkoxy-substituted PCs [253, 152].

As they grow they coalesce to a homeotropically aligned sample whereby some linear defects are formed, Fig.7.5. These appear as bright birefringent lines in the dark background under crossed polarisers.

The origin of these linear defects has been proposed in Ref. [253] whereas other defects are studied in Refs [31, 30]. The birefringent lines can be the results of a deformation mode as illustrated in Fig.7.6.

Heating of a sample of the cobalt derivative (CoPcSC12) to 280 °C revealed another, more common, characteristic texture of a columnar phase, the focal conic texture, see Fig.7.7. The shown texture was retained during cooling down to room temperature.

The thermal stability of the phthalocyanines was investigated by thermogravimetric analysis (TGA) at a heating rate of 10K/min, see Fig.7.8. For example, initial decomposition of CuPcSC12 under nitrogen atmosphere occurs at about 320°C, then

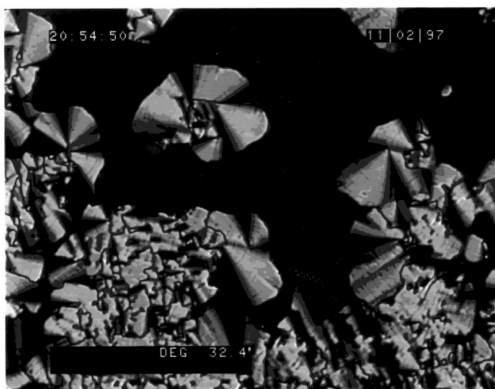


Figure 7.7: The focal conic texture of CoPcSC12 as it is observed under crossed polarizers at 280°C after cooling from the liquid phase.

the main decay takes place at 380°C. The mass loss around 400°C corresponds exactly to the relative mass loss of the eight side chains.

In air, see Fig.7.8, the temperatures for initial and main decomposition are decreased by about 40°C. We note that heating and cooling of both the device samples and samples for optical microscopy was typically done with the hotstage purged with nitrogen to minimize possible degradation effects at higher temperatures.

The absorption spectra of the metal-free phthalocyanine in chloroform shows two intense transitions (Q bands) at 702 and 730 nm (see Fig.7.10) which are about 30 nm red-shifted compared with their alkoxy-substituted analogues [253].

The Q bands appear generally less intense and are blue-shifted in more polar (ethyl acetate) as well as in less polar (toluene, n-hexane) solvents due to formation of aggregates[166].

Photoluminescence is only detectable in very good solvents such as chloroform and only at concentrations lower than 10^{-3} mg/ml since aggregation quenches the fluorescence drastically. Fig.7.10 shows both PL and absorption of such a dilute solution.

We note that in the following section we use HPC at room temperature in a single layer solar cell whereas double layer devices comprising a LC phase where the columns are oriented parallel to the substrate are investigated in Chapter 4.

For all liquid crystalline phthalocyanines the intra-molecular charge transfer step occurs on a pico-second time scale even in the liquid crystalline

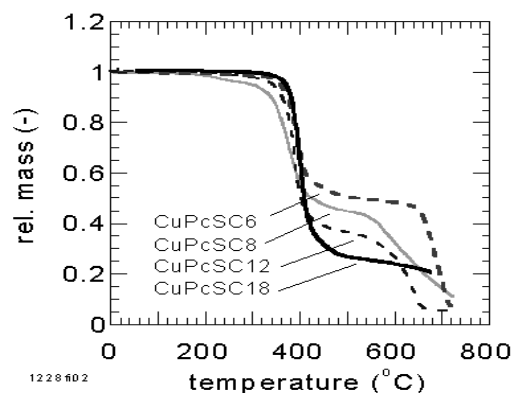


Figure 7.8: TGA of a series of phthalocyanine with different chain lengths measured under nitrogen.

phase [57]. Although the PR-TRMC method does not allow to differentiate between mobilities of electrons and holes, TOF measurements on discotic materials identified the hole as majority charge carrier.

From the fact that range of mobilities for a large variety of side chains spans less than an order of magnitude can be inferred - as expected - that the aromatic core of the phthalocyanine mainly determines the transport properties.

7.4 Photovoltaic Properties of HPC

Absorption and EQE Spectra

Fig.7.11 shows the linear absorption spectrum of an ITO/HPC/Al device (80nm thick) when illuminated through the ITO contact as well as the linear absorption spectrum. The Q band here is considerably smoother and absorbs stronger in the long wavelength range compared to the one in dilute solution in Fig.7.10. Such behaviour is usually assigned to strong aggregation as it is expected for this mesogenic compound.

The onset of absorption is around 900nm which corresponds to a semiconductor bandgap of 1.38eV. A sufficiently thick layer of HPC can therefore absorb up to 64 % of the solar radiation on earth - see table in Chapter 8.

The EQE in Fig.7.11 follows the absorption spectrum closely suggesting that the whole bulk of 80nm contributes to the photocurrent when illuminated through the ITO contact. The somewhat pro-

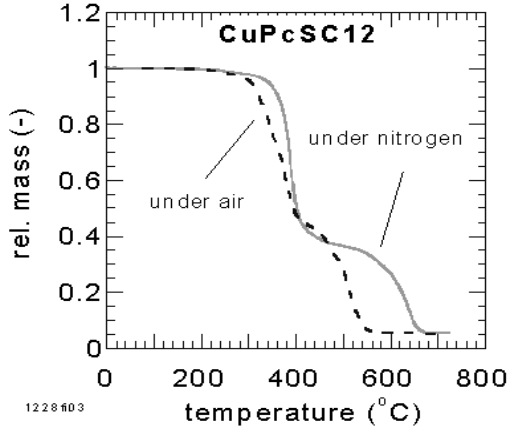


Figure 7.9: TGA of CuPcSC12 under nitrogen and air. Even in air the material is stable up to about 300°C.

nounced EQE in the absorption onset is probably due to enhanced exciton dissociation in aggregates as suggested in a study of photocurrent peaks in MEH-PPV [120] and not a signature of an optical filter effect.

The other EQE features coincide well with the absorption⁴ and there is no offset at the short wavelength side of the Q band.

Fig.7.12 shows the EQE and absorption upon illumination through ITO for a much thicker device (450nm). The first absorption peak (0-0 transition) appears stronger than in the thin film. This is more likely an artifact in conjunction with the background correction during the absorption measurement and therefore not significant.

However, here in this rather thick device, the EQE shows the familiar antibatic behaviour as it is usually observed in p-type semiconductors between ITO and Al when illuminated through ITO.

At the beginning of Chapter 3 we describe a method how the maximum thickness $d_{opt.}$ of the active region can be estimated from the absorption and EQE spectrum using the formula:

$$d_{opt.} = \frac{OD(\lambda_e)}{OD(\lambda_0)} \cdot d_0 \quad (7.1)$$

We have chosen to take the required input parameters from Fig.7.12 (thick device) since the shape EQE of the thin device does not allow a clear de-

⁴Note that a slight offset may be caused by a non horizontal baseline in the EQE spectrum.

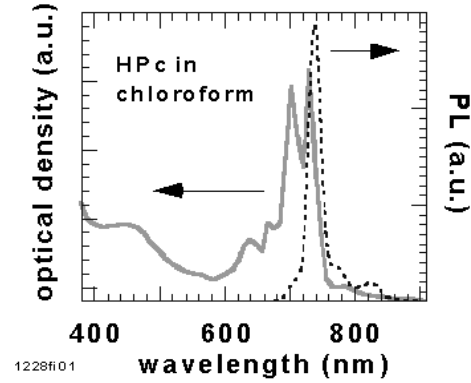


Figure 7.10: Absorption and photoluminescence of a very dilute solution of HPcSC12 in chloroform.

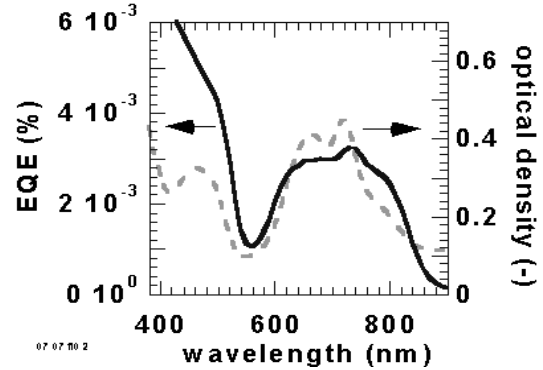


Figure 7.11: The EQE of the thin HPc device (in air) follows the absorption features when illuminated through ITO.

termination at what wavelength we ought to take the value for $OD(\lambda_e)$.

From Fig.7.12 we extracted the following data: $OD(\lambda_e) = 0.55 \pm 0.2$, $OD(\lambda_0) = 1.24 \pm 0.01$ and $d_0 = 450 \pm 30\text{nm}$. Using Eq. (7.1) we obtain:

$$d_{opt} = 200 \pm 80\text{nm} \quad (7.2)$$

The large error for $OD(\lambda_e)$ is due to the steep slope and the relatively broad peak in the EQE spectrum of the thick device. To avoid the occurrence of a filter effect we suggest not to exceed 120nm in this material.

Note that the absolute EQE values for both HPc devices are surprisingly low - only about a tenth of the EQE in e.g. a ITO/MEH-PPV/Al device - considering the large active range of at least 120nm for

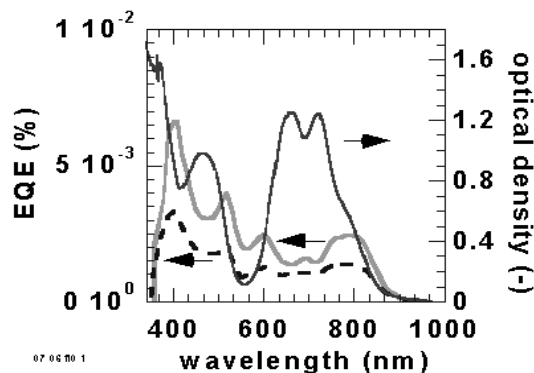


Figure 7.12: The EQE (solid line: 5hrs in air; dashed line: in vacuum) of the thick HPc cell shows antibatic behaviour when illuminated through the ITO contact.

HPc. We believe that a considerably higher series resistor due to a low concentration of free charge carriers may cause the low photocurrent in HPc. This possibility will be considered in the subsequent paragraph focusing on the IV characteristics.

The EQE spectra of both HPc devices - see Fig.7.14 and Fig.7.13, follow the absorption as expected if illumination occurs through the semitransparent Al contact.

However, the EQE of the thicker device is then about 3 times higher than the EQE of the 80nm device. This suggests that the active region is actually around 240nm, favouring a larger value within the error bars for the maximum active range as obtained above.

According to the discussion in Chapter 2 the filter effect in the thick device (ITO/HPc/Al, illumination through Al) can be caused either by a limiting exciton diffusion range or a limiting electron mobility (or both). Although both the charge and exciton transport are likely increased due to the strong $\pi - \pi$ interaction, the high value for the mobility ($\mu_e + \mu_h$) value obtained from PR-TRMC in Ref. [57] do not allow to exclude the possibility that the electron drift range is still a limiting factor in these devices. Hence, we can only say that the exciton diffusion range *plus* the electron drift range in these devices is around $200\text{nm} \pm 80\text{nm}$.

We want to note that this number means that the exciton can be over an order of magnitude larger than in typical polymers and is largely consistent with the suggested *several* hundred nanometers as suggested in Ref. [21] for a very similar compound,

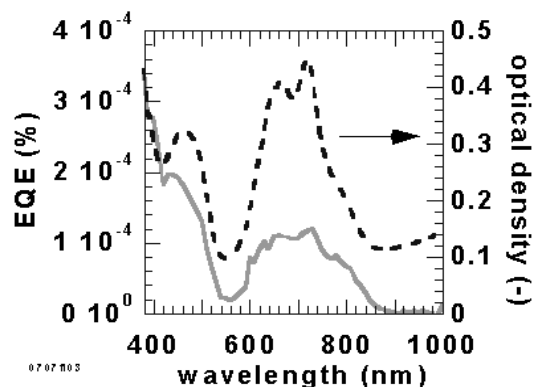


Figure 7.13: The EQE of the thin ($d=80\text{nm}$) device (solid line), illuminated through the Al contact and measured after 5hrs in air follows the linear absorption features (dashed line)

HPcOC12.

The lower absorption coefficient of HPc allows a 10nm layer of MEH-PPV to absorb as much light as the 80nm HPc film. Thus, since both films are thinner than their maximum active region they should give approximately the same photocurrent i.e. EQE numbers - provided all other parameters are comparable.

Charge Carrier Mobilities

In Table 7.2 we give a survey over published charge carrier mobilities in organic semiconductors including several liquid crystals. Recently published values using pulse radiolysis time resolved microwave conductivity (PR-TRMC) reveals even higher mobilities in the *crystalline* phase of many discotic materials [57]. The results are promising in that the compound we used for fabrication of solar cells showed the highest mobility for the discotic phase among all investigated compounds in this reference.

The latter includes other metal free phthalocyanines as well as porphyrins and triphenylenes with various lengths and types of side chains [57]. In the crystalline phase the HPc derivative with 8 instead 12 carbon atoms gave the highest mobility ($0.54\text{cm}^2\text{V}^{-1}\text{s}^{-1}$).

However, note that HPcSC12 is in its liquid crystalline phase starts to form already at 20°C according to our results whereas the $\text{K} \rightarrow \text{D}$ transition occurs only at 77°C according to Ref. [57]. Provided our number is true, significantly higher values for the mobility were expected for slightly lower tem-

Table 7.2: Survey of electron (e) and hole (h) mobilities of important organic and inorganic semiconductors. For abbreviations see Chapter 1. Σ denotes the sum of charge carrier mobilities.

material	type	mobility	source/method	comment
	-	$\text{cm}^2 \text{V s}^{-1}$	-	-
Si-monocr.	h/e	450/1500	[241]	inorganic
Si-amorph	e	0.1-1.0	[85]	inorganic
HPcS8 (K-phase)	Σ	0.54	PR-TRMC [57]	liquid crystal
HPcS8 (D-phase)	Σ	0.16	PR-TRMC [57]	liquid crystal
HHTS6 (K-phase)	h	0.26	PR-TRMC [57]	liquid crystal
HHTS6 (H-phase)	h	0.1	TOF [2]	liquid crystal
HHTS6 (D-phase)	h	0.007	PR-TRMC [57]	liquid crystal
HPcS12 (K-phase)	Σ	0.25	PR-TRMC [57]	liquid crystal
HPcS12 (D-phase)	Σ	0.22	PR-TRMC [57]	liquid crystal
MgPc	h	0.1	[87]	pigment
PcOx	Σ	$2 \cdot 10^{-2}$	PR-TRMC [262]	pigment
HPc	h	$1 \cdot 10^{-3}$	FET [13]	pigment
PPV	h	$1 \cdot 10^{-4}$	TOF [168]	polymer
PT(alkyl)	h	$9 \cdot 10^{-5}$	[85]	polymer
PT	h	$1 \cdot 10^{-5}$	[85]	polymer

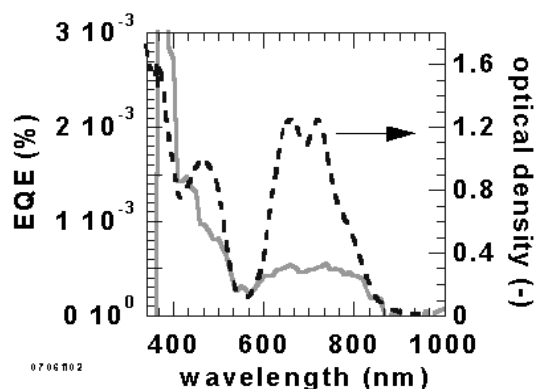


Figure 7.14: The EQE of the thick ($d=450\text{nm}$) HPc device (dashed line, in vacuum) increased when exposed to air for 5 hrs (solid line). The device was illuminated through the Al contact.

peratures since the value for the crystalline phase was measured at room-temperature.

It is worth considering that the mobilities obtained in PR-TRMC measurements usually refer to the *maximum* that could possibly be achieved in a two electrode device with a perfectly orthogonally oriented mono-domain of a discotic material [57]. Hence, one may conclude that the sample of HTP in the TOF experiments of Ref. [2] must have been

close to perfectly aligned, with the columnar axes orthogonal to the electrode surface and with complete columnar integrity across the entire 30μ electrode gap corresponding to as much as 10^5 macro cyclic units - a really thin molecular wire.

We note that rapid charge transport along self assembling graphite nanowires has recently been reported in the discotic molecule tetrakis coronene [58].

IV Characteristics

A numerical analysis of the IV curves in Fig.7.16 shows that both the series resistant and the shunt of the HPc devices are considerably higher ($R_s \approx 2 \cdot 10^9 \Omega$, $R_{sh} \approx 1 \cdot 10^{10} \Omega$ under illumination⁵ and air) than for the MEH-PPV devices ($R_s \approx 2 \cdot 10^6 \Omega$, $R_{sh} \approx 4 \cdot 10^8 \Omega$ under illumination).

Thus, it is likely that the very large R_s is responsible for the low dark and light currents. From the dark and light IV curves we can immediately see that the extra charge carriers due to photoexcitation indeed make a big difference.

7.5 Summary

In this Chapter we have shown that:

⁵Resistor values in the dark are: $R_s \approx R_{sh} \approx 3 \cdot 10^{11} \Omega$.

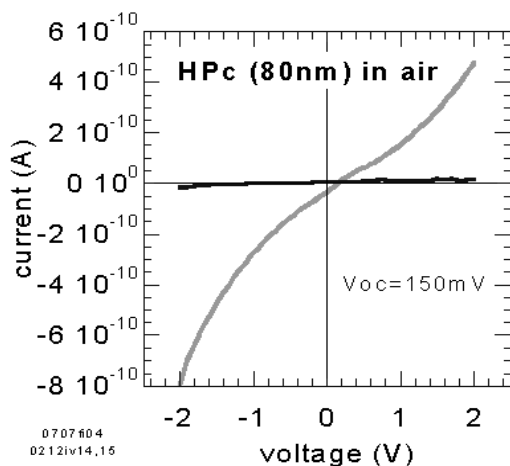


Figure 7.15: IV characteristics of the thin HPc device, after 5hrs in air, when illuminated ($\lambda = 700$ nm) through the ITO contact (dashed line) and in the dark (solid line).

1. It is possible to spin coat a monomer with a considerably smaller molecular mass than polymers like a phthalocyanine from non acidic solutions to build a working photovoltaic cell
2. The maximum thickness of the active region in a HPc film is estimated to lie around 200 ± 80 nm. This value is over an order of magnitude larger than for many polymers including MEH-PPV. Thus we can confirm that higher mobilities for charge carriers and/or excitons are possible in this material [57].
3. The low EQE values compared to e.g. MEH-PPV may be due to the very high series resistor in our devices. The reason for the high series resistor is probably a low concentration of free charge carriers.
4. The liquid crystalline phases of a series of phthalocyanines with varying center atoms and different lengths of side chains has been determined. Only one compound forms a liquid phase before decomposition. The same compound HPc is liquid crystalline already at room temperature ($> 20^\circ\text{C}$).

We want to emphasize that already the high solubility of the phthalocyanine derivatives represents an exciting novelty among organic solar cells with the potential of considerably simple and cheaper device processing compared to the usual sublimation of pigments.

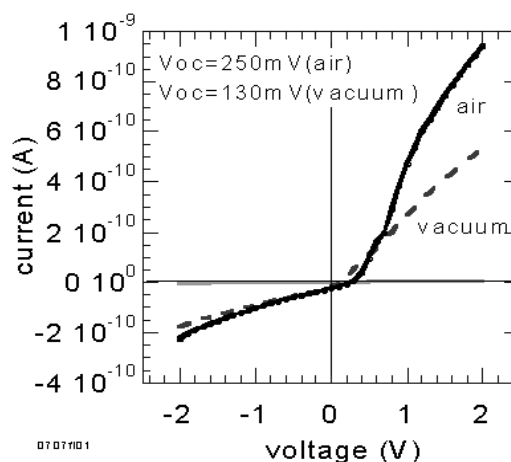


Figure 7.16: The IV characteristics ($\lambda = 700$ nm) of the thick HPc cell shows a linear behaviour under both forward and reverse bias when measured in vacuum. After 5hrs exposure to air the conductivity in forward direction increases showing to different slopes. Dark conductivity is very low and constant.

Further studies are desired to investigate the possibilities to increase the conductivity of HPc by the introduction of extra charge carriers via doping. The EQE may be thereby be increased considerably and make these materials also interesting candidates as active components in D/A systems. We also propose to study devices with discotic materials which are not necessarily liquid crystalline at room temperature but still well soluble.

Chapter 8

Determination of Solar Cell Efficiencies

8.1 Introduction

The ultimate method to test the overall performance of solar cells is outdoor exposure. However, reliable and reproducible results can only be obtained with solar simulators whose illumination conditions are designed to match an internationally standardised solar spectrum.

Commercially available solar simulators usually use a xenon arc lamp in conjunction with a spectral correction filter which *approaches* the terrestrial solar spectrum such that it is good enough for many applications [183].

Here we discuss to what extent a simulator based on a quartz tungsten halogen-lamp (QTH) can be used as a much cheaper ($\approx 1/10$) alternative. In particular, researchers in the field of organic solar cells may benefit from this alternative since their cells are usually not optimised for high stability and may therefore be reluctant to send them to an institute where a commercial simulator is available.

We also discuss and apply a numerical method that allows estimation of the power efficiency number that would be obtained if the cell was exposed to the solar light on Earth. The calculation is based on spectral response and intensity dependence measurements.

8.2 Solar Radiation

Radiant energy from the sun is vital for life on our planet. It determines the surface temperature of the Earth as well as supplying virtually all the energy for natural processes both on its surface and in the atmosphere. Every second the sun emits the energy of $3.90 \cdot 10^{26}$ J into space. Considering that the mean distance from Earth to sun is $150 \cdot 10^9$ m our planet receives the energy of 1395 J/m^2 , every second [66].

The sun is essentially a sphere of gas heated by a nuclear fusion reaction at its center with estimated temperature of up to $20\,000\,000\text{K}$ [97].

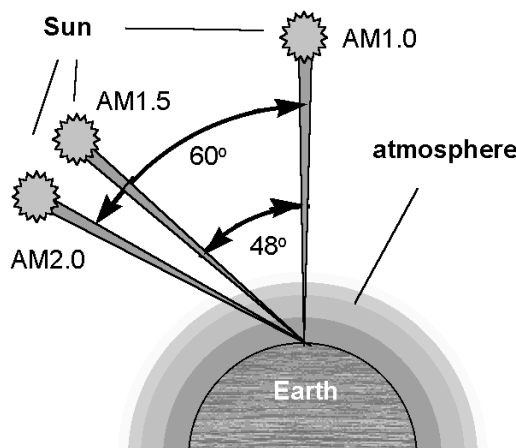


Figure 8.1: The path length of the solar radiation through the Earth's atmosphere in units of Air Mass (AM) increases with the angle from the zenith. It increases from unity for 0° (zenith) to 1.5 for 48° and 2.0 for 60° . The AM1.5 spectrum is the preferred standard spectrum for solar cell efficiency measurements in literature.

However, this is *not* the temperature that determines the characteristic electromagnetic emission from the sun since most of the intense radiation from the sun's deep interior is absorbed after a few millimeters (near the center) and by a layer of negative hydrogen ions¹ near the surface.

¹This ion can exist because the single electron of the neutral hydrogen atom does not completely screen the positive proton [280].

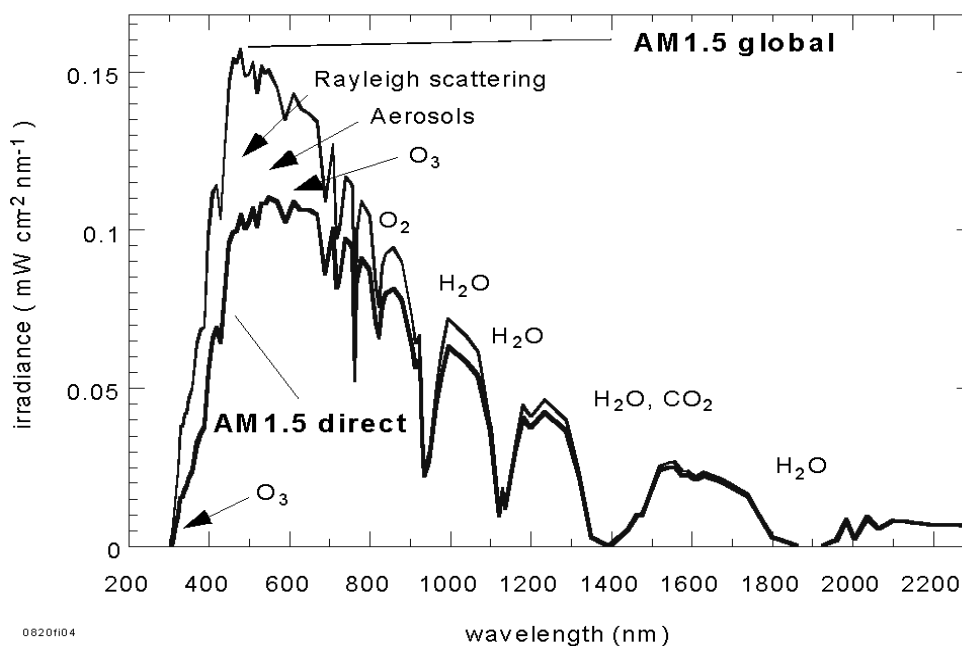


Figure 8.2: The two most commonly used standard spectra, AM1.5 direct and AM1.5 global. The global spectrum comprises the direct plus the diffuse sunlight. The difference is mainly in the shorter wavelength region since molecular scattering scales with λ^4 . Water (H_2O), ozone (O_3) and carbondioxide (CO_2) are the main absorbers of the solar radiation in Earth's atmosphere

(eV):	4.1	3.5	3.1	2.8	2.5	2.3	2.1	1.9	1.8	1.7	1.6	1.5	1.4	1.3	1.24	1.18	1.13	1.08	1.03	0.99	0.95	0.69	0.62	0.5
(nm):	300	350	400	450	500	550	600	650	700	750	800	850	900	950	1000	1050	1100	1150	1200	1250	1300	1800	2000	2500
300	0	0.7	2.9	7.6	14	21	28	35	42	48	54	59	64	67	70	74	77	79	81	84	86	96	96	100
350		0	2.2	6.9	14	21	28	35	41	47	53	58	63	66	69	73	77	78	80	83	85	95	96	99
400			0	4.7	11	18	25	33	39	45	51	56	61	64	67	71	74	76	78	81	83	93	93	97
450				0	6.7	14	21	28	34	40	46	51	56	59	62	66	70	71	73	76	78	88	89	92
500					0	7.0	14	21	28	34	39	44	50	52	56	60	63	64	67	69	72	81	82	86
550						0	7.1	14	21	27	32	37	42	45	49	53	56	57	60	62	65	74	75	79
600							0	7.1	14	20	25	30	35	38	42	46	49	50	52	55	58	67	68	72
650								0	6.5	13	18	23	28	31	35	39	42	43	45	48	51	60	61	65
700									0	6.1	12	17	22	25	28	32	35	37	39	42	44	54	54	58
750										0	5.6	11	16	19	22	26	29	30	33	35	38	48	48	52
800											0	5.1	10	13	16	20	24	25	27	30	32	42	43	46
850												0	5.1	8.0	11	15	19	20	22	25	27	37	37	41
900													0	2.9	6.3	10	13	15	17	20	22	32	32	36
950														0	3.3	7.3	11	12	14	17	19	29	29	33
1000															0	3.9	7.2	8.4	11	13	16	26	26	30
1050																0	3.2	4.5	6.8	9.5	12	22	22	26
1100																	0	1.2	3.5	6.2	8.7	18	19	23
1150																		0	2.3	5.0	7.5	17	18	21
1200																			0	2.7	5.2	15	15	19
1250																				0	2.5	12	13	16
1300																					0	10	10	14
1800																						0	0.5	4.3
2000																							0	3.8
2500																								0

Figure 8.3: Distribution of energy (in percent) within the AM1.5d spectrum. The Integral from 300 to 2500nm was taken as 100%. For example, silicon solar cells with a bandgap of 1.13eV (1100nm) can maximally absorb 77% of the terrestrial solar energy. Taking into account the region with the highest energy content (400-900nm, see values in the diagonal) a bandgap of 1.4eV is already sufficiently small to absorb 61% of the terrestrial solar radiation or 80% of the value for Silicon.

The accumulation of heat in this layer sets up convective currents that transport the excess energy through the optical barrier into the so called photosphere.

The temperature within the photosphere is only 5800K and emits an essentially continuous spectrum² of electromagnetic radiation closely approximating that expected from a black body at this temperature [280].

This is the solar spectrum we receive outside the Earth's atmosphere which is also known as extraterrestrial or Air Mass 0 (AM0) spectrum.

About 70% of the solar radiation in space can reach the surface after penetrating Earth's atmosphere. Apart from the reflection of clouds the reasons for such attenuation are [86]:

- Scattering by molecules in the atmosphere (Rayleigh scattering) which is most effective at short wavelengths.

- Scattering by aerosols and dust particles

- Absorption by the atmosphere and its constituent gases but mainly oxygen, O₃, H₂O, CO₂

The actual degree of attenuation through the Earth's atmosphere is highly variable. It depends mainly on two factors:

- Fraction of diffuse radiation scattered from the sky (and clouds) and surroundings
- Length of the light path through the atmosphere

The fraction of diffuse radiation received by a horizontal surface can reach 10 to 20% even in clear, cloudless skies. For completely covered skies most of the radiation will be diffuse.

Hence, for days between the sunny and cloudy extremes mentioned above, about 50% of the solar light will be diffuse [97]. Diffuse sunlight generally has a different spectral composition from direct sunlight - it will be richer in the shorter or "blue" wavelengths.

The standardised terrestrial spectra for direct and global sunlight are shown in Fig.8.2 where the global spectra comprises the direct *plus* the diffuse components.

The length of the light path through the atmosphere also undergoes changes during the day time - see Fig.8.1, but also depends on latitude and time of year. In any case, the path is shortest when the sun is directly overhead (zenith). The ratio of any actual path length to this minimum value is known as the optical air mass (AM). AM is unity when the sun is directly overhead or larger according to

$$AM = \frac{1}{\cos \theta} \quad (8.1)$$

where θ is the angle measured from the zenith.

Hence, when the sun is 48 degrees off overhead, the radiation is AM1.5. The easiest way to estimate the air mass in practice is to measure the length of the shadow s cast by a vertical structure of height h using:

$$AM = \sqrt{1 + \left(\frac{s}{h}\right)^2} \quad (8.2)$$

Consequently, as opposed to the situation outside the Earth's atmosphere, terrestrial sunlight varies greatly both in intensity and spectral composition. In order to allow meaningful comparison between the performances of different solar cells tested at different locations, a (preferably: terrestrial) standard has to be defined and measurements referred

²A fine structure appears due to absorption in the cool peripheral solar gas (Fraunhofer lines)

to this standard. The most widely used terrestrial standard at the time of writing are the AM1.5 direct and AM1.5 global spectrum as shown in Fig.8.2.

8.3 Simulation of Solar Radiation

Depending on the application, different parts of the solar spectrum become more important. For example, biological testing (sun screens, plant growth etc.) requires accurate simulation of the ultraviolet especially in the UV-B region, whereas for solar energy conversion the range between the visible to the near infrared light is the important part since it contains most of the solar power - see Fig.8.3.

The emission spectrum of a 100W QTH-lamp operating at 3200K colour temperature has an emission peak at 900nm - see Fig.8.4. It has a smooth continuous output over 350 to 2000nm. In order to determine solar efficiencies of organic solar cells we focus on the range between 400 to 1000nm which contains about 70% of the solar energy.

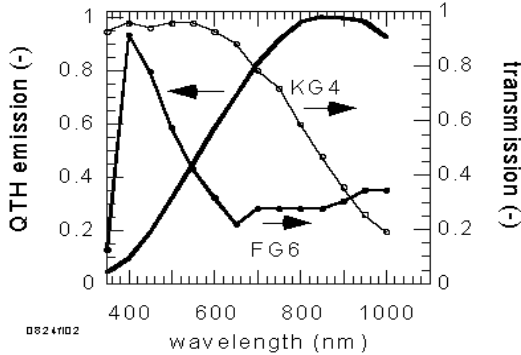


Figure 8.4: Emission spectrum of a 100W - QTH lamp (solid line) and transmission spectrum of the two coloured Schott-glass filters FG6 (6mm thick) and KG4 (3mm thick) which are used to shift the blackbody emission peak from 900nm (3200K) to 550nm (5800K) to approximate the AM1.5d spectrum.

8.3.1 Calculation of the Required AM1.5d Filter

In order to approach the AM1.5d spectrum, the emission peak at 900nm of the QTH lamp, operating at 3200K, has to be shifted towards 550nm by

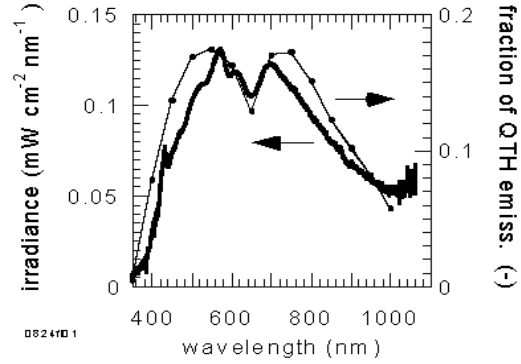


Figure 8.5: The actually measured spectrum (solid line) resembles the shape of the modeled spectrum (full circles). However, there is a significant difference - which we investigated further - see text.

suppressing the IR emission using suitable optical filter.

The transmission curves of the two selected coloured glass filter are also shown in Fig.8.4.

The spectral composition $X(\lambda)$ of the light from the quartz halogen tungsten lamp $QTH(\lambda)$ after passing through the two filters F1 and F2 with their transmission characteristics $T_1(\lambda)$ and $T_2(\lambda)$ is given by

$$X(\lambda) = QTH(\lambda) \cdot T_1^{\frac{d_1}{20}}(\lambda) \cdot T_2^{\frac{d_2}{20}}(\lambda) \quad (8.3)$$

with d_1 and d_2 being the thickness in mm. The denominator 20 is introduced since we used the catalogue data which were related to 20mm thick filters for the actual calculation. The best fit with the AM1.5d spectrum using integer thickness numbers (in mm) was found for filter 1 (FG6) with 6mm and filter 2 (KG4) with 3mm.

Fig.8.6 shows that this particular combination of filters approaches the desired AM1.5d filter quite well. The required filter transmission spectrum $F_{\text{requ.}}(\lambda)$ can be derived using

$$F_{\text{requ.}}(\lambda) = \frac{AM1.5d(\lambda)}{QTH(\lambda)} \quad (8.4)$$

All lenses in the setup (Fig.8.11) are made of optical crown glass providing a constant optical throughput over the 380 to 1000nm with less than 10% loss. Hence, they should not affect the spectral shape of the final light spot.

Using an ORIEL CCD spectrometer we measured the QTH lamp emission after the filters and lenses

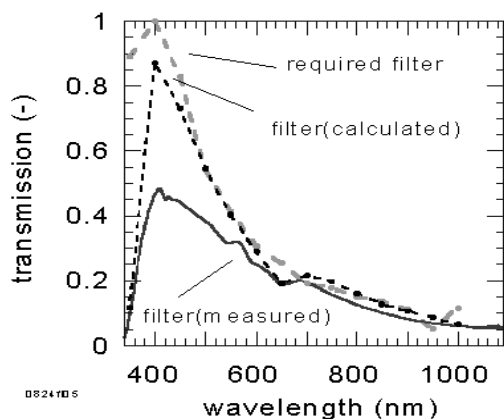


Figure 8.6: Transmission spectra of the required, modeled and measured AM1.5d filter. There is a clear deviation of the measured transmission from the expected (calculated) curve particularly in the 400nm to 500nm range by about 50%.

(Fig.8.5). Apart from the measured spectrum³ the figure also shows the AM1.5d spectrum. The spectra match well, in fact it appears comparable to the spectrum of commercial solar simulators [183].

However, there is some intensity lost in the UV and IR which was not predicted by the calculation (also shown in Fig.8.7). In order to understand the reason for this discrepancy we measured the transmission spectra of the filters as we received them and found a distinct deviation from the data according to the catalogue that have been used for the numerical simulation - see Fig.8.6 and Fig.8.8.

A new optimisation procedure using the new (more accurate) transmission data of the filters suggested 8mm FG6 and 4mm KG4 - see Fig.8.9 and Fig.8.10. It can be seen, although the UV range could be simulated better, the overall spectral match with the AM1.5d spectrum has not improved significantly. In addition the maximum available intensity would be further reduced which can only be compensated by using a stronger QTH-lamp and/or a smaller beam size.

Hence, the spectrum in Fig.8.7 represents our best result to simulate the AM1.5d spectrum. We believe that the spectrum provided by such a simulator is sufficient to allow reasonable comparisons of solar cell performance between different research

³Such an intense spectrum can be measured using e.g. metal coated neutral density filter with a known transmission spectrum for correction

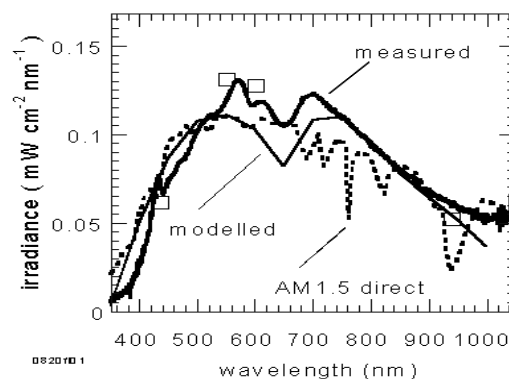


Figure 8.7: The calculated (see Eq. (8.3)) spectrum is shown here together with the standard spectrum (AM1.5d). The somewhat different measured spectrum (QTH+filter) has been shifted towards higher irradiance compared to Fig.8.5 to obtain a reasonable match almost as good as with a commercial simulator. The four squares represent irradiance levels measured with a powermeter to confirm the absolute values.

groups - particularly in the field of organic solar cells.

8.3.2 The Simulator Setup

The chosen optical arrangement of the simulator can be seen in Fig.8.11. The light generated from the QTH lamp is collimated after the first lens, passes through the above described filter system with subsequent concentration after the second lens.

The irradiance level of the final spot depends, apart from the optical throughput (lenses, filter), on the chosen focal distance of the two lenses as well as the actual sample position (since the final beam is divergent) and the distance x of the QTH lamp from the first lens.

Sample position and distance x has been adjusted to give the required irradiance ($0.11 \text{ mW cm}^{-2} \text{ nm}^{-1}$) using a calibrated photodiode masked with an interference filter at 550nm- taking into account its spectral width (6nm) and actual transmission factor (0.55).

To ensure that the sample cell always sees the correct (solar) intensity despite the divergent beam, a stripe of white paper was (temporarily) inserted

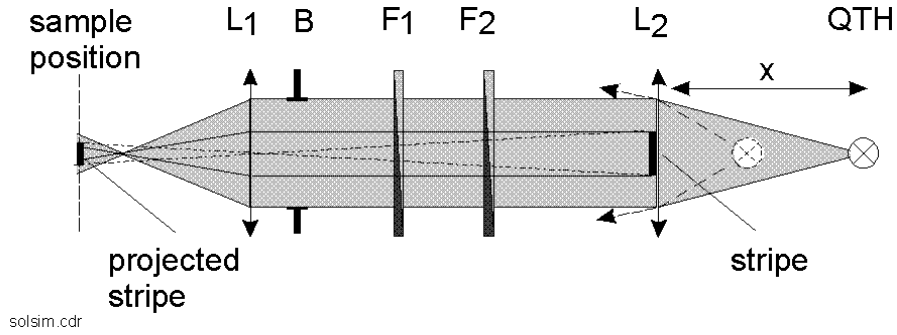


Figure 8.11: The solar simulator setup comprises the QTH-lamp (QTH), biconvex lenses (52mm diameter) made of optical crown glass L1 ($f=10\text{cm}$), L2 ($f=4\text{cm}$) the two filters F1 (FG6, 6mm thick) and F2 (KG4, 3mm thick) plus the iris B to define the spot size. The projection of a paper stripe (1cm wide) served as sample positioning tool⁵ allowing to reproduce the sample position within $\pm 1\text{mm}$ and irradiance within about 5%. Variation of the distance x allowed for fine tuning of the irradiance level.

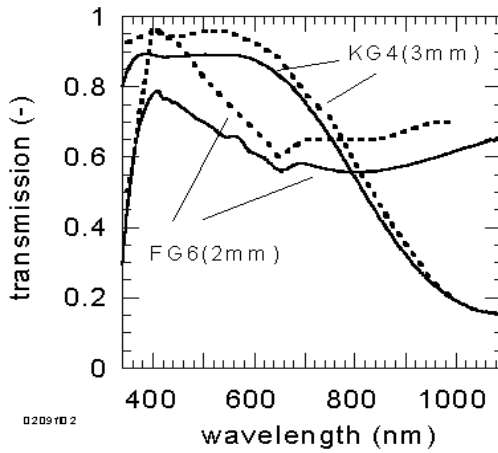


Figure 8.8: We found that the actual supplied filter transmission curves (solid lines) deviate up to 20% from the catalogue data (dotted lines). For 3x2mm FG6 filter this means a deviation of up to $1 - 0.8^3 = 0.5$ (50%) which is in good agreement with the deviation found in Fig.8.6.

into the light path at a position⁶ where its sharp projected image has the desired irradiance thereby defining the sample position. In this way, any sample solar cell or calibration device such as e.g. a thermopile could be positioned within $\pm 1\text{mm}$.

The irradiance can still be controlled i.e. fine adjusted via the distance x . Variation of the voltage and/or current of the QTH lamp allows mainly for

⁶which was just behind the first lens here

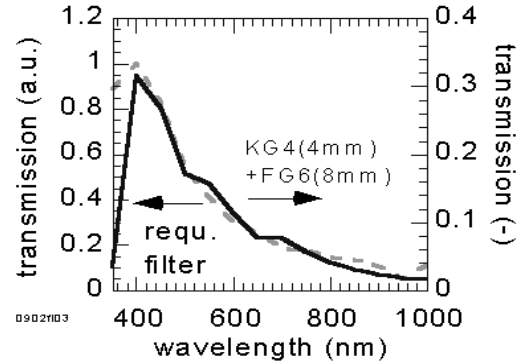


Figure 8.9: Using the measured filter data from Fig.8.8 we found that 4mm of KG4 and 8mm of FG6 would approximated the required filter better. However, transmission will then be reduced further by a factor of 2 - compare with Fig.8.6.

changes in colour temperature of the filament and thereby tune the spectral composition. With the described setup we could obtain the intensity of 1 sun with a spot diameter of 8mm which could almost illuminate all pixels of our standard devices (12x12mm) at once.

8.4 “Numerical” Simulation

An alternative way to estimate the solar power efficiency for a solar cell is to take the short circuit current (I_{sc}) and open circuit voltage (V_{oc}) data from the spectral response measurements at low illumina-

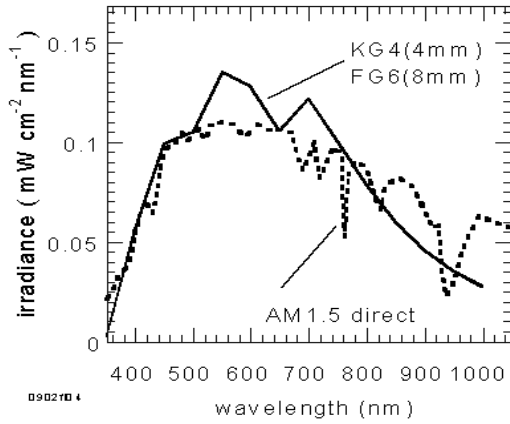


Figure 8.10: The simulated spectrum using the new filter combination approaches the standard AM1.5d spectrum much better in the short wavelength range than the previous - see Fig.8.6.

tion intensities, and scale them up to the standard AM1.5d condition.

The I_{sc} and V_{oc} extrapolated to the solar light intensities can then be used to calculate the power efficiency that is expected under AM1.5d condition by integrating over the entire solar spectrum.

This procedure requires the intensity dependence of the current and voltage and should ideally be performed for a large number of wavelengths. In addition IV curves should be taken for all these wavelengths to allow for changes of the fillfactor.

However, even when performed carefully and with much consideration this method can certainly not replace solar simulator measurements since it relies on a number of assumptions which may not apply for the concerned cell types.

The main problem is that we do not really know if we can simply integrate (add) the number of photons at higher intensities without considering Coulomb-Coulomb interaction of the charge carriers. We have tested this calculation on a standard silicon diode (HAMAMATSU) and obtained a reasonable efficiency of about 5% suggesting it is applicable at least to silicon - solar cells.

However, inorganic solar cells generally have 1000 times higher charge carrier mobilities and function in a different way.

Here we demonstrate the procedure with data taken from the laminated solar cell described in Chapter 6. The intensity dependence of V_{oc} and I_{sc}

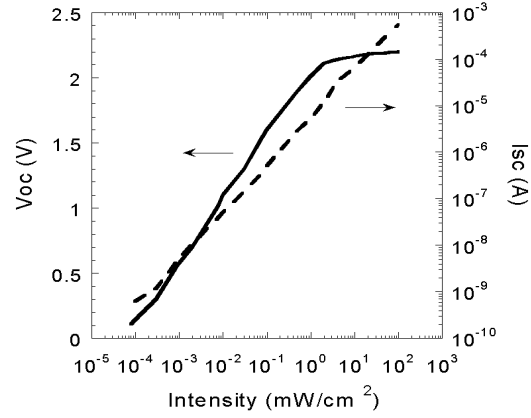


Figure 8.12: V_{oc} and I_{sc} versus intensity ($\lambda = 488\text{nm}$). The current goes virtually linear while the voltage saturates around the workfunction difference of the electrodes.

over a few orders of magnitude is plotted in Fig.8.12. The photocurrent varies virtually linearly with the irradiance E , hence we can write:

$$I_{sc}(\lambda) \sim E(\lambda) \quad (8.5)$$

In other words, the current scales by the same factor as the irradiance such that

$$I_{sc\text{AM1.5d}}(\lambda) = \frac{E_{\text{AM1.5d}}(\lambda)}{E_m(\lambda)} \cdot I_{sc_m}(\lambda) \quad (8.6)$$

with AM1.5d indicating quantities under AM1.5d condition and m indicating the actually measured quantity obtained during the spectral response measurements.

The wavelength dependent V_{oc} values for solar irradiance levels were taken from Fig.8.12. Fill-factors were derived from IV curves measured with irradiance E_m and found to be virtually independent of the excitation wavelength ($FF=0.33$). Now we can compute the power efficiency under AM1.5d condition expected for this cell using:

$$\eta_{\text{AM1.5d}}(\lambda) = \frac{J_{sc}(\lambda) \cdot V_{oc\text{AM1.5d}}(\lambda) \cdot FF_{\text{AM1.5d}}(\lambda)}{E_{\text{AM1.5d}}(\lambda)} \quad (8.7)$$

with

$$J_{sc\text{AM1.5d}}(\lambda) = \frac{I_{sc\text{AM1.5d}}(\lambda)}{A} \quad (8.8)$$

where A is the illuminated area of the device (5mm^2).

Since the spectral width of the light used for the SR measurements was set to 10nm - the same value as the chosen spectral resolution we could obtain the integral by simple adding all obtained values together. We took the mean values of the open circuit voltage and FF and applied:

$$\eta_{AM1.5d} \approx \frac{\left(\sum_{\lambda_1}^{\lambda_2} J_{scAM1.5d}(\lambda) \right) \cdot \bar{V}_{oc} \cdot \bar{FF}}{P_{AM1.5d}} \quad (8.9)$$

with $P_{AM1.5d} \equiv 76.6\text{mW}$ being the sum (integral) of the light power over the entire AM1.5d spectrum and A as the area of the sample cell (5mm^2).

The result for the power efficiency with this method was $\eta_{AM1.5d} = 1.84\%$.

Alternatively we could calculate the power per device area $J_{scAM1.5d5} \cdot V_{oc}$ for every wavelength interval before we built the integral (sum) as in:

$$\eta_{AM1.5d} \approx \frac{\left(\sum_{\lambda_1}^{\lambda_2} J_{scAM1.5d}(\lambda) \cdot V_{oc}(\lambda) \right) \cdot \bar{FF}}{P_{AM1.5d}} \quad (8.10)$$

Using this equation we obtained a slightly higher value $\eta_{AM1.5d} = 1.87\%$.

Since both methods can be justified equally, we decided to take the mean of both numbers so that our final result (after rounding) is $\eta_{AM1.5d} = 1.9\%$. The latter is the number cited in Ref. [94].

We note that a similar method has been applied to calculate $\eta_{AM1.5d}$ of a double layer cell using a perylene diimide and a ZnPc [214]. The calculated value (1.05%) in this reference was in satisfying agreement with the result using a solar simulator. In order to justify the integration over the wavelength range in Eq. (8.10) the short circuit current I_{sc} should continue its linearity up to the full solar intensity of $76\text{mW}/\text{cm}^2$ - which is the case here.

We also want to note that building the sum of I_{sc} ⁷ over the relevant wavelength range (here about 400nm) means that the resulting intensity i.e. number of photons/area can be about 2 orders of magnitude higher than the intensity extracted from 10nm of the solar spectrum.

- A good match with the standard spectrum for direct solar radiation on Earth (AM1.5d) can be achieved with a solar simulator using a QTH lamp. Although clearly more tedious and inconvenient to operate in comparison with commercial simulation equipment, such a simulator may still be interesting as a low cost evaluation device for researchers investigating solar cells with potential stability problems and/or (in comparison with inorganic cells) low conversion efficiencies such as organic solar cells.

In any case, if the cell reaches commercially interesting efficiencies (5%) we recommend to do outdoor performance tests and/or entrust internationally accepted solar energy research and test laboratories such as the Fraunhofer Institute for Solar Energy (FISE) in Freiburg, Germany or the National Renewable Energy Lab (NREL) in Golden, USA with their more sophisticated simulation facilities.

- An AM1.5d efficiency value for a silicon solar cell has been calculated by extrapolating the V_{oc} and I_{sc} values from the spectral response measurements to solar condition. By applying the same method to a laminated polymeric solar cell we obtained a value for the power conversion efficiency under AM1.5d conditions of 1.9 %.

Although this method appears to give reasonable results it would be desirable to investigate the theoretical assumptions (integration over the spectrum, wavelength independent fillfactor, extrapolation of the intensity dependency etc.) further. However, it may be considered as another possibility to characterise and compare the performance of organic photovoltaic devices among researchers in this field.

8.5 Summary

In this Chapter we have shown:

⁷with a spectral width of 10nm

Chapter 9

Summary and Bibliography

9.1 Summary

The aim of this work has been the investigation of different classes of organic semiconducting materials using various types of solar cell architectures with respect to their photovoltaic properties.

In Table 9.3 we have summarised the photovoltaic key parameters of the devices investigated in this thesis or reported by other research groups. It can be seen that, on average, devices using pigments (still) perform better than polymer, dye and liquid crystal containing devices.

Among devices that include at least one component which is a pigment, the type of cell architecture does only little affect the overall performance - see Table 9.1. Note that only monochromatic EQE values are considered here - cells comprising two or more molecular components have a better chance to absorb over wide spectrum to give higher solar efficiencies (AM1.5) than single layer structures.

Table 9.1: Overall assessment (*=low, **=medium, ***=high) of the different solar cell architectures. Devices must include at least one pigment component.

	including pigments		
device architecture	EQE	V_{oc}	FF
—	%	V	%
single layer	***	***	**
double layer	***	**	***
blend	***	**	**
laminated	—	—	—

It is important to keep in mind that pigments - in contrast to polymers and dyes - can not simply be processed from solution and that the best pigment devices suffer from severe problems related to the electrode materials [164, 224].

If only (the production friendly) soluble semiconductors are considered (see Table 9.2), the EQE but also the overall performance can vary considerably for different device architectures. The following order (best device architecture on top) for solar cell overall performance has been found:

1. laminated device
2. blend device
3. double layer device
4. single layer device

Table 9.2: Overall assessment of the different solar cell architectures. Soluble semiconductors only.

	only soluble materials		
device architecture	EQE	V_{oc}	FF
—	%	V	%
single layer	*	***	*
double layer	**	***	*
blend	***	**	**
laminated	***	***	**

If we focus only on the EQE of soluble materials, we find that double layer structures give about 10-100 times higher numbers than single layers whereas blends and the laminated structure allow a further enhancement by another factor of 5 to 10.

If all types of organic semiconductors are considered, we can see that each architecture seems to reach highest numbers for a different evaluation parameter:

- Highest **EQE**¹ in **single layer** devices

¹at peak wavelength

- Highest V_{oc} in **laminated** devices
- Highest FF in **double layer** devices
- Highest **SR-range** in **blend** devices

We note that the laminated device structure which is particularly efficient among soluble semiconductors has been introduced and investigated as part of this work. This technologically interesting structure opens many new possibilities in terms of combination of semiconductors and semiconductor treatment such as selective doping or heating.

Moreover, we have investigated, for the first time, dye/dye and liquid crystal/dye interfaces with respect to their photovoltaic properties.

9.1.1 Suggestions for Future Investigations

In future, the investigation and exploitation of the effects of doping using organic semiconductors or gases like oxygen as dopants will most likely allow further enhancements of efficiencies.

Another interesting subject to explore will be the use of photonic bandgap structures [203] to extend the range of available low bandgap materials.

Such photonic structures may even be realised in an highly ordered structure consisting of co-block polymers.

Table 9.3: Summary of important performance parameters of various organic solar cells including all types of architectures. The abbreviation for materials are listed in Chapter 1. In D/A cells the donor material is followed by the acceptor material. For clarity the electrode materials who were always Al and ITO in D/A devices have been omitted. Best parameters are printed using **bold** characters while *italic* letters mark devices investigated in this thesis. EQE values were taken at peak wavelength.

EQE %	V_{oc} V	FF %	range nm	device –	comments –	year
Single Layer Devices						
73	0.45	33	400-800(?)	In/HPc+polymer/NESA	pigment in polymer [164]	1981
62	1.1	33	400-800(?)	Al/HPc+polymer/SnO ₂	pigment in polymer [43]	1979
36 ¹	0.96 ¹	0.47 ¹	400-850	Al/pentacene/ITO	pigment [224]	2000
33	1.2	25	400-800(?)	Al/merocyanine/Ag	pigment [43]	1978
14	0.7	39	400-800(?)	Al/CuPc/Au	pigment [43]	1981
3	0.6	34	400-800(?)	Al/merocyanine/Au	pigment [43]	1978
1	1.2	20	400-500	PPV	polymer [168]	1994
0.7	0.32	25	400-700(?)	Cr/chlorophyll-a/Hg	dye [43]	1975
0.5	1.0	23	400-500	Al/PPV+PEDOT/ITO	polymer [8]	1998
0.15	0.85	25	400-800(?)	Al/MgPc/Au	pigment [43]	1974
0.1	0.7	25	400-750	Al/THPF/ITO	<i>polymer</i>	2000
0.1	0.1	25	400-560	Al/LPPP/ITO	<i>polymer</i>	2000
0.09	0.5	27	400-570	Al/CN-MEH-PPV/ITO	polymer [114]	1997
0.08	0.19	25	400-600	Al/Per/ITO	<i>dye</i>	2000
0.07	0.7	25	400-570	Al/MEH-PPV/ITO	<i>polymer</i> [196]	2000
0.05	0.37	25	400-750	Al/PTV/ITO	<i>polymer</i>	2000
0.03	< 0.02	25	400-650	Al/P3HT/ITO	polymer [63]	2001(?)
0.015	0.1	25	400-650 ⁺	In/HPc/Au	pigment [68]	1978
0.007	0.15	25	400-820	Al/HPc/ITO	<i>liquid crystal</i>	2000
0.005	< 0.02	25	400-1000	Al/PIF/ITO	<i>polymer</i>	2000
Double Layer Devices						
30⁺	0.5	65	400-800	CuPc/Per1	pigment/pigment [244]	1985
23	0.5	≈30	400-700 ⁺	HPc1/Per2	pigment/pigment [131]	1990
23	0.3*	40*	400-600	PEDOT/PEOPT/C60	polymer/pigment [213]	1998
9	0.8	48	400-560	PPV/C60	polymer/pigment [111]	1996
6	1.0	60	400-620	PPV/Per3	polymer/pigment [113]	1996
≈ 3 ⁺	1.0	23	400-620	PPyV/P3HT	polymer/polymer [242]	1997
2	1.0	51	400-590	PEDOT/PPV/Per	polymer/dye [9]	1999
0.6	0.12	25	400-800	CuPc2/Per	<i>dye/dye</i> [200]	2000
0.5	0.35	20	400-850	HPc/Per3	<i>liquid crystal(dye)/pigment</i> [199]	1999
Blend Devices						
29	0.5	≈25	400-550	MEH-PPV+C60	polymer+dye [278]	1995
23	0.4	≈33	400-550	MEH-PPV/C60	polymer+pigment [83]	1998
12	0.5	26	400-640	MEH-PPV+CdSe	polymer+nanocrystals [102]	1996
11	0.35	41	400-620	P3HT+Per	polymer+dye [65]	2000
6	0.6	25	400-600	MEH-PPV+CN-PPV	polymer+polymer [112]	1995
1.8	0.9	23	400-500	PPV+MWNT	polymer+nanotubes [3]	1999
1.0	0.1	25	400-800	HPc+Per	<i>liquid crystal+dye</i> [200]	2000
0.7	0.4	44	400-600	MEH-PPV+Per	<i>polymer+dye</i> [62]	1999
0.4	0.2	25	400-850	PTV+Per	<i>polymer+dye</i>	2000
0.4	0.12	25	400-900	PTV+Ter	<i>polymer+dye</i>	2000
0.2	0.6	25	400-800	PTV+THPF	<i>polymer+polymer</i>	2000
0.02	<0.01	25	400-1000	PTV+PIF	<i>polymer+polymer</i>	2000
0.0007	<0.01	25	400-1100	HPc+PIF	<i>polymer+liquid crystal</i>	2000
Laminated Devices						
30	1.3	33	400-700	POPT/MCP	<i>polymer/polymer</i> [94]	1998
0.2	0.37	23	400-900	HPc/Per	<i>liquid crystal/dye</i> [200]	2000

[1] IQE instead of EQE, illumination conditions are: AM1.5 (100mW/cm²) resulting in $\eta = 2.4\%$

Bibliography

- [1] D. Adam, F. Closs, T. Frey, D. Funhoff, D. Haarer, H. Ringsdorf, P. Schuhmacher and K. Siemensmeyer "Transient photoconductivity in a discotic liquid crystal." *Phys.Rev.Lett.* **70**, 457-460 (1993)
- [2] D. Adam, P. Schuhmacher, J. Simmerer, L. Haeussling, K. Siemensmeyer, K. H. Etzbach, H. Ringsdorf and D. Haarer "Fast photoconduction in the highly ordered columnar phase of a discotic liquid crystal (hexhexylthio-triphenylene)." *Nature* **371**, 141-143 (1994)
- [3] H. Ago, K. Petritsch, M.S.P. Shaffer, A.H.Windle and R.H. Friend "Composites of carbon nanotubes and conjugated polymers for photovoltaic devices" *Adv.Mat.* **11**, 1281-1285 (1999)
- [4] M. R. Andersson, D. Selse, M. Berggren, H. Jaervinen, T. Hjertberg, O. Inganaes, O. Wennerstroem and J. E. Oesterholm "Regioselective polymerization of 3-(4-octylphenyl)thiophene with FeCl₃." *Macromolecules* **27**, 6503-6506 (1994)
- [5] M. R. Andersson, M. Berggren, O. Inganaes, G. Gustafsson, J. C. Gustafsson-Carlberg, D. Selse, T. Hjertberg and O. Wennerstroem "Electroluminescence from substituted polythiophenes: From blue to near infrared." *Macromolecules* **28**, 7525-7529 (1995)
- [6] A.C. Arias, M. Granstrom, D.S. Thomas, K. Petritsch and R.H. Friend. "Doped conducting-polymer-semiconducting-polymer interfaces: their use in organic photovoltaic devices" *Phys.Rev.B - Cond. Matt.* **60**, 1854-1860 (1999)
- [7] A.C. Arias, M. Granstrom, K. Petritsch and R.H. Friend. "Organic photodiodes using polymeric anodes" *Synth. Met.* **102**, 953-954 (1999)
- [8] A.C. Arias, K. Petritsch, M. Granstrom, J.J. Dittmer, E.A. Marseglia and R. H. Friend "Efficient Polymeric Photovoltaic Devices." *Proc. CBECIMAT* (1998)
- [9] A.C. Arias, K. Petritsch, M. Granstrom, J. J. Dittmer, E. A. Marseglia and R. H. Friend "Efficient Polymeric Photovoltaic Devices." *Proc. CBECIMAT* (1998)
- [10] R. Ash *Incredible Comparisons*, DK, London (1997)
- [11] U. Bach et. al. "Solid state dye sensitized mesoporous TiO₂ solar cells with high photon to electron conversion efficiencies" *Nature* **395**, 583-585 (1998).
- [12] S. Barth and H. Baessler "Intrinsic photoconduction in PPV-Type conjugated polymers." *Phys.Rev.Lett.* **79**, 4445-4448 (1997)
- [13] Z. Bao, A. J. Lovinger and A. Dodabalapur "Highly ordered vacuum deposited thin films of metallophthalocyanines and their applications in field effect transistors." *Adv.Mat.* **9**, 42 (1997)
- [14] H. Becker, A. Lux, A. B. Holmes and R. H. Friend "PL and EL quenching due to thin metal films in conjugated polymers and polymer LEDs." *Synth.Met.* **85**, 1289-1290 (1997)
- [15] H. Becker, P. L. Burns and R. H. Friend "Effect of metal films on the photoluminescence and electroluminescence of conjugated polymers." *Phys.Rev.B* **56**, 1893-1905 (1997)
- [16] S. Becker et al. to be published.
- [17] P. Benett, "Earth: The Incredible Recycling Machine", Wayland (Publishers) Ltd, East Sussex (1993)
- [18] M. Berggren et al. "Thermal control of near infrared and visible electroluminescence from substituted polythiophenes" *Appl.Phys.Lett.* **65**, 1489-1491 (1994)
- [19] J. Bharathan, Y. Yang, *Appl. Phys. Lett.* **72**, 2660 (1998)
- [20] J. Billard, J.C. Dubois, H.T. Nguyen, A.Zann *Nouv.J.Chim.* **2**, 535 (1978)
- [21] G. Blasse, G. J. Dirksen, A. Meijerink, J. F. Van der Pol, E. Neeleman and W. Drenth "Luminescence and energy migration in the solid state and in the ordered columnar mesophase of peripherally octa-n-dodecoxy-substituted phthalocyanine." *Chem.Phys.Lett.* **154**, 420-424 (1989)
- [22] N. Boden, R. J. Bushby and J. Clements "Mechanism of quasi one dimensional electronic conductivity in discotic liquid crystals." *J.Chem.Phys.* **98**, 5920-5931 (1993)
- [23] N. Boden, R. C. Borner, R. J. Bushby and J. Clements "First observation of an n-doped quasi one dimensional electronically-conducting discotic liquid crystal hexakis(hexylthio)tricycloquinazino (HTTQ)." *J. Am. Chem. Soc.* **116**, 10807-8 (1994)
- [24] N. Boden, R. J. Bushby and J. Clements "Electron transport along molecular stacks in discotic liquid crystals." *J.Mater.Science: Mat.Electronics* **5**, 83-88 (1994)
- [25] N. Boden, R. J. Bushby and A. N. Cammidge "Triphenylene based discotic liquid crystalline polymers: A universal, rational synthesis." *J. Am. Chem. Soc.* **117**, 924-927 (1995)

- [26] N. Boden, R. J. Bushby, J. Clements and R. Luo "Characterization of the cationic species formed in p-doped discotic liquid crystals." *J. Mater. Chem.* **5**, 1741-1748 (1995)
- [27] N. Boden, R. Bissell, J. Clements and B. Movaghar "Discotic liquid crystals. References for charge and exciton transport and mobilities." *Liquid Crystals - Today* **6**, (1996)
- [28] N. Boden, R. J. Bushby, A. N. Cammidge, S. Duckworth and G. Headdock "Halogenation of triphenylene based discotic liquid crystals: towards a chiral nucleus." *J. Mater. Chem.* **7**, 601-606 (1997)
- [29] P.M. Borsenberger & D.S. Weiss "Organic Photoreceptors for Imaging Systems" Dekker, New York (1993)
- [30] Y. Bouligand "Geometry of non smectic hexagonal mesophases." *J. Physique* **41**, 1297-1306 (1980)
- [31] Y. Bouligand "Defects and textures of hexagonal discotics." *J. Physique* **41**, 1307-1315 (1980)
- [32] D. Braun and A. J. Heeger "Visible light emission from semiconducting polymer diodes." *Appl. Phys. Lett.* **58**, 1982 (1991)
- [33] T. M. Brown, J. S. Kim, R. H. Friend, F. Cacialli, R. Daik and W. J. Feast. "Built-in field electroabsorption spectroscopy of polymer light-emitting diodes incorporating a doped poly(3,4-ethylene dioxythiophene) hole injection layer" *Appl. Phys. Lett.* **75**, 1679-1681 (1999)
- [34] J. H. Burroughes, D. D. C. Bradley, A. R. Brown, R. N. Marks, K. Mackay, R. H. Friend, P. L. Burns and A. B. Holmes "Light emitting diodes based on conjugated polymers." *Nature* **347**, 539 (1990)
- [35] F. Cacialli, unpublished results.
- [36] C. J. Campbell and J. H. Laherrere "The end of cheap oil." *Scientific American March*, 60 (1998)
- [37] A. N. Cammidge, I. Chambrier, M. J. Cook, A. D. Garland, M. J. Heeney and K. Welford "Octaalkyl- and octaalkoxy-2,3 naphthalocyanines." *J. Porphyrins and Phthalocyanines* **1**, 77-86 (1997)
- [38] Y. Cao, P. Smith and A. J. Heeger "Counter-ion induced processibility of conducting polyaniline and of conducting poly-blends of poly-aniline in bulk polymers." *Synth. Met.* **48**, 91-97 (1992)
- [39] S. A. Carter, M. Angelopoulos, S. Karg, P. J. Brock and J. C. Scott "Polymeric anodes for improved polymer LED performance." *Appl. Phys. Lett.* **70**, 2067-2069 (1997)
- [40] R. R. Chance, A. Prock and R. Silbey *Adv. Chem. Phys.* **37**, 1 (1978)
- [41] G.A. Chamberlain P.J. Cooney and S. Dennison "Photovoltaic properties of merocyanine solid state photocells" *Nature* **289** 45-47 (1981)
- [42] G. A. Chamberlain "Organic PN junction solar cells." *Mol. Cryst. Liq. Cryst.* **93**, 369-379 (1983)
- [43] G. A. Chamberlain "Organic solar cells: A review." *Solar Cells* **8**, 47-83 (1983)
- [44] S. Chandrasekhar, B. K. Sadashiva and K. A. Suresh "Liquid crystals of disc-like molecules." *Pramana* **9**, 471-480 (1977)
- [45] S. Chandrasekhar "Liquid crystals of disc-like molecules." *Phil. Trans R. Soc. Lond. A* **309**, 93-103 (1983)
- [46] D. M. Chapin, C. S. Fuller and G. L. Pearson "A new silicon p-n junction photocell for converting solar radiation into electrical power." *J. Appl. Phys.* **25**, 676-677 (1954)
- [47] N. Chawdhury, M. Younus, P. R. Raithby, J. Lewis and R. H. Friend "The effect of air exposure on the photocurrent in a conjugated platinum poly-yne." *Opt. Mat.* **9**, 498-501 (1998)
- [48] G. Cheek, A. Genis, J. B. DuBow and V. R. P. Vernecker "Antireflection properties of ITO on silicon for photovoltaic applications." *Appl. Phys. Lett.* **35**, 495-497 (1979)
- [49] M. Chandross, S. Mazumdar, S. Jeglinski, X. Wei, Z.V. Vardeny, E.W. Kwock and T.M. Miller *J. Phys.: Condens. Matter* **6**, 1379-1394 (1994)
- [50] N. Chawdhury, M. Younus, P. R. Raithby, J. Lewis and R. H. Friend "The effect of air exposure on the photocurrent in a conjugated platinum poly-yne." *Opt. Mat.* **9**, 498-501 (1998)
- [51] G. Cheek, A. Genis, J. B. DuBow and V. R. P. Vernecker "Antireflection properties of ITO on silicon for photovoltaic applications." *Appl. Phys. Lett.* **35**, 495-497 (1979)
- [52] V. Choong, Y. Park, Y. Gao, T. Wehrmeister, K. Muellen, B. R. Hsieh and C. W. Tang "Dramatic PL quenching of PPV oligomer thin films upon submonolayer Ca deposition." *Appl. Phys. Lett.* **69**, 1492-1494 (1996)
- [53] T. Christ, B. Gluesen, A. Greiner, A. Kettner, R. Sander, V. Stuempfen, V. Tsukruk and J. H. Wendorff "Columnar discotics for LEDs." *Adv. Mat.* **9**, 48-52 (1997)
- [54] J. Cornil, A.J. Heeger, and J.L. Bredas, *Chem. Phys. Lett.* **272**, 463-470 (1997)
- [55] R. Corradi and S. P. Armes "Chemical synthesis of poly(3,4-ethylenedioxy thiophene)" *Synth. Met.* **84**, 453-454 (1997)
- [56] P. G. d. Costa and E. M. Conwell "Excitons and the band gap in PPV." *Am. Phys. Soc.-Rap. Comm.* **48**, 1993-1997 (1993)
- [57] A. van de Craats, P.G. Schouten, J.M. Warman "Charge Transport in Discotic Liquid Crystalline Materials Studied by Pulse-Radiolysis Time Resolved Microwave Conductivity (PR-TRMC)" *J. Jap. Liq. Cryst. Soc.* **2**, 12-27 (1998)
- [58] A. van de Craats, J.M. Warman, K. Muellen, Y. Geerts, J.D. Brand "Rapid charge transport along self assembling graphite nanowires" *Adv. Mat.* **10**, 36-38 (1998)

- [59] G. M. Delacote, J. P. Fillard and F. J. Marco "Electron injection in thin films of copper phthalocyanine." *Solid State Communications* **2**, 373-376 (1964)
- [60] S. Demmig and H. Langhals "Leichtloesliche, lichtechte Perylen- Fluoreszenzfarbstoffe." *Chem.Ber.* **121**, 225-230 (1988)
- [61] J.J. Dittmer, K. Petritsch, E.A. Marseglia, R.H. Friend, H. Rost and A.B. Holmes "Photovoltaic properties of MEH-PPV/PPEI blend devices" *Synth.Met.* **102**, 879 (1999)
- [62] J.J. Dittmer, P. Lazaroni, P. Leclerc, P. Moretti, M. Granstrom K. Petritsch, E.A. Marseglia, R.H. Friend, H. Rost and A.B. Holmes "Crystal Network Formation in Organic Solar Cells" *Sol.En.Mat.Sol.Cells* **61**, 53-61 (2000)
- [63] J.J. Dittmer to be published
- [64] J.J. Dittmer, private communication
- [65] J.J. Dittmer, E.A. Marseglia, R.H. Friend submitted to *Adv.Mat.*
- [66] *Fachlexikon der Physik*, Verlag Harri Deutsch, 2. Auflage (1989)
- [67] F. R. Fan and L. R. Faulkner "Photovoltaic effects of metal free and Zn phthalocyanines." *J.Chem.Phys.* **69**, 3334 (1978)
- [68] F. R. Fan and L. R. Faulkner "Photovoltaic effects of metal free and Zn phthalocyanines." *J.Chem.Phys.* **69**, 3341-3349 (1978)
- [69] L. Feiler, H. Langhals and K. Polborn "Synthesis of perylene- 3,4 dicarboximides - Novel highly photostable fluorescent dyes." *Liebigs Ann.*, 1229-1244 (1995)
- [70] Fesser, Bishop and Campbell "Optical absorption from polarons in a model of polyacetylene" *Phys.Rev.B* **27**, 4804-4825 (1983)
- [71] L. Fleury, B. Sick, G. Zumhofen, B. Hecht, U.P. Wild *Mol.Phys.* **95**, 1333 (1998)
- [72] T. Foerster, "Fluoreszenz Organischer Verbindungen", Vandenhoeck und Ruprecht, Goettingen (1951)
- [73] W. T. Ford, L. Summer, W. Zhu, Y.H. Chang, P. Um, K.H. Choi, P.A. Heiney, N.C. Maliszewski *New J. Chem.*, **18** 495 (1994)
- [74] M. Forster, K.O. Annan, U. Scherf, "Conjugated Ladder Polymers Containing Thienylene Units" *Macromol.* **32** 3159 (1999)
- [75] J. Frenkel, *Phys. Rev.* **38**, 309-320 (1931)
- [76] R. H. Friend, D. D. C. Bradley and P. D. Townsend "Photoexcitation in conjugated polymers." *J. Phys. D: Appl. Phys.* **20**, 1367 (1987)
- [77] R. H. Friend, J. H. Burroughes and D. D. C. Bradley "Electroluminescent Devices." Patent Nr: US5247190 (1993)
- [78] R. H. Friend, G. J. Denton, J. J. M. Halls, N. T. Harrison, A. B. Holmes, A. Koehler, A. Lux, S. C. Moratti, K. Pichler, N. Tessler and K. Towns "Electronic processes of conjugated polymers in semiconductor device structures." *Synth.Met.* **84**, 463-470 (1997)
- [79] R. H. Friend, G. J. Denton, J. J. M. Halls, N. T. Harrison, A. B. Holmes, A. Koehler, A. Lux, S. C. Moratti, K. Pichler, N. Tessler, K. Towns and H. F. Wittmann "Electronic excitations in luminescent conjugated polymers." *Solid State Communications* **102**, 249-258 (1997)
- [80] Fu Y, H. Cheng and R. L. Elsenbaumer "Electron Rich Thienylene - Vinylene low bandgap polymers." *Chem. Mater.* **9**, 1720-1724 (1997)
- [81] A. Fujii, A. A. Zakhidov, V. V. Borovkov, Y. Ohmori and K. Yoshino "Organic photovoltaic cell with donor-acceptor double heterojunction." *Jpn. J. Appl. Phys.* **35**, L1438-1441 (1996)
- [82] S. Fujita, T. Sakamoto, K. Ueda, K. Ohta and S. Fujita "Surface treatment of ITO substrates and its effects on initial nucleation processes of diamine films." *Jpn. J. Appl. Phys.* **36**, 350-353 (1997)
- [83] J. Gao, F. Hide and H. Wang "Efficient photodetectors and photovoltaic cells from composites of C60 and conjugated polymers: photoinduced electron transfer." *Proc. ICSM96 (Snowbird)* (1996)
- [84] J. Gao, Yu G and A. J. Heeger "Polymer PIN Junction Solar cells." *Adv.Mat.* **9**, 692-695 (1998)
- [85] F. Garnier, G. Horowitz, X. Z. Peng and D. Fichou "Structural basis for high carrier mobility in conjugated oligomers." *Synth.Met.* **45**, 163-171 (1991)
- [86] P.R. Gast, "Solar Radiation", in *Handbook of Geophysics*, ed. C.F. Campen et al., p14-30 (1960).
- [87] A. K. Ghosh, D. L. Morel, T. Feng, R. F. Shaw and C. A. Rowe "Photovoltaic and rectification properties of Al/Mg-phthalocyanine/Ag Schottky-barrier cells." *J.Appl.Phys.* **45**, 230-236 (1974)
- [88] A. K. Ghosh and T. Feng "Merocyanine organic solar cells." *J.Appl.Phys.* **49**, 5982-5989 (1978)
- [89] A.K. Ghosh and T. Feng "Photovoltaic Device containing an Organic Layer" US-Patent Nr.: US4127738 (1978)
- [90] F. Goldoni, R.A.J. Janssen and E.W. Meijer "Synthesis and characterization of new poly(thienylenevinylene)s with thioether side chains" *Polymer Preprints* **39**, 1049 (1998)
- [91] F. Goldoni, D. Iarossi, A. Mucci, L. Schenetti, M. J. Zambianchi, *J. Mater. Chem.* **7**, 593 (1997)
- [92] H. L. Gomez, P. Stallinga, H. Rost, A. B. Holmes, M. G. Harrison and R. H. Friend "Analysis of deep levels in a phenylenevinylene polymer by transient capacitance methods." *Appl.Phys.Lett.* **22**, (1999)
- [93] P. L. Gourley "Photonic lattices block light." *Scientific American March*, 43 (1998)

- [94] M. Granstrom, K. Petritsch, A. C. Arias, A. Lux, M. R. Andersson and R. H. Friend "Laminated fabrication of polymeric photovoltaic diodes." *Nature* **395**, 257-260 (1998)
- [95] M. Granstrom and K. Petritsch: Patent Nr.: WO9949525A1: Multilayer photovoltaic or photoconductive devices; Filing date: Febr.02. (1999)
- [96] W. Graupner, G. Leditzky, G. Leising, U. Scherf *Phys. Rev.B* **54** 7610 (1996)
- [97] M.A. Green. *Solar Cells - Operating Principles, Technology and System Applications*. University of New South Wales, Kensington, (1992).
- [98] M.A. Green *Silicon Solar Cells. Advanced Principles and Practice*. University of New South Wales, Sydney, (1995).
- [99] B. A. Gregg "Evolution of photophysical and photovoltaic properties of perylene bisphenylimide films upon solvent vapor annealing" *J.Phys.Chem.* **100**, 852-859 (1996)
- [100] N. C. Greenham, S. C. Moratti, D. D. C. Bradley, R. H. Friend and A. B. Holmes "Efficient light emitting diodes based on polymers with high electron affinities." *Nature* **365**, 628 (1993)
- [101] N. C. Greenham and R. H. Friend "Semiconductor device physics of conjugated polymers." *Solid State Physics* **49**, 1 (1995)
- [102] N. C. Greenham, X. Peng and A. P. Alivisatos "Charge separation and transport in conjugated -polymer (MEH PPV)/CdSe -nanocrystal composites studied by PL quenching and photoconductivity." *Phys.Rev.B* **54**, 17628 (1996)
- [103] J. Gruener, M. Remmers and D. Neher "Direct determination of the emission zone in a polymer LED." *Adv.Mat.* **9**, 964-968 (1997)
- [104] M.S. Gudipati, *J. Phys. Chem.* **98**, 9750-9763 (1994)
- [105] A. G. Guerek and O.E. Bekaroglu "Octakis(alkylthio)-substituted (Cu, Co, Ni, Zn) phthalocyanines and their interactions with silver and palladium ions. *J. Chem. Soc. Dalton Trans* 1419, (1994)
- [106] J. Hagen, W. Schaffrath, P. Otschik, R. Fink, A. Bacher, H. W. Schmidt and D. Haarer "Novel hybrid solar cells consisting of inorganic nanoparticles and an organic hole transport material." *Synth.Met.* **89**, 215-220 (1997)
- [107] A. Hagfeldt, B. Didriksson, T. Palmqvist, H. Lindstroem, S. Soedergren, H. Rensmo and S. E. Lindquist "Verification of high efficiencies for the Graetzel-cell." *Sol.En.Mat.Sol.Cells* **31**, 481-488 (1994)
- [108] T. W. Hagler, K. Pakbaz, K. F. Voss and A. J. Heeger "Enhanced order and electronic delocalization in conjugated polymers oriented by gel processing." *Phys.Rev.B* **44**, 8652 (1991)
- [109] D. A. Halliday, P. L. Burn, R. H. Friend, D. D. C. Bradley, A. B. Holmes and A. Kraft "Extended Pi conjugation in PPV from a chemically modified precursor polymer." *Synth.Met.* **55-57**, 954-959 (1993)
- [110] D. A. Halliday, B. L. Burn, D. D. C. Bradley, R. H. Friend, O. M. Gelsen, A. B. Holmes, A. Kraft, J. H. F. Martens and K. Pichler "Large changes in optical response through chemical pre ordering of PPV." *Adv.Mat.* **5**, 40 (1993)
- [111] J. J. M. Halls, K. Pichler, R. H. Friend, S. C. Moratti and A. B. Holmes "Exciton diffusion and dissociation in a PPV/C60 heterojunction photovoltaic cell" *Appl.Phys.Lett.* **68**, 3120-3122 (1996)
- [112] J. J. M. Halls, C. A. Walsh, N. C. Greenham, E. A. Marseglia, R. H. Friend, S. C. Moratti and A. B. Holmes "Efficient photodiodes from interpenetrating polymer networks." *Nature* **376**, 498 (1995)
- [113] J. J. M. Halls and R. H. Friend "The photovoltaic effect in a PPV/perylene heterojunction." *Synth.Met.* **85**, 1307-1308 (1996)
- [114] J. J. M. Halls "Photoconductive properties of conjugated polymers" *PhD thesis*, Cambridge (1997)
- [115] J.J.M. Halls and R.H. Friend "Photoresponsive device with a photoresponsive zone comprising a polymer blend." *US Patent* 5670791 (1997)
- [116] M. Hanack "Synthesis and properties of conducting bridged macrocyclic metal complexes." *Mol.Cryst.Liq.Cryst.* **105**, 133-149 (1984)
- [117] M. Hanack, A. Beck and H. Lehmann "Syntheses of liquid crystalline phthalocyanines." *Communications* 703-705 (1987)
- [118] M. Hanack and M. Lang "Conducting stacked metallophthalocyanines and related compounds." *Adv.Mat.* **6**, 819-833 (1994)
- [119] M. Hanack, K. Duerr, A. Lange, J. Osio Barcina, J. Pohmer and E. Witke "Synthesis of low band gap polymers - a challenge for organic chemists." *Synth.Met.* **71**, 2275-2278 (1995)
- [120] M. G. Harrison, J. Gruener and G. W. C. Spencer "Analysis of the photocurrent action spectra of MEH-PPV photodiodes." *Phys.Rev.B* **55**, 7831-7849 (1997)
- [121] M. G. Harrison, J. Gruener and G. W. C. Spencer "Investigations of organic electroluminescent diodes by impedance spectroscopy, photo-impedance spectroscopy and modulated photovoltage spectroscopy" *Synth.Met.* **76**, 71-75 (1996)
- [122] K. S. Harsha Sree, K. J. Bachmann, P. H. Schmidt, E. G. Spencer and F. A. Thiel "n-indium tin oxide/p-indium phosphide solar cells." *Appl.Phys.Lett.* **30**, 645-646 (1977)
- [123] C. B. Hatfield "Oil back on the global agenda. Permanent decline in global oil is virtually certain to begin within 20 years." *Nature* **387**, 121 (1997)
- [124] A.J.Heeger et al. *Appl. Phys. Lett.* **58** 1982-1984 (1991)
- [125] J. Heinze "Cyclovoltametry - die "Spektroskopie" des Elektrochemikers" *Angewandte Chemie* **96**, 823 (1984)

- [126] J. Heinze, J. Mortensen, K. Muellen and R. Schenk "The charge storage mechanism of conducting polymers: A voltametric study on defined soluble oligomers on the phenylene-vinylene type." *J. Chem. Soc., Chem. Commun* 701-703 (1987)
- [127] J. Heinze, M. Stoerzbach, J. Mortensen and polymers(conducting) "Electrical and theoretical studies on the redox properties of conducting polymers." *Ber. Bunsenges. Phys. Chem.* **91**, 960-967 (1987)
- [128] D. Hertel, U. Scherf, H. Baessler *Adv. Mat.* **10** 1119 (1998)
- [129] F. Hildebrandt, J. A. Schroeter, C. Tschierske, R. Festag, M. Wittenberg and H. Wendorff "Formation of columnar mesophase by rod-like molecules: Facial amphiphilic p-terphenyl derivatives." *Adv. Mat.* **9**, 564-567 (1997)
- [130] M. Hiramoto, M. Suezaki and M. Yokoyama "Effect of thin gold layer on the photovoltaic properties of tandem organic solar cell." *Chem. Lett* 327-330 (1990)
- [131] M. Hiramoto, Y. Kishigami and M. Yokoyama "Doping effect on the two layer organic solar cell." *Chem. Lett* 119-122 (1990)
- [132] M. Hiramoto, T. Katsume and M. Yokoyama "Light amplification in a new light transducer combining an organic LED with photoresponsive organic pigment film." *Opt. Rev.* **1**, 82-84 (1994)
- [133] M. Hiramoto, T. Imahigashi and M. Yokoyama "Photocurrent multiplication in organic pigment films" *Appl. Phys. Lett.* **64**, 187-189 (1994)
- [134] G. Horowitz, F. Kouki, P. Spearman, D. Fichou, C. Nogues, X. Pan and F. Garnier "Evidence for n-type conduction on a perylene tetracarboxylic diimide derivative." *Adv. Mat.* **8**, 242-244 (1997)
- [135] K. Hunger, W. Herbst "Industrielle Organische Pigmente: Herstellung, Eigenschaften, Anwendungen." 1st edition, VCH, Weinheim (1987).
- [136] Intergovernmental Panel on Climate Change (IPCC) "Second Assessment Report - Climate Change 1995", (1995) Web site: www.meto.gov.uk
- [137] K.Y. Jen, H. Eckhardt, T.R. Jow, L.W. Shackette, R. Elsenbaumer *J. Chem. Soc. Chem. Commun* 215 (1988)
- [138] K. C. Kao and W. Hwang "Electrical Transports in Solids - with Particular Reference to Organic Semiconductors" *Pergamon Press*, Oxford (1981)
- [139] N. Karl and Ziegler, *J. Chem. Phys. Lett.* **32**, 438-442 (1975)
- [140] M. Katayose, S. Tai, K. Kamijima, H. Hagiwara and N. Hayashi "Novel silicon naphthalocyanines: Synthesis and molecular arrangement in thin films." *J. Chem. Soc. Perkin Trans. 2*, 403-409 (1992)
- [141] M. Khan et. al. *Synth. Met.* **101**, 246-247 (1999)
- [142] M. Khan personal communication (1999)
- [143] M. Khan, unpublished results.
- [144] J. S. Kim, M. Granstrm, R. H. Friend, N. Johansson, W. R. Salaneck, R. Daik, W. J. Feast and F. Cacialli. "Indium-tin oxide treatments for single- and double-layer polymeric light-emitting diodes: the relation between the anode physical, chemical, and morphological properties and the device performance", *J. Appl. Phys.* **84**, 6859-6870 (1998)
- [145] K. H. Koch and K. Muellen "Synthesis of tetra alkyl-substituted oligo (1,4-naphthylene)s and cyclization to soluble oligo(peri-naphthylene)s. From the perylene to pentarylene." *Chem. Ber.* **124**, 2091-2100 (1991)
- [146] A. Koehler, H. F. Wittmann, R. H. Friend, M. S. Khan and J. Lewis "Enhanced photocurrent response in photocells made with platinum-poly-yne/C60 blends by photoinduced electron transfer." *Synth. Met.* **77**, 147 (1996)
- [147] A. Koehler, H. F. Wittmann, R. H. Friend, M. S. Khan and J. Lewis "The photovoltaic effect in a platinum poly-yne. Effect of triplet excitons on the photogeneration of charge carriers" *Synth. Met.* **67**, 245 (1994)
- [148] A. Koehler, J. Gruener, R. H. Friend, K. Muellen and U. Scherf "Photocurrent measurements on aggregates in LPPP. additional response in the yellow part (at 2.25 eV) attributed to aggregates." *Chem. Phys. Lett.* **243**, 456 (1995)
- [149] A. Koehler, D. A. Dos Santos, D. Beljonne, Z. Shuai, J. L. Bredas, A. B. Holmes, A. Kraus, K. Muellen and R. H. Friend "Charge separation in localized and delocalized electronic states in polymeric semiconductors." *Nature* **392**, 903-906 (1998)
- [150] A. Koehler, private communication.
- [151] K. Kogo, T. Goda, M. Funahashi and J. Hanna "Polarized light emission from a calamitic liquid crystalline semiconductor doped with dyes." *Appl. Phys. Lett.* **73**, 1595-1597 (1998)
- [152] J. M. Kroon, R. B. M. Koehorst, M. Van Diik, G. M. Sanders and E. J. R. Sudhoelter "Self assembling properties of non-ionic tetraphenyl - porphyrins and discotic phthalocyanines carrying oligo(ethylene oxide) alkyl or alkoxy units." *J. Mater. Chem.* **7**, 615-624 (1997)
- [153] F. Kulzer, F. Koberling, T. Christ, A. Mews and T. Bache *Chem. Phys.* **247**, 23 (1999).
- [154] K. Y. Law "Organic photoconductive materials: Recent trends and developments." *Chem. Rev.* **93**, 449-486 (1993)
- [155] K. Y. Law "Organic photo conductive materials for xerographic photo receptors." *Handbook Org. Cond. Mol. Polym.* **1**, 488-545 (1997)
- [156] B. M. W. Langeveld-Voss, E. Peteer, R. A. J. Janssen and E. W. Meijer, *Synth. Met.* **84**, 611 (1997)
- [157] H. Langhals *Heterocycles* **40**, 477 (1995)
- [158] C.H. Lee, G. Yu, D. Moses and A.J. Heeger, *Phys. Rev. B* **49**, 2396-2407 (1994)
- [159] O. Lehmann, *Z. Phys. Chem.* **4**, 462 (1889)

- [160] U. Lemmer, S. Heun, R.F. Mahrt, U. Scherf, M. Hopmeier, U. Siegner, E.O. Goebel, K. Muellen, H. Baessler *Chem. Phys. Lett.* **240** 373 (1995)
- [161] C.C. Leznoff, A.B.P. Lever (Eds), "Phthalocyanines, Properties and Applications" VCH Weinheim, Vol. 2 (1993)
- [162] H. J. Lewerenz and H. Jungblut "Photovoltaic - Grundlagen und Anwendungen" Springer, Berlin, Heidelberg, New York (1995)
- [163] E.J.W. List, J. Partee, J. Shinar, U. Scherf, K. Mullen, E. Zojer, K. Petritsch, G. Leising and W. Graupner "Localized triplet excitations and the effect of photo-oxidation in ladder-type poly(p-phenylene)s and oligo(p-phenylene)s" *Phys. Rev. B* in print (2000)
- [164] R. O. Loutfy, J. H. Sharp, C. K. Hsiao and Ho R "Phthalocyanine organic solar cells." *J. Appl. Phys.* **52**, 5218 (1981)
- [165] A. Lux, G.G. Rozenberg, K. Petritsch, S.C. Moratti, A.B. Holmes and R.H. Friend, "A series of novel liquid crystalline octakis(alkylthio)-substituted phthalocyanines" *Synth. Met.* **102**, 1527-1528 (1999)
- [166] A. Lux, private communication.
- [167] A. Lux, A. B. Holmes, R. Cervini, J. E. Davies, S. C. Moratti, J. Gruener, F. Cacialli and R. H. Friend "New CF₃ substituted PPV type oligomers and polymers for use as hole blocking layers in LEDs" *Synth. Met.* ? (1997)
- [168] R. N. Marks, J. J. M. Halls, D. D. C. Bradley, R. H. Friend and A. B. Holmes "The photovoltaic response in PPV thin film devices." *J. Phys.: Cond. Mat.* **6**, 1379-1394 (1994)
- [169] J. C. Mello, F. Wittmann and R. H. Friend "An improved experimental determination of external photoluminescence quantum efficiency." *Adv. Mat.* **9**, 230-232 (1997)
- [170] H. B. Michaelson "The workfunction of the elements and its periodicity" *J. Appl. Phys.* **48**, 4729-4733 (1977)
- [171] L. Q. Minh, T. Chot, N. N. Dinh, N. N. Xuan, N. T. Binh, D. M. Phuoc and N. T. Binh "A new organic photoconductor in the near infrared region of diode lasers. absorption maxima between 780nm and 850nm. Soluble in alpha-chloronaphthalene (?)." *Phys. Stat. Sol. (a)* **101**, K143 (1987)
- [172] E. Moons, M. Eschle and M. Graetzel "Determination of the energy diagram of the dithioketopyrrole / SnO₂:F heterojunction by surface photovoltage spectroscopy" *Appl. Phys. Lett.* **71**, 3305-3307 (1997)
- [173] D. L. Morel, E. L. Stogryn, A. K. Ghosh, T. Feng, P. E. Purwin, R. F. Shaw, C. Fishman, G. R. Bird and A. P. Piechowski "Organic photovoltaic cells" *J. Phys. Chem.* **88**, 923-933 (1984)
- [174] S. C. Moratti et al, "High electron affinity polymers for LEDs." *Synth. Met.* **71** 2117-2120 (1995)
- [175] N. F. Mott, *Trans. Faraday Soc.* **34** 500-506 (1938)
- [176] N. F. Mott "Note on the contact between a metal and an insulator or semiconductor." *Proc. Cambr. Phil. Soc.* **34**, 568-572 (1938)
- [177] M. Mueller, F. Morgenroth, U. Scherf, T. Soczka-Guth, G. Klaerner and K. Muellen "The benzene ring as modulus: Synthesis and supramolecular ordering of novel conjugated polymers." *Phil. Trans R. Soc. Lond. A* **355**, 715-726 (1997)
- [178] F. Nuesch, L. Si-Ahmed, B. Francois and L. Zuppiroli "Derivatized electrodes in the construction of organic LEDs." *Adv. Mat.* **9**, 222-225 (1997)
- [179] C. K. Ober and G. Wegner "Polyelectrolyte surfactant complexes in the solid state: Facile building blocks for self organizing materials." *Adv. Mat.* **9**, 17-31 (1997)
- [180] A. R. Oezkaya, A. G. Guerek, A. Guel and Bekaroglu Oe "Electrochemical and spectral properties of octakis(hexylthio)-substituted phthalocyanines." *Polyhedron* **16**, 1877-1883 (1997)
- [181] Ohnishi et al. *Synth. Met.* **57** 4174-4179 (1993)
- [182] B. O'Regan and M. Graetzel "A low cost, high efficiency solar cell based on dye-sensitized colloidal TiO₂ films." *Nature* **353**, 737 (1991)
- [183] ORIEL Corporation, "Solar Simulation", *Solar Simulator Product Guide*, (1993).
- [184] L. Oriol and J. L. Serrano "Metallomesogenic polymers." *Adv. Mat.* **7**, 348-369 (1995)
- [185] B. Ottenbours, H. Paulussen, P. Adriaensens, D. Vanderzande and J. Gelan "Characterization of poly(isothianaphthene) derivatives and analogs by using solid state C13 NMR" *Synth. Met.* **89**, 95-102 (1997)
- [186] K. Pakbaz, C. H. Lee, A. J. Heeger, T. W. Hagler and D. McBranch "Nature of the primary photoexcitation in poly arylene vinylene" *Synth. Met.* **64**, 295-306 (1994)
- [187] P. Panayotatos, G. Bird, R. Sauers, A. Piechowski and S. Husain "An aproach to the optimal design of p-n heterojunction solar cells using thin film organic semiconductors." *Solar Cells* **21**, 301-311 (1987)
- [188] Y. Park, V. Choong, Y. Gao, B. R. Hsieh and C. W. Tang "Work function of ITO transparent conductor measured by photoelectron spectroscopy." *Appl. Phys. Lett.* **68**, 2699-2701 (1996)
- [189] Y. Park, V. Choong, E. Ettegui, Y. Gao, B. R. Hsieh, T. Wehrmeister and K. Muellen "Energy level bending and alignment at the interface between Ca and a phenylene vinylene oligomer." *Appl. Phys. Lett.* **69**, 1080-1082 (1996)
- [190] Parrott "Thermodynamics of solar cell efficiency" *Sol. En. Mat. Sol. Cells* **25**, 73-85 (1992)
- [191] H. Paulussen, D. Vanderzande and J. Gelan "The synthesis and characterization of soluble poly(isothianaphthene)- derivatives." *Synth. Met.* **84**, 415-416 (1997)

- [192] D. Pede, E. Smela, T. Johansson, M. Johansson and O. Inganaes "A general purpose conjugated polymer device array for imaging." *Adv.Mat.* **10**, 233-237 (1998)
- [193] Q. Pei, G. Zuccarello, M. Ahlskog and O. Inganaes "Electrochromic and highly stable PEDOT switches between opaque blue black and transparent sky blue." *Polymer* **35**, 1347-1351 (1994)
- [194] J. B. Pendry "Photonic band structures." *J. Modern Optics* **41**, 209-229 (1994)
- [195] R. Peierls, *Ann. Phys.* **13**, 905-952 (1932)
- [196] K. Petritsch and R. H. Friend "Ultrathin Organic Photovoltaic Devices." *Synth.Met.* **102**, 976 (1998)
- [197] K. Petritsch, W. Graupner, G. Leising and U. Scherf "Photoinduced absorption in a Poly(para-phenylene) ladder type polymer." *Synth.Met.* **84**, 625-626 (1997)
- [198] K. Petritsch "Optical Modulation Spectroscopy in Organic and Inorganic Semiconductors" *Diploma Thesis*, Technical University Graz (1996)
- [199] K. Petritsch, R.H. Friend, A. Lux, G. Rozenberg, S.C. Moratti and A.B. Holmes "Liquid crystalline phthalocyanines in organic solar cells" *Synth.Met.* **102**, 1776 (1999)
- [200] K. Petritsch, J.J. Dittmer, E.A. Marsegia A. Lux, G. Rozenberg, S.C. Moratti and A.B. Holmes and R.H. Friend "Dye based Donor/Acceptor Solar Cells" *Sol.En.Mat.Sol.Cells* **61/1**, 63-72 (2000)
- [201] K. Petritsch, M. Granstrom, A.C. Arias, R.H. Friend, A. Lux, G.G. Rozenberg, S.C. Moratti, A.B. Holmes and M.R. Andersson "Towards inexpensive solar cells" *Proc. 2nd World Conference and exhibition on photovoltaic solar energy conversion* Vienna, 1998
- [202] K. Petritsch et. al, unpublished results
- [203] J. B. Pendry "Photonic band structures." *J. Modern Optics* **41**, 209-229 (1994)
- [204] A.P. Piechowski, G.R. Bird, D. L. Morel and E.L. Stogryn "Desirable properties of photovoltaic dyes " *J.Phys.Chem.* **88**, 934-950 (1984)
- [205] M. Pope and C.E. Swenberg, *Electronic Processes in Organic Crystals*, Clarendon Press, Oxford (1982)
- [206] M. B. Prince "Silicon Solar Energy Converters." *J.Appl.Phys.* **26**, 534-540 (1955)
- [207] H. Quante, P. Schlichting, U. Rohr, Y. Geerts and K. Muellen "Novel perylene-containing polymers." *Macromol. Chem.Phys.* **197**, 4029-4044 (1996)
- [208] E. Rabinowitch, "Photosynthesis", Wiley, New York (1969)
- [209] A. Rademacher, S. Maerkele and H. Langhals "Loesliche perylen- Fluoreszenzfarbstoffe mit hoher photostabilitaet." *Chem.Ber.* **115**, 2927-2934 (1982)
- [210] H. Reisch, U. Wiesler, U. Scherf and N. Tuytuykov "Poly(indenofluorene)(PIF), a novel low band gap polyhydrocarbon" *Macromolecules* **29**, 8204-8210 (1996)
- [211] L. S. Roman, I. A. Huemmelgen, F. C. Nart, L. O. Peres and de Sa E L "Determination of electro-affinity and ionization potential of conjugated polymers via Fowler-Nordheim tunneling measurements: theoretical formulation and application to PPV " *J.Chem.Phys.* **105**, 10614-620 (1996)
- [212] L. S. Roman, M. R. Andersson, T. Yohannes and O. Inganaes "Photodiode performance and nano-structure of polythiophene/c60 blends." *Adv.Mat.* **9**, 1164-1168 (1997)
- [213] L. S. Roman, W. Mammo, L. A. A. Pettersson, M. R. Andersson and O. Inganaes "High quantum efficiency polythiophene/C60 photodiodes." *Adv.Mat.* **10**, 774-777 (1998)
- [214] J. Rostalski and D. Meissner "Monochromatic versus Solar Efficiencies of Organic Solar Cells" *Solar Energy Mater. Solar Cells* **61**, 87-95 (2000)
- [215] L. J. Rothberg, M. Yan, S. Son, M. E. Galvin, E. W. Kwock, T. M. Miller, H. E. Katz, R. C. Haddon and F. Papadimitrakopoulos "Intrinsic and extrinsic constraints on PPV electroluminescence." *Synth.Met.* **78**, 231-236 (1996)
- [216] L. J. Rothberg, M. Yan, A. W. P. Fung, T. M. Jedju, E. W. Kwock and M. E. Galvin "Photogeneration mechanism and exciton binding energy in phenylenevinylene polymers." *Synth.Met.* **84**, 537-538 (1997)
- [217] H. Quante, P. Schlichting, U. Rohr, Y. Geerts and K. Muellen "Novel perylene-containing polymers." *Macromol. Chem.Phys.* **197**, 4029-4044 (1996)
- [218] R. J. Regensburger, J. J. Jakubowski; *U.S. Patent* 3,904,407 (**1975**)
- [219] F. Reinitzer, *Monatsh. Chem.* **9**, 421 (1888)
- [220] E. H. Rhoderick and R. H. Williams, *Metal-Semiconductor Contacts*, Clarendon Press, Oxford
- [221] M. Samoc, A. Samoc, B. L. Davies and U. Scherf "Saturable absorption in PIF - a picket fence polymer." *Opt.Lett.* in print (1998)
- [222] D. J. Sandman "Semiconducting polymers and their solid state properties." *TRIP* **2**, 44 (1994)
- [223] Savenije et al. *Phys.Rev.Lett*
- [224] J.H. Schon, C. Kloc, E. Bucher, B. Batiogg, "Efficient organic photovoltaic diodes based on doped pentacene" *Nature* **403** 408-410 (2000)
- [225] W. Schottky, *Naturwiss.* **26**, 843 (1938)
- [226] A. J. Schouten, J. M. Warman, M. P. de Haas, M. A. Fox and H. L. Pan "Charge migration in supramolecular stacks of peripherally substituted porphyrins." *Nature* **353**, 736-737 (1991)
- [227] P. G. Schouten, J. F. Van der Pol, J. W. Zwikker, W. Drenth and S. J. Picken "Peripherally octasubstituted phthalocyanines with branched alkoxy chains." *Mol.Cryst.Liq.Cryst.* **195**, 291 (1991)

- [228] P. G. Schouten, J. M. Warman, M. P. de Haas, C. F. van Nostrum, G. H. Gelinck, R. J. M. Nolte, M. J. Copyn, J. W. Zwikker, M. K. Engel, M. Hanack, Y. H. Chang and W. T. Ford "The effect of structural modifications on charge migration in mesomorphic phthalocyanines." *J. Am. Chem. Soc.* **116**, 6880-6894 (1994)
- [229] W. Shockley "The Theory of p-n Junctions in Semiconductors and p-n junction transistors." *Bell Syst. Techn. Journ.* **28**, 435-489 (1949)
- [230] W. Shockley and H. J. Queisser "Detailed balance limit of efficiency of PN junction solar cells" *J. Appl. Phys.* **32**, 510 (1961)
- [231] J. Simon and J. J. Andre "Molecular Semiconductors." *Springer Verlag*, Heidelberg (1985)
- [232] H. Sirringhaus, N. Tessler and R.H. Friend, *Science* **280**, 1741 (1998)
- [233] T.A. Skotheim "Handbook of Conducting Polymers", New York & Basel, Vol1 (1986)
- [234] G. Smestad and H. Ries "Luminescence and current voltage (IV) characteristics of solar cells and optoelectronic devices." *Sol.En.Mat.Sol.Cells* **25**, 51-71 (1992)
- [235] G. Smestad "Testing of dye sensitized TiO₂ solar cells II: Theoretical voltage output and photoluminescence efficiencies." *Sol.En.Mat.Sol.Cells* **32**, 237-288 (1994)
- [236] G. Smestad, C. Bignozzi and R. Argazzi "Testing of dye sensitized TiO₂ solar cells I: Experimental photocurrent output and conversion efficiencies." *Sol.En.Mat.Sol.Cells* **32**, 259-272 (1994)
- [237] Solar Cell Efficiency Tables (Version12), *Progress in Photovoltaics: Research and Applications* **7** (1998). Website (University of New South Wales): www.pv.unsw.edu.au/eff/
- [238] Stampfl, W. Graupner, G. Leising and U. Scherf "Photoluminescence and UV-VIS absorption study of PPP-type ladder polymers." *Journal of Luminescence* **63**, 117-123 (1995)
- [239] Stampfl, S. Tasch, G. Leising and U. Scherf "Quantum efficiencies of electroluminescent poly para phenylenes" *Synth.Met.* **71**, 2125-2128 (1995)
- [240] M. Stevens, B. Weir, G. Denton and R.H. Friend "Laser Ablation of Conjugated Polymers" *Synth. Met* **101**, 234-235 (1999)
- [241] S. M. Sze "Physics of Semiconductor Devices.", John Wiley & Sons, New York (1981)
- [242] K. Tada, M. Onada, A. A. Zakhidov and K. Yoshino "Characteristic of poly(p-pyridyl vinylene)/poly (3-alkyl-thiophene) heterojunction photocell." *Jpn. J. Appl. Phys.* **36**, L306-L309 (1997)
- [243] K. Tada and K. Yoshino "Conducting polymer color sensor." *Jpn. J. Appl. Phys.* **36**, L1351-53 (1997)
- [244] C. W. Tang "Two-layer organic photovoltaic cell." *Appl. Phys. Lett.* **48**, 183 (1986)
- [245] C. W. Tang "Multilayer organic photovoltaic elements." *US Patent* 4,164,431 (1981)
- [246] S. Tasch, E. J. W. List, O. Ekstroem, W. Graupner, G. Leising, P. Schlichting, U. Rohr, Y. Geerts, U. Scherf and K. Muellen "Efficient white light emitting diodes realized with new processable blends of conjugated polymers." *Appl. Phys. Lett.* **71**, 2883-2885 (1997)
- [247] S. Tasch, C. Brandstaetter, F. Meghdadi, G. Leising, G. Froyer and L. Athouel "Red green blue light emission from a thin film electroluminescence device based on parahexaphenyl." *Adv. Mat.* **9**, 33-36 (1997)
- [248] N. Tessler, N. T. Harrison, R. H. Friend *Adv. Mat.* **10**, 64 (1998)
- [249] N. Tessler, G. J. Denton and R. H. Friend "Lasing from conjugated polymer microcavities." *Nature* **382**, 695 (1996)
- [250] N. Tessler, P. L. Burns, H. Becker and R. H. Friend "Suppressed angular color dispersion in planar microcavities." *Appl. Phys. Lett.* **70**, 556-558 (1997)
- [251] T. Tsuzuki, Y. Shiota, J. Rostalski, D. Meissner "The Effect of Fullerene Doping on Photoelectric Conversion Using Titanyl Phthalocyanine and a Perlene Pigment" *Sol.En.Mat.Sol.Cells* **61**, 1-8 (2000)
- [252] United Nations Environment Programme (UNEP) "Global Environment Outlook (GEO)-2000", Earthscan Publications Ltd., London (2000). Web site: www.unep.org
- [253] J. F. Van der Pol, E. Neeleman, J. W. Zwikker, R. J. M. Nolte, W. Drenth, J. Aerts, R. Visser and S. J. Picken "Homologous series of liquid-crystalline metal free and copper octa-n-alkoxy phthalocyanines." *Liq. Cryst.* **6**, 577-592 (1989)
- [254] J. F. Van der Pol, E. Neeleman, J. C. Van Miltenburg, J. W. Zwikker, R. J. M. Nolte and W. Drenth "A POLYMER with the mesomorphic order of liquid crystalline phthalocyanines (Polymerization in the mesophase)." *Macromolecules* **23**, 155-162 (1990)
- [255] J. F. Van der Pol, M. P. de Haas, J. M. Warman and W. Drenth "Sudden conduction (10E-3 to 0.1 S/m) at the solid to mesophase transition of octa n alkoxy substituted phthalocyanines." *Mol. Cryst. Liq. Cryst.* **183**, 411-420 (1990)
- [256] J. F. Van der Pol, M. P. de Haas, J. M. Warman and W. Drenth "Erratum - Contributions from dipolar relaxation to microwave conductivity." *Mol. Cryst. Liq. Cryst.* **195**, 307-308 (1991)
- [257] J. A. E. H. Van Haare, L. Groenendaal, H. W. I. Peerlings, E. E. Havinga, J. A. J. M. Vekemans, R. A. Janssen and E. W. Meijer "Unusual redox behavior of oligoheteroaromatic compounds: An Increasing first oxidation potential with increasing conjugation length." *Chemistry of Materials* **7**, 1984 (1995)
- [258] J. A. E. H. Van Haare "A general procedure toward colorless transparent conducting polymer films." *PhD thesis* (1997)
- [259] C. F. van Nostrum and R. J. M. Nolte "Supramolecular architectures from phthalocyanine building blocks." *Macromol. Symp.* **77**, 267-276 (1994)

- [260] C. F. van Nostrum, A. W. Bosman, G. H. Gelinck, P. G. Schouten, J. M. Warman, A. P. M. Kentgens, A. C. Devillers, A. Meijerink, S. J. Picken, U. Sohling, A. J. Schouten and J. M. Nolte "Supramolecular structure, physical properties, and Langmuir Blodgett film formation of an optically active liquid crystalline phthalocyanine." *Chem. Eur. J.* **1**, 171-182 (1995)
- [261] C. F. van Nostrum, S. J. Picken, A. J. Schouten and R. J. M. Nolte "Synthesis and supramolecular chemistry of novel liquid crystalline crown ether substituted phthalocyanines: Toward molecular wires and molecular ionoelectronics." *J. Am. Chem. Soc.* **117**, 9957-9965 (1995)
- [262] C. F. van Nostrum "Self assembled wires and channels." *Adv.Mat.* **8**, 1027-1030 (1996)
- [263] J.A.E.H. Van Haare "A general procedure toward colorless transparent conducting polymer films." - Title of thesis: Redox states of conjugated oligomers and polymers." *PhD thesis* (1997)
- [264] S. C. Veenstra, G. G. Malliaras, H. J. Brouwer, F. J. Esselink, V. V. Krasnikov, P. F. van Hutten, J. Wildeman, H. T. Jonkman, G. A. Sawatzky and G. Hadziioannou "Sexithiophene+C60 blends as model systems for photovoltaic devices." *Synth.Met.* **84**, 971-972 (1997)
- [265] G.H. Wannier *Phys. Rev.* **52**, 191-197 (1937)
- [266] V. Wan unpublished results.
- [267] J. B. Whitlock, P. Panayotas, G. D. Sharma, M. D. Cox, R. R. Sauers and G. R. Bird "Investigations of materials and device structures for organic semiconductor solar cells." *Optical Engineering* **32**, 1921-1933 (1993)
- [268] D. Woehrle and D. Meissner "Organic solar cells" *Adv.Mat.* **3**, 129 (1991)
- [269] D. Woehrle, M. Eskes, K. Shigehara, A. Yamada, *Syn-thesis* 194 (1993)
- [270] J.P. Wolfe and A. Mysyrowicz, "Excitonic Matter" *Scientific American* **250** No.3, 70 (1984)
- [271] C.C. Wu, C.I. Wu, J. C. Sturm and A. Kahn "Surface modification of ITO by plasma treatment: An effective method to improve the efficiency, brightness, and reliability of organic LEDs" *Appl.Phys.Lett.* **70**, 1348-1350 (1997)
- [272] F. Wudl, M. Kobayashi and A.J. Heeger *J.Org.Chem.* **49** 3382 (1984)
- [273] Y. P. Yadava, G. Denicolo, A. C. Arias, L. S. Roman and I. A. Huemmelgen "Preparation and characterization of transparent conducting tin oxide (TO) film electrodes by chemical vapour deposition from reactive thermal evaporation of SnCl₂." *Mat.Chem.Phys.* **48**, 263-267 (1997)
- [274] Y. Yang, Q. Pei and A. J. Heeger "Efficient blue polymer light emitting diodes from a series of soluble PPP derivatives." *J.Appl.Phys.* **79**, 934-939 (1996)
- [275] S. Yamada, S. Tokito, T. Tsutsui, S. Saito *J. Chem. Soc., Chem Commun.* 1448 (1987).
- [276] K. Yoshino, K. Tada, M. Hirohata, H. Kajii, Y. Hironaka, N. Tada, Y. Kaneuchi, M. Yoshida, A. Fujii, M. Hamaguchi, H. Araki, T. Kawai, M. Ozaki, Y. Ohmori, M. Onada and A. Zakhidov "Novel properties of molecularly doped conducting polymers and junction devices." *Synth.Met.* **84**, 477-482 (1997)
- [277] K. Yoshino, K. Tada, A. Fujii, E. M. Conwell and A. A. Zakhidov "Novel photovoltaic devices based on donor-acceptor molecular and conducting polymer systems." *IEEE trans. Electron Devices* **44**, 1315-1324 (1997)
- [278] Yu G, J. Gao, C. Hummelen Jan, F. Wudl and A. J. Heeger "Polymer photovoltaic cells: Enhanced efficiencies via a network of internal donor acceptor heterojunctions." *Science* **270**, 1789 (1995)
- [279] C. Zenz, W. Graupner, S. Tasch, G. Leising, K. Muellen, U. Scherf *Appl. Phys. Lett* **71** 2566 (1997).
- [280] M. Zeilik and E.v.P. Smith "Introductory: Astronomy and Astrophysics", 2nd Edition, CBS College Publishing (1987)
- [281] F. Zhu and J. Singh "On the optical design and thin film amorphous silicon solar cells." *Sol.En.Mat. Sol.Cells* **31**, 119-131 (1993)
- [282] F. Zhu, P. Jennings, J. Cornish, G. Hefter and K. Luczak "Optimal optical design of thin film photovoltaic devices." *Sol.En.Mat.Sol.Cells* **49**, 163-169 (1997)
- [283] "Method lets pigments be processed like dyes." *Chemistry and Engineering News* **21**, 56 (1998)

Chapter 10

Appendices

10.1 Details of the Sample Preparation

Unless stated otherwise, the preparation of substrates and devices that have been used in the Chapters of this thesis has been performed as described in the following Sections.

10.1.1 ITO Substrates

The ITO substrates have been patterned by removing 2.5mm wide stripes of ITO from either side via etching in 20% HCl. The results is a conducting area of the form of a 7mm wide stripe in the middle of the substrate which is used as electrode. During the etching process the stripe in the middle was protected with a solid self adhesive photoresist sheet¹.

Note that the photoresist was only used as *protective* layer during etching and was illuminated with a UV lamp (before etching) for 2min so that it can be readily removed in two mechanical cleaning steps: rubbing the ITO surface with cotton buds using acetone and isopropanol (IPA).

The ITO substrates were then cleaned in ultrasonic baths with acetone (5min) followed by IPA (5min) in a laminar flow box.

10.1.2 Preparation of the Dye and Polymer Solutions

In order to obtain the desired concentrations of the polymer or dye solutions (typically between 2 and 30mg/ml), we were weighing the required amount of powder using a micro-scale in small vials (<2ml).

¹Later we used substrates which we received already pre-patterned. However, when received from the supplier/cutter the substrates were hold in place with a scotch tape. We used the same (pre-)cleaning procedure to remove remaining parts of the tape for these pre patterned substrates as for the home etched ones.

The solvent - usually chloroform - was added using disposable poly-propylene syringes and medium size needles. We did not use syringes with standard rubber plunges since the rubber dissolves quickly in chloroform which could lead to unknown effects in the organic film².

The solution was then shaken using an automatic roller device for typically more than an hour while avoiding to touch the vial caps³.

The solution was then filtered using polypropylene filters with pore sizes between 0.1 and 2.5 μ m - depending on the size of the molecule. Small molecules like dyes (Per or HPc) could be filtered using 0.1 μ m while polymers with high molecular weight require larger pore sizes. For example MEH-PPV may only be filtered through 2.5 μ m. The required minimal pore size can be estimated if the average size (length) of the specific molecule is calculated. Since we preferred to use fresh solutions so the required amount of solvent was usually less than 1ml. We found that about 3 films can be spun with 0.25ml solvent using 5 drops per substrate.

10.1.3 Film Deposition

The substrate was briefly (1-3s) rinsed with (IPA) and subsequently blow dried (\approx 10s) with nitrogen gas. About 5 drops of the solution were then dropped onto the patterned ITO substrates using disposable glass cuvettes - in a laminar flow box. Spin-speeds were typically 2000rpm with spinning times of 60s. The spun film was then transferred into the evaporation chamber where the top contact - usually Al - was sublimed.

²We could find significant absorption and PL of the dissolved rubber in solution.

³The vial caps had teflon layers inside which should be fairly resistant against chloroform - however, the long term exposure might allow solvent vapor to reach the vial cap which is actually made of some less resistant plastic material.

10.1.4 Sublimation of the Top Electrode

In order to complete the photovoltaic device, the top electrode - usually Al - was thermally sublimed onto the organic film. The pattern of the top electrodes was initially that shown in Fig.10.1 - so that 8 different electrodes allowed contacting of 8 different pixels on one substrate. Later the pattern was changed to 6 electrodes (pixels) to obtain larger pixel areas.

The larger pixel areas have been chosen so that the *whole* light beam could illuminate the electrode. Since the intensity of the whole light beam is the same as measured with the silicon photodiode the actual device area does not need to be known to calculate the EQE. This allowed more accurate determination of the EQE compared to the previously method where the pixels have been smaller than the light beam. In the latter, the actual size of the pixel and photodiode had to be determined which increased the error-bar of the final EQE number. The more accurate method was chosen since some devices (like the laminated polymer cell) reached high EQE numbers where higher accuracy was desired.

Typical pressures during evaporation were around 10^{-6} mbar.

The sublimation-mask used was made of brass with 9 substrate positions. When semi-transparency ($T > 20\%$) was required the Al film was between 10 and 20nm thin - otherwise the thickness was between 50 and 100nm.

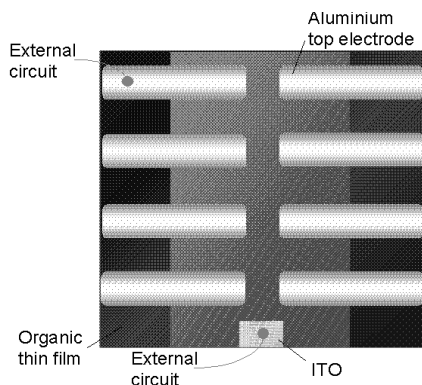


Figure 10.1: Planar view of the substrate - electrode pattern with the 8 pixel mask. The vertical stripe in the middle represents the ITO area (=bottom electrode). The substrate dimensions are 12x12mm. Figure courtesy of Ref. [63].

10.2 Details of the EQE and IV Measurements

After the sublimation of the top electrode the substrates were taken to the setup and dots of silver-paste solution were applied where the wires of the sample holder contact the electrodes in order to ensure a good electrical connection. Unless stated otherwise, all devices have been exposed to air for at least 24hrs prior to the measurement. After this period air molecules are assumed to have penetrated the entire bulk so that all devices can be compared even though some have seen air for one or two days longer than others.

In this way we were able to obtain fairly reproducible results. The fabrication of a set of 9 substrates - each containing 6 to 8 devices or pixels can be finished within 12hrs including dissolving the molecules and patterning the ITO.

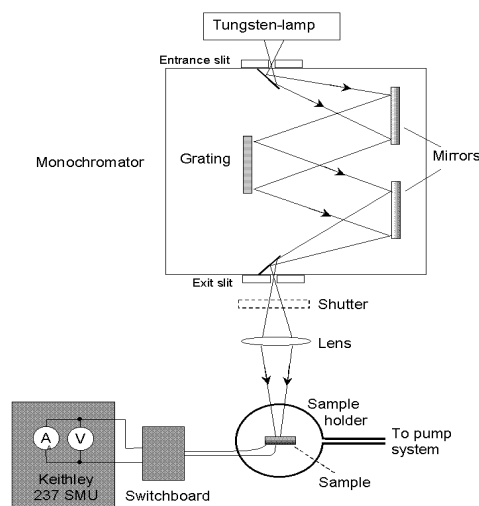


Figure 10.2: Experimental setup for the EQE and IV measurements. Figure courtesy of Ref. [63].

The experimental setup used for the EQE and IV measurements is shown in Fig.10.2. The light source is a 100W Bentham quartz tungsten halogen lamp with a spectral emission range larger than 350nm to 1300nm and an intensity peak at 880nm. The lamp is driven by a Bentham 505 current stabilised power supply. The white light was dispersed by a Czerny-Turner Bentham M300 single grating monochromator using a 1200 lines/mm grating and a blaze wavelength of 500nm.

The sample holder allowed automatic contacting

of the 8 or 6 pixels + the ITO contact using spring contacts made of beryllium-copper. The holder can be closed to apply a vacuum and is still optically accessible through quartz windows. A remotely controlled shutter allowed convenient switching between light and dark measurements for both the IV and the SR measurements. A switchboard serves to switch between different electrodes/pixels.

The setup was initially designed and built by Anna Koehler and later modified by the author.

A 580nm filter was used for the range from 600-1200nm to block the higher orders of the monochromator grating.

We note that the photocurrent can vary considerably between different pixels for various reasons (shorts, quality of the contact, poor film quality etc.). A quick method to find the best working pixel is to expose the entire substrate to a white light source (e.g. a 100W desk lamp) and switch between the pixels while observing the differences between dark and light current⁴.

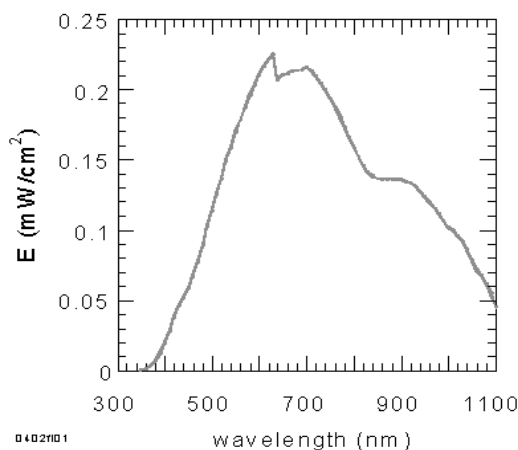


Figure 10.3: Typical light intensities (E) at the sample position as a function of wavelength. The offset at 620nm is due to the filter change.

Every set of SR measurements was preceded by a measurements of the light intensity using a silicon photodiode (HAMAMATSU 5106) with a known spectral response. The light intensity can vary depending on setup details but is generally constant within $\pm 20\%$ for different sets of measurements (on different days/weeks). Within the same set, we

could not find a significant variation of the light intensity.

A typical dependence of the light intensity at the sample position on the wavelength is shown in Fig.10.3. The offset around 620nm is due to a 580nm edge filter which is manually removed when the response to wavelengths smaller than 620nm is measured. The dark current was always assumed to be wavelength independent and subtracted from the photocurrent before the calculation of EQE.

The EQE was determined using Eq. (2.33) in Chapter 2. The EQE spectrum of the silicon reference diode using this procedure is shown in Fig.10.4. Both absolute values and the shape are as expected for commercial silicon photodiodes and confirm the validity of the applied mathematical procedure. The calculation of the EQE and irradiance was performed using an Excel spreadsheet designed by the author.

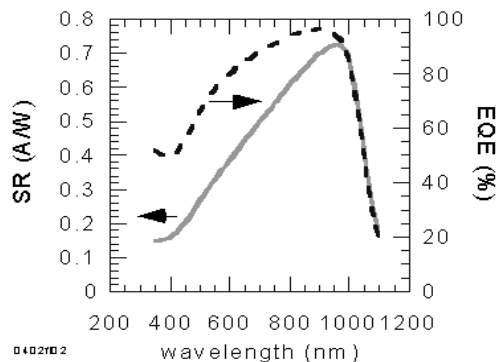


Figure 10.4: EQE spectrum and spectral response of the silicon reference diode (Hamamatsu S5106).

We assumed that the efficiency of our cells does not vary significantly with intensity in the used irradiance range. This assumption appears reasonable since results on e.g. MEH-PPV gave similar results using a completely different setup using a xenon lamp. Hence the intensity distribution of the incident photons was assumed to have no effect on the calculated EQE.

The IV curves were typically measured for wavelengths which gave the highest currents - which is not necessarily the highest EQE - starting in the negative voltage range. The voltage range was roughly scanned manually avoiding high currents which can destroy the device.

Depending on the open circuit voltage and the chosen voltage range the step size was between 20

⁴A negative bias may be used to enhance the effect for devices with very low EQE.

and 100mV. The dark characteristic was measured before and (again) after the light characteristic has been measured to confirm that the device behaviour did not change i.e. the device was destroyed.

As observed by other researchers in the same group the shape of the IV curves can vary more for different pixels than the EQE spectra [114, 64, 150]. We note that we did not use any mathematical smoothing procedure in more than 90% of the IV or EQE curves in this thesis. When smoothing was applied then to a very low extent ($< 1 - 3\%$) only to remove obvious and disturbing artifacts.

10.2.1 Note on the Dark Current at 0V

It can be assumed that the sometimes observed occurrence of a dark current (I_d) at 0V is - at least partly - due to the limited ability of the source measure unit (SMU) to apply *exactly* $0V \pm 0V$. The zero point error of the SMU cannot be much smaller than a few mV due to a finite resolution and non-ideal ground levels. Thus, these few mV can drive the current I_d through the cell with the actual size depending on R_{sh} .

The sign of I_d depends on the sign of the usually non zero ground potential plus the zero point error of the SMU itself. Note that devices with a very low shunt (e.g. partly shorted or doped devices) can show positive or negative⁵ I_d values of many nA. Note that upon illumination such devices can still generate a negative photocurrent and therefore still work as solar cells. These devices show usually no significant open circuit voltage.

Another possibility to explain the existence of such a dark current is to consider the capacity (C) of the device:

$$C = \epsilon_0 \epsilon_r \frac{A}{d} \quad (10.1)$$

with $\epsilon = 8.9 \cdot 10^{-12} J^{-1} C^2 m^{-1}$, $A \approx 10^{-6} m^2$, $\epsilon_r \approx 2$ we obtain capacities between 10 and 100pF for a thickness d ranging between 10 and 100nm respectively.

Together with the (series) resistor data from Table 3.5 we obtain time constants (τ):

$$\tau = RC \quad (10.2)$$

⁵In this thesis negative currents at $\geq 0V$ are defined as currents which are generated by the device upon illumination. However, the dark current due to externally applied voltage has always to be considered (subtracted) to obtain the actually photogenerated current.

between ms and several 10s. Considering the equation for discharging a capacitor:

$$U = U_0 \cdot e^{-\frac{t}{\tau}} \quad (10.3)$$

this means that, once a device has seen light (i.e. charged), it can take many seconds i.e. minutes to discharge via the series resistor even if the device is externally shorted ($V=0V$).

10.3 Absorption Measurements

Optical absorption spectra of solutions and thin films were measured with a Hewlett Packard 8453 UV-Vis spectrometer. The spectra were corrected for the transmission of the substrate (ITO on quartz) which was measured before a set of absorption spectra was taken. Most absorption spectra were taken from the actual device by directing the light beam through the space between the pixels using a suitable (diameter=0.8mm) mask.

10.4 Thickness Measurements

The thickness of the organic films was measured using a profilometer (Sloan Dektak IIa) by scratching the film carefully with a sharp tweezer or a toothpick avoiding to scratch into the substrate. We typically took 3 measurements at different positions on the substrate and calculated the mean value. For films thinner than 30nm or particularly soft materials like the liquid crystal HPc we also used the absorption data to determine the film thickness. In these cases the absorption coefficient was obtained using thicker films where the profilometer results are accurate enough.

In order to measure the thickness of very soft films we sublimed a layer of Al on top of the film with the scratch. For some materials like MEH-PPV we found that drying in air at room temperature for about three days makes the surface harder so that it can be readily measured using the profilometer. In very doubtful cases AFM scans across a scratch could be used.

10.5 Thermal Polarisation Microscopy

For the investigations of liquid crystalline phases a standard microscope was equipped with a video capturing system (PC+video camera+software) and a hotstage (LINKAM). Moreover, the microscope was fitted with a set of polarization filters one of which could be rotated easily to any desired angle with respect to the other.

The hotstage was also fitted with a cooling system using liquid nitrogen that allowed us not only to cool and heat the sample quickly to any temperature between -180° and 300° but also to purge the hotstage and sample environment with a constant flux of nitrogen gas to avoid effects of air at those temperatures.

The geometry of the hotstage requires a special microscope objective (20x) with a long working distance when higher magnifications were desired. We note that higher magnification could also be achieved using stronger magnifying eye-pieces.

10.6 List of Publications

1. H. Ago, Th. Kugler, F. Cacialli, K. Petritsch, R.H. Friend, W.R. Salaneck, Y. Ono, T. Yamatabe and K. Tanaka "Workfunction of Purified and Oxidised Carbon Nanotubes." *Synth.Met.* **103**, 2494-2495 (1998)
2. H. Ago, K. Petritsch, M.S.P. Shaffer, A.H.Windle and R.H. Friend "Composites of carbon nanotubes and conjugated polymers for photovoltaic devices" *Adv.Mat.* **11**, 1281-1285 (1999)
3. A.C. Arias, K. Petritsch, M. Granstrom, J. J. Dittmer, E. A. Marseglia and R. H. Friend "Efficient Polymeric Photovoltaic Devices." *Proc. CBECIMAT* (1998)
4. A.C. Arias, M. Granstrom, D.S. Thomas, K. Petritsch and R.H. Friend "Doped conducting-polymer-semiconducting-polymer interfaces: their use in organic photovoltaic devices" *Phys.Rev.B - Cond. Matt.* **60**, 1854-1860 (1999)
5. A.C. Arias, M. Granstrom, K. Petritsch and R.H. Friend "Organic photodiodes using polymeric anodes" *Synth. Met.* **102**, 953-954 (1999)
6. J.J. Dittmer, K. Petritsch, E.A. Marseglia, R.H. Friend, H. Rost and A.B. Holmes "Photovoltaic properties of MEH-PPV/PPEI blend devices" *Synth.Met.* **102**, 879 (1999)
7. J.J. Dittmer, P. Lazaroni, P. Leclerc, P. Moretti, M. Granstrom K. Petritsch, E.A. Marseglia, R.H. Friend, H.Rost and A.B. Holmes "Crystal Network Formation in Organic Solar Cells" *Sol.En.Mat.Sol.Cells* **61**, 53-61 (2000)
8. M. Granstrom, K. Petritsch, A.C. Arias, A. Lux, M.R. Andersson and R. H. Friend "Laminated fabrication of polymeric photovoltaic diodes." *Nature* **395**, 257-260 (1998)
9. M. Granstrom, K. Petritsch: World Patent Nr.:WO9949525A1: MULTILAYER PHOTO-VOLTAIC OR PHOTOCONDUCTIVE DEVICES, Filing date: Febr.02.1999
10. M. Granstrom, K. Petritsch: Australia Patent Nr.: AU2433799A1: MULTILAYER PHOTO-VOLTAIC OR PHOTOCONDUCTIVE DEVICES, Filing date: Febr.02.1999
11. M. Granstrom, K. Petritsch, A.C. Arias and R. H. Friend "High Efficiency Polymer Photodiodes." *Synth. Met.* **102** 957-958 (1999)
12. W. Graupner, K. Petritsch, G. Leising, G. Lanzani, M. Nisoli, S. Desilvestri, U. Scherf, "Femtosecond optical dynamics in a poly(paraphenylene) type ladder polymer.", *MRS-Proceedings* **413** 615 (1996)
13. W. Graupner, S. Eder, K. Petritsch, G. Leising and U. Scherf "Origin and Stabilization of Photoexcitations in Conjugated Polymers" *Synth.Met.* **84**, 507-510 (1997)
14. W. Graupner, T. Jost, K. Petritsch, S. Tasch, F. Meghdadi, G. Leising, W. Graupner and A. Hermetter "Optoelectronic Properties of Polyphenyls." *ANTEC97-Plastics saving planet earth* **1-3**, 1339-1343 (1997)
15. E.J.W. List, J. Partee, J. Shinar, U. Scherf, K. Mullen, E. Zojer, K. Petritsch, G. Leising and W. Graupner "Localized triplet excitations and the effect of photo-oxidation in ladder-type poly(p-phenylene)s and oligo(p-phenylene)s" *Phys. Rev. B* in print (2000)
16. A. Lux, G.G. Rozenberg, K. Petritsch, S.C. Moratti, A.B. Holmes and R.H.Friend,

- "A series of novel liquid crystalline octakis(alkyl-thio)-substituted phthalocyanines" *Synth.Met.* **102**, 1527-1528 (1999)
17. K. Petritsch "Optical Modulation Spectroscopy in Organic and Inorganic Semiconductors" *Diploma Thesis*, Technical University Graz (1996)
 18. K. Petritsch, W. Graupner, G. Leising and U. Scherf "Photoinduced absorption in a Poly(para-phenylene) ladder type polymer." *Synth.Met.* **84**, 625-626 (1997)
 19. K. Petritsch and R. H. Friend "Ultrathin Organic Photovoltaic Devices." *Synth.Met.* **102**, 976 (1998)
 20. K. Petritsch, M. Granstrom, A.C. Arias, R.H. Friend, A. Lux, G.G. Rozenberg, S.C. Moratti, A.B. Holmes and M.R. Andersson "Towards inexpensive solar cells" *Proc. 2nd World Conference and exhibition on photovoltaic solar energy conversion* Vienna, (1998)
 21. K. Petritsch, R.H. Friend, A. Lux, G.G. Rozenberg, S.C. Moratti and A.B. Holmes "Liquid crystalline phthalocyanines in organic solar cells" *Synth.Met.* **102**, 1776 (1999)
 22. K. Petritsch, J.J. Dittmer, E.A. Marseglia, A. Lux, G.G. Rozenberg, S.C. Moratti, A.B. Holmes and R.H. Friend "Dye based Donor-Acceptor Solar Cells" *Sol.En.Mat.Sol.Cells* **61/1**, 63-72 (2000)
- Dec. 3-5, 1998: "European Conference on Organic Solar Cells" (ECOS'98), Cadarache (France); 1 talk (30min.)
 - July 6-10, 1998: "2nd World Conference and Exhibition on Photovoltaic Solar Energy Conversion" (WCPEC), Vienna (Austria); 1 poster presentation.

10.8 Curriculum Vitae of the Author

1969 02. 02.	Born in Graz (Austria)
1975 - 1979	Elementary School
1979 - 1983	Grammar School
1983 - 1988	Technical Grammar School of Electronics and Telecommunications
1988 - 1996	Study of Applied Physics at the Technical University Graz
Febr.,1996	Research project (2 months) at the Max Planck Institut für Festkörperforschung in Stuttgart (Germany) in the field of thin film monocrystalline silicon solar cells.
Sept.,1996	Final exam with honours
1996-1999	Post as research assistant at the University of Cambridge, UK, in the opto-electronics group lead by Prof. R.H. Friend. The project was focused on the development of efficient organic solar cells.
1999-2000	Completion of the PhD thesis using the results from the work in Cambridge

10.7 Conferences

I have presented results of my research at the following conferences:

- Spring 1999: European network meeting on "Synthesis and Structure of Electroactive Organic Architectures" (SELOA), Bologna (Italy); 2 talks (5min. and 20min.)
- July 12-18, 1998: "International Conference on Science and Synthetic Metals" (ISCM'98), Montpellier (France); 7 poster presentations.
- August, 1998: European network meeting "Synthesis and Structure of Electroactive Organic Architectures" (SELOA), Faro (Portugal); 1 talk (20min.)

The author can be contacted under email:

klaus.petritsch@solarpassion.com